Investigating mechanisms of acquired resistance to the AKT inhibitor capivasertib (AZD5363)

Jasmine Marie Jakubowski

August 2019

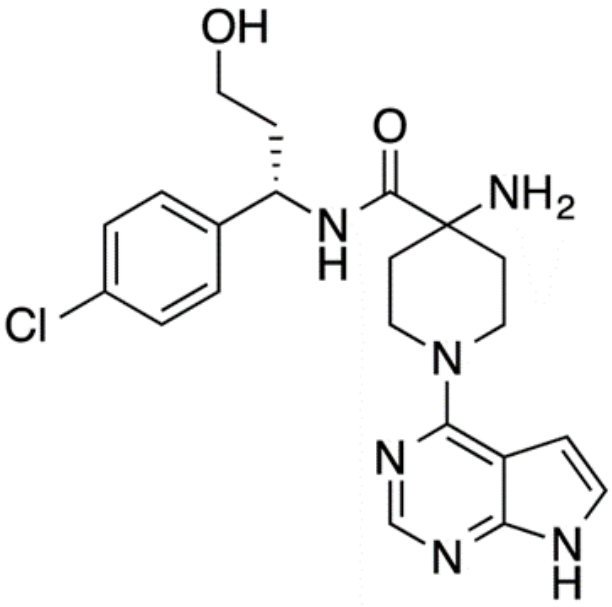

This thesis is submitted for the degree of PhD Cell Biology

Faculty of Sciences
School of Biosciences
University of Kent

Declaration

No part of this thesis has been submitted in support of an application for any degree or other qualification of the University of Kent, or any other University or Institution of learning.

Jasmine Marie Jakubowski

August 2019

Abstract

The PI3K/AKT/mTOR (PAM) pathway is a major driver of cell growth, proliferation and survival and is hyperactivated in 70% of ovarian cancers. PAM inhibitors, such as the AKT-kinase inhibitor capivasertib (AZD5363; currently in Phase III clinical trials), have therefore been `developed as novel cancer therapeutics. Acquired resistance to kinase inhibitors is a major threat to their clinical success, thus understanding resistance mechanisms can support their utility in the clinic. The aim of this thesis was to elucidate resistance mechanisms to capivasertib, using the A2780 human ovarian carcinoma parental and capivasertib-resistant cell lines as models, which harbour hyperactivating PAM pathway mutations.

The isogenic capivasertib-resistant subclone, A2780 254R-B, exhibited cross-resistance to both allosteric and multiple ATP-competitive AKT inhibitors. Additionally, they were also cross-resistant to allosteric and kinase inhibitors of mTORC, although no resistance was observed for the cap-dependent protein synthesis inhibitor, 4EGI-1. Furthermore, 4EBP1 expression was reduced and S6RP S235/6 phosphorylation was capivasertib-resistant, which correlated with overexpression of p90RSK. The induced interaction of 4EBP1 and eIF4E with increased 4EBP1 phosphorylation inhibition was not as great in 254R-B (4-fold) compared to PAR (9-fold), which was associated with a 9-fold increase in cap-dependent protein synthesis, determined by dual-luciferase report assay. Overexpression of 4EBP1 in 254R-B cells reduced resistance to capivasertib by 6-11 fold. Exogenous 4EBP1 additionally reverted the 4EBP1-eIF4E interaction in 254R-B cells sensitive to 4EBP1 phosphorylation inhibition, suggesting that the resistance mechanism may also be dependent on an mTORC1-independent kinase.

Another isogenic capivasertib-resistant subclone, A2780 254R-D, exhibited cross-resistance to ATP-competitive but not allosteric inhibitors of AKT which suggests that resistance may involve a non-AKT target of capivasertib.

Overall, this thesis provides evidence that acquired resistance to capivasertib is associated with increased cap-dependent protein synthesis, mediated through reduced 4EBP1 activity. Reduced 4EBP1 expression in tumours may therefore be used as a predictive biomarker for screening patients for acquired resistance to capivasertib.

Acknowledgments

On the outset of my PhD, I had absolutely no idea how life-changing the following four years would be. For this I have so many people to thank.

To begin I would like to acknowledge the University of Kent for providing the GTA scholarship and resources allowing me to conduct my PhD project.

Secondly, I would like to thank my supervisor, Professor Michelle Garrett, for putting her trust in me and seeking extra GTA funding, so both Nathan and I could work in her laboratory. I am also so grateful for her down-to-earth, open and friendly attitude and her always on-point feedback.

To all Garrett lab members, past and present, especially Nathan, Helen, Daniel, and Denis, I would like to say a big thank you for your support, trouble-shooting ideas, jokes, patience and many a cried-upon shoulder over these last four years. Special never-ending thanks goes to our lab superhero, Edith Blackburn for her priceless work, keeping the lab equipment, storage, finances and us all in check, being the ever caring and thoughtful 'Lab-Mum' supplier of egg-free biscuits, on top of managing that temperamental FACS machine!

Thank you to everyone who has also helped with my project including, Dr Tobias von der Haar, Dr Lyne Jossé, Dr Charlotte Godfrey, Dr Emma Mead, Dr Matt Badham and Mr Ian Brown. Also, I would like to thank all those past and present in the School of Biosciences, especially those whom have shared fond times in the Stacey Dungeon office, co-demonstrating or lengthy chats in the corridors. Special thanks to my epic and patient thesis proof-readers. Also, thank you to all the beautiful people outside of my PhD who have helped and supported me in one way or another, especially Kathryn, Becca, Rich, Phil and all the Kent and BIHS Hare Krishna devotees.

To Seb, my very best of friends, you have been there throughout my highest and lowest, you taught me so many life skills, you cooked amazing food for me when I couldn't and you completely changed my life in a way I never imagined. For that, I am eternally grateful.

To my wonderful parents, for without which, I most certainly would not be here in the first place, I thank you both so much for your amazing support and unconditional love.

Finally, I would like to give my thesis as a humble offering to His Divine Grace A.C. Bhaktivedanta Swami Prabhupada, who continuously inspires the inner scientist in me.

Table of Contents

List of Figures

List of Tables

Abbreviations

254R-B	A2780 CCT129254-resistant subclone B
254R-B-4EBP1-5A	A2780 CCT129254-resistant subclone B, 5A mutant 4EBP1 transfected
254R-B-4EBP1-WT	A2780 CCT129254-resistant subclone B, WT 4EBP1 transfected
254R-B-4EBP1-WT/5A	A2780 CCT129254-resistant subclone B, WT or 5A mutant 4EBP1 transfected
254R-D	A2780 CCT129254-resistant subclone D
254Rp	A2780 CCT129254-resistant polyclonal
4EBP1	eukaryotic translation initiation factor 4E binding protein 1
5’	5 prime end of DNA
5A	5 alanine (T36, T47, T70, S83 and S65) 4EBP1 mutant
ABC	ATP-binding cassette
aCGH	array comparative genomic hybridisation
AGC	related to cAMP/cGMP-dependent protein kinases and protein kinase C
AKT	v-akt murine thymoma viral oncogene homolog
ALK	anaplastic lymphoma receptor tyrosine kinase
ALP	alkyl phospholipids
AMP	adenosine monophosphate
AMPK	AMP-activated protein kinase
ASO	antisense oligonucleotides
ATG13	autophagy related 13
ATM	ataxia telangiectasia mutated
ATP	adenosine triphosphate
BAD	BCL-2-associated agonist of cell death
BCA	bicinchoninic acid
BCL-2	B-cell lymphoma 2
BCL-xL	B-cell lymphoma-extra large
BCR-ABL	breakpoint cluster region-Abelson murine leukaemia viral oncogene homolog 1
BSA	bovine serum albumin
C+	cleaved PARP positive control
CDK	cyclin dependent kinase
CDPS	cap-dependent protein synthesis
CHX	cycloheximide
CIPS	cap-independent protein synthesis
CM	canonical motif

CML	chronic myeloid leukaemia
CREB	cAMP-response element binding protein
C-terminal	carboxy-terminal
DAP1	death-associated protein 1
ddH2O	double-distilled water
DEPTOR	DEP-domain containing mTOR-interacting protein
DLRA	dual luciferase reporter assay
DMEM	Dulbecco's modified Eagle's medium
DMSO	dimethyl sulfoxide
DNA	deoxyribonucleic acid
DT	doubling time
DTT	dithiothreitol
ECL	Enhanced chemiluminescence
EDTA	ethylenediaminetetraacetic acid
eEF2	eukaryotic elongation factor 2
eEF2K	eukaryotic elongation factor 2 kinase
EGF	epidermal growth factor
eGFP	enhanced green fluorescent protein
EGFR	epidermal growth factor receptor
EGTA	ethyleneglycoltetraacetic acid
eIF	eukaryotic translation initiation factor
eIF4A	eukaryotic translation initiation factor 4A
eIF4E	eukaryotic translation initiation factor 4E
eIF4F	eukaryotic translation initiation factor complex 4F
eIF4G	eukaryotic translation initiation factor 4G
ELK	ETS domain-containing protein Elk-1
EMT	epithelial-mesenchymal transition
En	endogenous
ERBB2	v-Erb-B2 avian erythroblastic leukaemia viral oncogene homolog
ERK	extracellular signal-related kinase
EtOH	ethanol
Ex	exogenous
F2	flexitube 2 oligonucleotide
F5	flexitube 5 oligonucleotide
FBS	foetal bovine serum
FGF	fibroblast growth factor
FGFR	fibroblast growth factor receptor
FL	firefly luciferase
FOXO	forkhead box O

G418	geneticin
GAB	GRB2-associated binding partner
GAP	GTPase activating protein
GAPDH	glyceraldehyde 3-phosphate dehydrogenase
GDP	guanosine diphosphate
GEF	guanine nucleotide exchange factor
GI_{50}	half-maximal growth inhibitory concentration
GIST	gastrointestinal stromal tumour
GMP	guanosine monophosphate
GPCR	G-protein coupled receptor
GRB	growth factor receptor-bound protein
GSK-3β	glycogen synthase kinase-3 beta
GTP	guanosine triphosphate
HDM2	human double minute 2
HEPES	4-(2-hydroxyethyl)-1-piperazineethanesulfonic acid
HER2	human epidermal growth factor receptor 2
hERG	human ether-a-go-go-related gene
HGSOC	high-grade serous ovarian carcinoma
HIF	hypoxia-inducible factor
HMW	high molecular weight protein
HRP	horseradish peroxidase
hrs	hours
ICR	The Institute of Cancer Research, London
IGF	insulin-like growth factor
IL	interleukin
IRES	internal ribosome entry site
IRS	insulin receptor substrate
JNK	c-Jun N-terminal protein kinase
kDa	kilo Dalton
LARP1	La-related protein 1
LGSOC	low-grade serous ovarian carcinoma
LKB1	liver kinase B1
LMW	low molecular weight protein
m^7GTP	7-methyl GTP
MAPK	mitogen activated protein kinase
MCL1	myeloid cell leukaemia 1
MDR	multidrug resistance
MEK	mitogen-activated protein kinase kinase
mLST8	mammalian lethal with sec-13 protein 8
MNK	MAPK-interacting kinases

mSin1	mammalian stress-activated MAP kinase-interacting protein 1
MSK1	mitogen and stress activated protein kinase 1
mTOR	mammalian/mechanistic target of rapamycin
mTORC	mTOR complex 1 and/or 2
mTORC1	mTOR complex 1
mTORC2	mTOR complex 2
mTORK	mTOR kinase
MYC	myc Avian Myelocytomatosis Viral Oncogene
(N)SCLC	(non) small cell lung cancer
NT	non-targeting (oligonucleotide)
N-terminal	amino-terminal
OC	ovarian carcinoma
OCCC	clear cell ovarian carcinoma
OD	optical density
ORR	objective response rate
OS	overall survival
p(protein)	phosphorylated (protein)
P+	pull down positive control
p27kip1	cyclin-dependent kinase inhibitor 1B
p53	protein 53
p70S6K	p70 ribosomal S6 kinase
p90RSK	p90 ribosomal S6 kinase
PAM	PI3K/AKT/mTOR
PAR	A2780 parental
PARP	poly-ADP ribose polymerase
PBS	phosphate-buffered saline
PCR	polymerase chain reaction
PDCD4	programmed cell death 4
PDGF	platelet derived growth factor
PDGFR	platelet derived growth factor receptor
PDK1	phosphoinositide-3-kinase dependent kinase 1
PFS	progression free survival
PH	pleckstrin homology
PHLPP	PH-domain leucine-rich repeat protein phosphatase
PI	phosphatidylinositol
PI(3,5)P2	phosphatidylinositol 3,5-bisphosphate
PI(4,5)P2	phosphatidylinositol 4,5-bisphosphate
PI3K	phosphoinositide-3-kinase
PIC	pre-initiation complex

PIKK	phosphoinositide 3-kinase related kinase
PIP2	phosphatidylinositol bisphosphate
PIP3	phosphatidylinositol 3,4,5-trisphosphate
PKA	cAMP dependent protein kinase
PKB	protein kinase B
PKC	protein kinase C
PMSF	phenylmethylsulfonyl fluoride
PP1	protein phosphatase 1
PP2A	protein phosphatase 2A
PRAS40	proline-rich AKT substrate of 40 kDa
PROTOR	protein observed with RICTOR 1 and 2
PTEN	phosphatase and tensin homolog
PVDF	polyvinylidene fluoride
RAF	v-raf murine sarcoma viral oncogene homolog
RAPTOR	regulatory associated protein of mTOR
RAS	rat sarcoma viral oncogene homolog
RCC	renal cell carcinoma
REDD1	regulated in DNA damage and development 1
RF	resistance factor
RHEB	RAS-homolog enriched in brain
RICTOR	rapamycin insensitive companion of mTOR
RL	*Renilla* luciferase
ROCK	Rho-associated coiled-coil kinase
RT	room temperature
RTK	receptor tyrosine kinase
S(amino acid)	serine residue
S6RP	S6 ribosomal protein
SD	standard deviation
SDS	sodium dodecyl sulfate
SDS-PAGE	sodium dodecyl sulfate - polyacrylamide gel electrophoresis
SGK	serum and glucocorticoid-induced protein kinase
SH2	Src homology 2
SHIP	SH2-containing inositol phosphatase
shRNA	short hairpin ribonucleic acid
siRNA	small interfering ribonucleic acid
SLL	small lymphocytic lymphoma
SMT	somatic mutation theory
SOS	son of sevenless
SRB	sulforhodamine B

SREBP	sterol-regulatory element-binding protein
T(amino acid)	threonine residue
t0	time at 0hrs
t96	time at 96hrs
TBST	Tris buffered saline with Tween20 buffer
TGF-β	transforming growth factor beta
TNBC	triple negative breast cancer
TOP	terminal oligopyrimidine
TOS	TOR signalling
TSC	tuberous sclerosis complex
TSC1	tuberous sclerosis complex subunit 1 (hamartin)
TSC2	tuberous sclerosis complex subunit 2 (tuberin)
TSG	tumour suppressor gene
ULK1	Unc-51 like autophagy activating kinase 1
v/v	volume/volume
VEGF	vascular endothelial growth factor
w/v	weight/volume
Wnt	Wingless-related integration site
WT	wildtype
Y(amino acid)	tyrosine residue
YAP	Yes-associated protein

Chapter 1

Introduction

1. Introduction

1.1. Introduction to cancer

Current statistics for cancer occurrence state that for persons born since 1960, the likelihood of being diagnosed with cancer at some point during their lifetime is greater than 50% (Ahmad et al., 2015). According to GLOBOCAN 2018, it was estimated that there were 9.6 million deaths caused by cancer (17% of all deaths globally) in 2018 and that it is the second leading cause of death after cardiovascular disease. With 18.1 million new cancer cases diagnosed last year, the importance of research into cancer prevention and treatment is very clear (Bray et al., 2018; Global Burden of Disease Collaborative Network., 2018).

Cancer is a class of over 200 diseases which are characterised as uncontrolled cell proliferation, which may invade and spread from a primary site to other organs of the body. These can invade and impair the function of vital organs leading to death. There are several proposed theories that offer explanations into how normal cells transform into cancer cells; those include tissue organisation field theory, metabolic theory of cancer and somatic mutation theory (SMT; Christofferson, 2014; Baker, 2015; Seyfried, 2015; Pecorino, 2016). SMT is the currently the best studied and is the model of carcinogenesis assumed by this work. SMT describes that cancer is a genetic disease, which originally arises from a single somatic cell that has accumulated several permanently acquired DNA mutations, sometimes in combination with inherited mutations, such as those found in the *BRCA1* and *APC* genes of familial breast and colorectal cancers respectively (Stella *et al.*, 1992; Keisell *et al.*, 1993). Although there may be a correlation between cancer risk and stem-cell divisions, it is generally accepted that cancer risk is predominantly a result of internal and external genotoxic factors, such as reactive oxygen species, tobacco smoke and ultraviolet light which can generate DNA damage (Tomasetti and Vogelstein, 2015; Pecorino, 2016). The cell can combat the generation of novel somatic mutations through a number of DNA repair pathways. However, if DNA lesions are not repaired, or repaired incorrectly before a cell replicates, a

permanent alteration is fixed into the DNA and may contribute to carcinogenesis (Lord and Ashworth, 2012). Recent research has also identified that epigenetic alterations may also contribute towards oncogenesis (Weinstein and Joe, 2006; Stottrup *et al.*, 2016; Mansoori *et al.*, 2017).

Most mutations that arise in a somatic cell are passenger mutations, but mutations in oncogenes and tumour suppressor genes (TSGs) can disrupt normal cell proliferation and survival processes to promote clonal expansion. Oncogenes and tumour suppressors are genes that encode for proteins that positively and negatively regulate cell growth respectively. Mutations may occur in either the regulatory promotor region or the coding region itself to alter translation of the mRNA (Pecorino, 2016). Alternatively, recent research has also identified that epigenetic alterations can also contribute to carcinogenesis (Weinstein and Joe, 2006; Earwaker *et al.*, 2018; Ravegnini *et al.*, 2019). The mutations in oncogenes that lead to cancer usually involve increased production of the protein product or activity, whereas mutations in TSGs often downregulate expression or activity. An example of a commonly mutated oncogene is *RAS* (30% of cancers harbour this mutation), which induce a loss in GTPase activity, rendering the RAS protein permanently active leading to increased growth-promoting signalling. An example of a frequently mutated TSG is *TP53* (50% of cancers) which is important for sensing DNA damage (Higashitsuji *et al.*, 2007; Pecorino, 2016).

The acquisition of dysregulated oncogenes and tumour suppressor genes culminate in several characteristics present in most, if not all tumours. These are termed the “Hallmarks of Cancer” and include: growth signal autonomy; evasion of inhibitory growth signals; evasion of immune destruction; unlimited replicative potential; invasion and metastatic potential; angiogenesis; evasion of cell death and reprogrammed energy metabolism. Tumour-promoting inflammation and genomic instability are also included as characteristics that promote acquisition of the other hallmarks (Hanahan and Weinberg, 2011). Cancer cells are notoriously difficult to distinguish from normal somatic cells at a molecular basis, and therefore further understanding of these hallmarks of cancer may improve the development of novel cancer therapeutics.

1.2. History of cancer therapeutics

Historically, treatment of cancer dates back to the ancient Greek and Egyptian civilisations which often involved ineffective surgical means. Although radiotherapy was used in the late nineteenth century, cancer treatment received its major breakthrough during the First World War, with the accidental discovery of the cytotoxic anti-tumour activity of nitrogen mustard gas. Similarly following chemotherapies (alkylating agents, antimetabolites, anti-mitotics, and cytotoxic antibiotics) primarily target the rapidly dividing cells. The goal of these cytotoxic therapies is to cause severe DNA damage to trigger apoptosis in rapidly dividing cells. The major problem with these broad-acting therapies is that they cannot distinguish between neoplastic cells and rapidly dividing healthy tissue such as hair follicles and digestive epithelia, which are therefore also affected by these drugs (Falzone *et al.*, 2018).

Increased understanding in the 1980s and 1990s into the molecular mechanisms causing oncogenic transformation of cells drove the discovery and development of small selective inhibitory compounds (such as BCR-ABL tyrosine kinase inhibitor, imatinib) and monoclonal antibodies that targeted and inhibited oncogenic proteins (such as HER2 receptor targeting, trastuzumab). Research from the human genome project spurred the development of molecular targeted therapies such as BRAF inhibitor vemurafenib. The selectivity of these therapies allowed suppression of growth in cancerous cells whilst incurring minimal effects on normal tissue. This greatly increased the therapeutic window, which in turn minimised side effects (Falzone *et al.*, 2018).

At the turn of the 20th century, Bernard Weinstein introduced the concept of oncogenic addiction whereby despite the diverse array of somatic DNA mutations that may arise within a tumour, a predominant reliance on one single oncogene for continuous tumourigenesis was common in many cancers (Weinstein and Joe, 2006). The concept of “oncogene addiction” promoted exciting clinical implications and a large body of evidence supported that therapeutic intervention targeting a single dependent oncogene is sufficient for tumour regression. The most famous

application of this concept, despite its discovery prior to the coining of oncogenic addiction is the small Philadelphia chromosome in chronic myeloid leukaemia (CML). The small Philadelphia chromosome is a chromosomal translocation that produces a fusion transcript (BCR-ABL) encoding for a constitutively active tyrosine kinase (Druker *et al.*, 1996). This lead to the development of imatinib, which exhibited highly promising pre-clinical and phase I trial results, which encouraged the fast-track FDA approval of the drug within three years of clinical trials (Torti and Trusolino, 2011).

Kinases are particularly easy targets for small molecule inhibitor development due to the availability of ATP or co-factor binding pockets, which small molecule mimics can be easily designed (Roskoski, 2016). Therefore, signalling cascades of kinases that contain commonly mutated oncogenes or TSGs are attractive areas for oncotherapeutic development. One such promising signalling cascade is the phosphoinositide 3-kinase (PI3K)/AKT/mammalian target of rapamycin (mTOR; PAM) pathway (Yap *et al.*, 2008; Martini *et al.*, 2013).

1.3. The PAM signalling pathway

The PAM pathway (illustrated in Figure 1.1) is one of several signalling pathways which allow the cell to interact and adapt to its external environment by converting extracellular stimulation to intracellular signals to influence a cellular response. PAM pathway signalling promotes positive regulation of metabolism, proliferation, cell survival, cell cycle progression, angiogenesis and protein synthesis in response to external cues (Fruman *et al.*, 2017).

These pathways consist of a cascade of protein kinases that transmit the extracellular signal by a series of phosphorylation events from one kinase to another. Phosphorylation is one of the most common and reversible post-translation modifications of a protein, which involves the transfer of a phosphate group (PO_4) from ATP (adenosine triphosphate) to form ADP (adenosine diphosphate), onto the hydroxyl (-OH) group of a serine, threonine or tyrosine residue of a protein (Ardito *et al.*, 2017). All protein kinases contain two lobes (N-

terminal and C-terminal) to catalyse phosphorylation reactions. The phosphorylatable residue of the substrate is positioned in a shallow groove of the C-terminal lobe, whereas ATP is positioned within the hydrophobic pocket of the N-terminal lobe, thereby allowing the phosphorylatable residue of the substrate and the terminal phosphate of ATP to be adjacent to one another. An aspartate residue in the substrate binding pocket acts as a base and removes the proton from the substrate residue hydroxyl group. The remaining oxygen attacks the terminal phosphoryl group of ATP to form a metaphosphate intermediate. Mg^{2+} is important to electrostatically stabilise the intermediate in this reaction. ADP becomes displaced and the protein-residue phosphate is formed and both products are released from the active site (Roskoski, 2016). The addition of a phosphate group on a protein can affect the charge on the residue and induce a conformational change to activate or deactivate the substrate protein or affect its ability to form protein complexes (Ardito *et al.*, 2017).

Hormones and growth factors, such as insulin and insulin-like growth factor (IGF) stimulate receptor-coupled tyrosine kinases (RTKs) which are present on the cell surface membrane. Ligand binding activates pre-existing RTK dimers or induces receptor dimerization and subsequent autophosphorylation of the intracellular domains. This alone or with adapter proteins such as IRS1 (insulin receptor substrate) form a docking site for PI3K binding. PI3K can catalyse the phosphorylation of $PI(4,5)P_2$ (phosphatidylinositol 4,5-bisphosphate) to $PI(3,4,5)P_3$ (phosphatidylinositol 3,4,5-trisphosphate), which facilitates AKT recruitment to the plasma membrane. AKT is then subsequently phosphorylated by PDK1 (phosphoinositide-dependent kinase-1) and mTORC2 (mTOR complex 2) at T308 and S473 respectively. Once activated, AKT can phosphorylate over 100 substrates to induce a positive role on cell function. Examples of AKT substrates include: GSK-3β (glycogen synthase kinase-3β) and PFK2 (phosphofructokinase-2) involved in metabolism; HDM2 (human double minute 2 homolog) and BAD (BCL-2-associated death promoter) for survival; FOXO (forkhead box O), and p27kip1 (cyclin-dependent kinase inhibitor 1B) for cell cycle regulation; and PRAS40 (proline-rich

AKT substrate of 40 kDa) and TSC2 (tuberin) for protein synthesis (Pearce *et al.*, 2010; Vanhaesebroeck *et al.*, 2010, 2012; Fruman *et al.*, 2017).

TSC2 is a subunit of the tuberous sclerosis complex (TSC). Both TSC2 and PRAS40 are negative regulators of mTORC1, through inhibition of Rheb (RAS homologue enriched in brain), or the complex directly, respectively. AKT phosphorylation of TSC2 or PRAS40 blocks their negative regulation of mTORC1, thus increasing the activity of the complex. The best studied substrates of mTORC1 are ULK (Unc-51 like autophagy activating kinase), p70S6K (ribosomal protein S6 [S6RP]-kinase) and 4EBP1 (eukaryotic translation initiation factor 4E [eIF4E]-binding protein 1), of which the latter two are heavily involved in protein synthesis. 4EBP1 is a negative regulator of the mRNA cap-binding protein, eIF4E, and p70S6K phosphorylates several translation initiation and elongation factors including S6RP (Roux and Topisirovic, 2018). The key nodes of the PAM pathway will be elaborated on in the following sections. Section 1.4 will describe what alterations of these nodes have been reported in cancer.

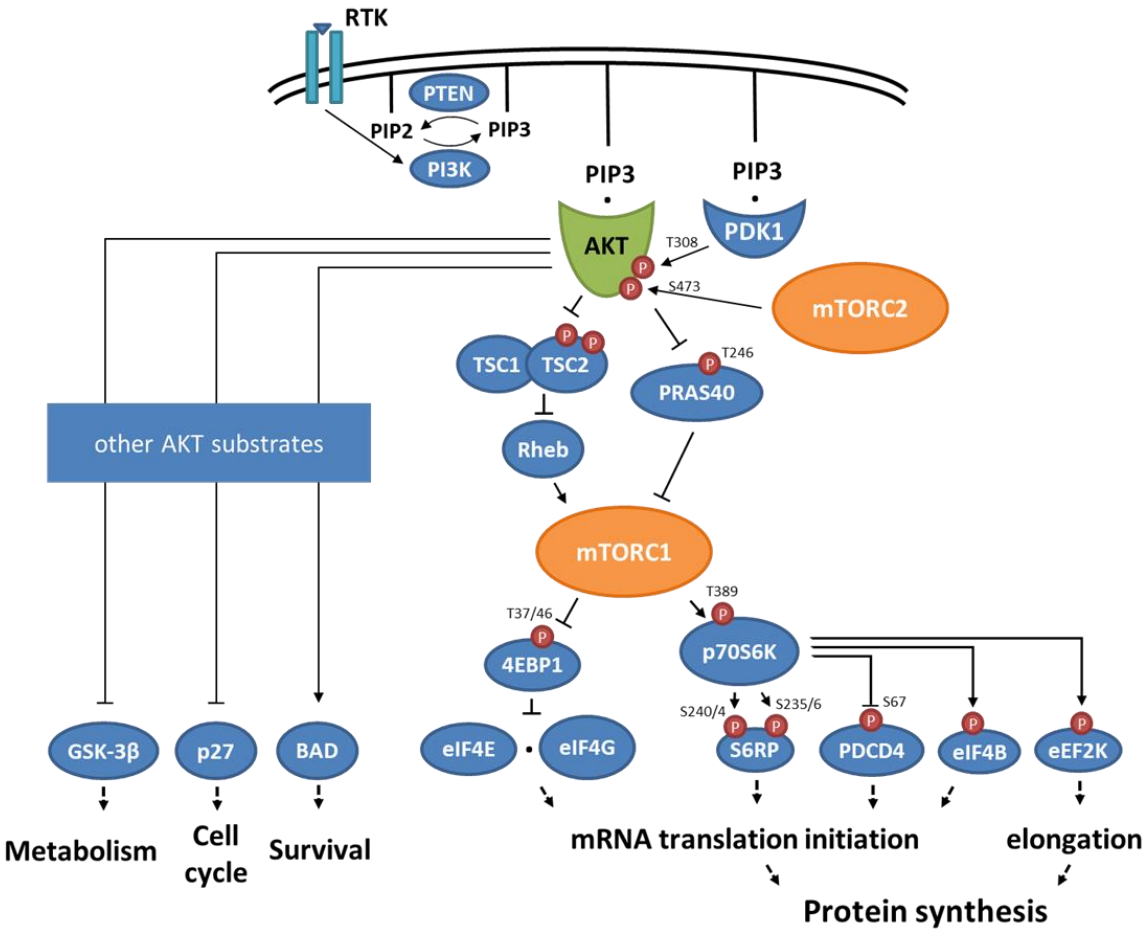

Figure 1.1 – The PAM pathway.
Phosphorylated residues are represented as dark red (P)s, with amino residue defined. Black arrows and block-headed arrows indicate phosphorylation of target induces activation or inhibition respectively. Black dotted arrows indicate phenotypic output. Based upon Fruman et al., (2017); Saxton and Sabatini, (2017) and Roux and Topisirovic, (2018).

1.3.1. PI3K family

PI3Ks are a family of at least eight lipid kinases that phosphorylate the 3-hydroxyl of the inositol head group of phosphatidylinositol (PI) of the plasma membrane. The catalytic subunits of all PI3K enzymes share a PI3K core structure which contains a C2 domain, a helical domain and a catalytic domain. PI3K isoforms are grouped into three classes; I, II and III based upon their structure and substrate specificity. Class I are heterodimeric, receptor-regulated PI(4,5)P_2 kinases and are further divided into two groups: IA and IB. (Vanhaesebroeck *et al.*, 2010, 2012).

Class IA PI3Ks are the subfamily involved in the PAM pathway. The three members of class IA contain a p110 catalytic subunit (p110α, β or δ, encoded by *PIK3CA,*

PIK3CB or *PIK3CD*, respectively) and one of five p85 regulatory subunit isoforms. These bind to the activated RTK or IRS1 via the SH2 (Src homology 2) domain of the p85 regulatory subunit, which reduces the domain's inhibitory action on the catalytic domain. This allows the p110α to phosphorylate $PI(4,5)P_2$ to $PI(3,4,5)P_3$ which can be reversed by PTEN. $PI(3,4,5)P_3$ may also be dephosphorylated to phosphatidylinositol 3,4-bisphosphate ($PI(3,4)P_2$) by SHIP1/2 (SH2 domain containing inositol polyphosphate 5-phosphatase 1 and 2). Both $PI(3,4,5)P_3$ and $PI(3,4)P_2$, but not $PI(4,5)P_2$ can recruit PH-domain containing PI3K effectors, such as AKT, to the plasma membrane (Figure 1.1; Vanhaesebroeck *et al.*, 2012; Fruman *et al.*, 2017).

1.3.2. AKT

AKT (also known as protein kinase B; PKB) is a 56 kDa serine/threonine kinase, of which there are three isoforms, AKT1, AKT2 and AKT3. The former two isoforms were initially identified as the human homologues of the AKT8 retroviral oncogene v-AKT (Staal, 1988). AKT1 was discovered to be closely related to PKA and PKC, and AKT3 was subsequently identified due to high homology with the other isoforms (Coffer and Woodgett, 1991; Konishi *et al.*, 1995).

AKT is an AGC kinase. The AGC kinase family contains 60 members (12% of the human protein kinome), and include PKA, PKC, SGK (serum and glucocorticoid-regulated kinase), p70S6K, p90RSK (ribosomal S6 kinase) and PDK1. The AGC kinases share a high degree of homology across the kinase domain (90% across all AKT isoforms) and the majority are fully activated by subsequent phosphorylation of highly conserved activation loop (T loop) and the non-catalytic hydrophobic motifs (Pearce *et al.*, 2010). The structure of AKT consists of three domains: a pleckstrin homology (PH) domain on the N-terminus, a kinase domain containing the AGC kinase T loop and a C-terminal extension containing the regulatory hydrophobic motif (Figure 1.2A). (Kumar and Madison, 2005).

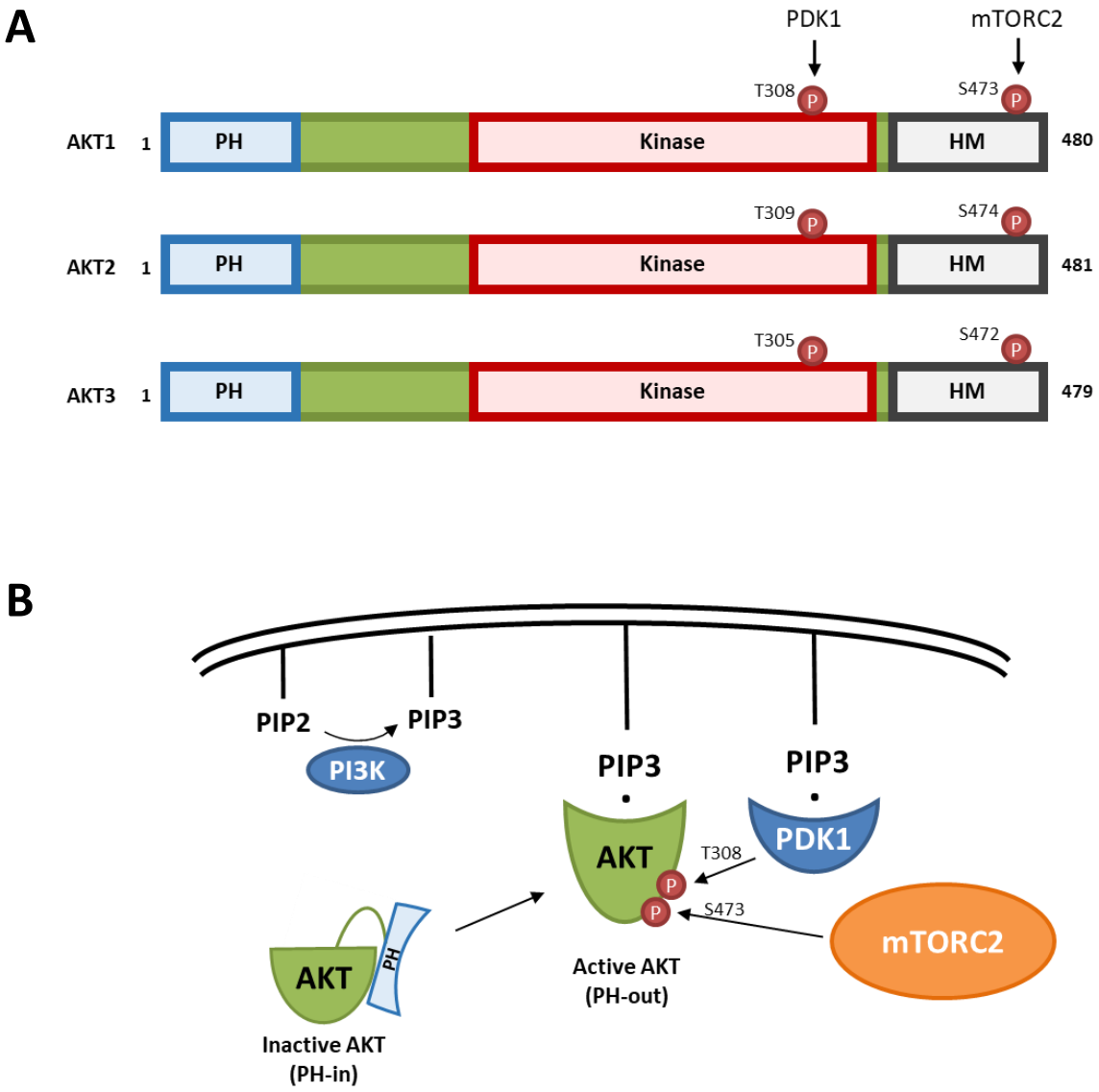

Figure 1.2 – AKT structure and activation.
(A) Domains for each AKT isoform. Phosphorylated residues (P). PH = PH domain; Kinase = kinase domain; HM = hydrophobic motif. Adapted from Martelli *et al.,* (2012). (B) When PH domain is in PH-in confirmation, inhibiting the kinase domain, AKT is inactive. When AKT binds to PI(3,4,5)P3 (PIP3) at the plasma membrane, the conformation changes to a PH-out structure. AKT is subsequently phosphorylated by PDK1 and mTORC2. Adapted from Pearce *et al.,* 2010.

Like many class I PI3K effectors, the PH domain of AKT binds to $PI(3,4,5)P_3$ or $PI(3,4)P_2$ to recruit it to the plasma membrane. This binding induces a conformational change in AKT from a 'PH-in' to 'PH-out' that relieves inhibition of the PH domain on the kinase domain (Figure 1.2B). Recent research has also identified that the activation of the different isoforms of AKT can be independently regulated by spatiotemporal coordination of $PI(3,4,5)P_3$ and $PI(3,4)P_2$ (Liu *et al.*, 2018). The active conformation enables AKT to be phosphorylated by PDK1 at

threonine 308 (T308) on the activation loop, stimulating enzymatic activity 100-fold (Kumar and Madison, 2005). Subsequent phosphorylation by mTORC2 on the hydrophobic motif at serine 473 (S473) induces maximal activation of AKT and regulates substrate specificity. FOXO1 and FOXO3A phosphorylation by AKT are dependent on maximal AKT activation, but substrates such as GSK-3β and TSC2 can be phosphorylated by AKT regardless of the S473 phosphorylation status (Guertin *et al.*, 2006; Jacinto *et al.*, 2006; Pearce *et al.*, 2010). AKT can also be dephosphorylated by PP2A (T308) and PHLPP1 (S473; Andjelković *et al.*, 1996; Brognard *et al.*, 2007).

Although over 100 proteins have been reported as AKT substrates over the past 20 years, the extent in which substrates have been validated is variable. A combination of phosphoproteomic analyses have assigned 20 proteins as AKT substrates with high confidence. Examples include GSK-3β, PRAS40, and TSC2 which all share the consensus sequence R-X-R-X-X-S/T-φ (where X is any amino acid and φ is a large hydrophobic residue; Cole *et al.*, 2019).

GSK-3β inhibits many pro-growth proteins by phosphorylating and targeting them for degradation. AKT enhances cell proliferation through inhibition of GSK-3β activity through phosphorylating serine 9 (S9) on the N-terminus, creating a pseudosubstrate motif that obstructs the catalytic domain (Cross *et al.*, 1995).

Both PRAS40 and TSC2 negatively regulate the AKT effector, mTORC1. Phosphorylation on threonine 246 (T246) on PRAS40 and several sites of TSC2 by AKT incur an inhibitory effect on these proteins and positively regulate mTORC1 signalling (Huang and Manning, 2008; Wiza *et al.*, 2012). Regulation of mTORC1 will be explained further in Section 1.3.3.2.

1.3.3. mTOR complexes 1 and 2

1.3.3.1. mTOR and complex structure

mTOR (previously known as FRAP), is a 289 kDa serine/threonine protein kinase of the PIKK (phosphoinositide 3-kinase related kinase) family. It contains several N-terminal tandem HEAT (Huntingtin, Elongation factor 3, A subunit of protein phosphatase 2A and TOR1) repeats, followed by a FAT (FRAP, ATM, TRRAP) domain and a FATC (FAT C-terminus) domain, which surround and are important for modulating the activity of the kinase domain. As shown in Figure 1.3A, mTOR also contains a PIKK regulatory domain (PRD) responsible for binding by the small GTPase mTORC1 activator, Rheb (Lovejoy and Cortez, 2009; Cargnello *et al.*, 2015).

The mTOR protein interacts with various proteins to form two functionally and structurally distinct complexes: mTORC1 and mTORC2. As shown in Figure 1.3B, both complexes share mTOR, mLST8 (mammalian lethal with SEC13 protein 8; also known as G protein beta subunit-like, GβL) and DEPTOR (DEP domain-containing mTOR-interacting protein). Specific subunits for mTORC1 are Regulatory-associated protein of mTOR (RAPTOR) and PRAS40, and specific for mTORC2 are RICTOR, mSIN1 and PROTOR (Laplante and Sabatini, 2009). Both RAPTOR and RICTOR act as scaffolding proteins for their respective complexes, facilitating the recruitment of substrates and regulators (Cargnello *et al.*, 2015). DEPTOR is a negative regulator of both complexes (Kim and Guan, 2019). mSIN1 is a particularly important subunit of mTORC2 as it contains a PH domain and allows transport of the complex to the plasma membrane for phosphorylation of substrates such as AKT and SGK1 (Jhanwar-Uniyal *et al.*, 2017).

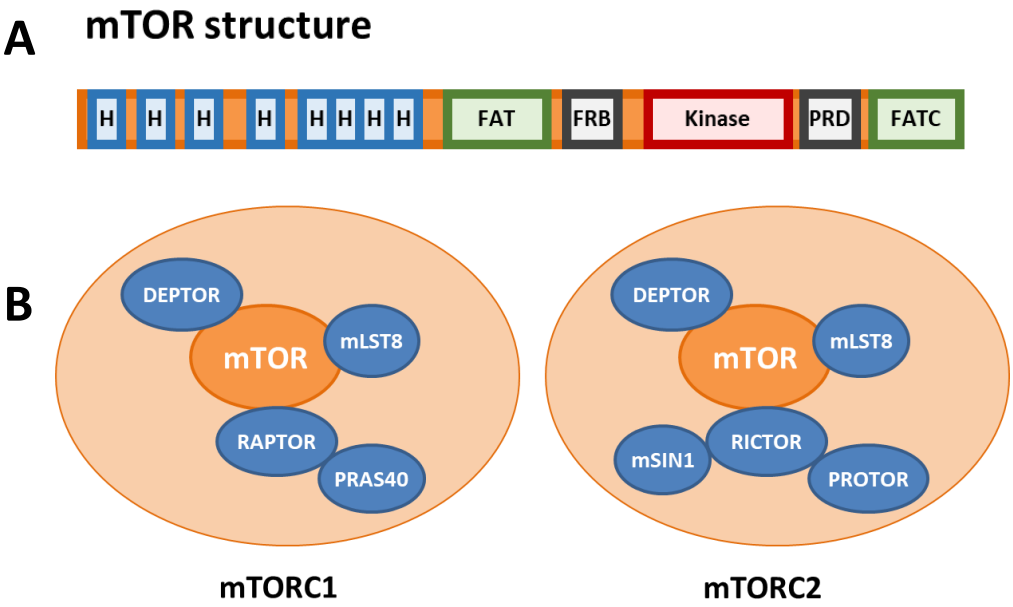

Figure 1.3 – mTOR structure and complexes.
(A) mTOR protein domains. H = HEAT domains. (B) mTORC1 and mTORC2 subcomponents. Adapted from Lovejoy and Cortez, (2009) and Cargnello et al., (2015).

1.3.3.2. mTORC1 regulation

mTORC1 is a key node for co-ordinating nutrient availability and external environmental signals, such as growth factors, with the regulation of intracellular signals important for cellular homeostasis. As such, the activity of mTORC1 is highly regulated by many mechanisms (Cargnello *et al.*, 2015), summarised in Figure 1.4.

Growth factor signals from the PAM axis are integrated with mTORC1 via PRAS40 and TSC2. As mentioned in Section 1.3.2, AKT regulates mTORC1 indirectly through the inhibitory phosphorylation of the negative regulators PRAS40 and TSC2. PRAS40 contains a five amino acid sequence TOR signalling (TOS) motif, found in all mTORC1 substrates that allows it to bind to the substrate binding site of RAPTOR, thus competing with mTORC1 substrates. Phosphorylation of T246 on the C-terminus of PRAS40 by AKT and subsequent serine 183 (S183) of the RAIP-motif by mTORC1 promotes its disassociation from the complex and sequestration by 14-3-3 proteins (Wiza *et al.*, 2012; Roux and Topisirovic, 2018).

TSC2 is a large 130 kDa protein which complexes with Hamartin (TSC1) and Tre2-Bub2-Cdc16-1 domain family member 7 (TBC1D7), to form the tuberous sclerosis

complex (TSC). TSC1 stabilises TSC2 and prevents its degradation and TBC1D7 promotes the association of TSC1 and TSC2 (Huang and Manning, 2008; Dibble *et al.*, 2012). TSC2 is a GTPase-activating protein (GAP) for the small GTPase, Rheb. TSC2 stimulates the hydrolysis of GTP to GDP on Rheb, rendering it inactive. TSC2 phosphorylation by AKT inhibits its activity by destabilising its interaction with TSC1 and Rheb at the lysosome. Activated Rheb-GTP can bind to mTOR and induce a conformational change to promote its activation (Menon *et al.*, 2014; Roux and Topisirovic, 2018).

Rheb is a potent activator of mTORC1, therefore the regulation of TSC2 also indirectly impacts on mTORC1 activity (Huang and Manning, 2008). AKT phosphorylates TSC2 at S939, S981, S1130, S1132 and T1462 (Kwiatkowski and Manning, 2005), which can all be phosphorylated by SGK1 as well (Castel *et al.*, 2016). ERK1/2 (Extracellular signal-regulated kinase; also known as MAPK) also phosphorylates TSC2 at S540 and S664 (Ma *et al.*, 2005), and p90RSK on S1798 (Roux *et al.*, 2004). Stressors can also play a role in regulating TSC2, such as through REDD1 in hypoxic conditions (Deyoung *et al.*, 2008), and AMPK at AKT-independent residues S1270 and S1387 in glucose starvation (Kwiatkowski and Manning, 2005). Wnt signalling promotes TSC2 activity by phosphorylation at S1337 and S1341 through GSK-3β (Kwiatkowski and Manning, 2005; Inoki *et al.*, 2006; Laplante and Sabatini, 2012).

Independently of signalling via Rheb, mTORC1 is also regulated by amino acid availability, particularly leucine, arginine and glutamine. There are four RagGTPases (A, B, C and D) which interact with RAPTOR to promote mTORC1 recruitment to the lysosome. These RagGTPases are dependent on the GAP and GEF activities of GATOR1 and Ragulator, respectively, in response to amino acid sensing (Cargnello *et al.*, 2015). Interestingly, nutrient availability and growth factor conditions do not regulate mTORC1 separately. Activation of mTORC1 occurs only at the lysosome when nutrient availability signalled by RagGTPases, and growth factor conditions signalled through Rheb, are both appropriate (Parmar and Tamanoi, 2010).

AMPK is an inhibitor of cell growth, and in line with this it can inhibit mTORC1 activation, both directly and indirectly. Under energy stress (high AMP or ADP levels), LKB-1 activates AMPK by phosphorylation of T172. AMPK can then inhibit mTORC1 by phosphorylating RAPTOR on S722 and S792, or TSC2 as described above. Negative feedback of the PAM pathway (as described in Section 1.3.5), allows mTORC1 to also negatively regulate AMPK through AKT-dependent phosphorylation of AMPK alpha subunits, which are associated with a decrease in T172 phosphorylation (Hindupur *et al.*, 2015).

The activity of mTORC1 can also be regulated by its substrates. For example, p70S6K phosphorylates mTOR at T2446 and S2448 to positively increase mTORC1 activity (Holz and Blenis, 2005). Additionally, mTORC1 can be regulated at a transcriptomic level, through the regulated expression of mTOR, RAPTOR and other proximally related proteins by the mTORC1 substrate, RNA-binding protein LARP1 (La-related protein 1) on the mRNA transcripts (Mura *et al.*, 2014).

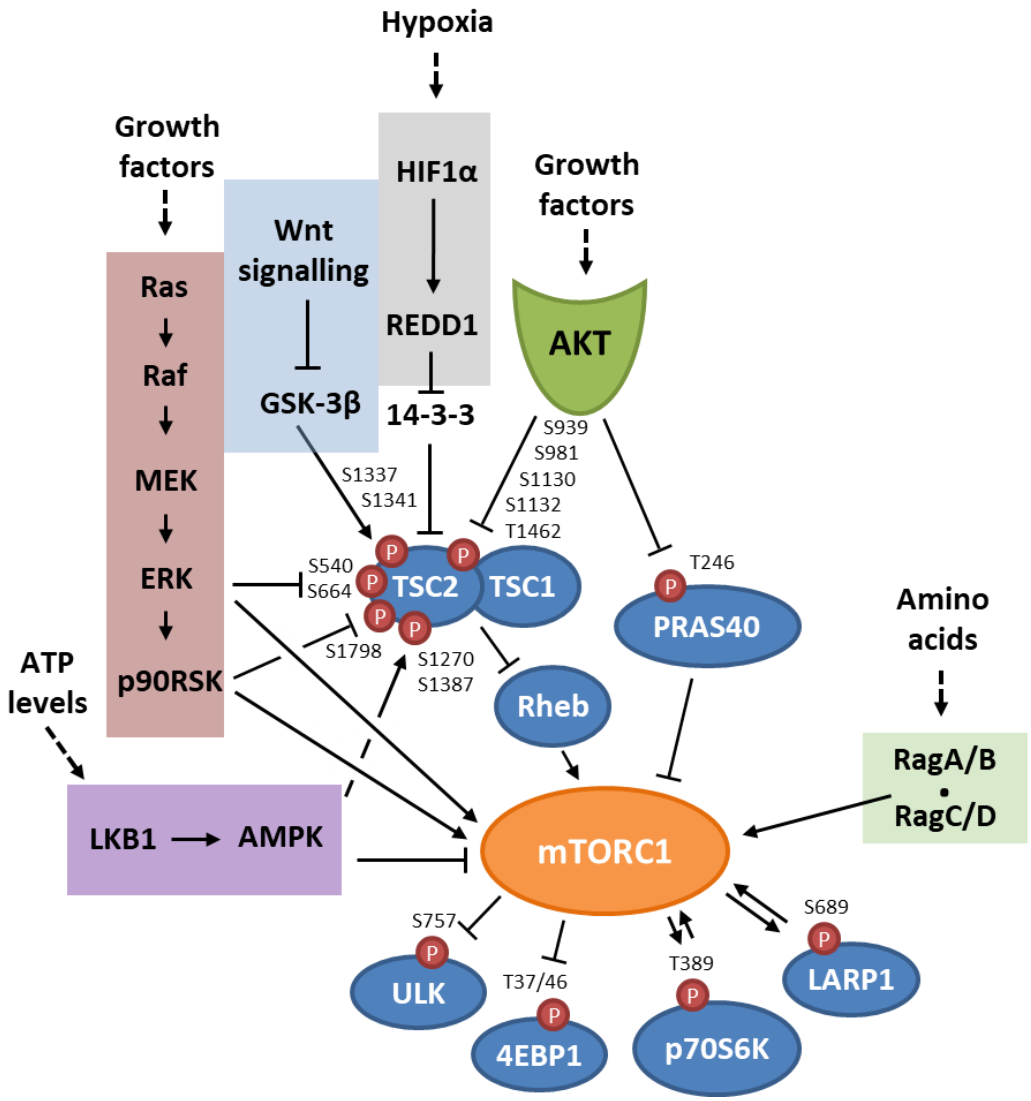

Figure 1.4 – Regulation of mTORC1.
Black arrows and block-headed arrows indicate phosphorylation of target induces activation or inhibition respectively. Based upon information from Kwiatkowski and Manning, (2005); Laplante and Sabatini, (2012) and Kim and Guan, (2019)

1.3.3.3. mTORC1 signalling

Many mTORC1 outputs increase growth and proliferation of the cell, therefore, when activated, the complex increases anabolic pathways such as protein, lipid and ribosome production whilst reducing catabolic pathways such as autophagy in response to environmental conditions (Saxton and Sabatini, 2017).

Autophagy is the central degradative process in the cell, whereby the formation of autophagosomes engulfs damaged and excess organelles for degradation and recycling at the lysosomes in response to nutrient availability. mTORC1

phosphorylates several components of autophagy such as ULK1 and WIPI2, which both drive autophagosome formation; the transcription factor, TFEB, preventing its translocation to the nucleus and DAP1, a negative regulator of autophagy (Kim *et al.*, 2011; Laplante and Sabatini, 2012; Saxton and Sabatini, 2017).

Many anabolic processes are controlled by mTORC1, including lipid and protein biogenesis. Fatty acid and sterol biogenesis are regulated at the transcriptomic level by SREBPs (sterol regulatory-element binding proteins) which are indirectly controlled by mTORC1 through p70S6K and Lipin-1 phosphorylation (Cargnello *et al.*, 2015). There are many effectors of mTORC1 that are involved in the initiation and elongation steps of protein synthesis which include p70S6K, p70S6K substrates and 4EBP1 and these will be further expanded on in the next section.

1.3.4. Protein synthesis

Protein biogenesis is one of the most energy consuming processes of the cell and thus requires careful regulation to ensure appropriate use of the process (Nandagopal and Roux, 2015). The canonical method of protein synthesis is cap-dependent (CDPS) of which the initiation is summarised below and illustrated in Figure 1.5. The ribosome is recruited onto the mRNA, via the m^7G-cap at the 5' terminus of mRNA, involving a concerted effort from a number of eukaryotic initiation factors (eIFs). The mRNA is first bound by the heterotrimeric eIF4F complex which is comprised of the eIF4G scaffolding protein, the eIF4E mRNA cap-binding protein and eIF4A, which is a DEAD-box RNA helicase. The mRNA cap is recognised and bound by eIF4E complexed with eIF4G (von der Haar et al., 2000; Youtani et al., 2000), which is dependent on the ratio of active 4EBP1 and eIF4E. 4EBP1 inhibits eIF4F assembly by binding and sequestration of eIF4E (Gingras et al., 2001; Nandagopal and Roux, 2015). The eIF4F complex then interacts with the 43S pre-initiation complex (PIC) in order to recruit the 40S ribosomal subunit preloaded with initiator methionyl tRNA (Met-$tRNA_i$; Gingras et al., 2001; Klann et al., 2004). The PIC is comprised of 40S ribsosomal subunit and several initiation factors, eIF2-ternary complex (eIF2-TC), eIF3 (for 40S subunit binding to PIC), eIF1 (to inhibit eIF2-

GTP hydrolysis), and eIF1A (for 40S and eIF2-TC binding). When eIF2 is phosphorylated on S51, it is fully capable of forming an initiation-competent eIF2-TC, which is a complex of eIF2 with GTP and Met-tRNA$_i$ (Jackson *et al.*, 2010). Subsequently, the helicase of the eIF4F complex, eIF4A, can unwind secondary structures within the 5'-UTR of the mRNA and allow the 43S complex to scan the 5'UTR (5' untranslated region) in the 5' to 3' direction to the AUG start codon. eIF1 dissociates from the initiation complex once the start codon has been recognised and thus the removal of inhibition on the hydrolysis of eIF2-bound GTP, mediated by eIF5. eIF5B facilitates the dissociation of eIF1, eIF1A, eIF3 and eIF2–GDP (Jackson *et al.*, 2010) and the recruitment of the 60S ribosomal subunit, to form a translation-competent 80S ribosome that can begin polypeptide chain synthesis, termed translation elongation (Gingras et al., 2001; Nandagopal and Roux, 2015).

Following translation initiation, the anticodon of Met-tRNA$_i$, based-paired with the start codon is in the middle P (peptidyl) site of the 80S ribosome. The appropriate complimentary aminoacyl-tRNA for the second codon of the open reading frame is delivered to the A (acceptor) site of the ribosome, by the eukaryotic elongation factor eEF1A, in a GTP-dependent manner. Codon recognition by the tRNA triggers GTP hydrolysis by eEF1A, releasing the factor and enabling the aminoacyl-tRNA to be accommodated into the A site. eEF1A-GDP is recycled to eEF1A-GTP by the exchange factor eEF1B. Peptide bond forms between the two amino acids in the peptidyl transferase centre of the ribosome during the translocation of tRNAs from the P and A sites to E and P sites respectively, which is facilitated by the binding and hydrolysis of GTP bound eEF2. The Met-tRNAi is released from the E site and the cycle of elongation continues with the binding of the next appropriate eEF1A-GTP-aminoacyl-tRNA to the A site, until the recognition of a stop codon. At this point, the eRF1-eRF3-GTP ternary complex binds to the A site, GTP is hydrolysed and eRF3 is released. eRF1 promotes peptide release from the ribosome (Dever and Green, 2012).

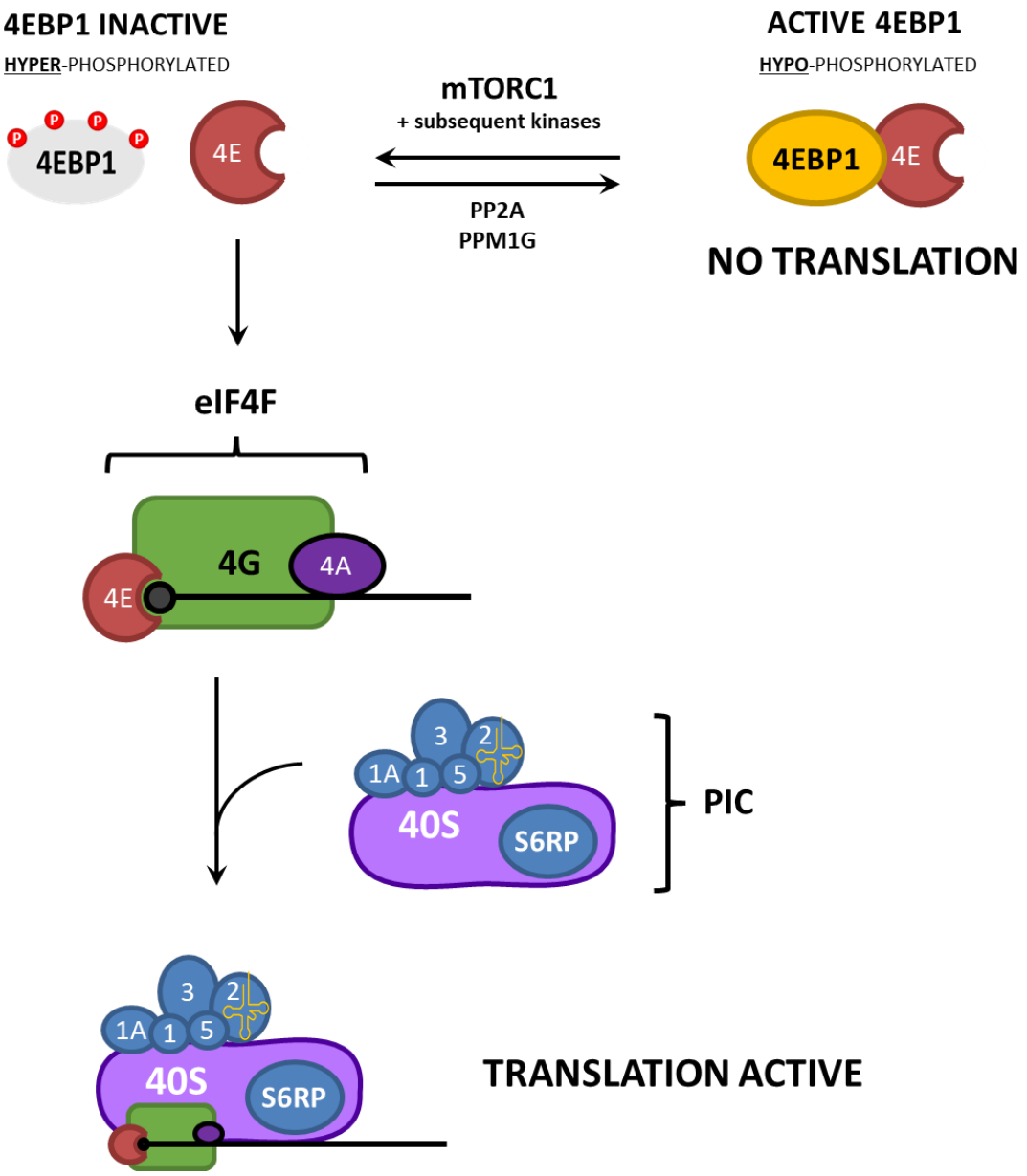

Figure 1.5 – Cap-dependent protein synthesis initiation.
When 4EBP1 is hypophosphorylated (yellow), it can bind to and sequester the mRNA cap-binding protein, eIF4E (4E). 4EBP1 becomes inactivated (grey) through phosphorylation of several residues and cannot bind with eIF4E. eIF4E brings the mRNA to the scaffold protein eIF4G (4G), and with eIF4A (4A) form the eIF4F initiation complex. This allows subsequent recruitment of the pre-initiation complex (PIC) for ribosomal docking. S6RP is bound to the 40S ribosomal subunit. 1 = eIF1; 1A = eIF1A; 2 = eIF2; 3 = eIF3; 5 = eIF5; 40S = 40S ribosomal subunit; P = phosphorylated residues; tRNA (yellow on eIF2). Black line with black and grey circle represents mRNA transcript with m^7G cap. Illustration based upon information from Ren-Jang, (2010).

A method of cap-independent protein synthesis (CIPS) uses internal ribosome entry sites (IRESs). These unique RNA structures recruit ribosomes independently of the mRNA m^7G-cap. IRESs require only a limited set of eIFs and therefore are commonly associated with viral protein production in an infected cell to overcome the high

complexity of CDPS initiation. The existence of cellular IRESs was also proposed as a means to maintain synthesis of selective proteins during times of low eIF4G availability, such as during stress and low nutrient availability. However, since 2004 these have been seriously challenged with the development of more stringent controls for IRES validation, and as a result, a controversy exists over cellular IRESs as means of protein synthesis (Jackson, 2013; Johnson *et al.*, 2017).

The PAM pathway feeds into CDPS via the two mTORC1 substrates, p70S6K and 4EBP1 and will be discussed in the following sections.

1.3.4.1. p70S6K

p70S6K is an AGC kinase family member, and as such requires phosphorylation at the activation loop (T229) by PDK1, and sequential phosphorylation of the hydrophobic motif (T389 by mTORC1), which are both are required to fully activate p70S6K.

p70S6K plays a role in protein synthesis initiation and elongation. At translation initiation, p70S6K phosphorylation is involved in the activation of the eIF4A helicase through phosphorylation (S67) and degradation of its negative regulator, PDCD4 and phosphorylation of its activator eIF4B at S422 (Dorrello *et al.*, 2006; Cargnello *et al.*, 2015). Translation elongation is regulated by the negative p70S6K phosphorylation S366 of eukaryotic elongation factor 2 (eEF2) kinase (Wang *et al.*, 2001), which phosphorylates eEF2 at T56, inhibiting it from shifting the nascent peptide between ribosomal sites A to P (Showkat *et al.*, 2014; Cargnello *et al.*, 2015; Thoreen, 2017). As well as protein synthesis, other substrates of p70S6K are also involved in cell survival (BAD1, HDM2), cytoskeletal rearrangements (Neurabin, Rac), proliferation (hnRNP), mRNA splicing (SKAR) and feedback regulation (IRS1, RICTOR and mTOR; Fenton and Gout, 2011).

S6RP is also key substrate of p70S6K, and its phosphorylation has been typically used as a readout of p70S6K activity. S6RP can be phosphorylated on the C-terminus at S235, S236, S240, S244 and S247. All residues can be phosphorylated by p70S6K, however phosphorylation of S235/6 is also directly regulated by a number

of kinases including, p90RSK, PKA, CDK1 and CDK4. S6RP is dephosphorylated by PP1 (protein phosphatase 1; Meyuhas, 2015). Interestingly, although S6RP has been associated with the 40S ribosomal subunit (Hutchinson *et al.*, 2011), its role in protein synthesis has yet to be elucidated. It was previously proposed to be involved in the translation of 5' terminal oligopyrimidine (TOP) mRNAs, however this was later proven to not be the case (Tang *et al.*, 2001). Mice knockout studies have suggested that S6RP may instead be associated with cell proliferation and cell size (Meyuhas, 2015).

1.3.4.2. 4EBP1

The eIF4F complex formation is highly dependent on the availability of eIF4E. This is further regulated by eIF4E-binding proteins (4EBPs), which sequester eIF4E. There are three isoforms: 4EBP1, 4EBP2 and 4EBP3. When 4EBP1 is hypophosphorylated, it strongly binds with eIF4E and inhibits its binding with eIF4G (Gingras *et al.*, 2001; Nandagopal and Roux, 2015).

4EBP1 and eIF4G compete for binding of the same site of eIF4E as both proteins contain a canonical eIF4E-binding motif (CM). 4EBP1 has a greater affinity for eIF4E due to the additional binding of a second less conserved non-canonical motif (NCM) to eIF4E. The NCM increases the affinity of 4EBPs to eIF4E by 1000-fold, allowing for displacement of eIF4G and inhibiting CDPS (Igreja *et al.*, 2014; Peter *et al.*, 2015).

When 4EBP1 is hyperphosphorylated, it becomes inactive and unable to bind eIF4E, thus allowing formation of the eIF4F complex (Gingras *et al.*, 2001; Nandagopal and Roux, 2015). As shown in Figure 1.6, 4EBP1 can phosphorylated on seven residues: T37, T46, S65, T70, S83, S101 and S112 (Gingras *et al.,* 2001; Martineau *et al.,* 2013; Musa et al., 2016; Qin et al., 2016). These residues are phosphorylated in a hierarchical order, with T37 and T46 phosphorylated by mTORC1, which are priming sites for sequential phosphorylation of T70 and S65 (Gingras *et al.*, 2001; Nandagopal and Roux, 2015; Qin *et al.*, 2016). Phosphorylation of S65 and T70 reduces the affinity of 4EBP1 for eIF4E. Additional studies have shown that phosphorylation of S101 is necessary for S65 phosphorylation, and that S112

phosphorylation directly affects eIF4E binding independently of other residues or mTORC1 activity due to phosphorylation by ATM (Wang *et al.*, 2003). Phosphorylation at S83 has no effect on CDPS (Martineau *et al.*, 2013). Alongside mTOR, other less studied 4EBP1 kinases include GSK-3β, p38MAPK, ERK, ATM, CDK1 and CDK4. These kinases however tend to target subsequent phosphorylation sites after T37 and T46 priming sites and may be mTOR dependent or independent and are also dependent on cell-type. PP2A and PPM1G are phosphatases known to target 4EBP1 (Gingras *et al.*, 2001; Roux and Topisirovic, 2018).

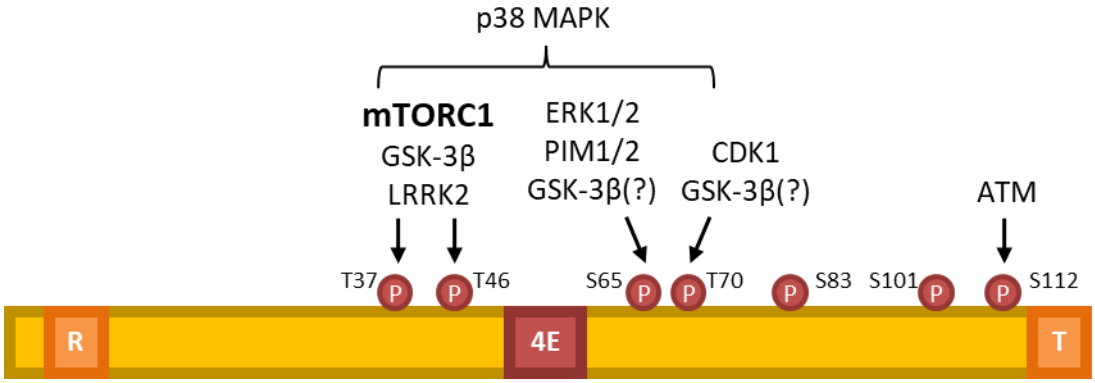

Figure 1.6 – 4EBP1 structure and phosphorylation residues.
Protein structure and currently known phosphorylation sites of 4E-BP1. 4E-BP1 (yellow) contains three functional domains: an N-terminal RAIP mTORC1 binding motif (R), the eIF4E- binding domain (4E) and a C-terminal TOS mTORC1 binding motif (T). Phosphorylated residues are represented as dark red (P)s, with amino residue defined – threonine = T, serine = S. Black arrows indicate phosphorylation of residue by kinases indicated. Brackets indicate phosphorylation of multiple sites. (?) = Possible kinase. Model based upon information from Gingras et al., (2001), Martineau et al., (2013), Musa et al., (2016) and Qin et al., (2016).

1.3.4.3. Regulation of specific mRNAs

The protein synthesis machinery can select for the translation of certain mRNAs including eIF4E-sensitive and 5'TOP mRNAs.

Several mRNA transcripts can also contain long and structured 5'UTRs. These are highly dependent on eIF4A helicase activity in unwinding the structure in order to allow for effective ribosomal scanning. As eIF4A activity is dependent on eIF4E availability for assembling the eIF4F complex, these mRNAs are termed, eIF4E-sensitive. This regulation is commonly found on mRNA transcripts encoding for oncogenes such as growth factors and cytokines (FGF-2, PDGF, TGF-β, VEGF, IL-15),

protein kinases (MOS, PIM-1), transcription factors (MYC, FOS), polyamine biosynthesis (ODC, OAT) and regulators of the cell cycle (Cyclin D1, Ras, CDK4; Polunovsky and Bitterman, 2002; Nandagopal and Roux, 2015; Qin *et al*., 2016).

5'TOP (5'terminal oligopyrimidine) mRNAs are another subset of mRNAs, which contain a cis-regulatory RNA element immediately downstream of the mRNA cap. Although translation of these mRNAs was highlighted to be S6RP independent (section 1.3.4.2), it was shown to be highly dependent on mTORC1 activity (Cargnello *et al.*, 2015). Studies into this identified the mTORC1 substrate, LARP1 as a negative regulator of 5'TOP mRNA translation (Tcherkezian *et al.,* 2014). Previous studies have determined that LARP1 associates with RAPTOR when mTORC1 is active and dissociates when mTORC1 is inactive. Crystal structures showed that LARP1 binds to the 5'TOP motif and the m^7G-cap of TOP mRNAs via the DM15 region in the C-terminus of the protein and prevents eIF4E-dependent translation of these mRNAs (Lahr *et al.*, 2017). These mRNAs encode for components of the protein synthesis pathway and therefore, due to regulation by mTORC1, ribosome biogenesis and protein synthesis is heavily controlled by nutrient availability and growth factors (Cargnello *et al.*, 2015).

1.3.5. Negative feedback of the PAM pathway

The activity of the PAM pathway is finely tuned using several negative feedback loops. IRS1 is a signalling adapter protein that binds to RTKs, that is commonly targeted by negative feedback loops (Figure 1.7). It is phosphorylated by p70S6K at S270, which inhibits recruitment to RTKs and reduces protein stability. p70S6K has also been shown to negatively regulate IRS1 gene expression (Harrington *et al.*, 2004; O'Reilly *et al.*, 2006). RAPTOR has also been previously shown to bind IRS1 to promote mTORC1 phosphorylation of S636 and S639 (Tzatsos and Kandror, 2006). Secondly, mTORC1 also directly activates and stabilises GRB10 (growth factor receptor-bound protein 10). Grb10 interacts with IRS2 to target it for ubiquitination and degradation. Lastly, phosphorylation at T86 and T389 of mSIN1 by p70S6K

causes it to dissociate from mTORC2, inhibiting the signalling of the complex (Harrington *et al.*, 2005; Laplante and Sabatini, 2012; Martelli *et al.*, 2018).

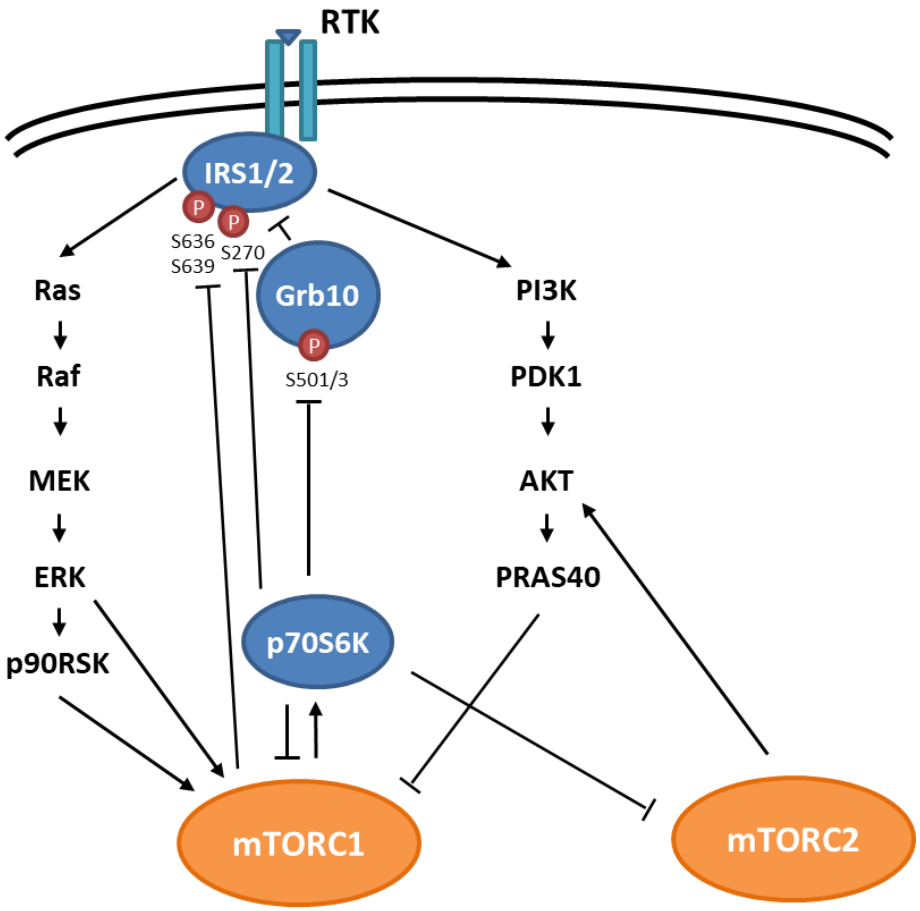

Figure 1.7 – Negative feedback loops of PAM pathway.
Black arrows and block-headed arrows indicate phosphorylation of target induces activation or inhibition respectively. Adapted from Pearce et al., (2010) and Martelli et al., (2018).

1.3.6. MAPK and PAM pathway crosstalk

Alongside the PAM pathway, the Ras/MEK/ERK (MAPK) cascade is also involved in the intracellular signal transduction to promote fundamental cellular processes such as cell growth and survival. Therefore, it is unsurprising that there are several nodes of crosstalk between MAPK and PAM pathways (Mendoza *et al.*, 2011).

Due to their promiscuity, ERK and p90RSK are the main nodes of crosstalk feeding from the MAPK pathway. As outlined in Section 1.3.3.2, ERK and its substrate p90RSK can directly phosphorylate TSC2 (Mendoza *et al.*, 2011; Aksamitiene *et al.*, 2012). Additionally ERK and p90RSK also phosphorylate S8, S696 and S863 of

RAPTOR (Carrière *et al.*, 2008; Carriere *et al.*, 2011). These all act to increase mTORC1 activity. ERK also phosphorylates MNK1 (MAPK-interacting kinases) which in turn targets S209 on eIF4E to increase its activity in CDPS (Siddiqui and Sonenberg, 2015; Brown and Gromeier, 2017). Additionally, the high kinase domain homology between p90RSK and p70S6K results in the sharing of several substrates including S235/6 of S6RP, eIF4B and eEF2K (Pearce *et al.*, 2010).

1.4. The PAM pathway in cancer

Considering the number of outputs of the PAM pathway that contribute towards the progression and hallmarks of oncogenesis, it is unsurprising that mutations within this pathway are common in many tumours. For example, mutations in *PIK3CA* have been reported to be present in 15% of tumours across all tumour types and whole-exome sequencing of 21 tumour types identified it as the second most frequently mutated gene, followed by PTEN mutations (Yap *et al.*, 2008; Lawrence *et al.*, 2014). Alterations of PAM genes can occur at multiple levels including amplification of oncogenes, deletion of tumour suppressor genes or mutations which may affect protein function. Alterations of PAM components are outlined below and summarised in Table 1.1.

1.4.1. RTKs in cancer

As outlined in Section 1.3, activation of RTKs stimulates growth factor signalling cascades, such as the PAM pathway. Therefore hyperactivation of these receptors can lead to dysregulated signalling to the PAM pathway (Rodon *et al.*, 2013). These can be observed through receptor gene amplification, receptor gene activating mutations or ligand gene amplification (Yap *et al.*, 2008). Gene amplification leads to increased protein expression on the cell plasma membrane and increased activation and signalling downstream. An example of this is ERBB2 that encodes for the HER2 receptor, which is commonly overexpressed in breast, ovarian and endometrial carcinomas (van Dam *et al.*, 1994; Livasy *et al.*, 2006; Yap *et al.*, 2008).

Missense mutations in exons 18-21, encoding the tyrosine kinase domain of EGFR are commonly found in non-small-cell lung cancer (NSCLC) and are associated with increased sensitivity to EGFR inhibitors (Douglas *et al.*, 2006; Metzger *et al.*, 2011). Additionally, the EGFRvIII mutation that causes truncation of the receptor and constitutive activation of intracellular domains is found in gliomas (Li *et al.*, 2004). Elevated circulation of IGF-1 and IGF-2, and reduction in their regulative binding partners have also been associated with breast and prostate cancers (Arcaro, 2013).

1.4.2. PI3K in cancer

As outlined in Section 1.3, signalling from RTKs to the PAM pathway generally occurs via class IA isoforms of PI3K. These kinases phosphorylate PIP_2 to PIP_3 to allow recruitment of AKT to the plasma membrane, therefore activating mutations of PI3K has been associated with increased PAM signalling in cancer (Fruman *et al.*, 2017). Alterations in both the catalytic and regulatory subunits of PI3K have been implicated in many tumours. Amplification of the *PIK3CA* gene which encodes for the p110α catalytic subunit has been associated with increased PI3K activity (Regad, 2015). Missense mutations in the helical domain such as E542K and E545K induce resistance of p110α to the inhibitory action of p85 and or increase interaction with IRS1, respectively (Hollestelle *et al.*, 2007; Thorpe *et al.*, 2015). Kinase domain mutations such as H1047R increase the interaction of p110α with its substrates. Additionally, other *PIK3CA* mutations have been shown to induce conformational changes that mimic those that occur during activation of PI3K, therefore resulting in a constitutively active kinase. Mutations in other class IA catalytic isoforms are rare, and alterations in cancer are usually through gene amplification (Thorpe *et al.*, 2015).

Mutations in *PIK3R1* gene which encodes for p85 have also been associated with many cancers. Many of these are substitutions or in-frame insertions or deletions which disrupt the ability of the SH2 domain to inhibit p110 isoforms (Thorpe *et al.*, 2015).

1.4.3. PTEN in cancer

PTEN reverses the function of PI3K, dephosphorylating PIP_3 to PIP_2 and acts as a tumour suppressor by negatively regulating the activity of AKT. Mutations in *PTEN* form the third most common mutation in cancer after *TP53* and *PIK3CA* (Lawrence *et al.*, 2014). Mutations in *PTEN* can include insertions, substitutions, deletions and epigenetic alterations which lead to loss of protein function (Regad, 2015; Thorpe *et al.*, 2015). Interestingly, loss or inactivation of one *PTEN* allele is sufficient for carcinogenesis (Haddadi *et al.*, 2018).

Additionally, micro RNAs mIR-21 and mIR-22, which both suppress PTEN by directly binding to its 3' UTR, are commonly upregulated in many tumours (Revathidevi and Munirajan, 2019)

1.4.4. AKT in cancer

AKT is the pivotal node of the PAM pathway, phosphorylating over 100 substrates contributing positively to oncogenesis, including substrates involved in metabolism, protein synthesis and cell survival (Fruman *et al.*, 2017). AKT itself is hyperactivated in a third of tumours, but these are more commonly due to alterations of AKT regulators, leading to increased activating phosphorylation, rather than dysregulating the protein itself. However several alterations of AKT itself have been identified in cancer, including overexpression, activating mutations and post-translational modifications (Rodon *et al.*, 2013; Revathidevi and Munirajan, 2019).

Gene amplification and protein overexpression of all three isoforms of AKT have been associated with many cancers including gastric, neck, pancreatic and breast cancers. Gene amplification of *AKT1* is the most common alteration of AKT (Regad, 2015).

Table 1.1 – Summary of molecular alterations in PAM pathway in cancer.
Based upon information from Yap et al., (2008); Rodon et al., (2013); Thorpe et al., (2015); Revathidevi and Munirajan, (2019); Bhat et al., (2015); *proteinatlas.org*; Leprivier *et al.*, (2013); Ng *et al.*, (2019). HNSCC = head and neck squamous cell carcinoma; NHL = non-Hodgkin's lymphoma; NSCLC = non-small cell lung cancer ; SCLC = small cell lung cancer.

Gene	Protein	Alteration	Tumour Type (% prevalence)
EGFR	EGFR1	Amplification	gliosarcoma (8%), ovarian (12%), endometrial carcinosarcoma (82%)
		Mutation	prostate (35%)
ErbB2	HER2	Amplification	ovarian (24%), endometrial carcinosarcoma (20%),
PDFGRA	PDGFRα	Amplification	gliosarcoma (3%)
PIK3CA	p110α	Amplification	HNSCC (9.1-100%), gastric (36.4%), colon (12%) breast (8.7-13.4%), cervical (9.1-76.4%), ovarian (13.3-39.8%), thyroid (30%), lung (9.5-69.6%)
		Mutation	breast (7.1-35.5%), endometrial (26%), colon (12%), colorectal (16.9-30.6%), glioblastoma (4.3-11.0%), lung (0.6-20.0%), oesophageal (5.5%), renal (1.0-2.9%), ovarian (33%)
PIK3R1	p85α, p55α, p50α	Mutation	glioblastoma (7.6-11.3%), colon (1.7%), ovarian (3.8%)
		Deletion	ovarian (22%)
PTEN	PTEN	Mutation	breast (5%), glioblastoma (30%), prostate (10%) endometrial (50%), colorectal (7%), liver (27%), cervical (16%), melanoma (17%)
		Deletion	glioblastoma (75%), colon (20%), breast (40-50%), lung (37%), prostate (42%), gastric (47%), thyroid (6.1%), NHL (3.7%), melanoma (26%)
AKT1	AKT1	Amplification	gastric (20%), breast (1%)
		Mutation	colon (1%), breast (4%), ovarian (1%)
AKT2/ AKT3	AKT2/ AKT3	Mutation/ Amplification	colon (1%), pancreatic (20%), ovarian (14%), breast (3-9.9%), melanoma (1.5%)
EIF4E	eIF4E	Overexpression/ Phosphorylation	breast (100%), HNSCC (100%), liver (70%), gastric (100%) breast, colon, gastric, and lung (63.4%)
EIF4EBP1	4EBP1	Overexpression	lung (40%), gastric (50%), colorectal (91%)
		Loss	pancreatic (50%)
EEF2K	EEF2K	Underexpression	colorectal (85%)
		Overexpression	breast (N/A), glioblastoma (N/A), medulloblastoma (N/A), liver (33%), colorectal (63%), prostate (27%)

A common somatic mutation of *AKT1* is E17K, located in the PH domain. This mutation enhances PIP_3 binding and ubiquitination of the PH domain which leads to constitutive localisation at the plasma membrane and phosphorylation at T308 by PH-domain containing PDK1 (Revathidevi and Munirajan, 2019). This mutation has also been reported in *AKT3*. Similar mutations which increase AKT membrane localisation include E49K, L52R, C77F, and Q79K (Regad, 2015; Revathidevi and Munirajan, 2019).

Altered methylation of genes of AKT regulators such as PHLPP2 and mTORC2 have shown to alter their expression towards activation of AKT and promote proliferation and tumorigenicity of endometrial cancer cells (Revathidevi and Munirajan, 2019). Many methods of post-translational modification of AKT have also been observed in cancers. Ubiquitination of the PH domain is an important mechanism for AKT hyperactivation which increases the translocation of AKT to the plasma membrane (Revathidevi and Munirajan, 2019).

1.4.5. mTOR in cancer

Similarly to AKT, mTORC1 and other components of the PAM pathway are not as frequently directly altered as PI3K and PTEN. However, 80% of tumours from one study showed aberrant mTORC1 hyperactivity (Menon and Manning, 2008; Jhanwar-Uniyal *et al.*, 2017), which result from dysregulated upstream growth factor signalling from the PAM as discussed above and aberrations from the MAPK pathway. Additionally, hyperactivity of mTORC1 can be affected by dysregulation of TSC activity through *LKB1* mutations (Agarwal *et al*., 2016). Additionally, alterations in components of nutrient sensing can dysregulate mTORC1 activity. All three subunits of the GATOR1 complex and RagC have been reported to harbour mutations in glioblastoma and follicular lymphoma respectively, and affect mTORC1 activity (Saxton and Sabatini, 2017).

Mutations in mTOR have also been reported. Two missense gain of function mutations were identified in mTOR in the C643 cell line and melanoma tumours. The H419R mutation is located at a linker region of the HEAT repeat domain, and

G2359E is located in the activation loop of the catalytic domain. These were associated with increased mTORC1 downstream signalling to p70S6K and 4EBP1 (Murugan *et al.*, 2019).

1.4.6. PAM-mediated protein synthesis in cancer

Hyperactivation of mTORC1 through the mutations described in previous sections will ultimately increase phosphorylation of substrates such as p70S6K and 4EBP1 to promote protein synthesis, however alterations in both proteins have been directly associated with oncogenesis as well.

Both p70S6K1 and p70S6K2 have been shown to be overexpressed in several cancers. Accumulation, particularly of p70S6K2 in tumour cell nuclei has also been observed and associated with cell growth and proliferation, likely through histone phosphorylation and gene expression of anti-apoptotic proteins such as BCL-xL and XIAP (Tavares *et al.*, 2015).

4EBP1 expression is severely reduced in over 50% of human pancreatic ductal adenocarcinomas, as well as many other tumours (Martineau *et al.*, 2013). Expression of 4EBP1 may be regulated by SMAD4, ATF4 and HIF-1α. This reduces its tumour suppressive activity on eIF4E, thereby increasing CDPS. However, 4EBP1 may not be considered a tumour suppressor gene on its own as 4EBP1-knockout mice did not develop tumours (Musa *et al.*, 2016). Phosphorylation of 4EBP1 (p4EBP1) is also shown to be increased in several tumours including colorectal, breast, lung and prostate carcinoma (Mi *et al.*, 2015; Nogami *et al.*, 2015; Musa *et al.*, 2016). However, the role of p4EBP1 in carcinogenesis highly depends on its ratio to 4EBP1 expression, as p4EBP1 may be increased due to increased 4EBP1 expression and may have no difference on the outcome with eIF4E (Alain *et al.*, 2012). Additionally, the stoichiometry of eIF4E/4EBP is also important for oncogenesis. An increased ratio has been previously associated with increased risk for head and neck cancer relapse (Musa *et al.*, 2016).

Paradoxically, the gene encoding 4EBP1, *EIF4EBP1* has also been observed in several studies to be amplified in tumours including breast and prostate cancer (Hsieh *et*

al., 2015; Rutkovsky *et al.*, 2019). 4EBP1 was suggested to play a role in a hypoxia-induced switch from cap-dependent to cellular IRES-mediated translation of selective mRNAs, such as proangiogenic factors, HIF-1α and VEGF. Decreased 4EBP1 was shown to reduce vascular density of xenografts and render tumours more sensitive to metabolic and genotoxic stresses. However, increasing research into the validity of cellular IRESs as discussed in Section 1.3.4 may put this hypothesis into question (Qin *et al.*, 2016).

Overexpression of eIF4E is increased in several kinds of tumours such as colon cancer. As explained in Section 1.3.4.2, this overexpression increases the formation of eIF4F complexes, enhancing the translation of selective eIF4E sensitive mRNAs which encode for oncogenes such as cyclin D1 and c-myc (Averous and Proud, 2006; Nina Ilic *et al.*, 2011; Cope *et al.*, 2014).

Along the p70S6K arm of mTORC1 signalling, eEF2K has been shown to be upregulated in cancers such as breast and glioblastoma, whereas in colorectal cancers eEF2K expression has been shown to be downregulated (Parmer *et al.*, 1999; Leprivier *et al.*, 2013; Ng *et al.*, 2019). Most studies into the role of eEF2K in cancer used xenograft and *in vitro* cell lines as models. For example, siRNA knockdown of eEFK2 or use of eEF2K inhibitors (TX-1718 and NH125) slowed the growth of breast cancer xenografts. In contrast, the intestinal crypt regeneration of APC deficient mouse models was reduced in association with eEF2K deletion. In summary, is unclear as to the cytoprotective or cytotoxic effect of eEF2K in tumours (Liu and Proud, 2016; X. Wang *et al.*, 2017).

1.4.7. PAM pathway in ovarian cancer

Ovarian cancer (OC) is the third most common gynaecological cancer worldwide with nearly 300,000 new diagnoses and an estimated 185,000 deaths in 2018 (GLOBOCAN., 2018). Due to the nature of symptoms presenting like common gastrointestinal or less lethal gynaecological issues, patients are commonly diagnosed at an advanced stage of the disease. 55-58% of patients are diagnosed at stage III or IV, where the tumour has spread to the abdomen or beyond the

peritoneal cavity (Cancer Research UK, 2017). Epithelial ovarian cancer makes up 90% of ovarian cancer diagnoses, which is heterogeneous and can be subdivided into high-grade serous (HGSOC), low-grade serous (LGSOC), endometrioid, clear cell (OCCC) and mucinous subtypes, with each presenting different aetiologies, tumour progression, and therapeutic responses (Meinhold-Heerlein and Hauptmann, 2014).

The PAM pathway has been reported to be activated in approximately 70% of ovarian cancers (Bast *et al.*, 2009). Gain of function *PIK3CA* mutations occur in 30-40% of OCCC, 12-20% of endometrioid OC, and *PIK3R1* mutations occur in 3.8% of all OC (Gasparri *et al.*, 2017). As described above, other methods of PAM pathway hyperactivation have also been associated with up to 39% of OC, including AKT amplification and mutations and PTEN loss of function alterations (Gasparri *et al.*, 2017).

1.5. Targeting the PAM pathway

The PAM pathway is one of the most commonly activated signalling pathways in cancer. As these cancers may be solely reliant on pathway mutations, as understood by Weinstein's concept of oncogene addiction, and the potential for many targetable components of the PAM pathway, this provides an attractive novel strategy for the development of molecular targeted therapies (Yap *et al.*, 2008; Martini *et al.*, 2013). However despite such promise, the clinical results for PAM inhibitors have fallen short of expectation, such as limited improvement in overall survival (OS) and objective response rate (ORR) in a meta-analysis of trials in solid tumours (Fruman *et al.*, 2017; Li *et al.*, 2018). This is mainly a result of drug resistance resulting from the remarkable plasticity of the pathway through multiple RTK activation, feedback loops and cross-talk from other signalling pathways and dose-limiting toxicities preventing sufficient target engagement (Fruman *et al.*, 2017). However, the PAM pathway is an important mediator for resistance to EGFR inhibitors and cytotoxic therapies, therefore in addition to testing PAM inhibitors as monotherapies, trials have also been designed to test the efficacy for combinations with cytotoxic therapies such as paclitaxel (Yap *et al.*, 2008; Banerji, Emma J Dean, *et al.*, 2018).

Inhibitors of the PAM pathway can be classified into 4 main categories: PI3K inhibitors, mTOR inhibitors, dual mTOR/PI3K inhibitors and AKT inhibitors (Gasparri *et al.*, 2017). However, other PAM inhibitors also include p70S6K (LY2584702), PDK1 specific inhibitors (GSK2334470) and inhibitors of cap-dependent protein synthesis initiation (Rodon *et al.*, 2013; Castel and Scaltriti, 2017). A summary of these inhibitors and their targets is shown in Figure 1.8.

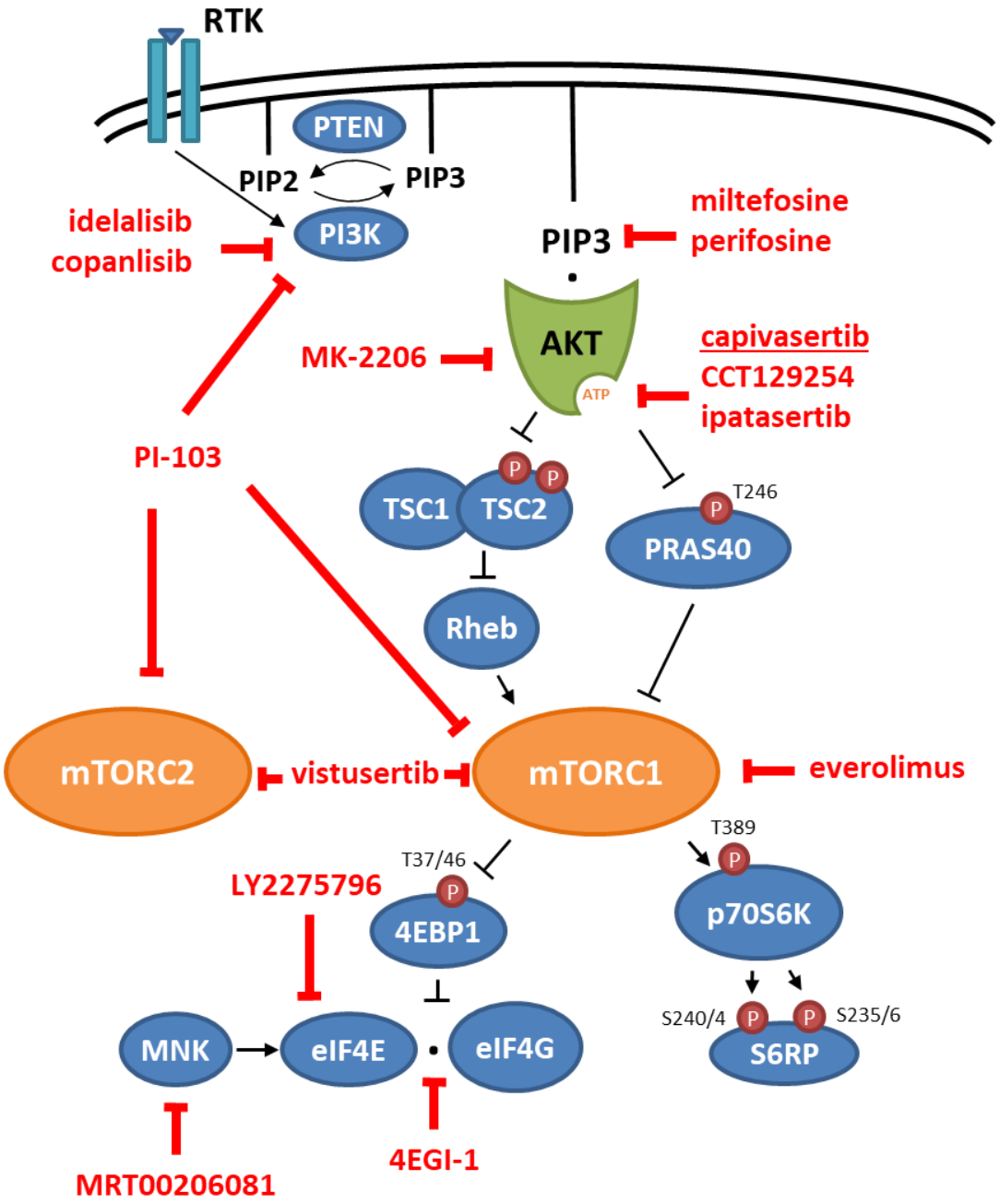

Figure 1.8 – Summary of drugs described in text and their targets.
Adapted from Martini et al., (2013); Lu et al., (2016); Nitulescu et al., (2016) and Teng et al., (2019)

1.5.1. PI3K inhibitors

As mutations in *PIK3CA* are common in cancer, the development of PI3K inhibitors is logical. The first group of PI3K inhibitors developed were pan-class I PI3K inhibitors including Wortmannin and LY2940002. These were useful tools in studying PI3K function, but poor pharmacokinetic and selectivity properties rendered their therapeutic use limited. More recently ATP-competitive pan-class I and isoform specific inhibitors have been developed with improved pharmacokinetic profiles, increased target specificity and minimized toxicity, however trials have reported unexpected autoimmune and infectious toxicities with these drugs (Martini *et al.*, 2013; Greenwell, 2017).

Idelalisib was the first FDA approved PI3K inhibitor. It is selective for the class I p110δ PI3K isoform and used for the treatment of relapsed chronic lymphocytic leukaemia, small lymphocytic lymphoma (SLL) and follicular lymphoma. The overall response rate as a single agent was 61% in SLL and 54% in FL (Greenwell *et al.,* 2017). Copanlisib, a pan-class I PI3K inhibitor has also been subsequently approved for relapsed follicular lymphoma. Phase III testing is currently undergoing for duvelisib (p110γ and p110δ selective) and pan-class I selective inhibitors, buparlisib and umbralisib (Greenwell *et al.,* 2017). Inhibitors including pan-class I selective, pictilisib (GDC-0941) and INCB050465 are undergoing Phase II and earlier testing (*clinicaltrials.gov*; Folkes *et al.*, 2008; Greenwell *et al.,* 2017). Interestingly, reports show that isoform-selective or pan-class I PI3K inhibitors are more effective in haematological tumours than solid tumours (Mundi *et al.*, 2016).

1.5.2. mTORC inhibitors

Rapalogues such as everolimus and temsirolimus were the first inhibitors of PAM pathway to be FDA approved for the treatment of renal cell carcinoma (RCC), neuroendocrine tumours and mantle-cell lymphoma (Schuler *et al.*, 1997; Rodon *et al.*, 2013). These are mTORC1-specific allosteric inhibitors and act by complexing with FKBP12 and binding to the FRB domain of mTOR, preventing substrate recruitment to the catalytic domain of mTOR by steric hinderance (Aylett *et al.*,

2016). The anti-tumour efficacy of these compounds beyond use in RCC was limited due to inherent resistance arising from p70S6K-dependent negative feedback to PAM and MAPK pathways via IRS1/2, and an incomplete suppression of 4EBP1 phosphorylation (Martelli *et al.*, 2018; Teng *et al.*, 2019).

Dual PI3K/mTOR inhibitors were developed to overcome the limitations of rapalogues by targeting three points of the PAM pathway, PI3K and the catalytic mTOR subunits in mTORC1 and mTORC2. This was possible due to the structural similarity of the kinase domains of both proteins as members of the PIKK family. PI-103 was the first compound in this class to be investigated and was more effective than rapalogues in glioblastoma or leukaemia cell line models, but due to its rapid *in vivo* metabolism, was never taken to clinical trials. Other members include dactolisib, voxtalisib, apitolisib and gedatolisib. However, contrary to expectations, clinical studies have revealed limited efficacy of this class of drugs as cancer therapeutics and commonly associated with severe adverse effects led to the reduction in the development of these drugs (Martelli *et al.*, 2018; Teng *et al.*, 2019).

To reduce the toxicity of dual PI3K/mTOR inhibitors, mTOR kinase (mTORK) only inhibitors were designed. PP242 was the initial prototype compound of this class, which blocked the phosphorylation of 4EBP1 and cap-dependent protein synthesis more effectively than rapamycin *in vitro* and *in vivo.* Many TORKIs have been subsequently developed including Torin 1, Torin 2 and vistusertib (AZD2014; Pike *et al.*, 2013; Martelli *et al.*, 2018). Interestingly, a phase II study in metastatic RCC showed vistusertib to perform worse than everolimus in progression free survival (PFS) and OS, with minimal improvement in adverse effects (Martelli *et al.*, 2018; Teng *et al.*, 2019).

The latest generation of mTOR inhibitors are RapaLinks, which simultaneously bind the ATP-binding pocket of mTOR and the FRB domain, acting like both a rapalogue and TORKI. RapaLink-1 was observed to reduce phosphorylation of S473 on AKT and T37/46 on 4EBP1 more efficiently than rapamycin and inhibits a more lasting mTOR kinase inhibition than mTORK inhibitors. These also showed strong anti-tumour

activity in mouse xenografts and are attractive compounds for future clinical trials (Martelli *et al.*, 2018; Teng *et al.*, 2019).

1.5.3. AKT inhibitors

AKT is one of the main effectors of PI3K that can promote oncogenesis through the phosphorylation and regulation of many substrates involved in cell growth and survival. Therefore, AKT poses an attractive target for oncotherapy.

There are two main categories of AKT inhibitor based upon their mechanism of inhibition: ATP-competitive and allosteric inhibitors. The development of AKT-specific and isoform-selective inhibitors was predicted to be difficult due to the high degree of homology in the ATP-binding pocket between AGC kinases, therefore allosteric AKT inhibitors are generally more AKT specific. This includes PH domain inhibitors as these domains can harbour 30% sequence homology (Morrow *et al.*, 2011; Rodon *et al.*, 2013). Additionally, there are other inhibitors such as irreversible AKT inhibitors (lactoquinomycin; Revathidevi and Munirajan, 2019). Currently, only one AKT inhibitor, the allosterically acting milefosine has been FDA-approved and is used as a topical treatment against parasites. It exhibited haemolytic toxicity with intravenous use and has therefore not been considered for cancer treatment. In recent years, development of new pan-AKT inhibitors has progressed with many in clinical trials. Isoform specific AKT inhibitors, A-674563 (AKT1) and CCT128930 (AKT2) are also in preclinical development (Mundi *et al.*, 2016; Revathidevi and Munirajan, 2019).

Allosteric AKT inhibitors bind to an alternative site from the kinase domain of AKT, in order to inhibit its activity. MK-2206 (Figure 1.9) is an allosteric AKT inhibitor which induces a conformational change in AKT so that the active site is no longer accessible by its substrates. MK-2206 has been shown to be potent and selective for AKT (AKT1 IC_{50} = 5 nM; AKT2 IC_{50} = 12 nM) and is currently in Phase II clinical trials as a single agent or in combinations such as with the MEK inhibitor selumetinib, and EGFR inhibitor erlotinib (Hirai *et al.*, 2010; Mundi *et al.*, 2016; *clinicaltrials.gov*). MK-2206 appeared to be tolerated well but failed to achieve satisfactory clinical

responses (Konopleva *et al.*, 2014; Do *et al.*, 2015). Alternative allosteric inhibitors target the PH domain of AKT thus preventing its recruitment and activation. Compounds such as the tricyclic purine nucleoside analogue, triciribine target the PH domain directly (Sampath *et al.*, 2013), whereas alkyl phospholipids (ALPs), such as miltefosine and perifosine, target indirectly through inference with PIP_2 and PIP_3 metabolism (structures in Figure 1.19; Richardson *et al.*, 2012). Perifosine is one of the few AKT inhibitors currently in Phase III clinical trials, in combination with capecitabine in colorectal tumours (Mundi *et al.*, 2016; Revathidevi and Munirajan, 2019).

ATP-competitive enzyme inhibitors act by competing with ATP to block the kinase domain of AKT and therefore inhibit their kinase activity. Although five broad classes of ATP-competitive AKT inhibitors have been developed, only a couple remain in clinical evaluation. This includes the thiophenecarboxamide derivatives, afuresertib (GSK2110183) and uprosertib (GSK2141795); and the pyrrolopyrimidines ipatasertib (GDC-0068) and capivasertib (AZD5363; Nitulescu *et al.*, 2016).

Afuresertib potently inhibits all AKT isoforms at nanomolar range and subnanomolar to AKT1 specifically (for structure see Figure 1.9). Afuresertib is most effective as a single agent against haematological malignancies, particularly multiple myeloma, and is currently in Phase II clinical trials (*clinicaltrials.gov*; Nitulescu *et al.*, 2016). Additionally, the effect of afuresertib in combination for example with bortezomib, ofatumumab or paclitaxel are also being investigated in haematological and solid tumours (*clinicaltrials.gov*). The drug was well-tolerated, with a relative low incidence and severity of hyperglycaemia which is likely due to the selectivity of afuresertib for AKT over other AGC kinases (Rodon *et al.*, 2013; Spencer *et al.*, 2014). Afuresertib also showed safe and promising clinical activity in a heavily pre-treated epithelial ovarian cancer in combination with carboplatin and paclitaxel (Blagden *et al.*, 2014)

Uprosertib is structurally similar to afuresertib (Figure 1.9), and unsurprisingly the potency for AKT inhibition and overall anti-tumour activity is also similar although uprosertib is more potent and exhibits greater off-target inhibition. It is currently in

Phase II clinical trials for several tumour types including cervical, melanoma, multiple myeloma, colon and breast cancers, either as a single agent or commonly in combination with the MEK inhibitor, trametinib, however several of the latter studies were terminated due to a lack of efficacy (*clinicaltrials.gov*; Nitulescu *et al.*, 2016).

Ipatasertib is an orally bioavailable inhibitor of all AKT isoforms, which also minimally targets other members of the AGC family (for structure see Figure 1.9; Lin *et al.*, 2013). Preclinical *in vitro* and xenograft studies have shown that the resultant AKT inhibition by ipatasertib decreases viability of cancer cell lines through decreased cell cycle progression (Lin *et al.*, 2013). It is another of the few AKT inhibitors currently in Phase III clinical trials as a combination therapy with several different cytotoxic therapies for metastatic prostate and breast cancers, and in Phase II for safety and efficacy as a monotherapy (*clinicaltrials.gov*; Nitulescu *et al.*, 2016).

1.5.3.1. Capivasertib

Capivasertib is an ATP-competitive AKT inhibitor and was developed as a result of a hit of a fragment-based drug discovery program as part of a collaboration between the Institute for Cancer Research (ICR) and Astex Pharmaceuticals (Rees *et al.*, 2004; Donald *et al.*, 2007; Akan, 2015). 300,000 low molecular weight compound fragments were screened *in silico* against the structure of AKT2 and hits were verified using crystallography with a PKA-AKT chimera and AKT2 kinase assay. Hits from the screen led to the development of pyrazoles such as AT7867 (precursor to AT13148) and pyrrolopyrimidines such as CCT128930 (precursor to capivasertib). CCT129254 was developed from CCT128930 from the addition of an amide linker to increase oral bioavailability and reduce plasma clearance, although this also reduced selectivity to AKT over PKA (McHardy *et al.*, 2010).

As shown in Table 1.2, CCT129254 is a potent inhibitor of AKT1, as well as other AKT isoforms and AGC kinases such as PKA, p70S6K, MSK1 (mitogen and stress activated protein kinase 1) and ROCK2 (Rho-associated coiled-coil kinase 2). CCT129254 was

subsequently licenced to and further developed by AstraZeneca, and the addition of an hydroxyethyl group at the amide linker lead to the discovery of capivasertib (AZD5363; Davies *et al.*, 2012; Addie *et al.*, 2013). As shown in Table 1.2, capivasertib is more selective for all AKT isoforms and p70S6K than CCT129254. Additionally, capivasertib exhibits reduced activity with the hERG ion channel which is involved in the electrical activity of the heart, thus reducing complications with later drug development (Addie *et al.*, 2013).

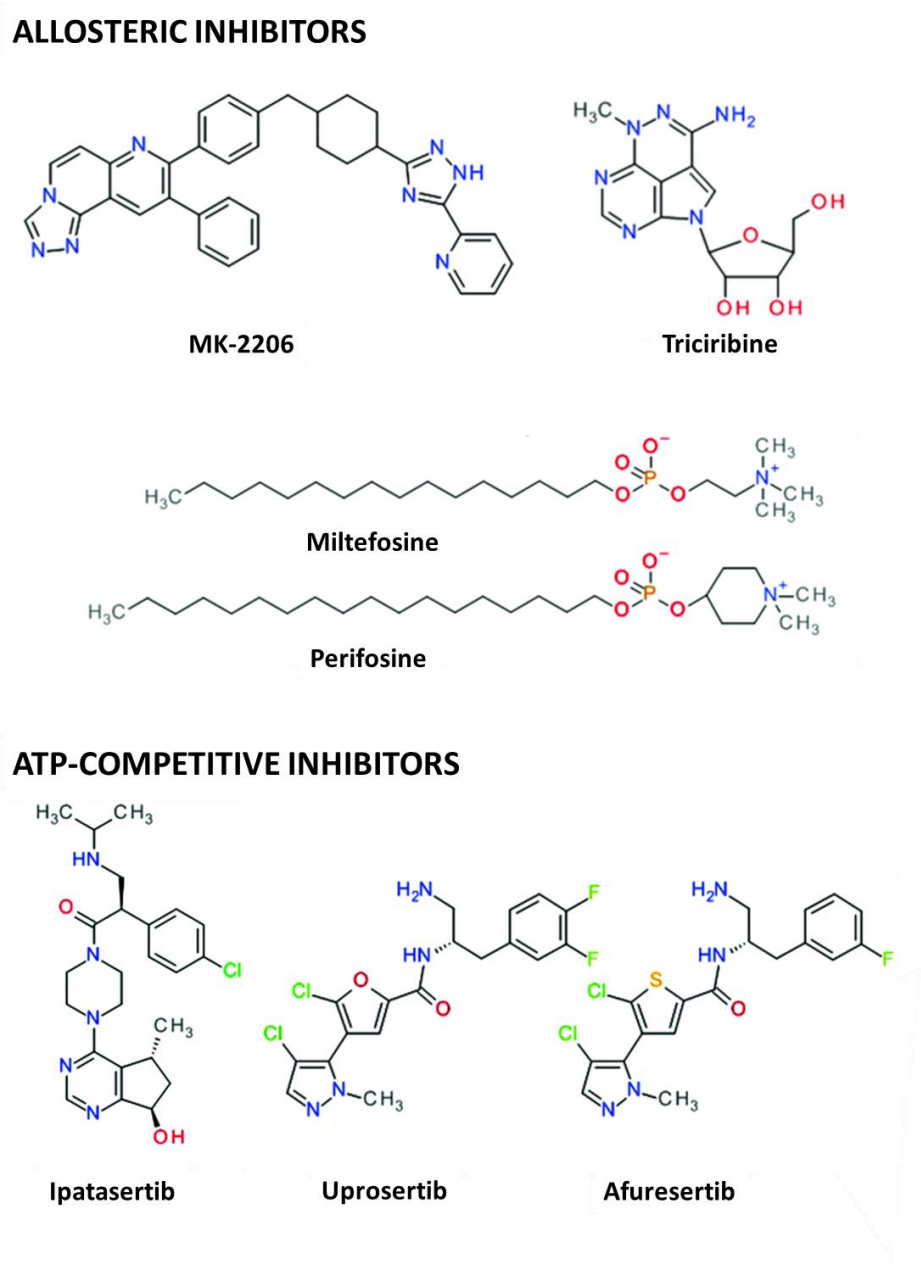

Figure 1.9 – Chemical structures of allosteric and ATP-competitive AKT inhibitors.
Adapted from Nitulescu et al., (2016).

Capivasertib targets the kinase pocket of AKT, and blood samples in trial patients have shown reduction in the phosphorylation of AKT substrates (such as GSK3β and PRAS40) as markers of target inhibition. Capivasertib showed good pharmacokinetic and pharmacodynamic properties in preclinical studies and also is well tolerated in trial patients; the most severe adverse effects being diarrhoea, hyperglycaemia, nausea, infection, neutropenia, rash and fatigue (Tamura *et al.*, 2016; Rinnerthaler *et al.*, 2018; Schmid *et al.*, 2018). Hyperglycaemia and the maculopapular rash are expected adverse effects of these drugs as the PAM pathway is important for regulating glucose metabolism and cytokine and chemokine regulation (Chia *et al.*, 2015). Cell lines and tumours with *PI3KCA* or *PTEN* mutations which increase PAM activity were found to be more sensitive to capivasertib (Davies *et al.*, 2012; Banerji *et al.*, 2018). As with many PAM inhibitors, clinical development of capivasertib is geared towards combinational strategies with cytotoxic therapies such as paclitaxel. The addition of capivasertib to paclitaxel in the PAKT Phase II trial in metastatic triple-negative breast cancer (TNBC) patients increased the PFS by 1.7 months and OS by 6.5 months. This amongst other successful trials prompted entry of capivasertib into Phase III trials in TNBC (*clinicaltrials.gov*; Rinnerthaler *et al.*, 2018; Schmid *et al.*, 2018). Capivasertib is also currently investigated in Phase I/II trials for prostate, gastric and gynaecological cancers as a mono- and combinational therapy (*clinicaltrials.gov*).

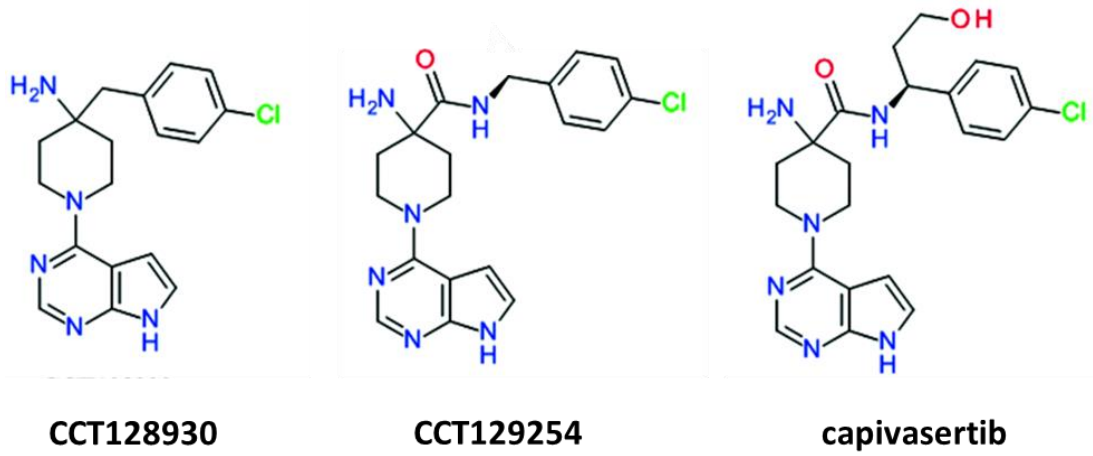

Figure 1.10 – Chemical structures of capivasertib and derivatives.
Adapted from Nitulescu et al., (2016).

Table 1.2 – Selectivity profile of CCT129254 and capivasertib.
Adapted from Davies et al. (2009) and Addie et al. (2013)

Kinase	IC_{50} (nM)	
	CCT129254	capivasertib
AKT1	13	3
AKT2	66	7
AKT3	57	7
p70S6K	18	6
PKA	30	7
MSK1	54	-
ROCK1	-	470
ROCK2	86	60
p90RSK1	136	-
CHK2	1271	-

1.5.3.2. AKT inhibitors and ovarian cancer

AKT inhibitors are introduced to patients in clinical trials, for the treatment OC that have commonly undergone alternative therapies and relapsed. As chemo-resistant cells are generally more aggressive than chemo-naïve cells (Donzelli *et al.*, 2014), this may suggest they may have greater genetic plasticity for development AKT inhibitor resistance (discussed further below). Table 1.X shows a summary of the response rates of AKT inhibitors in ovarian carcinomas in several clinical trials. Overall, AKT inhibitors appear to be effective in tumour regression of ovarian carcinomas, including those which are recurrent, with few adverse effects such as hyperglycaemia, rash, nausea and diarrhoea.

Table 1.3 – Response rates and main toxicities of completed AKT inhibitor clinical trials in ovarian cancer patients.
Based upon information from *clinicaltrials.gov*; Tamura *et al.*, (2016); Saura *et al.*, (2017); Banerji, *et al.*, (2018); Blagden *et al.*, (2019). ORR = overall response rate; PFS = progression free survival; RECIST = Response evaluation criteria in solid tumours; CA125 = Cancer Antigen 125 protein.

AKT inhibitor	Ovarian cancer	Response rates	Main toxicities
afuresertib (with carboplatin & paclitaxel)	recurrent, platinum sensitive, resistant or refractory epithelial ovarian cancer	ORR 52% (CA125) and 32% (RECIST). PFS 7.1 months	diarrhoea, nausea, fatigue, alopecia
ipatasertib	Ovarian carcinoma	Stable disease (no numerical data stated)	diarrhoea, nausea, asthenia, hyperglycaemia, decreased appetite, rash, vomiting
capivasertib	Ovarian Cancer	ORR 8% (RECIST)	Rash, diarrhoea, nausea, hyperglycaemia
capivasertib	Recurrent Ovarian Carcinoma	55.8% reduction in the sum of the longest diameter (1 OC patient in trial)	diarrhoea, hyperglycaemia, nausea, maculopapular rash

1.5.4. Inhibitors of PAM-mediated protein synthesis

As outlined in Section 1.3.4 and 1.4.6, PAM and MAPK growth factor signalling pathways converge onto CDPS, and there are multiple components of the eIF4F complex assembly process, thus providing many potential targets for therapy. Currently, the only FDA-approved CDPS inhibitors for oncotherapy are those that target CDPS indirectly, such as the PAM inhibitors described above. However, in the last 10 years, there has been great effort into development of novel CDPS inhibitors and therefore the eIF4E antisense oligonucleotide (ASO), LY2275796 is currently in Phase I clinical trials (*clinicaltrials.gov*). Other methods of targeting the eIF4F complex include, interfering with eIF4E-eIF4G interaction, suppressing phosphorylation of eIF4E and inhibiting eIF4A helicase activity (Bhat *et al.*, 2015; Lu *et al.*, 2016; Malka-Mahieu *et al.*, 2017).

Reducing eIF4E expression using ASOs such as LY2275796 (ISIS EIF4E Rx) showed promising activity in preclinical studies and was safely administered in Phase I trials. Currently in Phase II, more recent trials have shown no significant clinical response as a monotherapy. Combination Phase II trials are also underway (Pelletier *et al.*, 2015; Malka-Mahieu *et al.*, 2017). eIF4E dependent carcinogenesis relies on its cap-binding ability, therefore cap analogues such as ribavirin were developed. Phase II trials have shown anti-tumour activity in AML patients (Bhat *et al.*, 2015). Nucleotide analogues suffer from poor permeability and stability *in vivo*, but have been circumvented with pro-drugs such as 4Ei-1 (Bhat *et al.*, 2015; Lu *et al.*, 2016), which is effective in combination with gemcitabine in breast and lung cancer cell lines (Li *et al.*, 2013; Malka-Mahieu *et al.*, 2017).

Inhibitors of the eIF4E-eIF4G interaction act by mimicking 4EBP1 include 4EGI-1, 4E1RCat and 4E2RCat (Moerke *et al.*, 2007; Papadopoulos *et al.*, 2014; Sekiyama *et al.*, 2015). These have proved to reduce oncogenic phenotypes in breast cancer and lymphoma xenografts, multiple myeloma, Jurkat, A549 lung cancer cell lines and primary AML cells (Bhat *et al.*, 2015; Malka-Mahieu *et al.*, 2017). The highly oncogenic phosphorylation of S209 on eIF4E can be reduced by MNK inhibitors. Currently several MNK inhibitors are in preclinical development such as CGP052088, CGP57380, cercosporamide, eFT508 and MRT00206081 (Bhat *et al.*, 2015; Webster *et al.*, 2015; Lu *et al.*, 2016). Although these have shown some cytostatic properties in lung and leukemic cell lines alone, these drugs appear more promising as combination therapies to reduce resistance to drugs such as rapamycin, imatinib, gemcitabine and Herceptin (Bhat *et al.*, 2015; Lu *et al.*, 2016). Flavaglines (such as silvestrol), hippuristanol and pateamine A constitute the three classes of eIF4A inhibitors, which are all derived from natural products and display potent preclinical anti-tumour activity *in vivo* (Gupta *et al.*, 2011; Bhat *et al.*, 2015; Pelletier *et al.*, 2015; Malka-Mahieu *et al.*, 2017).

In addition to CDPS inhibitors, disabling cap-independent protein synthesis effectors of the PAM pathway, such as the eEF2K (section 1.3.4) through siRNA or via compound inhibition with NH125 was also shown to be effective to sensitise glioma cells to the pro-apoptotic stimulus, TRAIL. Use of NH125 has also proved effective in

enhancing the cytotoxic effects of MK-2206 by limiting autophagy. siRNA silencing of eEF2K also improved the pro-apoptotic effects of doxorubicin. Therefore, similar to the CDPS inhibitors described above, eEF2K inhibition may pose an attractive target for combination therapy in cancers (X. Wang *et al.*, 2017).

Regardless of the many ways to target the pathway, due to the genetic instability of tumours and the remarkable plasticity of the PAM pathway, drug resistance is a common occurrence in the development and clinical utility of the drugs described above (Fruman *et al.*, 2017). This will be elaborated in the next section.

1.6. Resistance to targeted therapies

Drug resistance is defined as the failure of cancer cells to respond to therapy, whether from the outset (intrinsic), or after an initial response to therapy (acquired; Holohan *et al.*, 2013). It remains as the biggest challenge to the clinical success of molecular-targeted therapies and is the main cause of death for patients with advanced cancer (Longley and Johnston, 2005; Konieczkowski, 2018).

The reliance of these therapies targeting the object of oncogenic addiction, allows for drug resistance to emerge through a combination of pathway plasticity, genetic instability of the tumour cells and presence of pre-existing resistant populations within a heterogenetic tumour (Fruman *et al.*, 2017; Konieczkowski *et al.*, 2018). Drug resistance in targeted therapies have been associated with drug efflux mechanisms involving increased expression of ABCB1 transporters, but the most common resistance mechanisms alter the oncogenic output of the targeted pathway (Konieczkowski *et al.*, 2018). These alterations converge into recognisable patterns to either exhibit 1) pathway reactivation; 2) pathway bypass or 3) pathway indifference. These are further explained below and summarised in Figure 1.11.

Pathway reactivation allows for re-engagement of the original pathway effectors by which the tumour relied for oncogenesis and may represent the most common resistance principle. Reactivation of the pathway may manifest as alterations in the drug target protein to render it insensitive to the drug, hyperactivation of upstream or parallel pathway components, or reactivation of downstream effectors

independent of upstream signalling. In addition to index pathway reaction, alterations of alternative signalling pathways may converge to reactivate downstream effectors through pathway crosstalk or re-engage other components of the oncogenic output. This is termed as pathway bypass. Pathway indifference describes alterations that result in cell states that are independent of the targeted oncogenic pathway, leading to activation of alternative oncogenic outputs that are not disrupted by drug action (Konieczkowski *et al.*, 2018). Examples of these resistance mechanisms will be elaborated on in the following sections for each category of PAM inhibitor (from section 1.5).

1.6.1. Resistance to PI3K inhibitors

Acquired and intrinsic resistance has been observed in PI3K inhibitors. Pathway reactivation was observed through parallel effectors, SGK1 overexpression, and upstream effectors through PTEN loss and RTK overregulation (Elkabets *et al.*, 2013; Juric *et al.*, 2015; Castel and Scaltriti, 2017; Zorea *et al.*, 2018). Pathway bypass mechanisms were observed such as through PIM1 or p90RSK3 and p90RSK4 overexpression feeding into PAM pathway components (Serra *et al.*, 2013; Le *et al.*, 2016). Additionally, epigenetic alterations to the genes *H19* and *PSTA1* in GISTs were observed as pathway indifferent mechanisms of resistance to PI3K inhibitors (Ravegnini *et al.*, 2019).

1.6.2. Resistance to mTOR inhibitors

Resistance to mTOR inhibitors has been extensively studied. There have been many reports that have identified intrinsic and acquired alterations of the eIF4F complex and reactivating the PAM pathway as a means to overcome allosteric or kinase inhibition of mTOR (Dilling *et al.*, 2002; Thoreen *et al.*, 2009; Alain *et al.*, 2012; Hoang *et al.*, 2012; Cope *et al.*, 2014; Hassan *et al.*, 2014; Mallya *et al.*, 2014; Y Martineau *et al.*, 2014; Mi *et al.*, 2015; Nogami *et al.*, 2015). These mainly involve upregulation of eIF4E or inactivation of 4EBP1 through reduced expression or increased phosphorylation. These are the most common methods of resistance to

mTOR inhibitors. Alterations in ERK have also contributed to pathway bypass resistance through cross-talk to mTORC1 for torkinib resistance (PP242; Hoang *et al.*, 2012) and pathway indifference resistance mechanisms by stabilising the transcription factor CREB and upregulating the transcription of oncogenes *MYC* and *YAP1* (Muranen *et al.*, 2016).

1.6.1. Resistance to AKT inhibitors

Currently, several studies have observed and defined intrinsic resistance mechanisms to both allosteric and ATP-competitive AKT inhibitors, however no reports of acquired resistance to AKT inhibitors have been published. Intrinsic mechanisms published against MK-2206 and ipatasertib have all shown PAM pathway reactivation through hyperactivation of upstream effectors such as the RTK, HER2 or target alteration of AKT3 (Qi *et al.*, 2015; Stottrup *et al.*, 2016; Wehrenberg-Klee *et al.*, 2016). Capivasertib specific intrinsic resistance mechanisms include pathway bypass by upregulation of Ras signalling and PAM pathway reactivation through parallel effector, SGK1 hyperactivation and reactivation of downstream effectors increasing autophagy (Davies *et al.*, 2012; Lamoureux *et al.*, 2013; Sommer *et al.*, 2013).

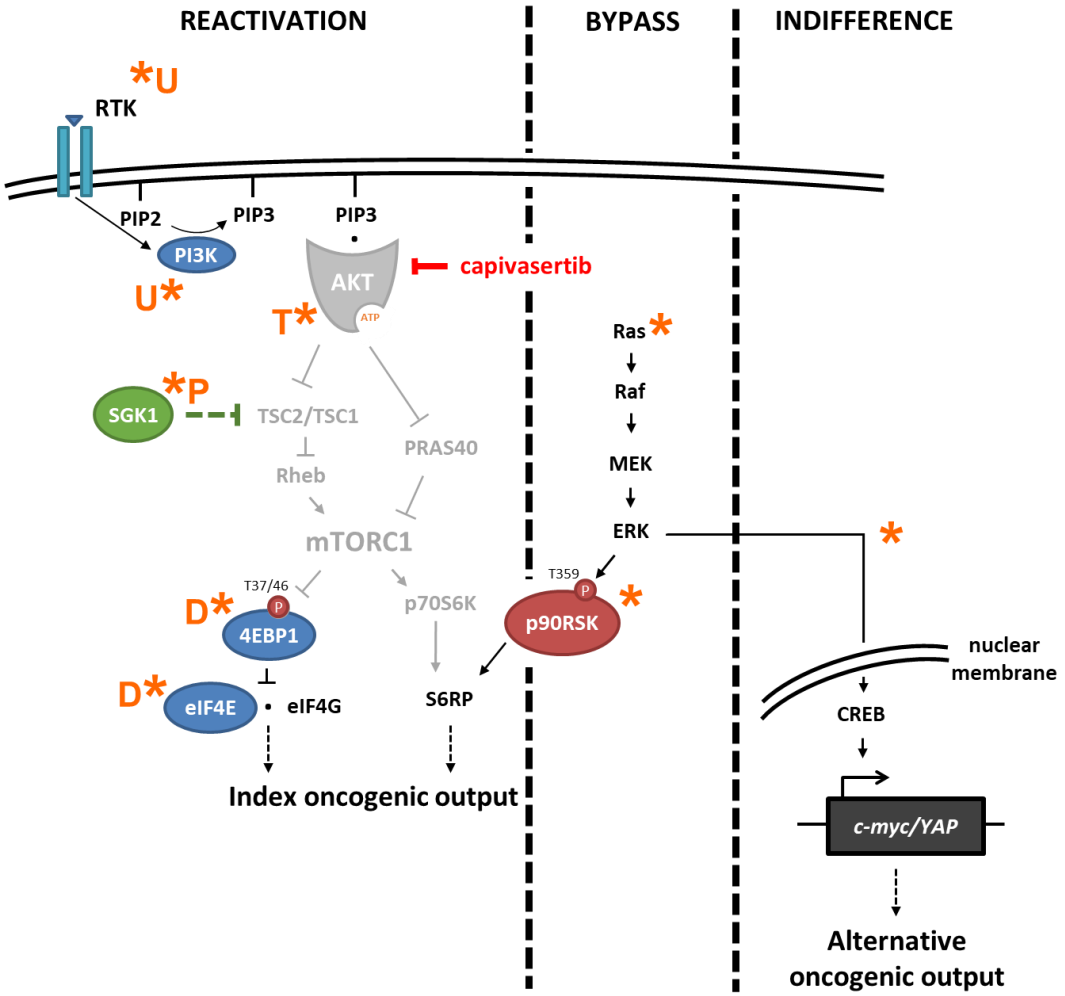

Figure 1.11 – Convergence of drug resistance mechanisms on PAM signalling.
Reported drug resistance mechanisms (*) against PAM inhibitors as described in text, illustrated according to mechanism type as Konieczkowski, (2018). U = upstream effector alterations; T = target alterations; P = parallel effector alterations; D = downstream effector alterations to AKT inhibition (capivasertib).

1.6.1. Resistance to CDPS inhibitors

As most of the CDPS inhibitors described here are in preclinical or early phase clinical development, potential resistance mechanisms of these drugs has been relatively unexplored. However, as CDPS is the convergence point of several growth factor pathways, alterations of CDPS components is a common mechanism in many chemo-naïve and drug resistant tumours. Many studies have shown that the inhibitors described in this section hold promise for combination therapy and reduce the likelihood of drug resistance to PAM and MAPK inhibitors and cytotoxic

therapies as well (Zhang *et al.*, 2008; Cencic *et al.*, 2011, 2013; Boussemart *et al.*, 2014).

1.7. Overview and aims of this thesis

The PAM pathway is one of several signalling pathways which is particularly important for regulating cell growth, proliferation, metabolism, survival and other phenotypes in the cell. As many of these phenotypes are also useful for oncogenesis, it is unsurprising that deregulation of this pathway is commonly observed in many cancers (Fruman *et al.*, 2017).

For this reason, AKT inhibitors such as capivasertib amongst other PAM inhibitors are undergoing development as a novel form of targeted cancer treatment. As described above, for many PAM inhibitors acquired resistance is a major barrier to their clinical success, and it is likely that the progression of AKT inhibitors will be impacted also. Understanding potential resistance mechanisms can support the clinical utility of these drugs through screening patients for intrinsic or acquired resistance and determining effective therapeutic strategies to prevent or counteract resistance.

One method to investigate drug resistance mechanisms is by using cell line models. Resistant isogenic lines are relatively cheap, require fewer ethical considerations and are less laborious to generate. In addition, these can be easily employed in high throughput and candidate screens for rapid identification of resistance mechanisms. However, monolayer culturing methods are limited in their capacity to properly represent a tumour environment and may limit or remove entirely the influences of intratumoural, microenvironment and immune interactions on resistance generation (McDermott *et al.*, 2014; Goodspeed *et al.*, 2016; Namekawa *et al.*, 2019). Regardless, there are several studies which have successfully demonstrated that cell line models can be used to identify clinically relevant drug resistance mechanisms (Dilling *et al.*, 2002; Thoreen *et al.*, 2009; Nazarian *et al.*, 2010; Alain *et al.*, 2012; Hoang *et al.*, 2012; Cope *et al.*, 2014).

This project uses the A2780 ovarian carcinoma cell line and its isogenic capivasertib-resistance subpopulation (A2780 254Rp) to identify and validate candidate resistance mechanisms and associated oncogenic phenotypes. The A2780 ovarian carcinoma cell line was selected as a model as this cell line harbours a loss-of-function PTEN mutation (383-391 deletion; Saito *et al.*, 2000), and a gain-of-function mutation on PIK3CA (G>A substitution at 1093; Oda *et al.*, 2008) which increases p110α PI3K activity; thus it represents a sensitive tumour type that might be selected for capivasertib treatment. The parental A2780 (PAR) cell line was exposed to dose-escalation of CCT129254 over a period of six months by Dr Denis Akan (Akan, 2015) to generate the CCT129254-resistant subline, A2780 254Rp. CCT129254 was employed as it is a close analogue to capivasertib (Figure 1.10) and large quantities of compound were more accessible at the time of resistance generation.

Aims:

This aim of this project was to investigate the A2780 PAR and 254Rp cell lines to identify and validate candidate acquired resistance mechanisms to capivasertib, associated oncogenic phenotypes and potential strategies to prevent or overcome resistance.

Objectives:

- Identify candidate resistance mechanisms *in vitro* in A2780 254Rp by:
  - Examination of morphological differences with A2780 PAR
  - Cross-resistance profiling to a range of targeted inhibitors
  - Examination of baseline and drug-treated PAM pathway signalling compared with A2780 PAR
- Validate identified resistance mechanisms in A2780 cell lines
- Devise therapeutic strategies for overcoming identified resistance mechanisms.

Chapter 2

Materials and Methods

2. Materials and Methods

2.1. Compounds and Materials

Compounds used on cultured cells were prepared and maintained in sterile conditions in solvents as per Table 2.1. Other chemicals and reagents were purchased from Sigma-Aldrich (Germany) unless otherwise indicated.

Table 2.1 – List of compounds used for cross-resistance profiling, western blotting and other cell-based experiments.

Drug	Target	Solvent	[Stock]	Supplier
4EGI-1	eIF4F initiation complex	DMSO	50 mM	Adooq, USA
capivasertib/ AZD5363	AKT (ATP-competitive)	DMSO	20 mM	Selleck Chemicals, USA
CCT129254	AKT (ATP-competitive)	DMSO	20 mM	Institute of Cancer Research, courtesy of John Caldwell and Ian Collins
cycloheximide (CHX)	Protein synthesis elongation	DMSO	100 mg/ml	Sigma Aldrich, Germany
everolimus/ RAD001	mTORC1 only (substrate recruitment)	DMSO	100 nM	Fluka Analytics, Switzerland
geneticin/ G418	Cytotoxic antibiotic (protein synthesis elongation)	Saline	50 mg/ml	Santa Cruz, USA
ipatasertib/ GDC-0068	AKT (ATP-competitive)	DMSO	20 mM	Selleck Chemicals, USA
MK-2206	AKT (allosteric)	DMSO	20 mM	
MRT00206081	MNK	DMSO	20 mM	MRC Technology (LifeARC), courtesy of Andy Merritt and Ed McIver
pictilisib/ GDC-0941	Pan PI3K class I mTOR kinase	DMSO	20 mM	Selleck Chemicals, USA
ravoxertinib/ GDC-0994	ERK	DMSO	20 mM	
selumetinib/ AZD6244	MEK	DMSO	10 mM	
vistusertib/ AZD2014	mTOR kinase	DMSO	10 mM	

2.2. Cell lines and culture

2.2.1. A2780 cell line

The A2780 cell line is a chemo-naïve human endometrioid ovarian adenocarcinoma cell line originated from a 53-year-old African female in 1982-86 (Beaufort *et al.*, 2014). Currently known mutations in A2780 include a 383-391 deletion (corresponding to a K128 – R130 amino acid deletion and loss of PTEN lipid phosphatase activity; Saito *et al.*, 2000), and a *PIK3CA* 1093 G>A substitution (corresponding to p110α E365K amino acid substitution, which increases p110α PI3K activity; Oda *et al.*, 2008). The parental A2780 cells were obtained from the Health Protection Agency (Salisbury, UK). A subpopulation of A2780 cells resistant to capivasertib analogue CCT129254 (A2780-254R) was generated by Dr Denis Akan (Institute of Cancer Research, UK; Akan, 2015).

2.2.2. Routine cell culture

All cell lines used were maintained in Dulbecco's Modified Eagle Medium (DMEM; ThermoFisher Scientific, USA) containing high glucose, L-glutamine but no pyruvate, and supplemented with 10% (v/v) heat-inactivated foetal bovine serum (FBS; ThermoFisher Scientific, USA) and no antibiotics. The cells were incubated in normal growth conditions at 37˚C in a humidified 5% CO_2 incubator. Cells were passaged when approximately 70-90% confluent. Cells grown in T25 flasks were rinsed with 2ml phosphate-buffered saline (PBS; Oxoid, UK) prior to detachment from flask with 0.5ml 0.05% Trypsin-EDTA solution (ThermoFisher Scientific). Detached cells were resuspended in complete DMEM and split appropriately (approximately 1:10-100 dilution) into 5ml complete DMEM into a fresh flask. Some remaining cells were reserved in the trypsinised flask as a backup. Volumes were tripled for use in T75 flasks and multiplied seven-fold for T175 flasks.

In order to seed a specific number of cells for an assay, cells were counted after trypsinisation and resuspension in complete DMEM. 10µl of suspended solution was diluted 1:5 in trypan blue to detect viability of cells and counted using a

BRAND® counting chamber. An appropriate volume of calculated concentration of cells was diluted in complete DMEM for plating.

Cell lines were routinely tested approximately every 6 months to ensure they were free from *Mycoplasma* contamination using the VenorGeM® Mycoplasma PCR detection kit (Minerva Labs, UK).

To prevent genetic deviation, cell populations were passaged continuously for no longer than 4-6 months. Freeze-downs of cells were thawed as quickly by warming in 37˚C water bath. Once fully thawed, DMSO was removed by diluting the cells in 5ml complete DMEM and centrifuged at 270 x g for five minutes at room temperature (RT). The culture medium was carefully aspirated and cell pellet was resuspended in fresh 5ml and transferred to a T25 flask to allow to settle overnight. To maintain resistant flasks, the drug was added to resistant cells five days post thawing. A confirmatory SRB growth assay (section 2.3.2) against CCT129254 was performed with newly thawed cells and old passaging cells to ensure response to drug is maintained.

A subpopulation of each cell line was frozen down within two passages of thawing. Cells were grown to approximately 80% of a T75, trypsinised, resuspended in complete DMEM (as section 2.2.1) and spun down at 270 x g for five minutes at RT. Culture medium was carefully aspirated and cell pellet resuspended in 3ml of freeze-down media (10% DMSO in complete DMEM). Cells were aliquoted into three cryovials each and cooled to -80˚C inside Mr. Frosty™ Freezing container (ThermoFisher Scientific, USA) supplied with RT propan-2-ol (replenished every five freeze-thaws).

2.2.3. Generation of CCT129254-resistant A2780 cells

Polyclonal CCT129254-resistant A2780 cells (A2780 254Rp) were generated by Dr Denis Akan (Akan, 2015). In brief, CCT129254 sensitive A2780 parental (PAR) cells were incubated in complete DMEM with half-maximal growth inhibitory concentration (GI_{50}) of CCT129254 in normal growth conditions until cells reached

70% confluency. Cells were treated with incrementally increased concentration of drug after passaging for a period of six months.

Clonal populations of A2780 254Rp were generated by seeding the cells at 0.5 cells/100µl in each well of a 96-well plate and checked once a day until visible colonies formed. Single colonies were picked for growing up to 24-well plates once reaching a sufficient colony size (approximately 1mm) within 11-21 days post plating. Culture medium was removed carefully by pipetting away from colony, and cells were incubated in 60µl trypsin for approximately two minutes at RT. Cells were agitated by resuspending with 200µl complete DMEM and transferred cells to a final volume of 500µl in 24-well plate, and complete DMEM added to trypsinised well as a backup. At 70% confluency, cells were washed with 200µl PBS, trypsinised with 100µl trypsin and resuspended in 2ml final volume in 6 well plate. This process was repeated with double volumes into T25 and passaged as section 2.2.1.

All resistant cells were routinely maintained in 56µM CCT129254 (the maximum concentration used for generation of resistant population by Dr Denis Akan (Akan, 2015) and removed from selective pressure into drug-free complete DMEM one week prior to plating for experiments.

2.3. Sulforhodamine B (SRB) growth assay

2.3.1. SRB growth assay

Sulforhodamine B dye (SRB) provides an estimate of the concentration of cells through binding to amino-acids, and therefore can be used to measure the proliferation of cells (Skehan *et al.*, 1990) both treated and untreated with drugs. Cells were seeded at cell concentrations as indicated in 160µl complete DMEM and allowed to attach for 48 hours prior to treatment. For investigation of cross-resistance to different compounds, cells were treated with a range of concentrations by serially diluting compounds (1.5-5 fold) in complete DMEM and adding 40µl of each concentration to wells, further diluting the compound 5-fold to the concentrations indicated. Cells were left to incubate for 96 hours in drug. After

this time, the culture medium was removed, and cells were fixed with 10% (w/v) trichloroacetic acid (TCA) for 30 minutes and washed three times with water. Fixed cells were stained with 0.4% (w/v) SRB solubilised in 1% (v/v) acetic acid (Fisher Scientific, UK) for 30 minutes, and subsequently washed thrice with 1% (v/v) acetic acid until wells became clear before drying for at least three hours at 37 ˚C. Protein-bound SRB was solubilised in 100µl 10mM Tris base and absorbances were read at a wavelength of 490nm in a Victor X4 Multilabel Plate Reader (PerkinElmer Life Sciences, USA). Raw values were blanked using cell-less wells with 10mM Tris and normalised to a percentage of the average of the untreated control per drug. The GI_{50} values were determined using GraphPad Prism 6 (GraphPad Software Inc, USA). Resistance Factors (RF) values were calculated as the ratio of CCT129254-resistant cells GI_{50} to PAR GI_{50}. RF presented in text, tables and bar charts as the average RFs of at least three independent experiments. Statistical significance of RF was calculated using the unpaired t test with Welch's correction of resistant to PAR GI_{50} values.

$$Resistance\ Factor\ (RF) = \frac{resistant\ GI_{50}}{parental\ GI_{50}}$$

2.3.2. SRB growth assay optimisation (determining 96-well seeding concentration)

The cell seeding concentration for 96-well format SRB growth assay was optimised per cell line to accommodate cell line differences in doubling times when responding to drug treatment. Cells were plated at several cell concentrations (as indicated in text) in seven 96-well plates in 200µl complete DMEM. Every 24 hours, one plate was fixed, stained and analysed as described for the SRB growth assay (section 2.3.1). Raw absorbances were used to generate growth curves in GraphPad Prism 6. The ideal cell concentration was that which the cells remained in logarithmic growth over the course of the hypothetical 96-hour drug incubation period (indicated by the dotted lines in Figures 2.1-2.4).

Logarithmic doubling times for each cell line was calculated using the following formulae where the duration in hours (hrs) is the difference in time between the time of the initial OD signal (48 hrs) and final OD (144hrs). This was averaged across at least three independent experiments as indicated.

$$Doubling\ Time\ (DT; hrs) = \frac{duration\ (hrs) \times \log(2)}{\log(final\ OD) - \log(initial\ OD)}$$

The growth of the A2780 PAR and 254Rp for SRB experiments in Chapter 3 were investigated at the following seeding concentrations: 200, 400, 800, 1600 and 3200 cells per well. Figure 2.1**Error! Reference source not found.** showed with increased cell concentration, both PAR and 254Rp cell lines reached logarithmic growth at earlier time points. The optimal seeding concentration for both PAR and 254Rp cell lines was 800 cells per well. Through examination of the optical density (OD) in $\log_{10}$ (Figure 2.1B and D), there was consistent logarithmic growth between the two time points indicated, with the least plateau by 146 hours and lag beyond 50 hours post cell plating of the five seeding concentrations tested.

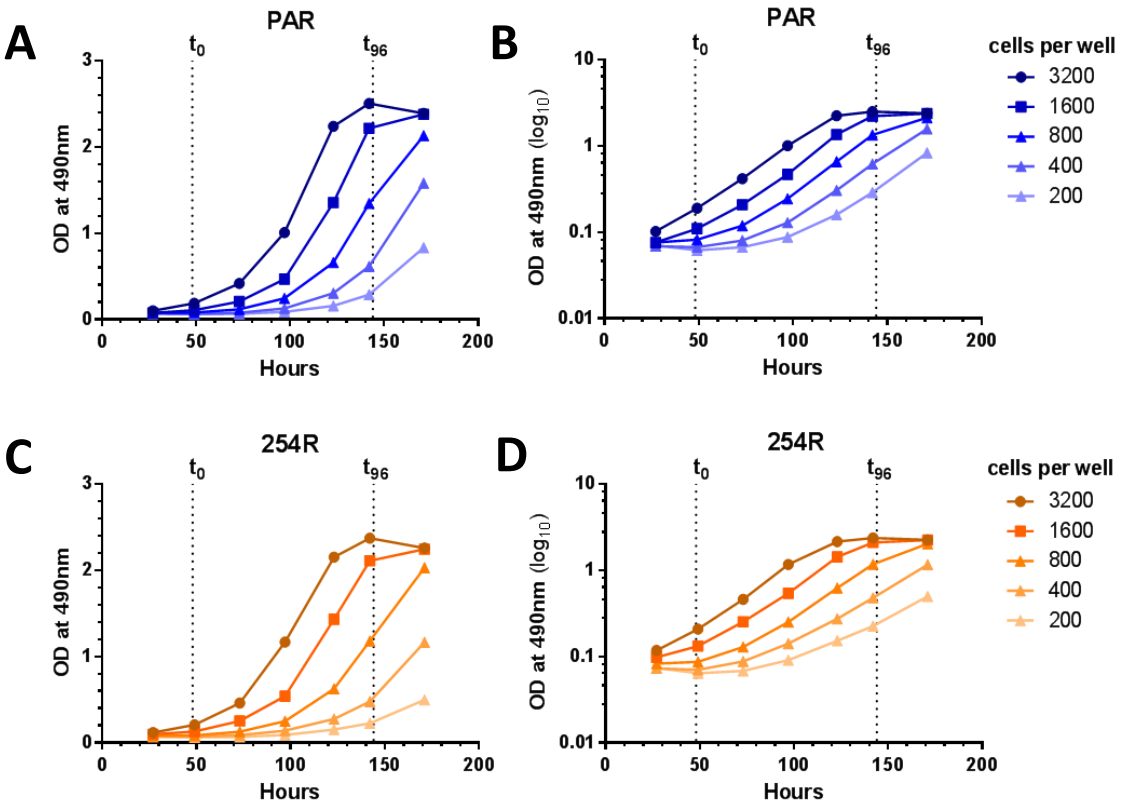

Figure 2.1 – A2780 PAR and 254Rp growth in 96-well plates.
Cells were plated at seeding concentrations indicated in the keys over seven plates, each fixed every 24 hours and analysed by SRB growth assay. Characterisation of growth of both cell lines were through analysis of decimal (A and C) or log_{10} (B and D) raw absorbance (OD_{490}) over time in hours after cell plating. Growth curves were generated using Graphpad Prism 6. The time between broken lines (t_0 and t_{96}) indicate the 96-hour time frame of hypothetical drug incubation, starting 48 hours post cell plating, in an SRB growth assay. Data points present the mean for five technical replicates. Data representative of four independent experiments.

As can be seen in Figure 2.2, by overlaying the growth curves for PAR and 254Rp cells plated at 800 cells per well, there was no difference in growth patterns throughout the entire assay and thus indicated 800 cells per well as the optimal seeding concentration for direct drug-profiling comparison. The average doubling times of the cells during the incubation period at 800 cells per well were calculated as 26.3 hours for PAR and 26.8 hours for 254Rp.

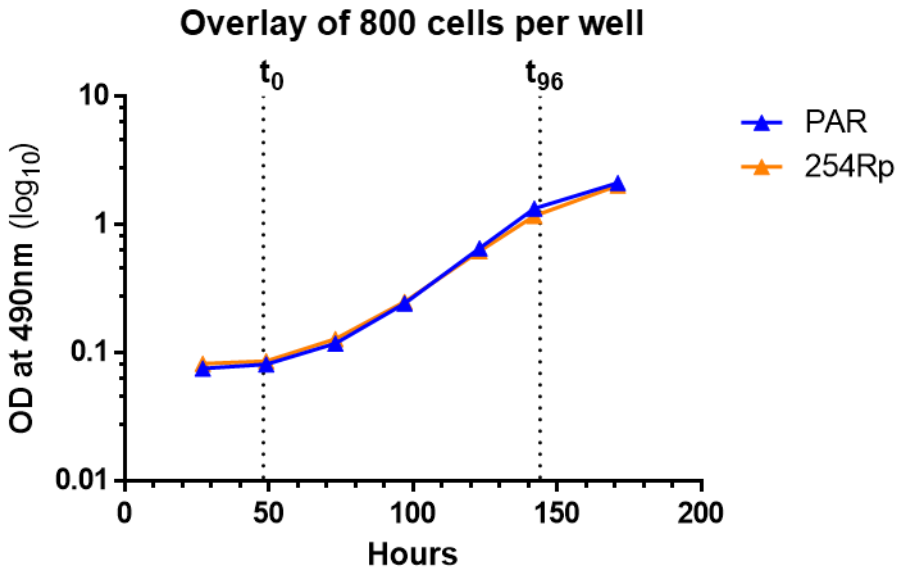

Figure 2.2 – Overlay of A2780 PAR and 254Rp growth in 96-well plates at optimal seeding concentration.
Data taken from Figure 2.1, to overlay growth characterisations of PAR and 254Rp cells. Growth curves were generated using Graphpad Prism 6. The time between broken lines (t_0 and t_{96}) indicate the 96-hour time frame of hypothetical drug incubation, 48 hours post cell plating, in an SRB growth assay. Data points present the mean ± SD for five technical replicates. Data representative of four independent experiments.

The growth of the A2780 254Rp subclones, 254R-B and 254R-D in Chapter 4, was investigated at the following seeding concentrations: 800, 1600 and 3200 cells per well. The optimal seeding concentration for both 254Rp subclones was 1600 cells per well. This concentration showed the most logarithmic growth during the incubation period, with the least plateau by 146 hours and least lag beyond 50 hours post plating the five seeding concentrations tested. Additionally, the growth for both 254R-B and D at 1600 cells per well overlapped the logarithmic growth for PAR and 254Rp at 800 cells per well (Figure 2.3).

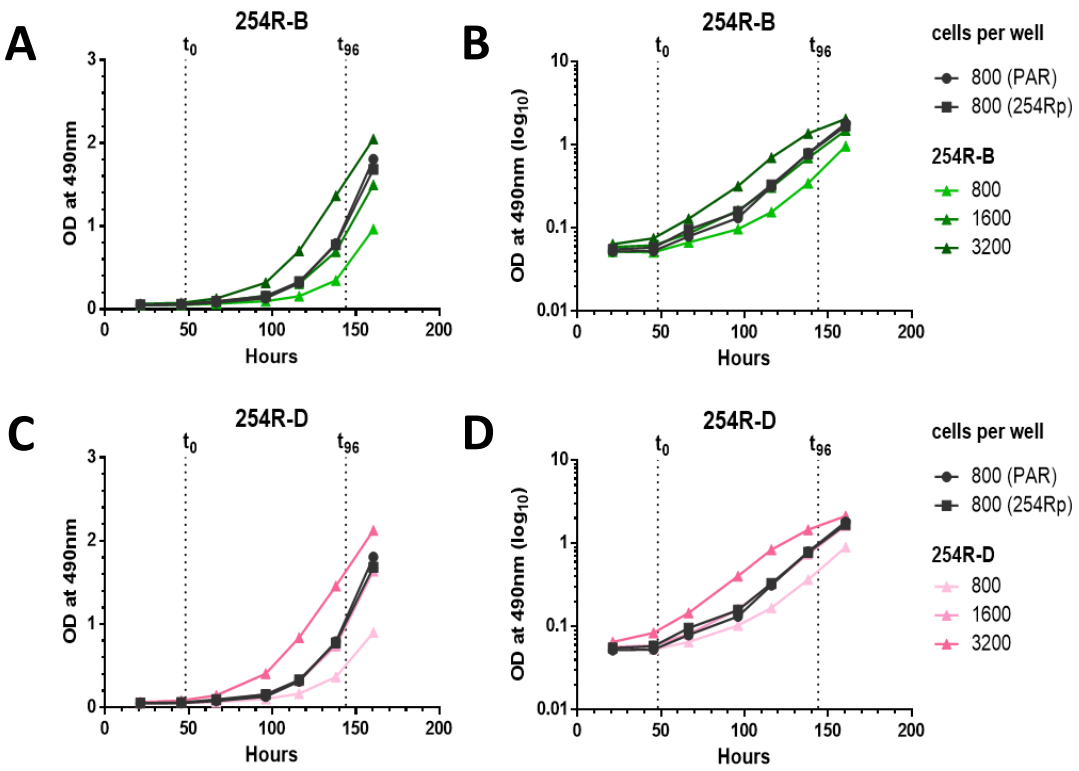

Figure 2.3 – A2780 254Rp subclones 254R-B and 254R-D growth in 96-well plates.
A2780 PAR, 254Rp, 254R-B and 254R-D cells were plated and fixed and growth curves generated as Figure 2.1. Characterisation of A2780 254R-B (A and B) and 254R-D (C and D) growth in 96-well plates through analysis of decimal (A and C) or $\log_{10}$ (B and D) raw absorbance (OD_{490}) over time. The time between broken lines (t_0 and t_{96}) indicate the 96-hour time frame of hypothetical drug incubation, starting 48 hours post cell plating, of an SRB growth assay. Data points present the mean for five technical replicates. Data representative of three independent experiments.

The seeding concentration was also optimised for the four selected 254R-B-4EBP1 subpopulations (Chapter 6), in order to accurately determine the GI_{50} and RF values to capivasertib. The ideal cell concentration was that which the growth of the cells mimicked best the untransfected 254R-B cells, remaining in logarithmic growth over the course of the hypothetical 96-hour drug incubation period (indicated by the dotted lines of Figure 2.4).

The optimal seeding concentration for all 254R-B-4EBP1 subpopulations was 3200 cells per well (Figure 2.4). This was the concentration that mimicked growth the best with 254R-B in all subclones. Although a higher concentration may have exhibited less lag beyond the drug incubation start point (48 hours), the growth remained logarithmic throughout most of the incubation period.

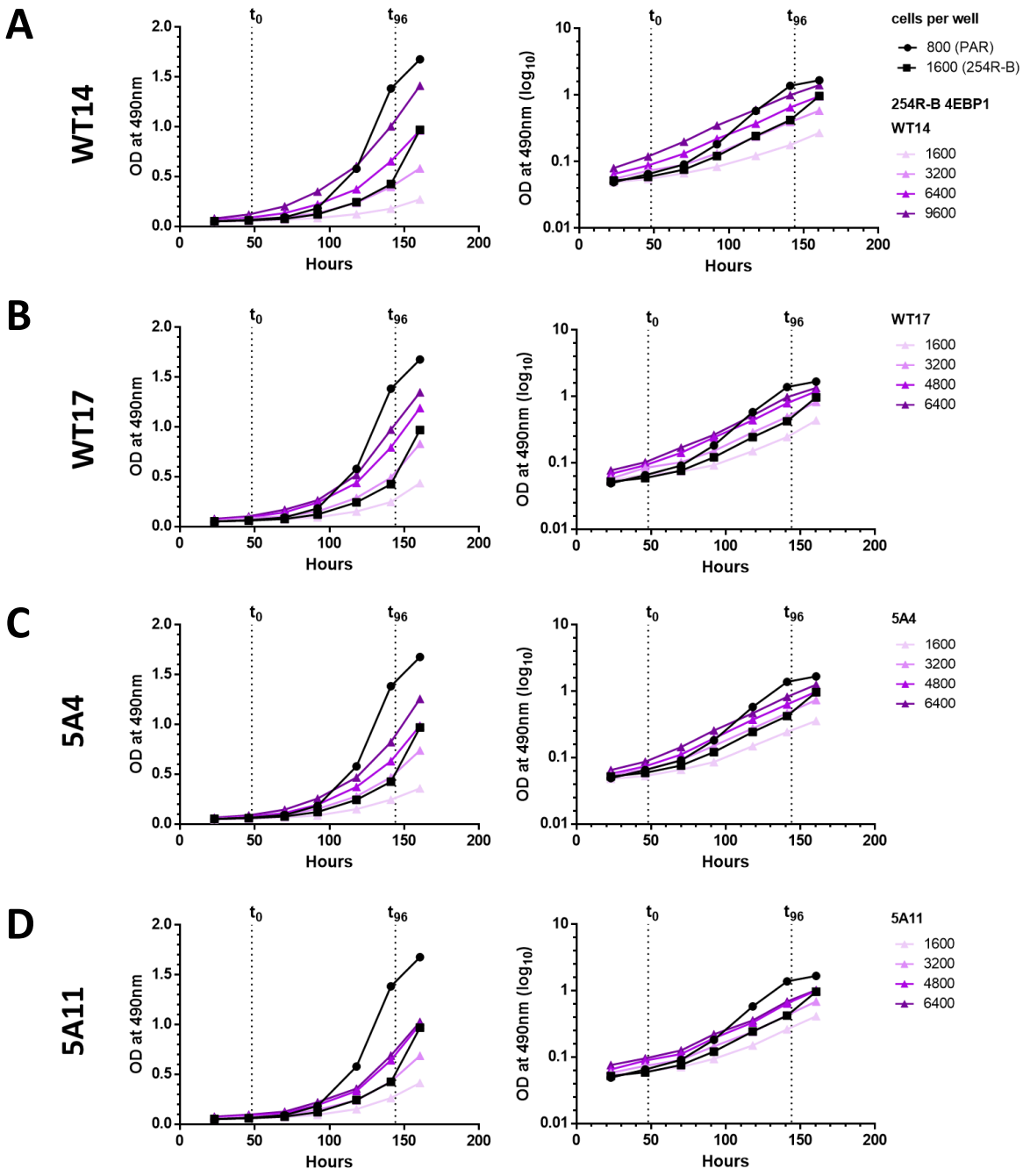

Figure 2.4 – A2780 254R-B-4EBP1 subpopulations growth in 96-well plates.
A2780 PAR, 254Rp, 254R-B and 254R-B-4EBP1 cells were plated and fixed and growth curves generated as Figure 2.1. Characterisation of 254R-B-4EBP1-WT14 (A), WT17 (B), 5A4 (C) and 5A11 (D) growth in 96-well plates through analysis of decimal (left) or log10 (right) raw absorbance (OD_{490}) over time. The time between broken lines (t_0 and t_{96}) indicate the 96-hour time frame of hypothetical drug incubation, starting 48 hours post cell plating, of an SRB growth assay. Data points present the mean for five technical replicates. Data representative of three independent experiments.

2.4. Cell lysis and western blotting

2.4.1. Cell lysis

Cells were plated at $5x10^5$ (or $1x10^6$ in A2780-254R subclones) in 10 cm dishes or $7.5x10^4$ in 6-well plates and allowed to adhere for up to 72 hours. If drug treatment was required, cell medium was replenished after 48hrs with drug-treated media (at concentrations indicated in text) and incubated for 24 hours unless otherwise indicated. At lysis, culture medium was removed, and plates rinsed twice with 2ml ice-cold PBS. Ice-cold lysis buffer (50mM HEPES pH 7.4, 250mM NaCl, 0.1% Nonidet-P40, 1mM DTT, 1mM EDTA pH8.0, 1mM NaF, 10mM β-glycerophosphate, 0.1mM sodium orthovanadate and Complete™ protease inhibitor cocktail [Roche, Switzerland]) was added and cells were manually scraped. Lysates were collected in pre-chilled microcentrifuge tubes and incubated on ice for 30 minutes. Insoluble material in lysates were cleared by centrifugation at 14,000 x g for 10 minutes at 4˚C, and the cleared lysate was transferred to a clean microcentrifuge tube and kept on ice for immediate use or snap-frozen on dry ice and stored at -80°C.

2.4.2. Determination of protein concentration

The bicinchoninic acid (BCA) assay was used to determine the protein concentration in cell lysates (Smith *et al.*, 1985). Cleared cell lysate was diluted 10 or 20-fold in double distilled (ddH_2O), and 10µl was added in triplicate to a 96-well plate. Copper(II) sulfate solution was mixed with BCA at a 1:50 dilution, and 200µl was added to each well. Samples were mixed thoroughly and incubated at 37˚C for 30 minutes. Absorbances were read at a wavelength of 560nm in a Victor X4 Multilabel Plate Reader (PerkinElmer Life Sciences, USA).

Concentrations of lysates were calculated by cross-comparing the lysate absorbance values against a standard curve, generated from including 10µl per well in triplicate of bovine serum albumin (BSA) protein standards (0.1-1mg/ml) or ddH_2O on every plate tested. Analysis was performed in Microsoft Excel 2016 (Microsoft, USA).

2.4.3. SDS-PAGE and western blotting

The levels of protein expression and phosphorylation at specific sites across cell lysates were semi-quantitively investigated by Laemmli sodium dodecyl sulfate-polyacrylamide gel electrophoresis (SDS-PAGE; Laemmli, 1970) and western blotting (Hirano *et al.*, 1993).

Cell lysates were normalised to the same protein concentration in lysis buffer, and 5X sample buffer (312.5mM Tris pH6.8, 6%(w/v) SDS, 50% glycerol, 25%(v/v) β-mercaptoethanol, 0.25%(w/v) bromophenol blue) was added. The samples were subsequently denatured and reduced by boiling samples at 95°C for five minutes.

Equal quantities of protein sample (20-70µg as required), depending on the protein molecular weight of interest, were loaded onto 6%, 10% or 15% Tris-glycine gels (6-15% acrylamide/bis(v/v), 0.375M Tris pH8.8, 0.1% SDS(w/v), 0.05% ammonium persulfate(w/v) and 0.005% tetramethylethylenediamine) with a 4% tris-glycine stacking gel (4% acrylamide/bis(v/v), 0.125M Tris pH6.8, 0.1% SDS(w/v), 0.05% ammonium persulfate(w/v) and 0.01% tetramethylethylenediamine) polymerised within 3 days of running. Gels were run in a Tris-glycine running buffer (25mM Tris, 190mM glycine, 0.1% SDS) at 150V for 60-90 minutes. 7.5µl of Dual Precision Prestained Protein Markers (BioRad, USA) or Page Ruler Plus prestained protein ladder (ThermoFisher Scientific, USA) were loaded in separate wells to the samples to identify the positions of relevant sized proteins within the gel.

Protein was transferred to methanol-activated 0.2µm pore Immobilon-P PVDF membrane (Millipore, USA) using the wet transfer system (Hirano *et al.*, 1993). Most transfers were run at 100V for 90-120 minutes, dependent on molecular weight and acrylamide percentage of gel, in pre-chilled transfer buffer (25mM Tris-base, 190mM glycine, 10%(v/v) methanol). For investigation of very high molecular weight proteins (i.e. eIF4G – 220 kDa), resolved 6% gels were transferred overnight (18-24 hours) at 30V in 4°C cold room.

Following transfer, membranes were re-activated in methanol and incubated in ponceau S solution (0.1% ponceau S in 5% acetic acid) for one minute and rinsed in

ddH_2O, to determine the quality of transfer. Membranes were appropriately sliced to separate proteins of interest for probing in primary antibody (Table 2.2).

Membranes were blocked on a rocking platform at RT for one hour in blocking buffer: Tris Buffered Saline Tween buffer (TBST; 50mM Tris pH8.0, 150mM NaCl, 0.1% Tween-20 (v/v)) containing 5% milk. Subsequently, membranes were incubated in primary antibody diluted in blocking buffer overnight at 4˚C (Table 2.2). Membranes were washed twice for 10 minutes with TBST, and incubated in goat anti-rabbit or anti-mouse secondary horseradish peroxidase-conjugated (HRP) antibody (BioRad, USA; Table 2.1) for one hour at RT. Membranes were washed four times for five minutes each, and detection was performed using Enhanced Chemiluminescence (ECL) Western Blotting Substrate (Pierce Biotechnology, USA) or Clarity™ Western ECL Blotting Substrates (Bio-Rad, USA). Bands were developed by exposure to Amersham Hyperfilm ECL (GE Healthcare, UK) or developed using Syngene GBox system and Genesys software (Syngene, USA).

Membranes were probed for phosphorylated proteins and stripped for detection of total protein expression. Antibodies stripped from the membrane by incubating in a stripping buffer (50mM glycine, 1%(w/v) SDS, pH2.0) for five minutes on a rocking platform, washed twice in TBST for five minutes each, and re-probed with relevant antibodies overnight at 4°C or 1-3 hours at RT depending on quality of the antibody.

2.4.1. Densitometric quantification of bands

Quantification of band density was performed using Image J software. Images were imported and band density was calculated as percentage of the sum density of analysed bands. Each sample band normalised to its respective loading control (GAPDH).

Table 2.2 – List of antibodies used for western blot analysis. Cat No., catalogue number; CST, Cell Signaling Technology; PD, antibody dilution used on m^7GTP agarose beads for eIF4E pull down.

Primary antibody	Supplier	Cat No.	Species	Dilution
4EBP1	CST, USA	9644	Rabbit	1:4000 PD: 1:5000
4EBP1 pT37/T46	CST, USA	2855	Rabbit	1:1000
AKT	CST, USA	4691	Rabbit	1:5000
AKT pS473	CST, USA	9271	Rabbit	1:1000
AKT pT308	CST, USA	4056	Rabbit	1:1000
Cleaved PARP	CST, USA	9541	Rabbit	1:500
c-Myc (G-4)	Santa Cruz, USA	sc-377552	Mouse	1:200
Cyclin D1 (HD-11)	Santa Cruz, USA	SC-246	Mouse	1:1000
eIF4E	CST, USA	2067	Rabbit	1:5000 PD: 1:3000
eIF4G	CST, USA	2469	Rabbit	1:5000 PD: 1:3000
ELK	Santa Cruz, USA	sc-365876	Mouse	1:200
ELK pS383	Santa Cruz, USA	sc-8406	Mouse	1:200
ERK	CST, USA	4695	Rabbit	1:1000
ERK pT202/Y204	CST, USA	4370	Rabbit	1:1000
GAPDH	Chemicon, USA	MAB374	Mouse	1:100,000
GSK-3β	CST, USA	9315	Rabbit	1:1000
GSK-3β pS9	CST, USA	5558	Rabbit	1:1000
His-probe Antibody (H-3)	Santa Cruz, USA	sc-8036	Mouse	1:200
MEK	CST, USA	9122	Rabbit	1:1000
MEK pS217/S221	CST, USA	9154	Rabbit	1:1000
p70 S6K	CST, USA	9202	Rabbit	1:500
p70 S6K pT389	CST, USA	9205	Rabbit	1:500
PRAS40	CST, USA	2691	Rabbit	1:4000
PRAS40 pT246	CST, USA	2640	Rabbit	1:2000
p90RSK	R&D Systems, USA	MAB2056	Mouse	1:500
p90RSK pT359	CST, USA	8753	Rabbit	1:500
S6RP	CST, USA	2217	Rabbit	1:4000
S6RP pS235/236	CST, USA	2211	Rabbit	1:4000
S6RP pS240/4	CST, USA	2215	Rabbit	1:4000
tubulin	Bio-Rad, USA	9280-0050G	Rabbit	1:1000
TSC2	CST, USA	4308	Rabbit	1:1000
TSC2 pS939	CST, USA	3615	Rabbit	1:1000
TSC2 pT1462	CST, USA	3617	Rabbit	1:500
TSC2 pS1387	CST, USA	5548	Rabbit	1:1000
Secondary antibody				
Anti-mouse HRP conjugate	Bio-Rad, USA	170-6516	Goat	1:10,000
Anti-rabbit HRP conjugate	Bio-Rad, USA	170-6515	Goat	1:10,000

2.4.2. Co-immunoprecipitation (eIF4E)

To investigate the interaction between eIF4E and its competitive binding partners eIF4G and 4EBP1, 7-methyl GTP (m^7GTP) immobilised on agarose beads were used as a 5' mRNA cap-mimetic to isolate eIF4E from cell lysates, and western blotting was used to semi-quantitatively determine the amount of each binding partner bound.

Cells were plated, drug-treated if necessary, lysed and protein concentration determined, as described above in section 2.5.1-2, using 200µl non-denaturing lysis buffer (NDLB; 1X Cell Lysis Buffer: 20mM Tris-HCl pH 7.5, 150mM NaCl, 1mM disodium EDTA, 1mM EGTA, 1% Triton, 2.5mM sodium pyrophosphate, 1mM sodium orthovanadate and 1µg ml-1 leupeptin; Cell Signaling Technologies, USA). Lysates were diluted to 0.5mg/ml in NDLB.

15µl immobilised γ-Aminophenyl-m7GTP agarose beads (30µl 50% slurry; Jena Bioscience, Germany) were washed twice with 200µl NDLB. 250µg sample was added to the washed beads and incubated on a rotating wheel at 4 ˚C overnight. Beads were centrifuged at 2,500 x g for one minute, to separate the output lysate from the beads and the beads were then washed three times with 400µl NDLB. 50µl 2X sample buffer was added, and bound proteins were denatured by incubating the beads at 60˚C for 10 minutes to prevent agarose melting. Bead-free input and output lysates samples were prepared as section 2.5.2.

eIF4G and 4EBP1 levels bound to eIF4E in prepared bead samples were analysed by western blotting (section 2.5.3). eIF4E was used as an equivalent loading control between sample conditions.

2.5. Gene expression microarray analysis

A2780 PAR and 254Rp cells were grown, lysed and RNA purified by Dr Denis Akan (Akan, 2015). RNA samples were run using the Agilent Two-Colour Microarray-Based Gene Expression Analysis at Oxford Gene Technology (Oxford, UK) and supplied data was analysed by Dr Akan using Genespring GX 12.6 (Agilent Technologies, USA). In brief, A2780 PAR and 254Rp were assessed for significant

changes in expression of mRNAs using a t-test. Significance was determined as greater than a 2-fold change in expression. Significant mRNAs were cross-examined in Reactome software to identify PAM pathway components with significantly altered expression in 254Rp compared to PAR.

2.6. Plasmid DNA preparation

2.6.1. Plasmids

All of the plasmids used in this project were obtained as kind gifts. The pRL-(PV)IRES-FL plasmid was received from Dr Simon Cook (The Babraham Institute, Cambridge, UK) and reconstituted by Denis Akan in 100µl TE buffer (10mM Tris pH 8.0, 1mM EDTA). The pcDNA5-FRT-eGFP plasmid was obtained from Professor Mark Smales (University of Kent, UK). The pcDNA3-4EBP1WT-HISMYC and pcDNA3-4EBP15A-HISMYC plasmids were received from Professor Chris Proud (SAHMRI, Australia).

2.6.2. Transformation of plasmid DNA

Plasmid DNA was grown up by transforming into XL-1 calcium competent DH5α *E.coli* cells (a kind gift from Professor Mark Smales, University of Kent, UK). 10ng of prepared plasmid DNA was spiked into 100µl freshly thawed glycerol stock of competent cells. The DNA:*E.coli* mixture was incubated on ice for 30 minutes, heat shocked at 42˚C for 90 seconds, and further incubated on ice for two minutes. 900µl SOB media (2% (w/v) bacto-tryptone, 0.5% (w/v) yeast extract, 0.05% (w/v) NaCl, 20mM $MgCl_2$ and 0.5% glucose) was added to cells and incubated at 200rpm at 37˚C for one hour. Transformed bacteria were plated onto LB agar plates (1% (w/v) bacto-tryptone, 0.5% (w/v) yeast extract, 1% (w/v) NaCl and 1.5% (w/v) agar) containing 100µg/µl ampicillin and incubated at 37˚C overnight. Individual colonies were used to inoculate 3ml lysogeny broth (LB) plates (1% (w/v) bacto-tryptone, 0.5% (w/v) yeast extract and 1% (w/v) NaCl) supplemented with 100µg/µl ampicillin and incubated at 37˚C, at 130rpm overnight. For large-scale purification of plasmid

DNA, 3ml cultures were used to inoculate 250ml 100µg/µl ampicillin LB broth for incubation overnight.

2.6.3. Plasmid preparations

Plasmid DNA was isolated from cells by transforming DH5α *E.coli* and cultured overnight in 250ml 100µg/µl ampicillin LB broth (as section 2.6.2) and cells were pelleted by centrifugation at 6,000 x g at 4˚C for 15 minutes. The plasmid DNA was harvested from the pellet using the QIAGEN Plasmid Maxi Kit (QIAGEN, Germany) following the manufacturer's instructions.

Ethanol precipitation was used to purify and concentrate plasmid DNA. $\frac{1}{10}$ volume 3M sodium acetate pH5.2 and two volumes -20˚C ethanol (EtOH) was added to extracted DNA, vortexed for 10 seconds and chilled at -80 ˚C for 20 minutes. Precipitated DNA was centrifuged for 5 minutes at 14,000 x g, washed with 500µl 4˚C 70% EtOH and air-dried. DNA was resuspended in sterile TE buffer and concentration measured using a Nanodrop ND-1000 UV/Vis spectrophotometer (Nanodrop, USA).

2.7. Lipid-mediated transfection

2.7.1. Transient transfection

To express exogenous proteins of interest, cells were transfected using TransIT®-LT1 (Mirus Bio, USA) and relevant protein coded plasmids. Cells were plated at $3x10^5$ cells per well in 6-well plate and allowed to adhere overnight. DNA-lipid complexes were prepared (as per manufacturer's instructions; 2.5µg plasmid DNA with 7.5µl lipid) in OptiMEM GlutaMAX (Life Technologies, USA) before addition to the cells and allowed 48 hours incubation for transfection and expression of plasmid to take place. Volumes were scaled up accordingly for the culture dish size used.

2.7.2. Plasmid transfection optimisation

Transfection efficiency was optimised utilising the transfection of pcDNA5-FRT-eGFP (from Professor Mark Smales) to visually compare transfection efficiency by fluorescence microscopy. Transfection reagents tested include TransIT®-LT1 (Mirus Bio, USA) and Lipofectamine 2000 (ThermoFisher Scientific, USA). Cells were transiently transfected with 2.5µg plasmid as section 2.7.1, following manufacturer's instructions and recommended DNA:lipid ratios. 48 hours post-transfection, cells were visualised using either Leica MZ FLIII (Leica Camera AG, Germany) or Lumascope 620 (Etaluma, USA) fluorescence microscopes. At time of transfection, cells were equally confluent (80-90%) confluent. Therefore, the transfection efficiency was calculated and compared based on the approximate intensity of eGFP fluorescence.

$$\text{Transfection efficiency } (\%) = \frac{\text{Area of GFP positive cells}}{\text{Total area of cells}} \times 100$$

The ideal lipid:DNA ratio was defined as the ratio which gave the greatest transfection efficiency for both PAR and 254R-B. Figure 2.5 and Figure 2.6 show the transfection in PAR cells using Lipofectamine 2000 and TransIT-LT1, respectively. The transfection in 254R-B cells using Lipofectamine 2000 and TransIT-LT1, were shown in Figure 2.7**Error! Reference source not found.** and Figure 2.8 respectively. No eGFP expression was observed in either of the mock-transfected PAR or 254R-B cells. The PAR cells exhibited equal intensity of transfected cells with either recommended lipid:DNA ratio using Lipofectamine 2000 (Figure 2.5). TransIT-LT1 exhibited a far greater transfection efficiency in 3:1 lipid:DNA ratio and no transfection at 1:1 (Figure 2.6). In 254R-B, the transfection efficiency was generally lower than the PAR cell line in similar conditions, however the best efficiency for Lipofectamine 2000 at 2:1 (Figure 2.7) exhibited a similar transfection efficiency to either TransIT-LT1 ratios tested (Figure 2.8). TransIT-LT1 was selected at ratio 3:1 to carry forward for the DLRA transfection for both cell lines as this was the most efficient and cost-effective condition for transfection.

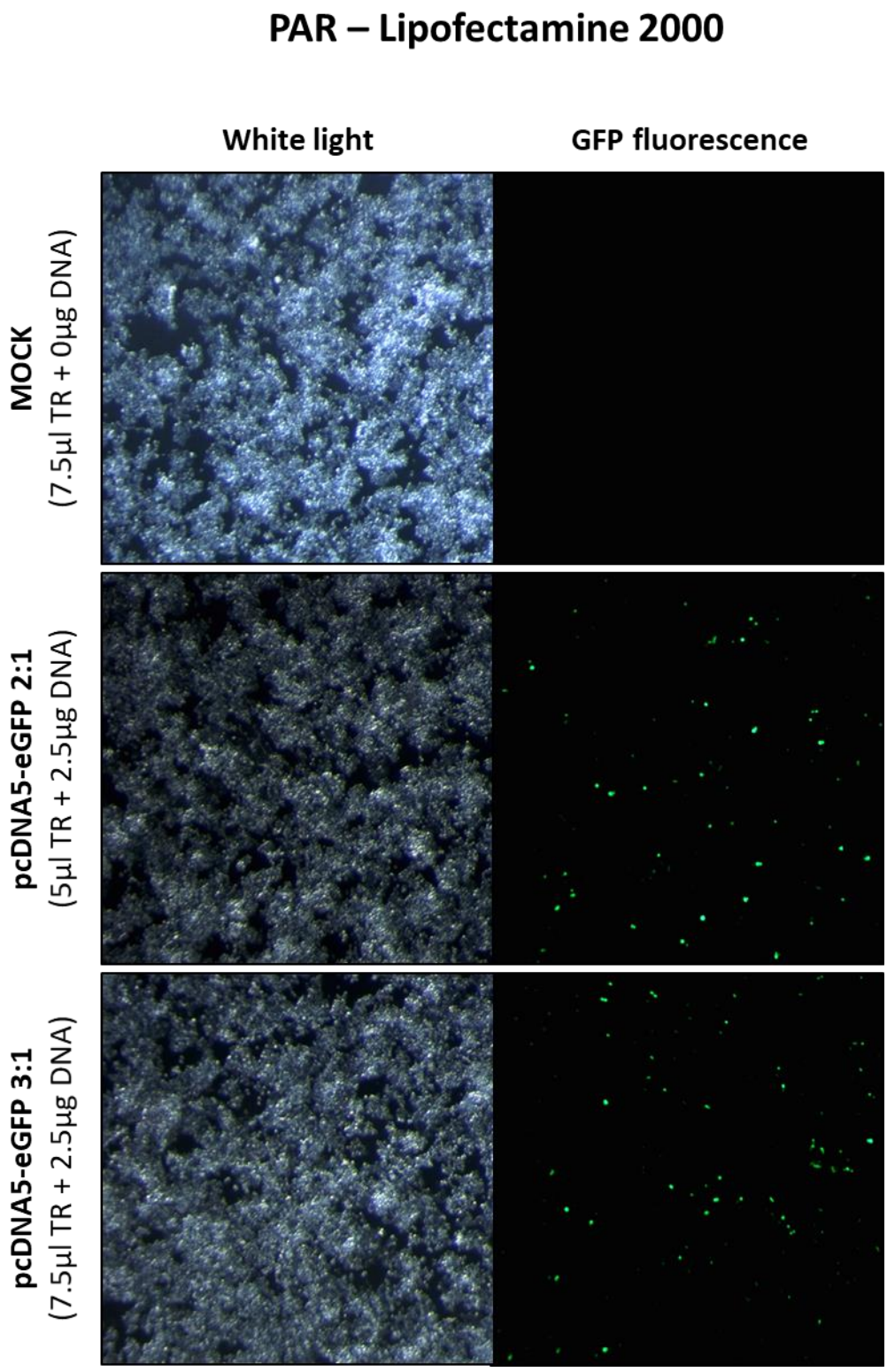

Figure 2.5 – Transfection of pcDNA5-FRT-eGFP in A2780 PAR cells using Lipofectamine 2000.
Cells were plated at $3x10^5$ cells per well in a 6-well plate, 24 hours prior to transfection. 2.5µg of pcDNA5-FRT-eGFP or RNAse free water (mock) was complexed with two recommended transfection reagent (TR):DNA ratios, and added to cells as per manufacturer's instructions. Cells were visualised at 40X magnification under FITC or brightfield, 48 hours post-transfection.

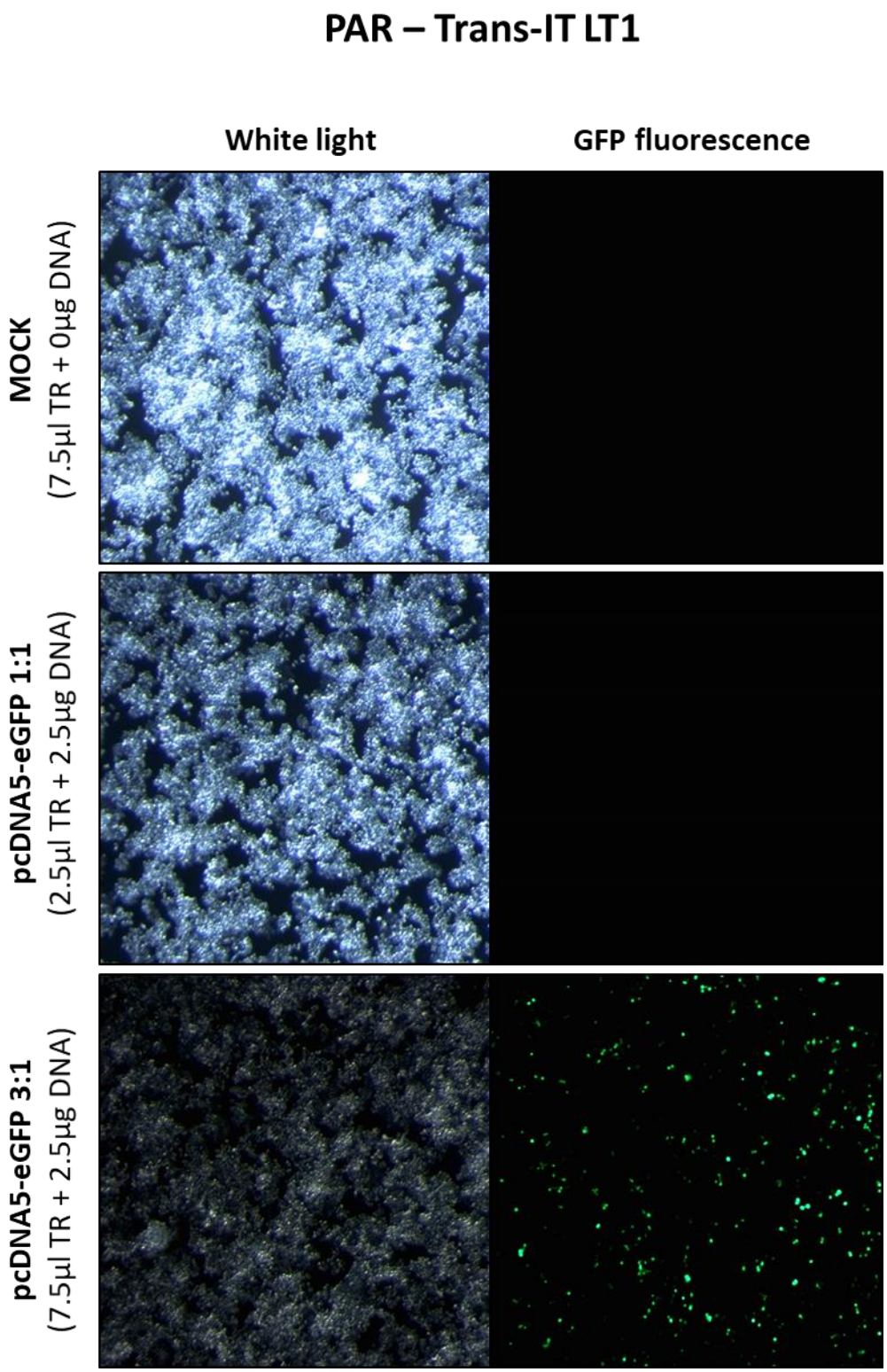

Figure 2.6 – Transfection of pcDNA5-FRT-eGFP in A2780 PAR cells using Trans-IT LT1.
PAR cells were plated, transfected and visualised as Figure 2.5, using Trans-IT as transfection reagent. 40X magnification.

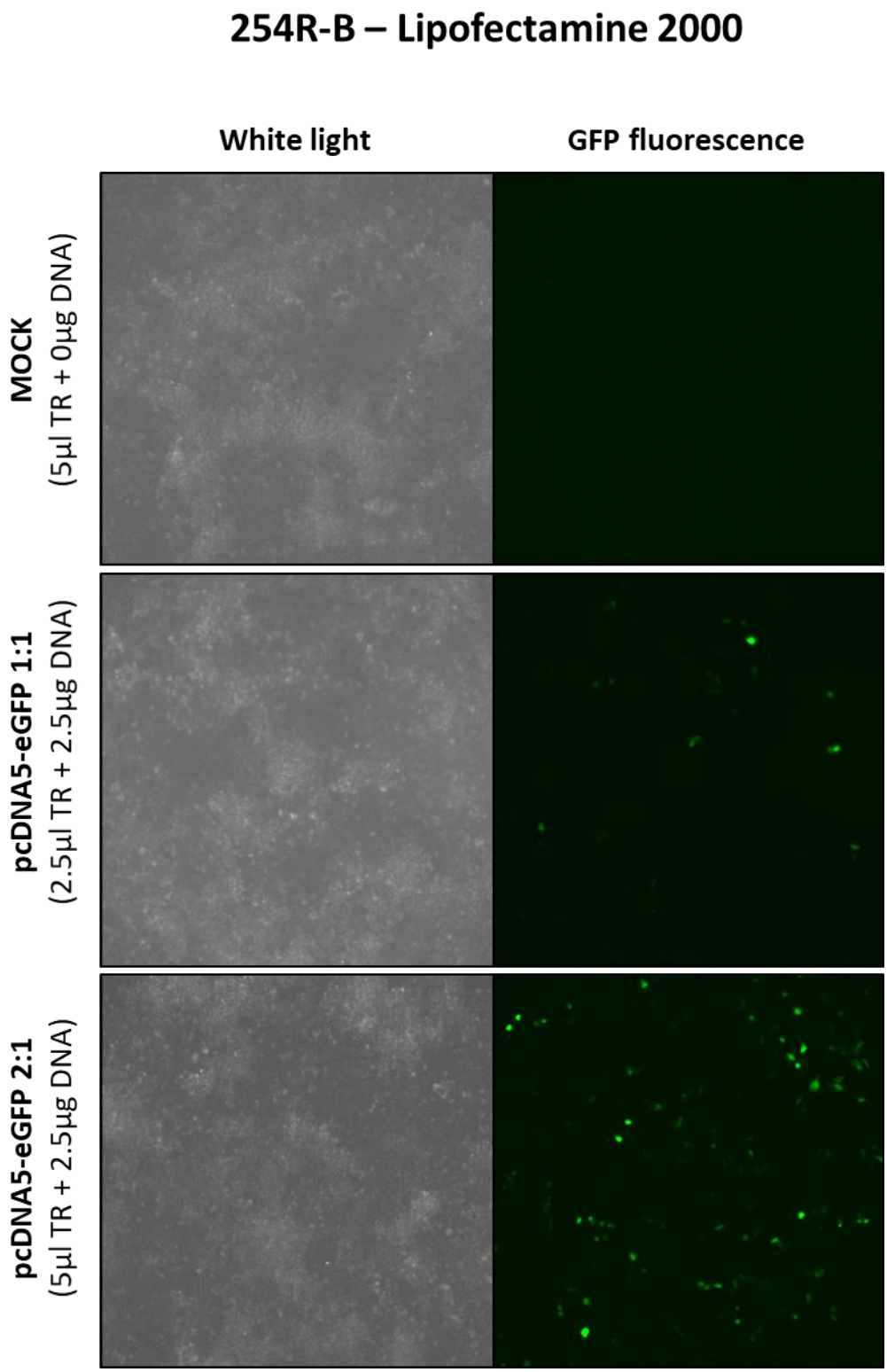

Figure 2.7 – Transfection of pcDNA5-FRT-eGFP in A2780 254R-B cells using Lipofectamine 2000. 254R-B cells were plated, transfected and visualised as Figure 2.5, using Lipofectamine 2000 as transfection reagent. 40X magnification.

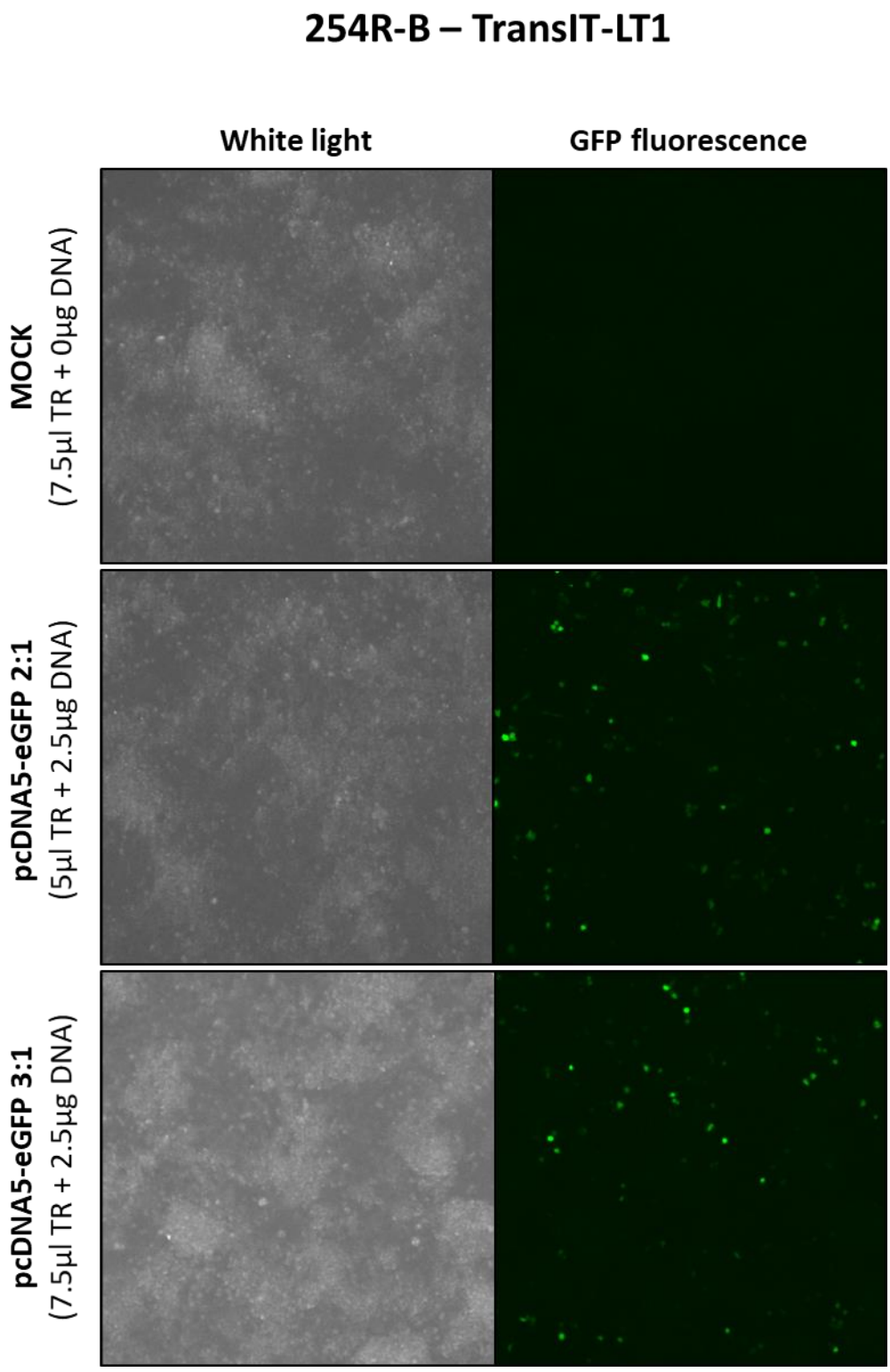

Figure 2.8 – Transfection of pcDNA5-FRT-eGFP in A2780 254R-B cells using Trans-IT LT1.
254R-B cells were plated, transfected and visualised as Figure 2.5, using Trans-IT LT1 as transfection reagent. 40X magnification.

2.7.3. Generation of stable over-expressing 4EBP1 cell lines

For stable expression of protein of interest (i.e. 4EBP1), transfected cells were treated with geneticin (G418) to select for cells with plasmid and geneticin resistance marker incorporated into the genome. Cells were plated at $5x10^5$ cells in T25 flasks and allowed to adhere overnight. 6.5µg plasmid DNA (pcDNA3, pcDNA3-4EBP1WT-HISMYC or pcDNA3-4EBP15A-HISMYC) was complexed with 18.75µl TransIT®-LT1 in OptiMEM GlutaMAX for 15-30 minutes, before addition to cells and allowed 48 hours incubation at normal growth conditions (section 2.2.1).

Transfected cells were subsequently trypsinised and cells were plated across all six wells of a 6-well plate and allowed to adhere for six hours. The cells were treated with a variety of concentrations of G418 (as determined by kill curve in section 2.7.4) between 0.25 and 1.5mg/ml under normal growth conditions, with drug-treated media replenished every 2-3 days until resistant populations developed. Mock transfected cells were run alongside transfected cells to identify when all remaining cells in plasmid transfected plates are resistant to G418.

Single colonies were isolated once reaching a sufficient colony size (approximately 1mm) within 11-21 days of plating. Culture medium was removed carefully by pipetting away from the colonies and transferred by sucking it up with a pipette tip pre-dipped in trypsin. Cells were resuspended in trypsin to break up the colony and immediately transferred to 500µl complete DMEM in a 24-well plate. At 70% confluency, cells were passaged to T25 flasks. After isolation of colonies, cells were maintained in half concentration of G418 used for their selection to ensure plasmid remained incorporated into the genome.

2.7.4. G418 kill curve

Cells were mock transfected with TransIT®-LT1 in T25 flasks as section 2.7.3 and RNAse-free dH_2O to replace plasmid DNA. Following plating into a 6-well plate, cells were drugged with 0.25, 0.5, 0.75, 1.0 and 1.5mg/ml G418. Drug-treated media was replenished every 2-3 days for a period of 10 days. Pictures of cells were taken using the Olympus CKX53 Inverted Microscope and GXCAM-U3-5 camera (Olympus, USA).

2.8. Cap-dependent protein synthesis assay

2.8.1. Dual luciferase reporter assay

A dual luciferase reporter assay was used to determine the relative level of cap-dependent mRNA translation through use of the bicistronic pRL-IRES-FL dual luciferase plasmid. The plasmid contains two luciferase genes, *Renilla* and firefly, separated by a polioviral IRES (Li *et al.*, 2002; Cope *et al.*, 2014). *Renilla* luciferase mRNA translation is an indicator of cap-dependent protein synthesis, whereas firefly luciferase mRNA translation is driven by IRES-mediated protein synthesis. *Renilla* expression was normalised to firefly luciferase expression as a control, in order to compare relative cap-dependent protein synthesis across transfected cells with differing transfection efficiencies.

Cells were plated at $1x10^5$ cells per well in six-well plates and allowed to adhere overnight. Cells were transfected with pRL-IRES-FL plasmid, pcDNA5-FRT-eGFP (transfection positive control) or RNAse-free ddH_2O (mock transfection) using TransIT®-LT1, as described in section 2.7.1. Cells were incubated in normal growth conditions for 48 hours post-transfection to allow gene expression before lysis.

Lysis and determination of luciferase expression was carried out as per manufacturer's instructions from the Dual-Luciferase Reporter Assay System (Promega, USA). For lysis, cells were washed twice with pre-chilled PBS, lysed and scraped in 250µl 1X Passive Lysis Buffer and collected in microcentrifuge tubes to incubate on ice for 15 minutes. Lysates were cleared by centrifugation at 14,000 x g for three minutes at 4°C, and either used immediately or snap-frozen and stored at -80˚C for later use. Protein concentration of cleared lysates was determined by BCA assay (section 2.4.2) and lysates were normalised to the same protein concentration in 1X Passive Lysis Buffer.

For the dual luciferase assay, 20µl of sample was pipetted into triplicate wells of opaque white-walled 96-well plates. To determine firefly luciferase levels, 100µl of Luciferase Assay Reagent II was added, and samples were mixed by pipetting up and down thrice. Luciferase activity as light emitted was immediately measured using

the default luciferase protocol on Victor X4 Multilabel Plate Reader (PerkinElmer Life Sciences, USA), utilising a one second measurement period. The firefly luciferase reaction was stopped and *Renilla* luciferase reaction initiated by adding 100µl Stop & Glo reagent and mixed thoroughly by pipetting. *Renilla* luciferase activity was immediately measured as described above.

Raw signals for *Renilla* and firefly were blank corrected with mock transfected cell lysate from the relevant cell line, and transfection efficiency ratio as calculated in section 2.8.2 was used to correct signals to the control (i.e. A2780 PAR) and observe comparative raw luciferase signals. Blank corrected *Renilla* values were normalised to blank corrected firefly luciferase signals in order to compare relative cap-dependent protein synthesis between A2780 PAR and resistant cells. Data analysis was performed in Microsoft Excel 2016.

2.9. Polysome Profiling

2.9.1. Cell lysis

Cells were plated at $15x10^6$ in T175 flasks and allowed to adhere overnight. At time of harvest, cells were spiked with cycloheximide to 0.1mg/ml final concentration and incubated for five minutes at 37°C. Culture medium was removed, and cells washed twice with ice-cold 0.1mg/ml cycloheximide in PBS. Ice-cold polysome profiling lysis buffer (300mM NaCl, 15mM Tris-HCl pH7.5, 15mM $MgCl_2$, 0.5% (v/v) TritonX-100, 5mM β-mercaptoethanol, 0.5mM phenylmethylsulfonyl fluoride (PMSF) and 0.1mg/ml cycloheximide in RNase/DNase free H_2O) was added and cells were scraped. Lysates were collected in pre-chilled RNase/DNase free microcentrifuge tubes and incubated on ice for five minutes. Lysates were cleared of insoluble material by centrifugation at 10,000 x g for three minutes at 4°C and were transferred to a fresh RNase/DNase free microcentrifuge tube and kept on ice for immediate use or snap-frozen on dry ice to store at -80°C. The protein concentration of lysates was determined using the BCA assay (section 2.4.2).

2.9.2. Polysome and sub-polysome separation by sucrose gradient and polysome profiling

1ml of each lysate was loaded onto separate 10-50% RNase/DNase free sucrose gradients (Acros Organics, USA; frozen when made and allowed to thaw and gradients diffuse overnight) in Beckman 14x96mm polyallomer tubes (Beckman Coulter, USA). These were centrifuged at 180,000 x g for 135 minutes at 4°C. Absorbance of gradient fractions were read at a wavelength of 254nm in a BR-188 Gradient Fractionation System (Brandel, USA) to draw a physical or digital trace over time. The traces were analysed either by importing the digital copy into Microsoft Excel 2016 software, or by scanning the hard copy using CanoScan LiDE120 (Canon., Japan), tracing in Inkscape and calculating the area under the curve using ImageJ software (Zuccotti and Modelska, 2016). The area under the curves were calculated separately to measure the relative sub-polysome and polysome percentages.

2.10. Knockdown of gene expression with small interfering RNA

2.10.1. siRNA knockdown

Transfection of small interfering RNA (siRNA) oligonucleotides was used to facilitate transient knockdown of target gene expression, using Lipofectamine 2000. The oligonucleotide sequences used to deplete gene expression are listed in Table 2.3. Oligonucleotide-lipid complexes were prepared (as per manufacturer's instructions) in OptiMEM GlutaMAX and incubated at RT for 15 minutes to allow for complex formation.

Meanwhile, cells were trypsinized and counted for reverse transfection. For 96-well plates, 50µl of oligonucleotide-lipid complex was added to each well before addition of $1x10^4$ cells in 110µl complete DMEM per well. Transfected cells were allowed 24 hours incubation in normal growth conditions for sufficient knockdown of target mRNA to take place, before drug treatment in 40µl per well (as SRB growth assay, section 2.4.2.) Cells were incubated for a further 72 hours in normal growth

conditions and plates were fixed, stained and analysed as SRB growth assay (section 2.4.2).

For analysis of protein knockdown levels by western blot, cells were transfected in three 6-well plates with 0.5ml oligonucleotide/lipid mixture and 1.1ml of $3x10^5$ cells per well and 400µl complete DMEM was added at time of 96-well plate drug treatment. Cells were harvested at 24 hours (96-well plate drug treatment), 48 hours (optimal knock down) and at 96 hours (SRB assay end time point) post reverse-transfection and analysed by western blot as described in section 2.5.

2.10.1. siRNA knockdown optimisation

To ensure the greatest target gene knockdown with limited toxicity (Chapter 6), transfection conditions such as cell seeding concentrations and transfection reagent percentage were optimised. Several transfection reagents including HiPerFect (QIAGEN, Germany), TransIT®-X2 (Mirus Bio, USA) and Lipofectamine 2000 (Life Technologies, USA) were tested at a range of 0.1-0.4% 5nM and 20nM Death control oligonucleotides (QIAGEN, USA) were transfected as a means of determining transfection efficiency, and mock transfection (RNAse-free water) and non-targeting oligonucleotides were used as a negative control to investigate toxicity of transfection reagent conditions.

Preliminary optimisation was carried out over three seeding concentrations of PAR cells: 4,000, 8,000 and 16,000 cells per well across all three transfection reagents.

The results in Figure 2.9 show that across all transfection reagents and seeding concentrations, an increase in titrated transfection reagent increased toxicity. At 4,000 cells per well, the culture viability of mock and NT transfected cells was reduced by at least 50% with the lowest concentration (0.1%) of either Lipofectamine 2000 or TransIT-X2. Although minimal toxicity was witnessed at 0.1% with HiPerFect (84% culture viability), the culture viability with either death oligonucleotide concentration was high (62-72% culture viability), indicating poor transfection efficiency at 4,000 cells per well.

At greater seeding concentrations, less toxicity with mock or NT transfection was witnessed for all transfection reagents. HiPerFect was again the least toxic of all lipids, regardless of concentration (55-98%), however it again exhibited the lowest growth inhibition with transfection of the death oligonucleotide. At 16,000 cells per well, HiPerFect exhibited no window between the mock, NT and the death oligonucleotide controls at 0.1-0.2% lipid. TransIT-X2 was less toxic than Lipofectamine 2000, and comparatively transfected 25nM death oligonucleotide more effectively than HiPerFect, however the transfection efficiency of the 5nM death oligonucleotide was poor, exhibiting no greater reduction in culture viability than the mock and NT controls. Although Lipofectamine 2000 was toxic at 4,000 cells per well, it appeared to have the greatest toxicity-effectivity window of all lipids at 8,000 (0.1% lipid) and 16,000 (0.2% lipid) cells per well seeded with a 57-59% difference in culture viability between mock and NT controls and death oligonucleotides. Therefore Lipofectamine 2000 was taken forward for further optimisation.

As large toxicity-effectivity windows existed for transfections for both 8,000 and 16,000 cells per well seeding concentrations at 0.1-0.2% Lipofectamine 2000, the seeding concentration was further optimised – investigating 10,000 and 13,000 cells per well. Figure 2.10 shows that both seeding concentrations exhibited larger toxicity-effectivity windows, particularly at 0.1% Lipofectamine. However, the culture viability of the mock and NT controls with 0.2% Lipofectamine 2000 was reduced from 82-89% with 16,000 cells per well to 54-69% with the lower concentrations. Figure 2.11**Error! Reference source not found.** presents a summary of the toxicity and effectivity of 0.1% Lipofectamine 2000 across the seeding concentrations tested in Figures 2.9 and 2.10. The greatest window was observed with a seeding concentration of 10,000 cells per well, with a culture viability of at least 95% for the mock and NT controls, and less than 13% for both death oligonucleotide controls. Therefore, the optimal conditions for PAR siRNA transfection were defined as 0.1% Lipofactamine 2000 and seeding 10,000 cells per well.

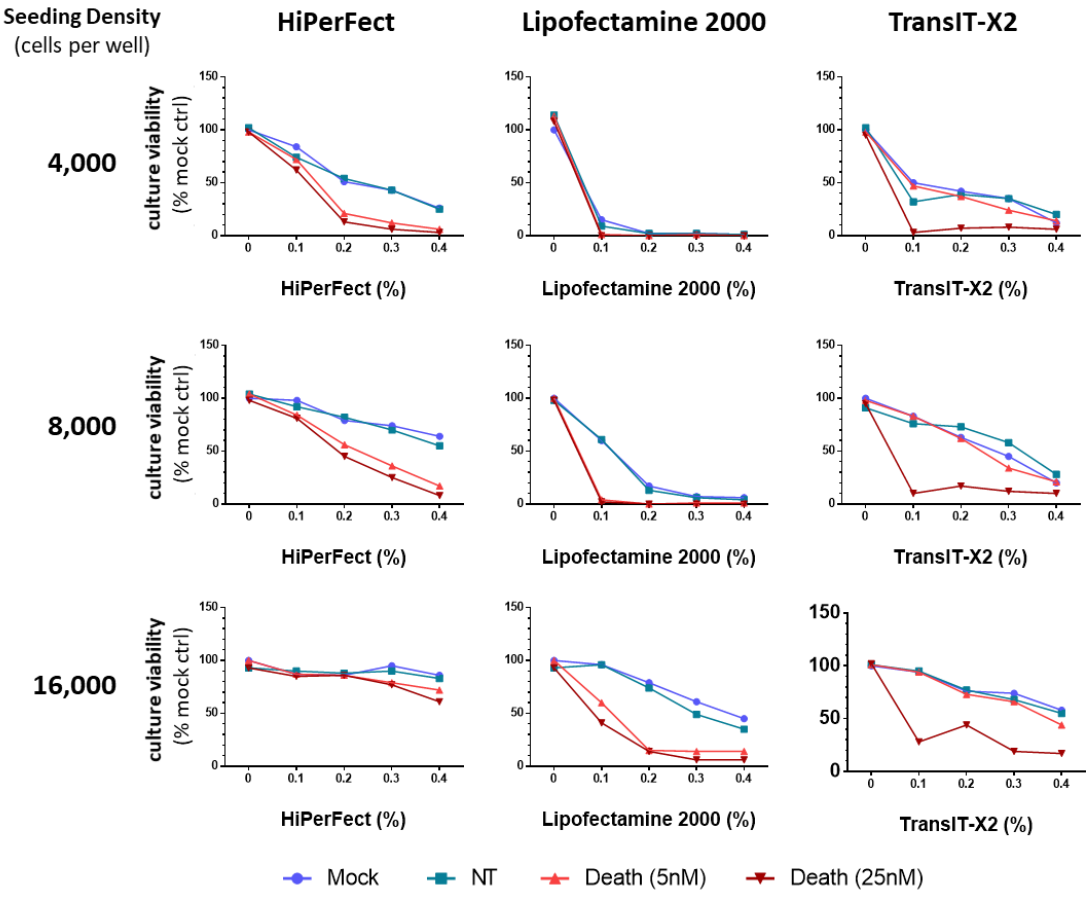

Figure 2.9 – Determining optimal transfection reagent for siRNA knockdown studies in PAR cells
A2780 PAR cells plated at 4,000 (top row), 8,000 (middle row) or 16,000 (bottom row) cells per well were reverse transfected with HiPerFect (left column), Lipofectamine 2000 (middle column) or TransIT-X2 (right column) at the concentrations indicated, with RNAse free water (mock), 25nM non-targeting Allstarnegative control oligonucleotide (NT), or 5 or 25nM Allstar positive control oligonucleotide (Death). After 96 hours cells were subsequently fixed and analysed using the SRB culture viability assay. All data were normalised to the mock untransfected control (0% transfection reagent) and analysed using GraphPad Prism 6.

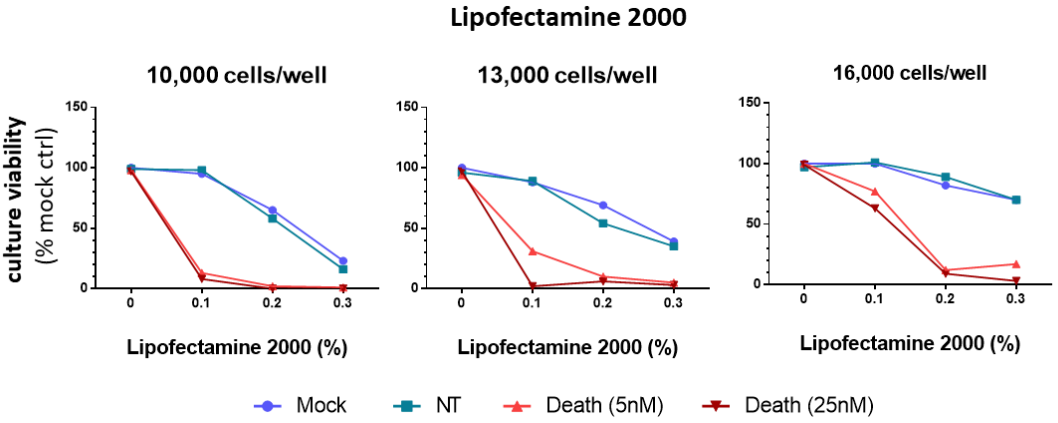

Figure 2.10 – Optimisation of PAR seeding concentration with lipofectamine 2000 reagent
A2780 PAR cells plated at 10,000 (left), 13,000 (middle) or 16000 (right) cells per well were reverse transfected with Lipofectamine 2000 (middle) at the concentrations indicated with oligonucleotides as Figure 2.9. SRB growth assay was performed and analysed as Figure 2.9.

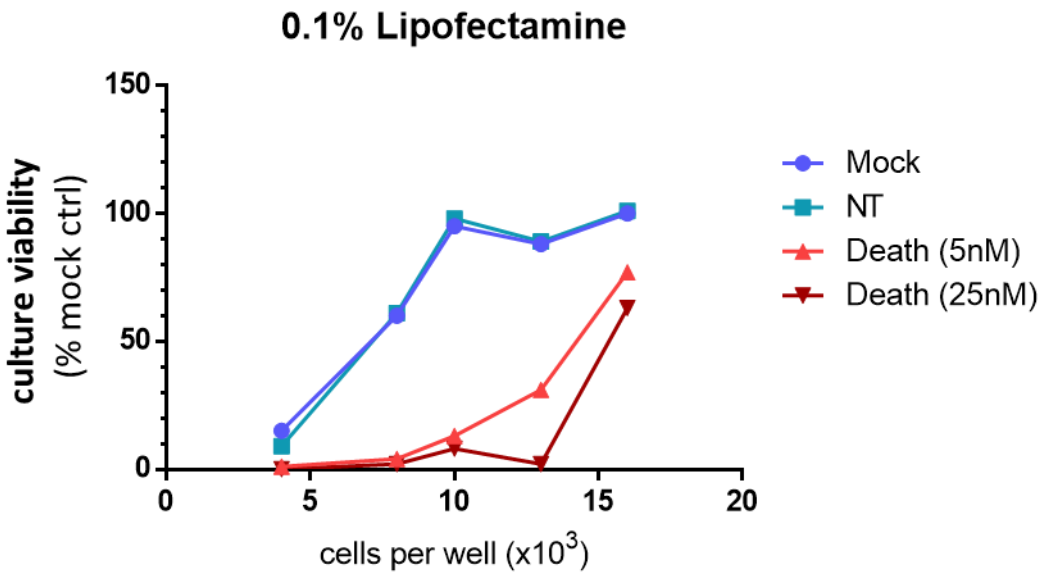

Figure 2.11 – Transfection efficiency and toxicity at 0.1% Lipofectamine across seeding concentrations
The effect on culture viability of A2780 PAR cells across the seeding concentrations investigated in Figure 2.9 and 2.10, after reverse-transfection with 0.1% Lipofectamine 2000.

After optimisation of cell seeding concentration and transfection reagent percentage, target gene knockdown was optimised. Reverse transfection of gene targeting oligonucleotides was performed as section 2.9.1 in 6 well plates with concentrations of 1, 3, 10 and 30nM.

Initially, three 4EBP1-targeting oligonucleotides were tested for their ability to knockdown 4EBP1 levels at two concentrations 3nM and 10nM after 48 hours. The oligonucleotides were Stealth, Flexitube 2 and Flexitube 5 and their targets on 4EBP1 mRNA are indicated on Figure 2.12A. The optimised reverse transfection conditions were scaled up to 6-well dishes to yield sufficient protein for western blotting. Figure 2.12B showed that the NT control transfection did not reduce 4EBP1 levels, compared with the mock transfection control. All three oligonucleotides tested reduced the expression of 4EBP1. Flexitube 5 gave the greatest reduction in 4EBP1 levels, especially at 10nM. Flexitube 2 exhibited some knockdown of 4EBP1 but not to the same level as Flexitube 5. The Stealth oligonucleotide gave the least effective knockdown. Therefore, Flexitube oligonucleotides 2 & 5 were taken forward for 4EBP1 siRNA knockdown in Chapter 6.

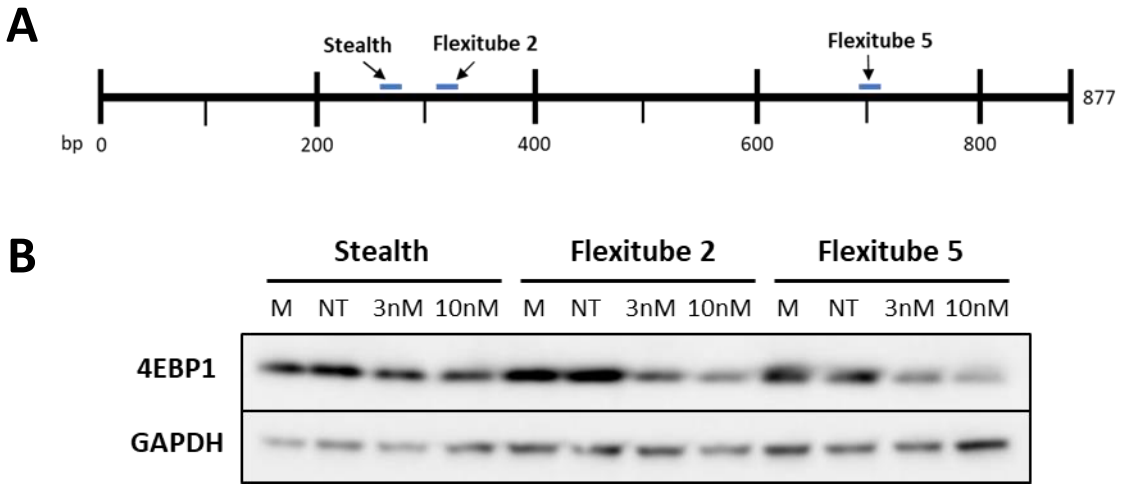

Figure 2.12 – Optimisation of 4EBP1 oligonucleotide knockdown
(A) Schematic of the regions of 4EBP1 mRNA where the 4EBP1 oligonucleotides, Stealth, Flexitube 2 and 5 target. (B) Western blot analysis of 4EBP1 knockdown with 4EBP1 oligonucleotides. A2780 PAR cells were reverse transfected with RNAse free water (mock; M), 25nM non-targeting Allstar negative control oligonucleotide (NT), or 4EBP1 oligonucleotide (Stealth, Flexitube 2 or 5) at concentrations indicated. Reverse-transfection was performed using 0.1% Lipofectamine 2000 in 6-well plates and incubated for 48 hours. Cells were subsequently lysed and analysed by western blotting. Lysate proteins were separated by SDS-PAGE, transferred to PVDF membranes and probed with antibodies against phosphorylated proteins and developed. Membranes were probed with antibodies as indicated. GAPDH was used as a loading control.

Chapter 3

Identification of candidate drivers of resistance to capivasertib in A2780 254Rp

3. Identification of candidate drivers of resistance to capivasertib in A2780 254Rp cells

3.1. Introduction

The majority of deaths from cancer are due to the failure of treatment by drug resistance, which is as high as 90% in metastatic cancers (Longley and Johnston, 2005). Despite the development of novel molecular-targeted therapies, drug resistance remains a major barrier to their success as well.

There are many research groups looking to identify mechanisms of drug resistance, and there are several methods by which to do this. Characterisation of patient-derived samples would be the ideal method to provide the most clinically relevant mechanisms. However, due to logistical issues, patient-derived samples may not necessarily be the most practical model. Regardless, these clinical samples have been applied to validate the clinical relevance of mechanisms identified through *in vitro* based methods (Nazarian *et al.*, 2010; Garraway and Jänne, 2012). The most common methodologies are the use of functional genomics; bioinformatic screens and comparative characterisation of isogenic and non-isogenic resistant cell lines (Garraway and Jänne, 2012).

Isogenic cell lines were used for this project, and may be acquired in two ways: 1) mimicking the cyclic treatment of chemotherapy by short-term pulsing of cells with a clinically relevant concentration of inhibitor over an extended period of time or, 2) by the dose-escalation method (Garraway and Jänne, 2012; McDermott *et al.*, 2014). Although 1) is the most clinically relevant method for generating acquired resistant populations, the resistance is often low and transient (McDermott *et al.*, 2014). The dose escalation method frequently generates resistance which is higher and more stable and thus more practical for investigation. Although this method is clinically artificial in comparison, it is a proven successful means of identifying clinically relevant resistance mechanisms (Nazarian *et al.*, 2010).

This thesis sets to carry on the work initiated by Dr Denis Akan (Akan, 2015) to identify candidate resistance mechanisms to capivasertib. The isogenic A2780 254Rp cell line was generated by dose escalating the heterogenetic A2780 parental (PAR) cells with the capivasertib-analogue, CCT129254 over time and monitored for increase in half-maximal growth inhibition concentrations (GI_{50}) to the drug. After 6 months, the resistant subpopulation GI_{50} to CCT129254 was twenty times greater than the original PAR line. The cells were also cross-resistant to capivasertib. A2780 254Rp showed no cross-resistance to cytotoxic chemotherapeutics, nor overexpressed MDR1 (multidrug resistance protein 1), compared to PAR, which thus suggested resistance was not due to a general drug-efflux mechanism. A2780 254Rp did exhibit resistance to multiple AKT, PI3K and mTORC inhibitors and changes in the baseline phosphorylation of S473 and T308 of AKT, indicative of increased activation. Sequencing of AKT isoforms observed no mutations between PAR and 254Rp. Exome sequencing identified a novel mutation in PHLPP1, an AKT and p70S6K phosphatase, however knockdown of PHLPP1 alone in PAR cells did not induce capivasertib resistance. Baseline expression of p70S6K was increased and 4EBP1 was decreased in the 254Rp cell line, and phosphorylation of both proteins was resistant to AKT inhibition by MK-2206 and CCT129254, but not to the mTORC inhibitors everolimus or vistusertib. The resistant cell line exhibited reduced 4EBP1 binding with eIF4E and concomitant increase in eIF4G to eIF4E binding and cap-dependent protein synthesis. As p70S6K and 4EBP1 are both mTORC1 substrates, the data taken together suggested that mTORC1 activity was increased in A2780 254Rp, resulting in increased cap-dependent protein synthesis driving acquired resistance to capivasertib (Akan, 2015).

This aim of this chapter was to validate the mTORC1 hyperactivity in A2780 254Rp cells as observed by Dr Akan and identify the acquired mechanism driving the mTORC1 hyperactivity and resistance to capivasertib.

3.2. Results

3.2.1. Investigation of morphology of A2780 PAR and 254Rp cell lines

Examining cellular morphology is a simple and direct way of characterising cells and can easily highlight any distinct changes between cell lines, which may be the phenotypic result of the resistance mechanism. An example is the epithelial to mesenchymal transition (EMT; Beaufort et al., 2014; Haslehurst et al., 2012).

Figure 3.1A shows the morphology of the A2780 PAR and 254Rp. Figure 3.1B also presents the morphology data in a quantifiable way, through the average number of protrusions per cell in a population. Both PAR and 254Rp cell lines were adherent and regularly shaped with few protrusions, consistent with epithelial-like cells such as A2780 (Haslehurst *et al.*, 2012). The individual cells of the PAR cell line were generally more rounded and appeared 'pebble-like', with on average 1.4 protrusions per cell. The untreated 254Rp cells (254Rp [UT]), were more polygonal in shape with on average 1.6 protrusions per cell.

254Rp were maintained in 56μM of CCT129254, to ensure retention of resistance mechanisms. This was the maximum concentration used in generation of this isogenic cell line by Dr Denis Akan (Akan, 2015). When maintained in CCT129254 (254Rp (T)), the cells exhibited a very flat morphology across the dish, with a greater number of protrusions per cell (2.6), compared with 254Rp (UT).

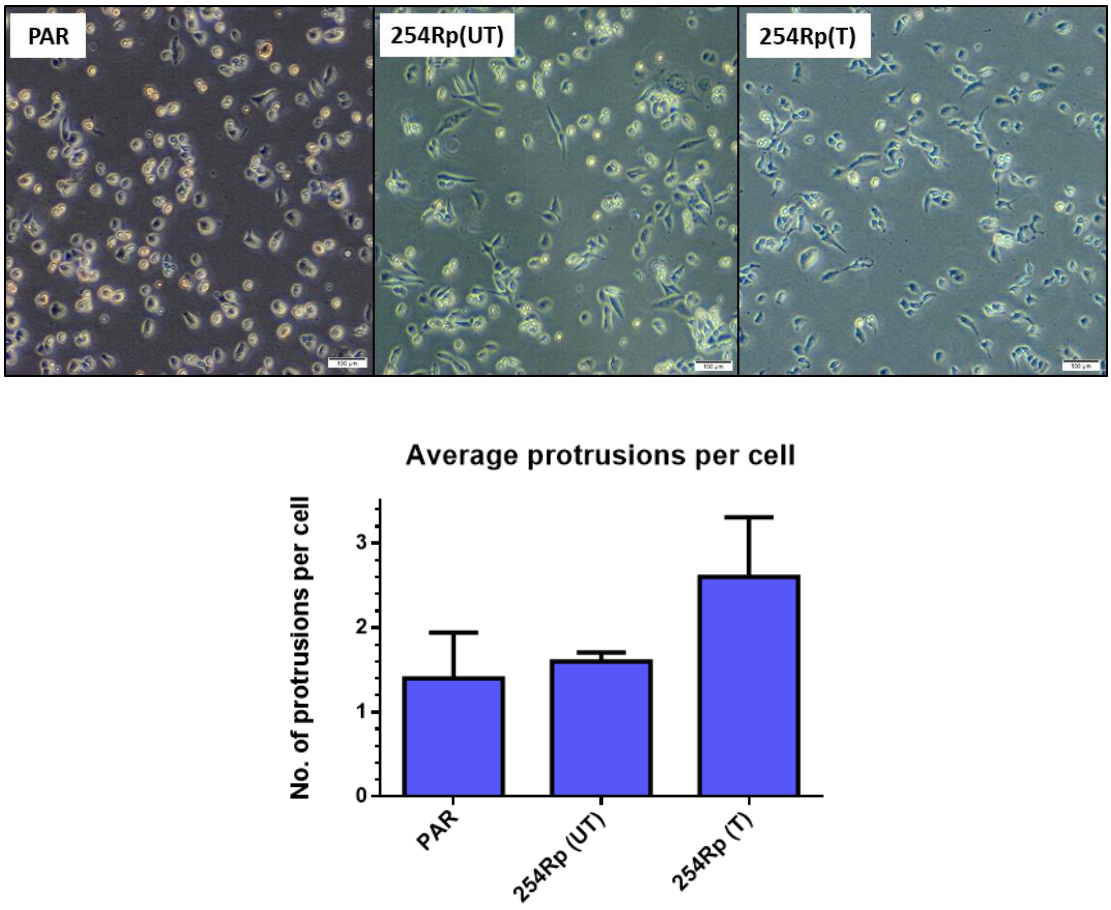

Figure 3.1 – Morphology of A2780 PAR and 254Rp cell lines.
(A) Morphology of A2780 PAR and 254Rp cell lines at 40x magnification, phase contrast. Cells were plated to the same cell concentration ($5x10^5$ cells in T25 flask) and left to adhere for 24 hours. UT= released from maintenance in CCT129254 for one week, T = maintained in 56µM CCT129254. Scale bar indicates 100µm. Representative of two repeats. (B) Bar chart of average protrusions per cell.

3.2.2. Profiling of A2780-254Rp cell line sensitivity to PAM inhibition

The A2780 254Rp cell line was generated by Dr Denis Akan (Akan, 2015) using CCT129254, an analogue of capivasertib. The cross-resistance of 254Rp to capivasertib was therefore investigated to confirm this cell line as a relevant model for identifying resistance mechanisms to the drug.

GI_{50} determinations for the PAR and 254Rp cell lines were carried out using the SRB growth assay. The wells were plated at the optimised seeding concentration (800 cells per well) and incubated with a serial dilution of inhibitor for 96 hours, and the percentage of remaining surviving cells was determined using the SRB dye (Skehan *et al.*, 1990). The GI_{50} was determined as the concentration by which the percentage of remaining cells was 50% of the untreated control. The ratio of 254Rp

GI_{50} to PAR GI_{50} was used to calculate the Resistance Factor (RF) and defined the level of resistance in 254Rp.

$$Resistance\ Factor\ (RF) = \frac{254Rp\ GI_{50}}{PAR\ GI_{50}}$$

As shown in the example dose response curves in Figure 3.2, the 254Rp cell line showed a clear difference in GI_{50} concentration to CCT129254 (15.73µM) compared with PAR (0.71µM), resulting in an RF value of 23.2. There was an even greater fold resistance to capivasertib, with a PAR GI_{50} of 0.11µM and 254Rp GI_{50} of 10.92µM, corresponding to nearly 100-fold resistance. This indicated that the 254Rp cell line was resistant to both CCT129254 and its analogue capivasertib and was thus confirmed to be a relevant model for identifying mechanisms of capivasertib resistance.

A

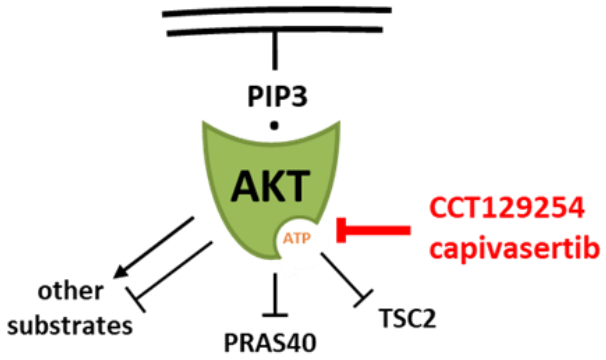

B

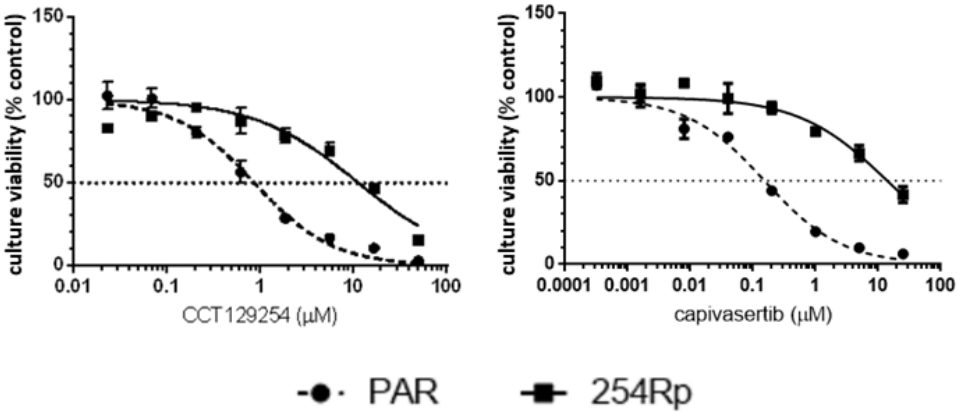

C

Drug	Target	GI_{50} (μM)		RF	N
		PAR	254R		
CCT129254	AKT (ATP-competitive)	0.71 ± 0.12	15.73 ± 4.15	**23.20*****	6
capivasertib AZD5363	AKT (ATP-competitive)	0.11 ± 0.03	10.92 ± 2.48	**99.77****	4

Figure 3.2 – Determination of resistance of A2780 254Rp cells to CCT129254 and capivasertib.
(A) A simplified schematic to show the target of capivasertib and its close analogue CCT129254 to the ATP-binding pocket of AKT. Pointed arrows indicate activation, block-head arrows indicate inhibition. PIP3 = PtdIns(3,4,5)P3. Periods (.) indicate protein interaction and binding. (B) Representative dose response curves for CCT129254 (left) and capivasertib (right). A2780 PAR and 254Rp cells were treated with serially diluted concentrations of drug for 96 hours and surviving cells were determined by SRB growth assay. Dose response curves generated and half-maximal growth inhibition concentrations (GI_{50}) were calculated using GraphPad Prism 6. Data points present mean ± SD of three technical replicates. The broken line on the Y-axis indicates the points on the curves where growth was inhibited by 50% (GI_{50}). Data representative of ≥four independent experiments. (C) Summary of GI_{50} concentrations and resistance factors (RF) to CCT129254 and capivasertib in A2780 PAR and 254Rp cells. GI_{50} values presented as mean ± SD of GI_{50} values from ≥four independent experiments. Resistance Factors (RF) presented as mean RF of ≥four independent experiments. Individual independent RF values calculated as the ratio of 254Rp GI_{50} to PAR GI_{50}. N = number of independent experiments. Statistics: Unpaired t test with Welch's correction of 254Rp to PAR GI_{50} values, *p<0.05, **p<0.01, ***p<0.001, N.S = non-significant. Values rounded to two decimal places.

Alteration of the drug target is one of the simplest resistance mechanisms that can reactivate the drug-targeted pathway (Konieczkowski *et al.*, 2018). Previous studies show that alterations in AKT lead to resistance to AKT inhibitors (Carpten *et al.*, 2007; Stottrup *et al.*, 2016). As 254Rp showed cross-resistance to capivasertib, cross-resistance profiling with other AKT inhibitors (ipatasertib and MK-2206) was investigated.

Ipatasertib (GDC-0068) is an ATP-competitive kinase inhibitor of AKT (Figure 3.3A; Blake *et al.*, 2012; Lin *et al.*, 2013) which is currently in Phase III clinical trials as a combination therapy with paclitaxel, abiraterone or palbociclib, particularly in breast and prostate cancers. Tumour populations with hyperactive PAM pathway signalling showed the greater sensitivity (*clinicaltrials.gov*; Tabernero *et al.*, 2011). The structure of ipatasertib is similar to capivasertib (Figures 1.9 and 1.10), so it is therefore unsurprising that 254Rp showed significant cross-resistance to ipatasertib (Figure 3.3) with a GI_{50} of 6.33µM compared with a PAR GI_{50} of 0.14µM, which equated to nearly 50-fold resistance.

MK-2206 is a non-ATP-competitive allosteric AKT inhibitor. It is highly selective for AKT and induces a 'closed' conformational change in the kinase to inhibit both its activation and activity (Lindsley, 2010; Mundi *et al.*, 2016). It is currently in Phase II clinical trials (*clinicaltrials.gov*). Interestingly, 254Rp was also significantly resistant to allosteric AKT inhibition by MK-2206 (Figure 3.3), with a GI_{50} value of 2.17µM compared with a PAR GI_{50} of 0.08µM, corresponding to a 27.2-fold RF.

Taken together, these data showed that 254Rp cells were resistant to AKT inhibitors despite inhibition by two different methods.

A

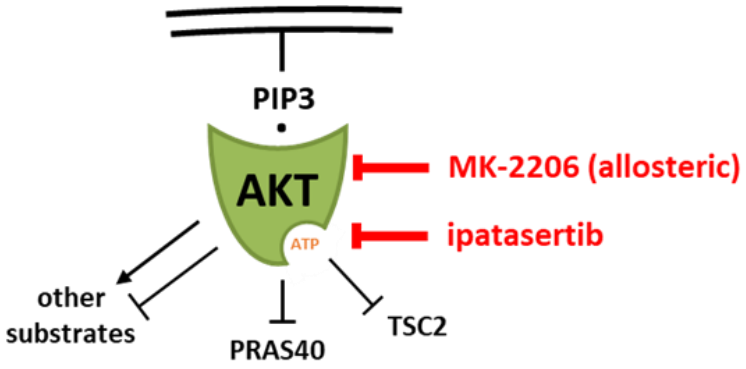

B

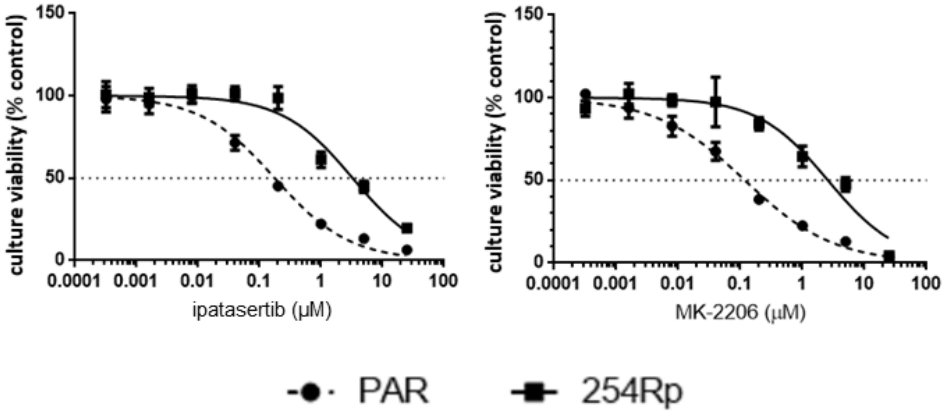

C

Drug	Target	GI_{50} (μM)		RF	N
		PAR	254R		
ipatasertib GDC-0068	AKT (ATP-competitive)	0.14 ± 0.03	6.33 ± 2.21	**49.82****	5
MK-2206	AKT (allosteric)	0.08 ± 0.02	2.17 ± 1.09	**27.19***	4

Figure 3.3 – Determination of resistance of A2780 254Rp cells to ipatasertib and MK-2206.
(A) A simplified schematic to show the target of the ATP-competitive inhibitor ipatasertib to the ATP-binding pocket of AKT and allosteric inhibitor MK-2206, through blocking the binding of AKT to PtdIns(3,4,5)P_3 (PIP3). Pointed arrows indicate activation, block-head arrows indicate inhibition. Periods (.) indicate protein interaction and binding. (B) Representative dose response curves for ipatasertib (left) or MK-2206 (right), as Figure 3.2. Data representative of ≥four independent experiments. (C) Summary of GI_{50} concentrations (GI_{50}) and resistance factors (RF) to MK-2206 and ipatasertib in A2780 PAR and 254Rp cells, analysed and formatted as Figure 3.2.

The most common resistance mechanisms to targeted therapies are those that reactivate the originally inhibited signalling pathway (Konieczkowski *et al.*, 2018). To further investigate whether the resistance mechanism may circumvent AKT activity by reactivating the PAM pathway, cross-resistance to inhibitors of other nodes of

the PAM pathway was examined, including PI3K inhibition with pictilisib (GDC-0941) and mTORC inhibitors everolimus (RAD001) and vistusertib (AZD2014).

Pictilisib is an ATP-competitive pan-class I PI3K inhibitor (Folkes *et al.*, 2008), targeting upstream of AKT. As observed in Figure 3.4, 254Rp was resistant to pictilisib showing a 9.8 fold increase in GI_{50} (21.8μM) compared to PAR (162.7μM).

Everolimus is an allosteric inhibitor of the mTOR complex 1 (mTORC1; Schuler *et al.*, 1997; Sedrani *et al.*, 1998). It is an analogue of rapamycin (rapalogue) and acts with a similar mechanism of action by forming a complex with FKBP12 which can bind to the FKBP12-rapamycin-binding (FRB) domain of mTOR and inhibit substrate recruitment to mTORC1 by steric hinderance (Yip *et al.*, 2010; Aylett *et al.*, 2016). Vistusertib is an ATP-competitive mTOR kinase inhibitor and negates the activity of both mTOR complexes 1 and 2 (Pike *et al.*, 2013). Figure 3.4 shows that 254Rp cells exhibited resistance to both inhibitors, however the cells were more resistant to inhibition of both complexes by vistusertib (4.6 RF) than mTORC1 specific inhibition by everolimus (2.8 RF).

As 254Rp cells were identified as resistant to mTORC1 inhibition, cross-resistance to inhibitors targeting downstream of this complex was investigated. Two of the best studied substrates are p70S6K and 4EBP1, both of which are involved in cap-dependent protein synthesis (CDPS; Wang and Proud, 2011; Huang and Fingar, 2014). Therefore, the response to the CDPS inhibitors, 4EGI-1 and MRT00206081 was investigated.

As illustrated in Figure 3.5A, 4EGI-1 is an inhibitor of the binding of eIF4E and eIF4G directly (Moerke *et al.*, 2007) and also indirectly by enhancing 4EBP1 activity to sequester eIF4E (Sekiyama *et al.*, 2015). Wang *et al.*, 2015 suggests it weakly targets mTORC1 as well. MRT00206081 is a selective MNK inhibitor kindly donated by Andy Merritt and Ed McIver from MRC Technology. Interestingly, no cross-resistance was observed to 4EGI-1 or MRT00206081, with resistance factors below 2-fold (1.4 and 1.7 RF respectively; Figure 3.5).

A

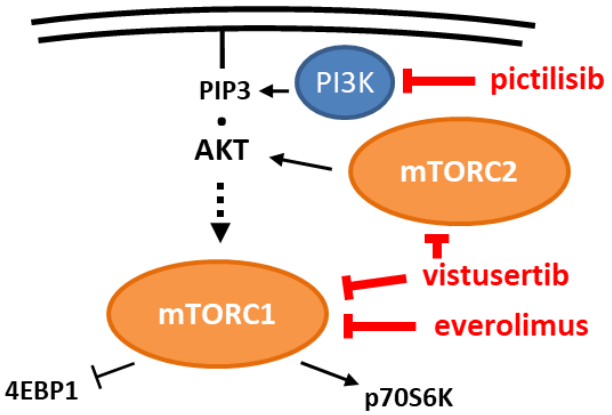

B

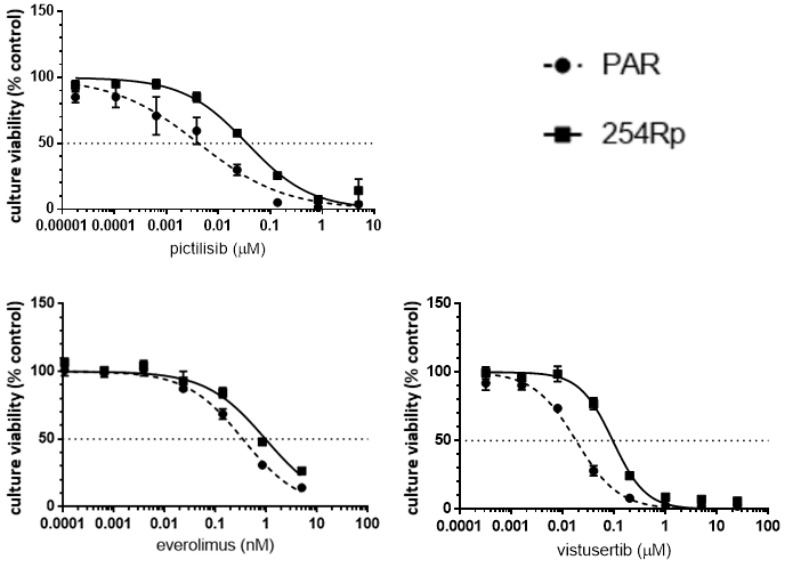

C

Drug	Target	GI_{50} (nM)		RF	N
		PAR	254Rp		
pictilisib GDC-0941	pan PI3K class I	21.80 ± 4.48	162.65 ± 76.23	**9.76***	3
everolimus RAD-001	mTORC1 only (substrate recruitment)	0.64 ± 0.22	1.77 ± 0.77	**2.78***	4
vistusertib AZD2014	mTORC1/2 (ATP-competitive)	12.99 ± 2.78	59.48 ± 24.27	**4.58***	4

Figure 3.4 – Determination of resistance of A2780 254Rp cells to PI3K and mTOR inhibitors.
(A) A simplified schematic to show the target of the mTORC1 specific rapalogue everolimus, mTOR kinase inhibitor vistusertib and PI3K inhibitor pictilisib. Pointed arrows indicate activation, block-head arrows indicate inhibition. Periods (.) indicate protein interaction and binding. (B) Representative dose response curves for pictilisib (top left), everolimus (bottom left) or vistusertib (bottom right), as Figure 3.2. Data representative of ≥three independent experiments. (C) Summary of GI_{50} concentrations (GI_{50}) and resistance factors (RF) to pictilisib, everolimus or vistusertib in A2780 PAR and 254Rp cells, analysed and formatted as Figure 3.2.

A

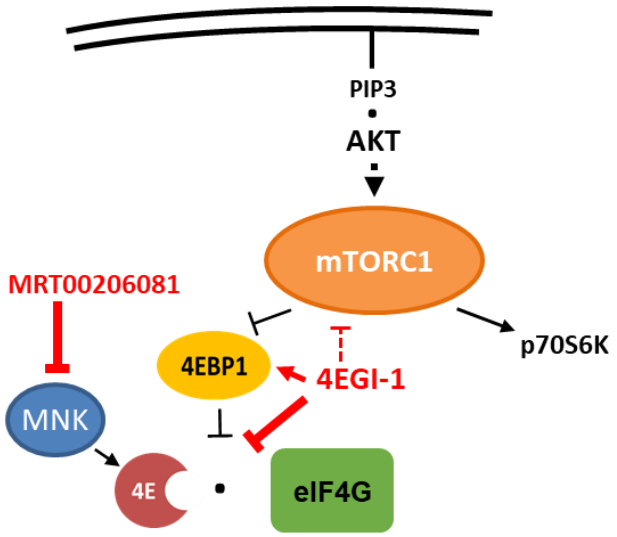

B

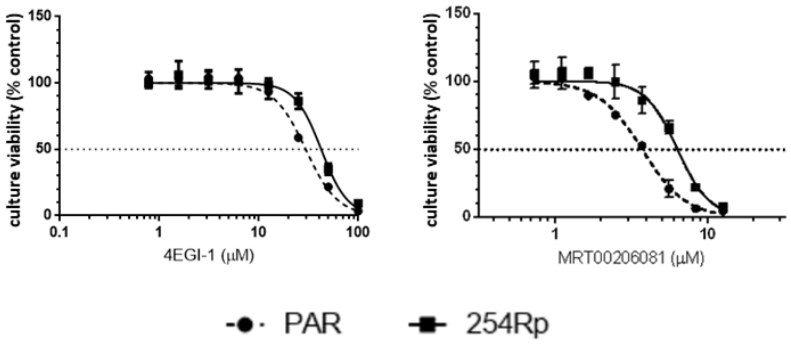

C

Drug	Target	GI_{50} (μM)		RF	N
		PAR	254Rp		
4EGI-1 (μM)	eIF4E/4G assembly	21.79 ± 6.89	31.33 ± 9.66	**1.44**$^{N.S}$	3
MRT00206081 (μM)	MNK1/2	4.65 ± 1.22	7.97 ± 2.43	**1.70**$^{N.S}$	3

Figure 3.5 – Determination of resistance of A2780 254Rp cells to protein synthesis inhibitors
(A) A simplified schematic to show the target of the eIF4E/eIF4G interaction inhibitor 4EGI-1, and MNK inhibitor MRT00206081. Pointed arrows indicate activation, block-head arrows indicate inhibition. Periods (.) indicate protein interaction and binding. (B) Representative dose response curves for 4EGI-1 (left), and MRT00206081 (right), formatted as Figure 3.2. Data representative of ≥three independent experiments. (C) Summary of GI_{50} concentrations (GI_{50}) and resistance factor (RF) values to 4EGI-1 and MRT00206081 in A2780 PAR and 254Rp cells, analysed and formatted as Figure 3.2.

Figure 3.6 shows a comparative summary of the resistance factors for all drugs tested. 254Rp cells were significantly resistant to AKT inhibitors (23-100 RF), less

resistant to PI3K and mTORC inhibitors (3-10 RF), whereas no significant cross resistance was observed with protein synthesis inhibitors.

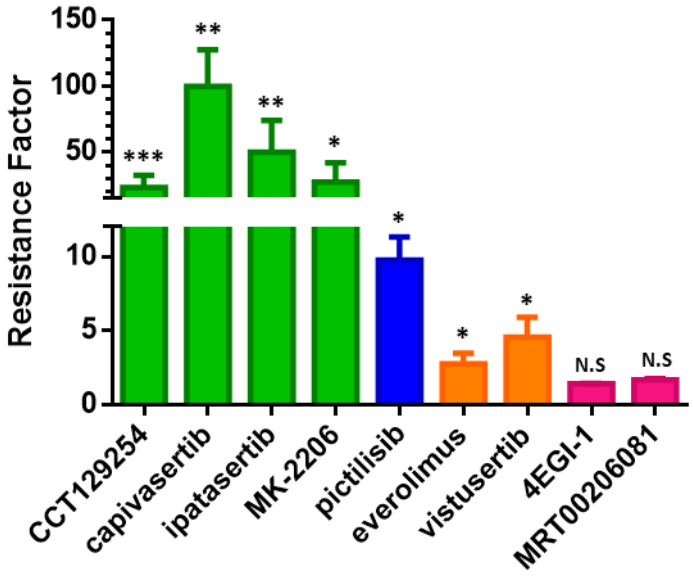

Figure 3.6 – Graphical summary of resistance factors of A2780 254Rp cells.
Bar chart representing mean and error bars as SD for 254Rp RF values for all AKT (green), PI3K (blue), mTORC (orange) and protein synthesis (pink) inhibitors investigated in chapter 3.2. Mean RF values and SD calculated as average of RF values and SD from ≥ three individual experiments. Individual RF values calculated as ratio of 254Rp GI_{50} to PAR GI_{50}. Statistics as calculated in Figure 3.2.

3.2.3. PAM pathway signalling in A2780 PAR and 254Rp cells

Cross-resistance to inhibitors of mTORC1 but not CDPS (Figure 3.6) suggested that the resistance mechanism may involve signalling downstream of mTORC1. Therefore, PAM pathway signalling proximal to mTORC1 was investigated by western blotting.

Clear differences in the baseline levels of phosphorylation were observed in several components of the PAM pathway (Figure 3.7). There was a small decrease in AKT phosphorylation at serine 473 (S473) between PAR and 254Rp, which is phosphorylated by mTORC2 and is indicative of decreased maximal activity of AKT (Pearce *et al.*, 2010). This may cause the reduction in serine 9 (S9) phosphorylation on GSK-3β but was not reflected in reduced signalling at threonine 246 (T246) of PRAS40; both direct substrates of AKT.

The most significant changes in signalling were downstream of mTORC1. There was a marked increase in phosphorylation of serine 235 and 236 (S235/6) of S6RP (S6 ribosomal protein), which is phosphorylated by p70S6K (p70 ribosomal S6 kinase) and p90RSK (p90 ribosomal S6 kinase; Roux *et al.*, 2007). 4EBP1 (eukaryotic translation initiation factor 4E [eIF4E]-binding protein 1), exhibited a reduction in expression and phosphorylation at threonine 37 and 46 (T37/46) in 254Rp compared to PAR, which is directly targeted by mTORC1 (Figure 3.7B). These residues are priming sites by mTORC1, which lead to phosphorylation of further residues on 4EBP1 to fully inhibit its ability to bind to eIF4E (Fadden *et al.*, 1997; Herbert *et al.*, 2002). The ratio of p4EBP1 to total 4EBP1 expression can influence 4EBP1/eIF4E stoichiometry, therefore densitometric analysis was performed on the baseline phosphorylation and expression of 4EBP1. Figure 3.9C shows there was a significant reduction in p4EBP1:4EBP1 ratio from 0.75 to 0.45, resulting in a 1.67 fold reduction between PAR and 254Rp, which suggests there may be an alteration on 4EBP1/eIF4E stoichiometry. Hyperphosphorylation of 4EBP1 has been previously reported to increase 4EBP1 degradation (Elia *et al.*, 2008), although other studies have directly conflicted with this finding (Yanagiya *et al.*, 2012).

Taken together, the increased S6RP activity may suggest increased mTORC1 activity, although it is unclear whether p4EBP1 is increased due to reduced 4EBP1 expression. Although PRAS40 is involved in mTORC1 regulation, there was no alteration of T246 phosphorylation in 254Rp and thus unlikely the cause of increased mTORC1 activity in 254Rp.

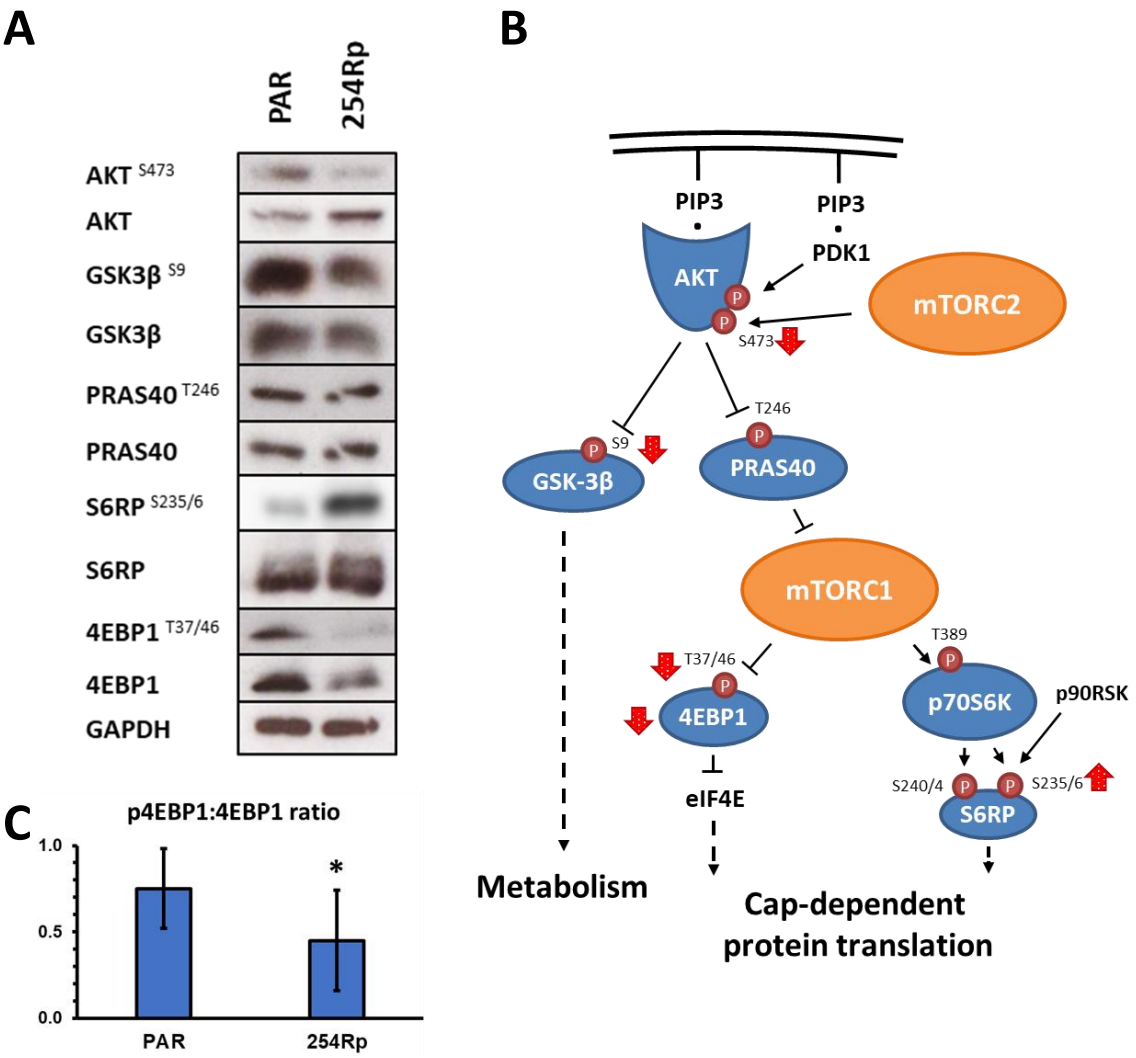

Figure 3.7 - Baseline signalling of key nodes in PAM pathway in A2780 PAR and 254Rp cell lines.
(A) Western blot of the baseline signalling in PAM pathway. Cells were plated at $5x10^5$ in 10cm tissue culture dishes and incubated at normal growth conditions for 72 hours. 254Rp cells were released from CCT129254 at least one week prior to plating. Lysate proteins were separated by SDS-PAGE, transferred to PVDF membranes and probed with antibodies against phosphorylated proteins and developed. Subsequently, blots were stripped and reprobed with antibodies against total proteins as indicated. Superscript (e.g. AKT ^{S473}) indicates signalling at phosphorylation site in superscript. GAPDH was used as a loading control. Data are most representative of six independent experiments. (B) A simplified schematic of the PAM pathway illustrating the relationship of the components (blue), investigated in (A). Phosphorylated residues are represented as dark red (P)s, with amino residue defined. Black arrows and block-headed arrows indicate phosphorylation of target induces activation or inhibition respectively. Black dotted arrows indicate phenotypic output. Fat red arrows illustrate increase or decrease of phosphorylated residue or protein in 254Rp, as per western blot in (A). Absence of red arrow indicates no change. C) Bar chart of average ratio of 4EBP1$^{T37/46}$:total 4EBP1. Band intensities were determined using Image J, and relative densities calculated and analysed in Microsoft Excel. Statistics: Welch's t test of PAR to 254Rp p4EBP1;t4EBP1 ratios, *p<0.05.

As both S6RP and 4EBP1 are downstream of mTORC1, their altered baseline signalling may suggest that the activity of mTORC1 was increased. PAM pathway signalling was examined to observe if 254Rp cells respond differently with inhibition of AKT, compared to PAR. MK-2206 was used for this investigation instead of

CCT129254 or capivasertib as MK-2206 as an allosteric inhibitor is more AKT-selective (Smyth and Collins, 2009; Hirai *et al.*, 2010). This is particularly important because both ATP-competitive inhibitors also target p70S6K, which is a substrate of mTORC1 (Davies *et al.*, 2012; Addie *et al.*, 2013).

Both PAR and 254Rp cells were exposed for 24 hours to a range of concentrations of MK-2206 and PAM pathway signalling was analysed by western blotting. As shown in Figure 3.8, treatment with MK-2206 reduced the phosphorylation of S473 of AKT with increasing concentrations of drug, indicative of reduced maximal activity of AKT. This phosphorylation was undetectable by 0.1μM of drug in both cell lines. Consistent with Figure 3.7, there was a slight decrease in baseline phosphorylation at this residue in 254Rp, compared with PAR. The phosphorylation of AKT substrates, GSK-3β (S9) and PRAS40 (T246) also exhibited a dose-dependent reduction in signal.

Interestingly, the phosphorylation of threonine 389 (T389) of p70S6K was resistant to AKT inhibition. This signalling was sensitive to MK-2206 in PAR, being completely undetectable by 0.01μM, compared with a detectable band in 254Rp even at the highest concentration tested (10μM). Additionally, despite a reduction in 4EBP1 expression in 254Rp, 4EBP1 phosphorylation appeared to be resistant to MK-2206 treatment. This was observed by hyperphosphorylated higher molecular weight (HMW) isoforms of total 4EBP1 requiring greater concentrations of MK-2206 in 254Rp to bandshift to hypophosphorylated low molecular weight (LMW) isoforms. These resistant hyperphosphorylated 4EBP1 isoforms were also phosphorylated at T37/46. T389 of p70S6K and T37/46 of 4EBP1 are directly phosphorylated by mTORC1, and thus the resistance to MK-2206 suggests that mTORC1 activity was independent of AKT signalling in 254Rp cells.

To investigate whether MK-2206 resistant phosphorylation of these sites was dependent on mTORC1 activity, these cells were treated for 24 hours with the allosteric mTORC1 inhibitor everolimus and PAM signalling examined by western blotting.

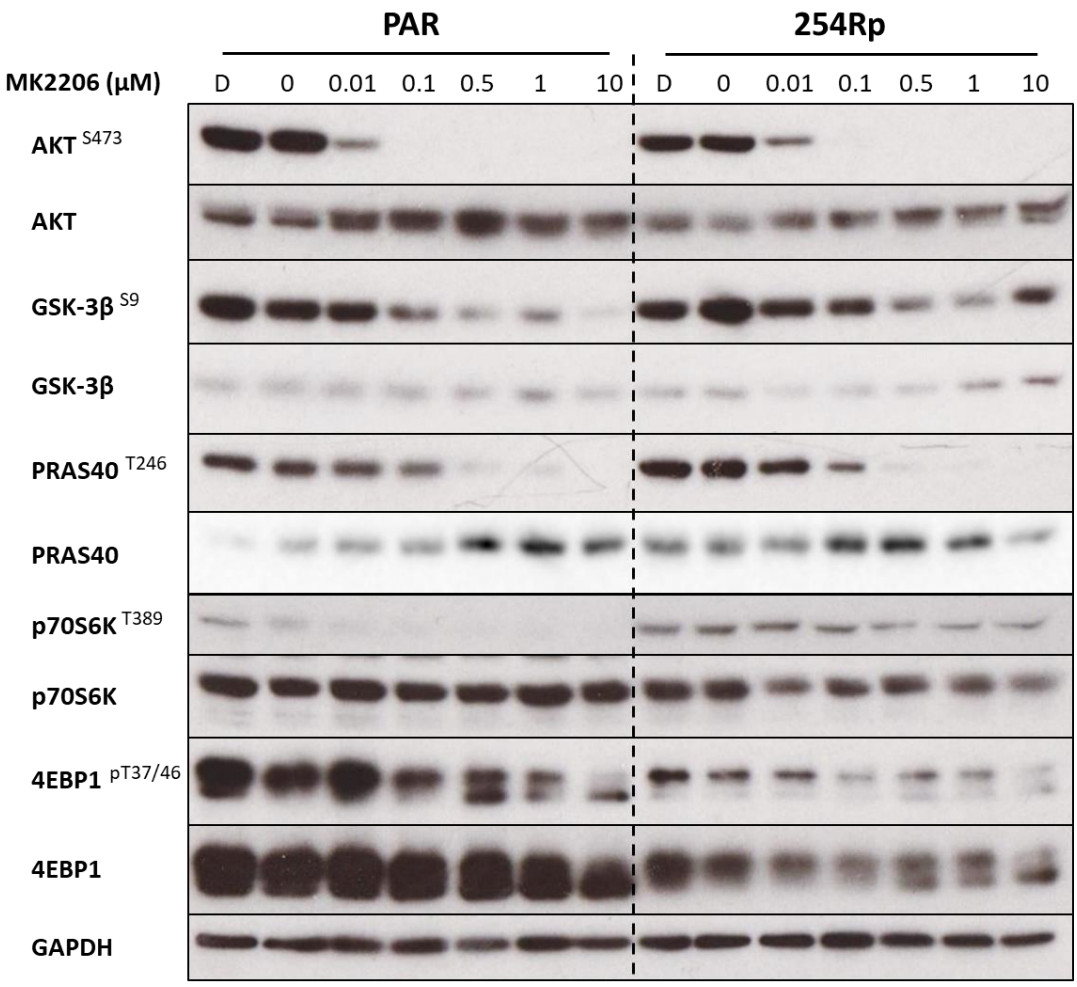

Figure 3.8 – PAM pathway signalling in A2780 PAR and 254Rp cells in response to MK-2206
A2780 PAR and 254Rp cells were plated at $5x10^5$ in 10cm tissue culture dishes and incubated at normal growth conditions for 72 hours. Plates were treated with a range of concentrations of MK-2206 for 24 hours prior to lysis. 254Rp cells were released from CCT129254 at least one week prior to plating. Western blot procedure used as described in Figure 3.7. Superscript (e.g. AKT ^{S473}) indicates signalling at phosphorylation site in superscript. GAPDH was used as a loading control. Data are representative of three independent experiments. D = DMSO only control.

In Figure 3.9, AKT S473 phosphorylation was not inhibited by everolimus as witnessed with MK-2206 (Figure 3.8). Instead, S473 was increased in 254Rp with increasing concentration of everolimus. This is an understood phenomenon with mTORC1 inhibition by rapamycin analogues, and was likely due to release of negative feedback via IRS-1 (O'Reilly *et al.*, 2006; Breuleux *et al.*, 2009). For all markers of the PAM pathway investigated, the response to everolimus in 254Rp was nearly identical to PAR. The complete abolishment of T389 on p70S6K and bandshift of 4EBP1 isoforms by 0.5nM for both cell lines was in marked contrast to that observed for AKT inhibition by MK-2206 in Figure 3.8. Taken together, p70S6K and 4EBP1 phosphorylation are not resistant to mTORC1 inhibition.

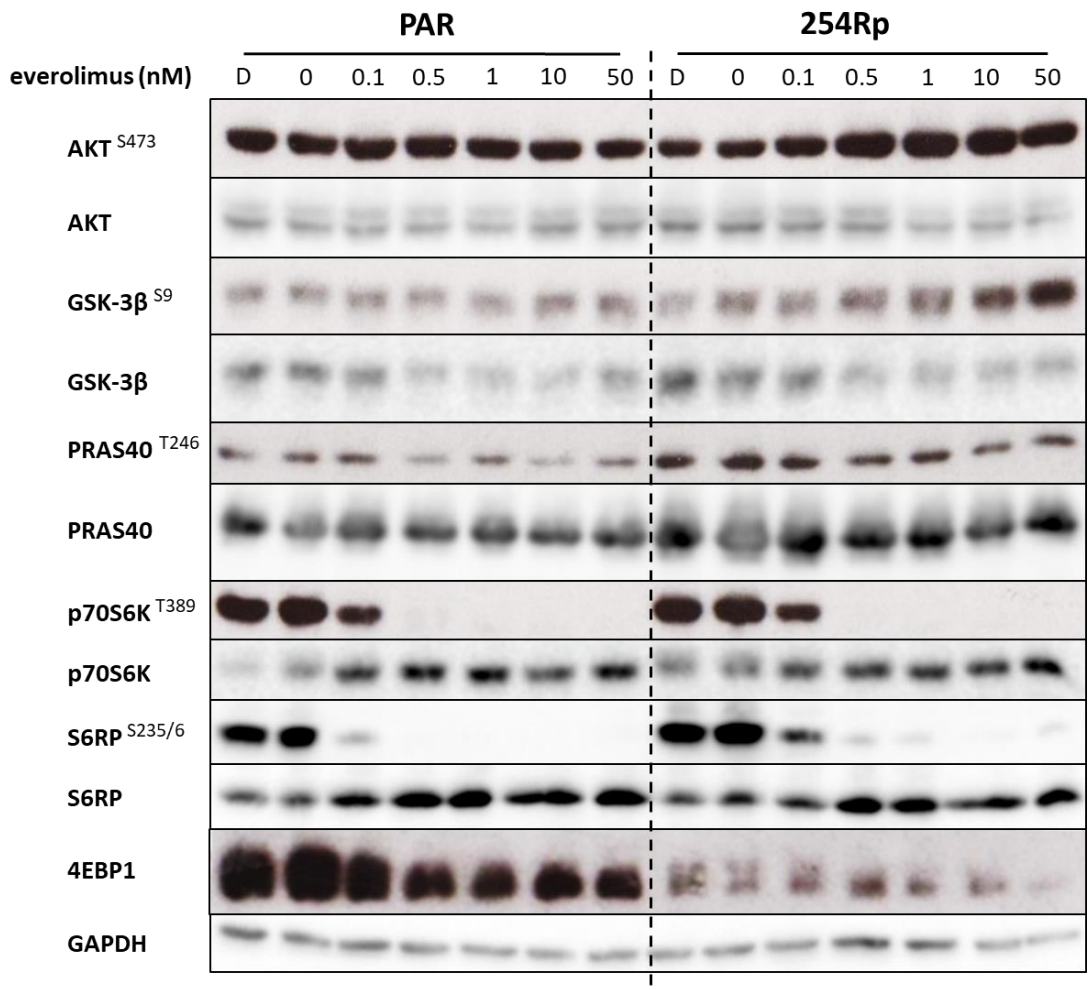

Figure 3.9 – PAM pathway signalling in A2780 PAR and 254Rp cells in response to everolimus
A2780 PAR and 254Rp cells were released and plated as described in Figure 3.8. Plates were treated with a range of concentrations of everolimus for 24 hours prior to lysis. Western blot procedure used as described in Figure 3.7. GAPDH was used as a loading control. Superscript (e.g. AKT ^{S473}) indicates signalling at phosphorylation site in superscript. Data are representative of three independent experiments. D = DMSO only control.

3.2.4. Investigation of SGK1 overexpression as a candidate resistance mechanism to capivasertib

Regulation of mTORC1 activity involves a complex network of regulators (Figure 1.4). Heightened mTORC1 activity may be a result of reduced activity of negative regulators; increased activity of positive regulators or alternatively a change in activity of the subunits of mTORC1 itself (Wang and Proud, 2011; Laplante and Sabatini, 2012).

One prominent activator of mTORC1 is the Ras-like GTPase Rheb (Groenewoud *et al.*, 2013). Rheb is negatively regulated through inhibition by the heterodimeric

tumour suppressor complex (TSC): hamartin (TSC1)/tuberin(TSC2) – shown in Figure 1.4. TSC2 harbours a GTPase activating protein (GAP) domain that drives Rheb into the inactive GDP-bound state, thereby inactivating it (Groenewoud *et al.*, 2013).

This branch of mTORC1 regulation was further investigated as TSC inhibition is regulated through several mechanisms independent of AKT, including ERK, p90RSK, AMPK and SGK1 (Groenewoud *et al.*, 2013; Castel *et al.*, 2016). SGK1 is of particular interest as it has been previously identified as a marker of intrinsic AKT inhibitor resistance (Sommer *et al.*, 2013), and Castel *et al.*, (2016) identified that SGK1 has high similarity in the kinase domain to AKT and can compensate for the inhibitory action on TSC1/TSC2 by phosphorylating all AKT-targeted residues on TSC2.

Array comparative genomic hybridisation (aCGH) using Agilent 4x44k aCGH platform was performed on RNA isolated from A2780 PAR and 254Rp cells and data were analysed using Genespring GX by Dr Denis Akan (Akan, 2015) to identify expression changes genes with significant fold change (>2 fold or <-2 fold) between the two cell lines. Identified genes were cross-examined in Reactome to highlight members of the PAM pathway that may reactivate the pathway in 254Rp. Table 3.1 presents a list of genes with significant fold change associated with the PAM pathway, including SGK1, identified in **red**, with 7.9-fold increase in mRNA expression.

AKT inhibits the TSC by phosphorylating TSC2 at serines 939 (S939), 981, (S981), 1130 (S1130), 1132 (S1132) and threonine 1462 (T1462; Kwiatkowski and Manning, 2005). Based upon the hypothesis that SGK1 may compensate AKT activity during AKT inhibition(Castel *et al.*, 2016), the phosphorylation levels at residues S939 and T1462 as well as AMPK-targeted serine 1387 (S1387) were investigated by western blot to observe whether AKT-targeted residues and not AMPK-targeted residues are resistant to AKT inhibition by MK-2206 in 254Rp cells compared with PAR.

Both AKT-targeted TSC2 phosphorylation sites (S939 and T1462) appeared to respond to AKT inhibition by MK-2206 in a dose-dependent fashion in both PAR and 254Rp populations at the highest concentrations. Reduction in signal at both residues requires a greater concentration of MK-2206 than S473 of AKT, with near undetectable signal at 10µM and 0.1µM respectively. Phosphorylation at these sites

are not resistant to MK-2206 in 254Rp compared to PAR. Interestingly, phosphorylation of the AMPK-targeted TSC2 site, S1387 was increased in both PAR and 254Rp cell lines with increasing MK-2206 concentration. Taken together, phosphorylation at AKT targeted residues of TSC2 is not resistant to AKT inhibition in 254Rp.

Table 3.1 – Gene expression microarray analysis in A2780 254Rp cells
Array comparative genomic hybridisation (aCGH) using Agilent 4x44k aCGH platform was performed on RNA isolated from A2780 PAR and 254Rp cells. Data was analysed using Genespring GX by Dr Denis Akan and cross-examined in Reactome to identify PAM pathway genes with significantly altered expression in 254Rp compared to PAR. Text in **red** indicates genes previously associated with AKT inhibitor resistance.

Gene	Protein	Fold change
PDGFA	platelet-derived growth factor alpha polypeptide	12.18
SGK1	**serum/glucocorticoid regulated kinase 1**	**7.90**
MET	met proto-oncogene	5.44
ITGA6	integrin, alpha 6	4.52
LAMC3	laminin, gamma 3	3.99
GEM	GTP binding protein overexpressed in skeletal muscle	2.86
AGO2	argonaute RISC catalytic component 2	2.13
FOXO3	forkhead box O3	-2.06
PIK3CA	phosphatidylinositol-4,5-bisphosphate 3-kinase, catalytic subunit alpha	-2.07
HDAC5	histone deacetylase 5	-2.56
GNG8	guanine nucleotide binding protein (G protein), gamma 8	-2.65
GAB2	GRB2-associated binding protein 2	-3.00
PCK2	phosphoenolpyruvate carboxykinase 2 (mitochondrial)	-3.95
APOL6	apolipoprotein L, 6	-6.15
LNX1	ligand of numb-protein X 1, E3 ubiquitin protein ligase	-9.48
CDK6	cyclin-dependent kinase 6	-12.94

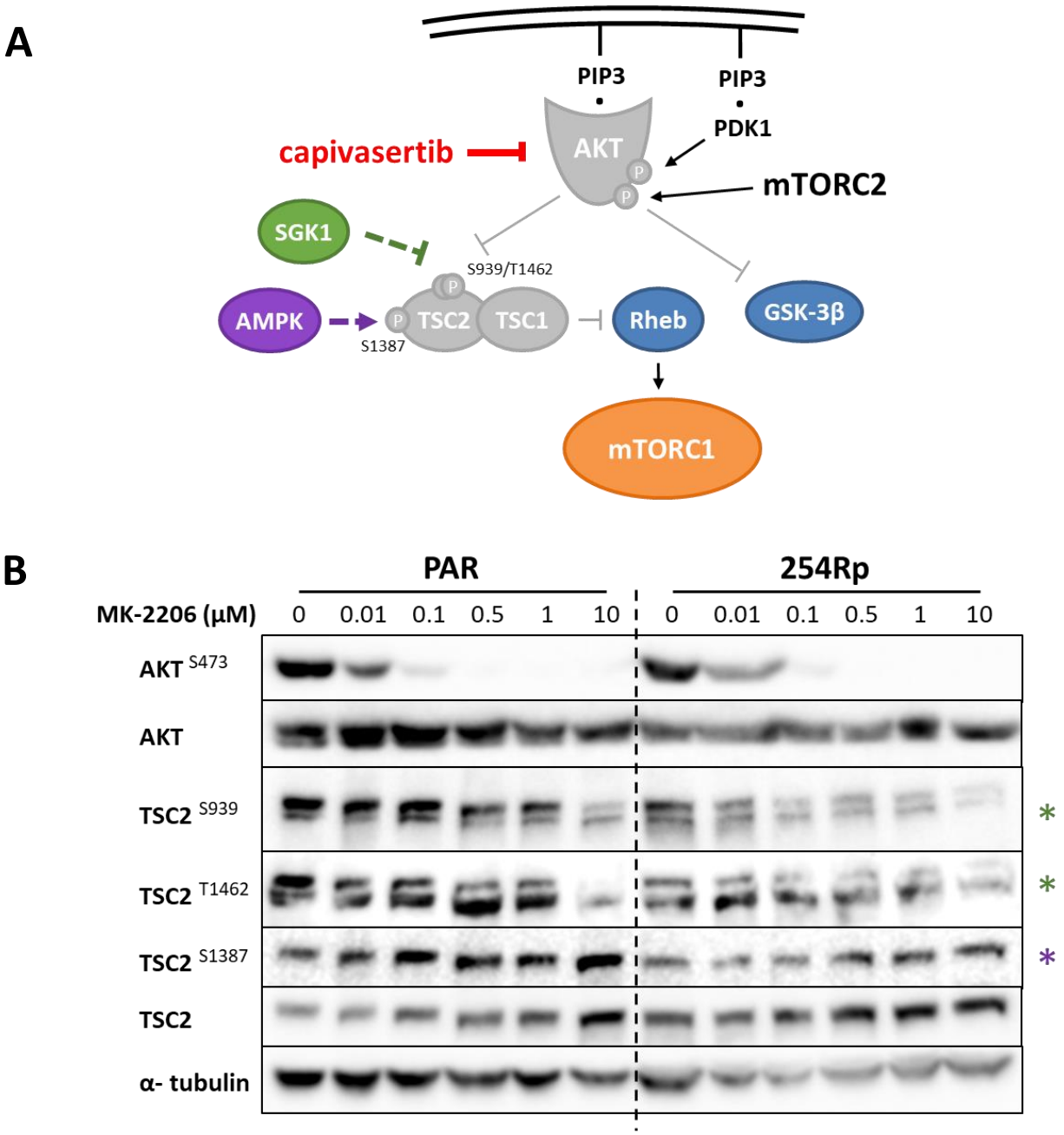

Figure 3.10 – Investigating SGK1 as a candidate to increase mTORC1 activity via TSC2 signalling
(A) A simplified schematic of a hypothetical model of SGK1 inducing activity of mTORC1 during capivasertib treatment in 254Rp cells through compensation for loss of TSC2 inhibition from AKT. Based upon Castel et al., (2016). (B) Western blot analysis of TSC2 signalling with treatment of MK-2206. A2780 PAR and 254Rp cells were plated and treated with a range of concentrations of MK-2206 and proteins separated and detected by western blot as described in Figure 3.8. Green asterisks indicated AKT-targeted TSC2 residues and purple asterisk indicates AMPK-targeted TSC2 residues as illustrated in (A). Superscript (e.g. AKT ^{S473}) indicates signalling at phosphorylation site in superscript. GAPDH was used as a loading control. Data are representative of three independent experiments. D = DMSO only control.

3.3. Discussion

This aim of this chapter was to validate the mTORC1 hyperactivity in A2780 254Rp cells observed by Dr Akan (Akan, 2015) through examination of the morphology, cross-resistance profiling and PAM signalling of the cells. These data were used to investigate acquired mechanisms driving the mTORC1 hyperactivity and resistance to capivasertib.

3.3.1. Morphology and cross-resistance profiling

The morphology was examined first as this is the simplest technique to narrow down candidate resistance mechanisms and phenotypes, such as EMT (Haslehurst *et al.*, 2012; Beaufort *et al.*, 2014). No stark changes in morphology were observed in 254Rp, compared with PAR, indicating that the resistance mechanism was unlikely to involve an invasive, migratory phenotype.

As 254Rp cells were also resistant to CCT129254 and capivasertib (Figure 3.2), these cells were taken forward for further study of resistance mechanisms to capivasertib.

As well as observing 100-fold resistance to capivasertib, 254Rp cells were also significantly resistant to the allosteric inhibitor MK-2206 (27-fold; Figure 3.3). This finding was significant as it highlights several properties of the resistance mechanism. Firstly, it suggests that the resistance mechanism was not specific to ATP-competitive AKT inhibitors, and thus less likely to involve AKT directly. To confirm this, *in vitro* kinase investigations of AKT in 254Rp by Dr Denis Akan showed no increase in AKT activity, nor were mutations found on any of the three AKT isoforms (Akan, 2015). Secondly, the resistance mechanism was unlikely to involve drug efflux through MDR1 overexpression (Gottesman *et al.*, 2002; Türk and Szakács, 2009), as the chemical structures of the AKT inhibitors possess little homology. Additionally, no cross-resistance to known MDR1 substrates, nor overexpression of MDR1 protein was found in 254Rp (Akan, 2015). Finally, the resistance mechanism was likely to be proximal to AKT as cross-resistance to two different methods of AKT inhibition was unlikely a result of adaptation of other off-target effects of CCT129254 such as p70S6K (McHardy *et al.*, 2010). There are

several other types of allosteric AKT inhibitors such as PH domain inhibitors (such as triciribine), alkyl phospholipids (such as miltefosine) and irreversible AKT inhibitors (such as lactoquinomycin). Investigation of 254Rp cross-resistance to these also would further validate 254Rp as a good model for resistance mechanisms to AKT inhibitors in general. Taken together, the resistance mechanism is likely to confer resistance via a regulator of AKT, or due to circumvention of AKT function downstream.

Alongside cross-resistance to AKT inhibition, 254Rp cells also demonstrated statistically significant cross-resistance to PI3K (9.8 RF) and mTORC (2.8 and 4.6 RF) inhibition (Figure 3.4), although the level of resistance was not as great as to AKT inhibitors (23.2-99.8 RF). There may be several reasons for this phenomenon: 1) The resistance mechanism feeds into both mTORC1-dependent and independent signalling, and thus mTORC1 inhibitors target one of multiple nodes required for AKT inhibitor resistance (e.g. SGK1). 2) The mechanism is an alteration of a subunit of mTORC1, which is not fully inhibited by mTORC inhibitors. 3) There are multiple resistance mechanisms in the heterogenetic 254Rp polyclonal population. A combination of these factors may also be possible.

Taking together the data so far, the resistance mechanism is likely to be downstream of AKT and therefore also downstream of PI3K. The relative reduction in level of resistance of pictilisib (Figure 3.4) compared to the AKT inhibitors suggests then that the resistance mechanism may be dependent on signalling from PI3K but also receives residual signalling from another PI3K-dependent source.

There was no cross-resistance of 254Rp to inhibitors of cap-dependent protein synthesis (Figure 3.5). As the inhibitors tested target components of CDPS downstream of mTORC1, tied with significant resistance to inhibitors upstream, it may suggest that the resistance mechanism lies in this area. It is worth taking note that both inhibitors may have off-target effects, since 4EGI-1 requires high concentrations for mechanism of action (Sekiyama *et al.*, 2015) it may interfere with targets other than eIF4E and 4EBP1, one previously reported weak target being mTORC1 (Wang *et al.*, 2015). The MNK inhibitor MRT00206081 is also a recently

developed drug, with high selectivity for both MNK1 and MNK2 and high specificity with 4 out of 250 (including MNKs) kinases tested observed with greater than 50% inhibition at 1µM treatment (data unpublished). It is possible that the sensitivity of both cells lines to both inhibitors may be due to a lack of intended target inhibition. Currently, there are no FDA-approved alternative inhibitors which acutely target the CDPS eIF4F complex. However, the eIF4E antisense nucleotide, LY2275796 which is currently the only CDPS inhibitor progressing through clinical trials, may be a more suitable alternative for cross-resistance profiling of CDPS inhibitors in the A2780 cell lines (*clinicaltrials.*gov; Lu *et al.*, 2016). Further development into CDPS targeting compounds is important for the clinical use of kinase therapies, as CDPS is being revealed as nexus of resistance for PAM and MAPK pathway targeting therapeutics (Cope *et al.*, 2014; Boussemart *et al.*, 2014).

Taken together, cross-resistance profiling data suggests that the resistance mechanism of 254Rp is likely to be circumventing the function of AKT, downstream of AKT and PI3K. This mechanism may also feed into mTORC1 signalling.

3.3.2. PAM pathway signalling analysis

Through observation of the baseline signalling of the PAM pathway in A2780 PAR and 254Rp cells (Figure 3.7), several alterations within the pathway were noted. A decrease in S473 phosphorylation on AKT suggests that AKT activation was reduced in 254Rp and the resistance mechanism may be less dependent on AKT activity. This supports the AKT inhibitor cross-resistance data that the resistance mechanism was unlikely to directly involve AKT itself. The most marked changes in baseline PAM signalling observed were downstream of mTORC1 with a significant increase in phosphorylation of S235/6 on S6RP and a reduction in T37/46 phosphorylation of and total 4EBP1 protein. S235/6 on S6RP are phosphorylated by p70S6K and p90RSK (Roux *et al.*, 2007), and thus could indicate an increase in the signalling by one or both kinases. Resistance of T389 p70S6K to exposure to MK-2206 highlights that p70S6K was likely to contribute towards increased S6RP phosphorylation. Additionally, 4EBP1 observed a greater maintenance of its hyperphosphorylated isoforms with increasing concentrations of MK-2206 (Figure 3.8), indicating that

although there was less 4EBP1 protein in 254Rp cells, proportionally, more of the total protein was in its phosphorylated state and was resistant to AKT inhibition. 4EBP1 phosphorylated at T37/46 residues also appeared to be resistant to MK-2206 as well. Since both observed p70S6K and 4EBP1 MK-2206-resistant residues are phosphorylated by mTORC1 (Pearce *et al.*, 2010; Showkat *et al.*, 2014), this may suggest an increase in mTORC1 activity. Interestingly, at the baseline level, proportional p4EBP1 appears to be reduced in 254Rp compared with PAR, based upon densiometric analysis in Figure 3.7. 4EBP1 turnover has been linked with its phosphorylation status (Elia *et al.*, 2008; Yanagiya *et al.*, 2012), however if phosphorylation of 4EBP1 is resistant to AKT and mTORC1 inhibition, the overall reduction in p4EBP1 may be due to a homeostatic mechanism to compensate for this. The effect of the p4EBP1:4EBP1 ratio on the turnover of 4EBP1 could be confirmed investigation of the half-life of 4EBP1 in both cell lines, using a cycloheximide time-course assay. Another explanation for reduced 4EBP1 expression may lie in alternative 4EBP isoforms (4EBP2 and 4EBP3) predominating in activity (Tsukumo *et al.*, 2016). The 4EBP1 antibody used does not cross-react with other 4EBP isoforms. This can be further investigated with pan-4EBP and 4EBP2 and 4EBP3 specific antibodies.

The increase in mTORC1 activity was further investigated by observing the response of PAM signalling in PAR and 254Rp cells when treated with everolimus (Figure 3.9). Interestingly, the phosphorylation of 4EBP1 and T389 p70S6K were not resistant to everolimus in 254Rp cells. This further highlighted that the MK-2206 resistant phosphorylation of these proteins was dependent on mTORC1 activity. As S235/6 S6RP is phosphorylated by p70S6K and p90RSK, depletion of p70S6K activity by everolimus shows minimal residual signalling of this site and thus was unlikely to contribute towards cross-resistance to everolimus (Figure 3.4) observed in drug-profiling or is otherwise significant in only a small population of the heterogenetic 254Rp cells. This could be validated using an p90RSK inhibitor in conjunction with everolimus.

An increase in mTORC1 activity can increase the activity of p70S6K and decrease activity of 4EBP1. Both S6RP and 4EBP1 have roles in cap-dependent protein

synthesis (CDPS): S6RP is a 40S ribosomal subunit protein (Hutchinson *et al.*, 2011) and 4EBP1 is an inhibitor of the eIF4F complex (Averous and Proud, 2006). p70S6K is known to phosphorylate other substrates involved in protein synthesis such as eIF4B – an activator of the eIF4A helicase; PDCD4 – an eIF4A inhibitor, which phosphorylation inactivates; and SKAR, an mRNA splicing factor (Fenton and Gout, 2011). CDPS has been previously reported to play a role in resistance to PAM inhibitors (Dilling *et al.*, 2002; N. Ilic *et al.*, 2011; Cope *et al.*, 2014; Tsukumo *et al.*, 2016) thus, it may be possible that capivasertib resistance in 254Rp cells is also driven by increased CDPS.

As hyperactivity of mTORC1 in 254Rp was confirmed, further investigations were carried out to investigate the mechanisms driving mTORC1 activity. Heightened mTORC1 activity may be a result of a reduction in regulation by mTORC1 inhibitors such as PRAS40, an increase in activity of positive regulators such as Rheb or alternatively a change in activity of the subunits of the complex itself (Wang and Proud, 2011; Laplante and Sabatini, 2012)

PRAS40 was eliminated as a potential candidate because phosphorylation at T246 was not resistant to MK-2206. This residue is important for the release of inhibitory binding to mTORC1 (Wang *et al.*, 2007), and thus a lack of resistance to MK-2206 at this site implies the dynamics of PRAS40 and mTORC1 binding was similar in both cell lines. This can be validated by analysis of PRAS40 binding with immunoprecipitation of RAPTOR. Additionally, as observed in Figure 3.4, 254Rp are cross-resistant to vistusertib, which targets both mTORC1 and mTORC2, the latter of which is important for AKT activation (Laura R. Pearce *et al.*, 2010). Therefore, the resistance mechanism will unlikely involve PAM pathway components along the AKT-mTORC1 axis, such as PRAS40. Consistent with this, no alterations were observed by exome sequencing or microarray analysis along this axis (Akan, 2015).

SGK1 was investigated as a resistance candidate because its signalling is not dependent on the PAM pathway, but Castel *et al.*, (2016) suggests that it may feed into mTORC1 signalling via TSC1/2. Additionally, microarray data exhibited a near eight-fold increase in mRNA expression in 254Rp cells. Although SGK1 may

compensate for AKT activity in JIMT1 and HCC1954 breast carcinoma cell lines (Castel *et al.*, 2016), the overexpression of SGK1 mRNA (Figure 3.10) in 254Rp did not correlate with TSC2 phosphorylation resistance to AKT inhibition, when compared with PAR. In fact, TSC2 S939 and T1462 phosphorylation appeared sensitive in 254Rp compared to PAR. However, as phosphorylation at AKT-targeted sites S939 and T1462 required over 100-fold greater concentration than S473 on AKT or S9 on GSK-3β (Figure 3.8) to exhibit the same reduction in signal, this may suggest that these sites are not very dependent on AKT signalling in A2780 cells. Interestingly, phosphorylation of the AMPK-targeted TSC2 site, S1387 was increased in both PAR and 254Rp cell lines with increasing MK-2206 concentration, suggesting that AMPK activity is increased. As AKT-dependent phosphorylation of AMPK alpha subunits negatively regulates its activity, MK-2206 alleviates this inhibition from AKT. SGK1 protein overexpression was not analysed by western blot as there are no good-quality commercial antibodies for this target. Although SGK1 may not necessarily be involved in mTORC1 hyperactivation, it may be important to determine whether the overexpression of SGK1 in 254Rp is a result of changes in *SGK1* gene transcription or altered mRNA or protein turnover. Taken together, SGK1 was not taken forward for further investigation as a mechanism of the increase in mTORC1 activity.

In summary, the data presented in this chapter suggests that resistance to capivasertib in the A2780 254Rp cell line circumvents the function of AKT through hyperactivation of mTORC1, which is modulated by a mechanism proximal to, but unlikely within the AKT-mTORC1 axis. SGK1 was investigated as a potential candidate but failed to demonstrate a role in increasing mTORC1 activity within the 254Rp cell line. Due to the polyclonal nature of this cell line, there may exist multiple mechanisms within this cell line. The following chapters aim to eliminate this issue through further characterisation of subclonal populations of the 254Rp cell line to identify candidate mechanisms driving resistance to capivasertib.

Chapter 4

Identification of candidate drivers of resistance to capivasertib in A2780 254Rp subclones

4. Identification of candidate drivers of resistance to capivasertib in A2780 254Rp subclones

4.1. Introduction

It has been well documented that tumours exhibit wide heterogeneity, both histopathologically and genetically, and also in the inter- and intra-tumoral setting. More recently it has been discovered that intra-tumour heterogeneity can exist at genetic, transcriptomic and proteomic levels. It is widely understood that a major source of such heterogeneity is the intrinsic genetic instability of cancerous cells, however diverse phenotypes can also be influenced by extrinsic factors such as pH, hypoxia, paracrine signalling, other microenvironment interactions, and drug exposure. All these drive different degrees of selection pressures. The heterogenetic cells within a tumour may respond to therapy in a variety of ways, leading to polyclonal drug resistance (Burrell and Swanton, 2014).

Polyclonal resistance to targeted therapies has been clinically identified within tumours, where drug resistance may be driven by more than one resistance mechanism within a tumour, which can arise from multiple clonal populations. For example, Bettegowda *et al.*, (2014) showed that tumours from 17/24 colorectal cancer patients with acquired resistance to cetuximab or panitumumab, harboured multiple mutations within the EGFR pathway that were not present pre-treatment. Another study showed one lung cancer patient with crizotinib-resistant non-small-cell lung cancer with two ALK (anaplastic lymphoma receptor tyrosine kinase) secondary mutations in two independent cell populations within the same tumour (Choi *et al.*, 2010).

The heterogeneous nature of tumours will ultimately lead to cancer cell lines that are also heterogeneic. This means that generation of drug-resistant isogenic cell lines by dose escalation drug-exposure of a polyclonal parental cell line (A2780 PAR in this case), may also produce a similar polyclonal drug resistance phenotype in the resistant population (A2780 254Rp; McDermott *et al.*, 2014).

A pooled population of cells exhibiting polyclonal drug resistance poses a challenge for identifying candidate resistance mechanisms. Many common forms of cellular analysis technologies such as exome-sequencing or western blotting require a large number of cells to yield sufficient nucleic acids or protein for evaluation. If a polyclonal drug resistant population is used for such techniques, the resulting data may be noisy and unclear, rendering the sample difficult for identifying resistance mechanisms. Subcloning resistant polyclonal populations may overcome these challenges by generating a population of cells that are more genetically identical.

Subcloning can be performed by isolating resistant colonies during drug selection or by limited dilution, plating 0.5 cells per well of a 96-well plate (McDermott *et al.*, 2014). Generating clonal populations by either method requires the cells to be able to grow independently of one another, which may not necessarily be the case for every cell in a heterogenetic population. Therefore, not all resistance mechanisms can be isolated in this way. This is particularly true for resistance mechanisms that may have co-evolved together and form co-dependence (Burrell and Swanton, 2014). However, resistance mechanisms investigated post-subcloning tend to be more stable, and thus easier to identify, and often do not require drug maintenance (McDermott *et al.*, 2014). Ultimately, subcloning of cells has been used to identify clinically relevant resistance mechanisms (Nazarian *et al.*, 2010), and thus is a legitimate method for identifying candidate resistance mechanisms to targeted therapies. These can be built upon to understand the nature of polyclonal drug resistance (Burrell and Swanton, 2014).

In Chapter 3, the morphology, cross-resistance and PAM (PI3K/AKT/mTOR) signalling of A2780 parental (PAR) and CCT129254-resistant (254Rp) cells were investigated to identify candidate resistance mechanisms to capivasertib. However, the 254Rp cells displayed conflicting results, as AKT inhibitor-resistant mTORC1 signalling was sensitive to the mTORC1 inhibitor everolimus, despite displaying statistically significant cross-resistance to the drug. This phenomenon may occur if 254Rp is a polyclonal drug resistant population. The aim of this chapter, therefore, was to subclone the A2780 254Rp cell line and investigate the clonal populations to identify candidate resistance mechanisms driving resistance to capivasertib.

4.2. Results

4.2.1. Generation and screening of A2780 254Rp subclones

To generate the A2780-254Rp subclonal populations, the limited dilution method was employed. Cells were seeded at 0.5 cells per well across a 96-well plate and left to grow in the absence of CCT129254 for one week until colonies became visible. These were passaged into larger plates and treated with 56μM CCT129254 (as 254Rp) once passaged into T25 flasks. From a total of 11 colonies originally isolated, eight of these survived growing up into T25 flasks. These populations are 254R- A, B, D, E, F, H, J and K. 254R-C, G and I did not survive expansion into larger flasks.

As with A2780 254Rp cells, the morphology of the 254Rp subclones were examined (Figure 4.1). All subclones, except 254R-F exhibited similar morphology to 254Rp. Cells were adherent and regularly shaped with few protrusions, characteristic of epithelial-like cells. All subclones except 254R-E and F exhibited between 1.4-1.6 protrusions on average per cell, thus were similar to PAR and 254Rp. 254R-F cells were more elongated in shape compared with 254Rp, which is more characteristic of fibroblast-like cells and may be indicative of an epithelial to mesenchymal transition (EMT) phenotype.

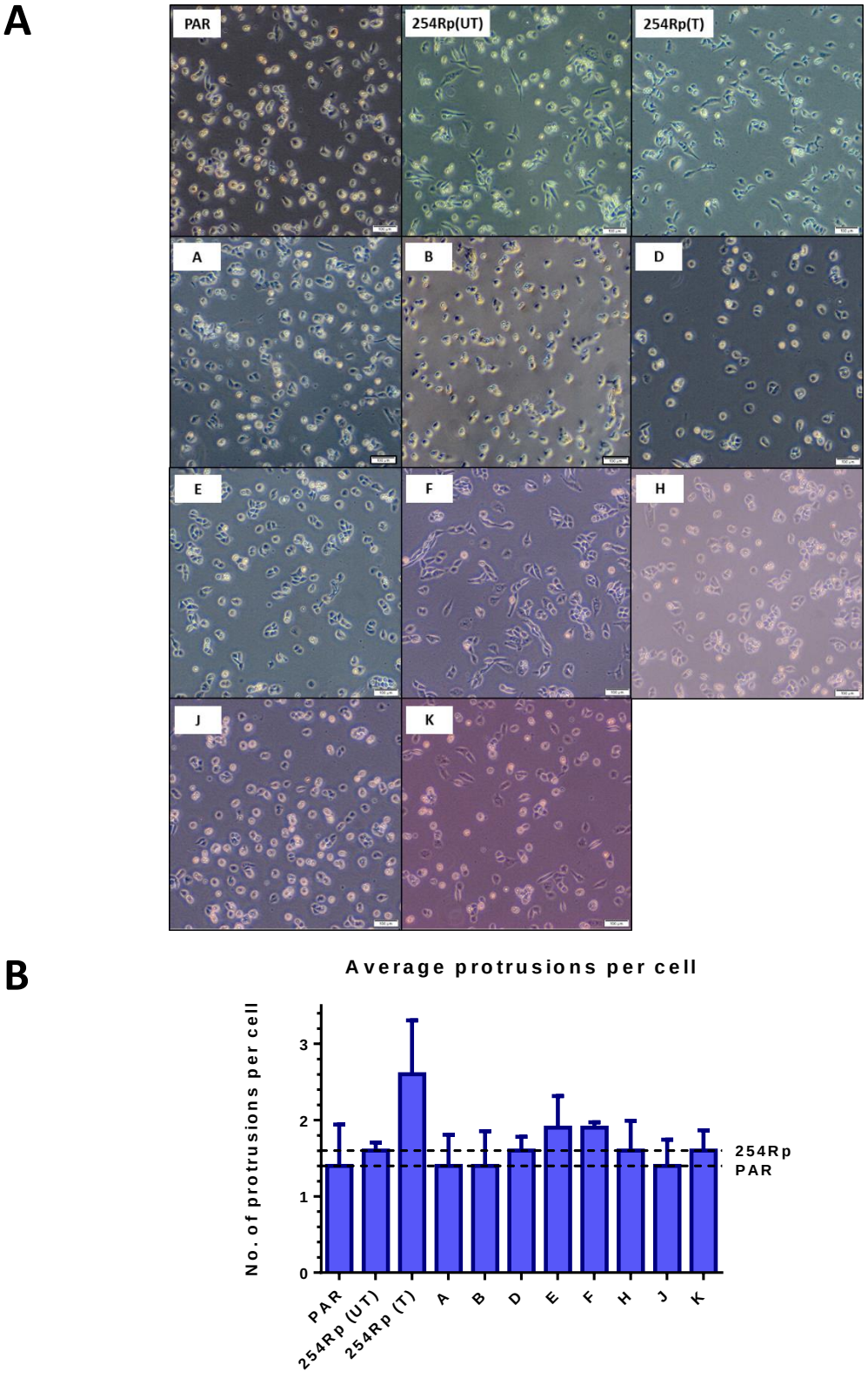

Figure 4.1 – Morphology of A2780 PAR, 254Rp and 254Rp subcloned cell lines, A-K.
(A) Morphology of A2780 PAR, 254Rp and 254Rp subclones A-K at 40x magnification, phase contrast. Cells were plated to same cell concentration and left to adhere for 24 hours. UT= released from maintenance in CCT129254 for one week, T = maintained in 56µM CCT129254. Scale bar indicates 100µm. Representative of two repeats. (B) A bar graph of average protrusions per cell.

The resistance factor (RF) values were determined for CCT129254 and its close analogue capivasertib (AZD5363) for the 254Rp subclones. Figure 4.2 shows that all the subclones were significantly resistant to both CCT129254 (6.3-11 RF) and capivasertib (16-54 RF), with similar RFs to 254Rp (9.6 and 37 RF respectively). As all subclones were resistant to capivasertib, none were excluded at this stage.

Cross resistance to mTORC1 inhibitors was also investigated in the 254Rp subclones. Figure 4.3 shows that although all subclones exhibited a greater GI_{50} value than PAR for the allosteric mTORC1 inhibitor, everolimus (RAD001; >2 RF), none were statistically significant according to Welch's t test. The standard deviation for all cell lines treated with everolimus was very high. The response to mTORC inhibitors across the 254Rp subclones was varied. 254Rp exhibited 4.9 RF, therefore the resistance of 254R-A (5.5 RF) was similiar. 254R-B and E observed the greatest resistance (11-13 RF) and the rest of the subclones were less resistant than 254Rp (2.5-3.5 RF).

Most subclones were significantly resistant to the mTOR kinase inhibitor vistusertib (AZD2014; 4.3-5.8 RF), with levels similar to 254Rp (6.7 RF) except 254R-D and J (3.6 and 3.0 RF, respectively).

A

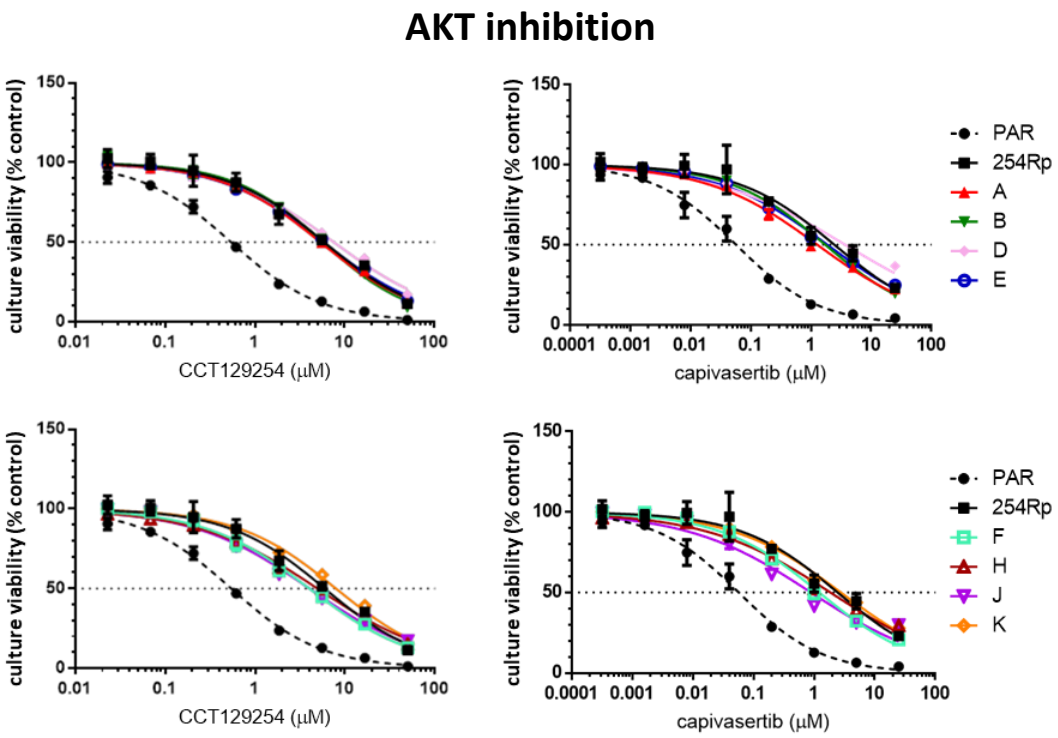

B

		PAR	A	B	D	E
CCT129254	GI_{50} (μM)	0.66 ± 0.21	5.32 ± 1.45	6.64 ± 3.63	7.30 ± 1.58	5.03 ± 1.24
	RF	-	8.03*	11.08*	11.17*	8.07**
capivasertib (AZD5363)	GI_{50} (μM)	0.06 ± 0.01	1.35 ± 0.47	1.71 ± 0.81	3.24 ± 0.68	1.30 ± 0.48
	RF	-	21.90*	28.61*	54.10*	22.77*

		F	H	J	K	254Rp
CCT129254	GI_{50} (μM)	4.12 ± 0.64	5.47 ± 1.30	3.82 ± 0.75	6.28 ± 1.45	5.90 ± 0.57
	RF	6.34**	8.27*	5.88*	10.12*	9.63***
capivasertib (AZD5363)	GI_{50} (μM)	1.09 ± 0.13	1.81 ± 0.25	1.01 ± 0.34	2.28 ± 0.44	2.34 ± 1.03
	RF	18.80**	30.34**	16.42*	38.80*	37.31*

Figure 4.2 – Determination of resistance of A2780 254Rp subclones to CCT129254 and capivasertib. (A) Representative dose response curves for CCT129254 (left) or capivasertib (right), for 254R-A, B, D, E (top), F, H, J and K (bottom). A2780 PAR, 254Rp (800 cells per well) and 254Rp subclones (3200 cells were well) were plated and after 48 hours treated with serially diluted concentrations of drug for 96 hours and surviving cells were determined by SRB growth assay. Dose response curves generated and half-maximal growth inhibition concentrations (GI_{50}) were calculated using GraphPad Prism 6. Data points present mean ± SD of three technical replicates. The broken line on the Y-axis indicates the points on the curves where growth was inhibited by 50% (GI_{50}). Data representative of ≥three independent experiments. (B) Summary of GI_{50} concentrations and resistance factors (RF) to CCT129254 and capivasertib in A2780 PAR and resistant cells. GI_{50} values presented as mean ± SD of GI_{50} values from ≥three independent experiments. Resistance Factors (RF) presented as mean RF of ≥three independent experiments. Individual independent RF values calculated as the ratio of 245R(X) GI_{50} to PAR GI_{50}. Statistics: Unpaired t test with Welch's correction of 254R(X) to PAR GI_{50} values, *p<0.05, **p<0.01, ***p<0.001, N.S = non-significant.

A

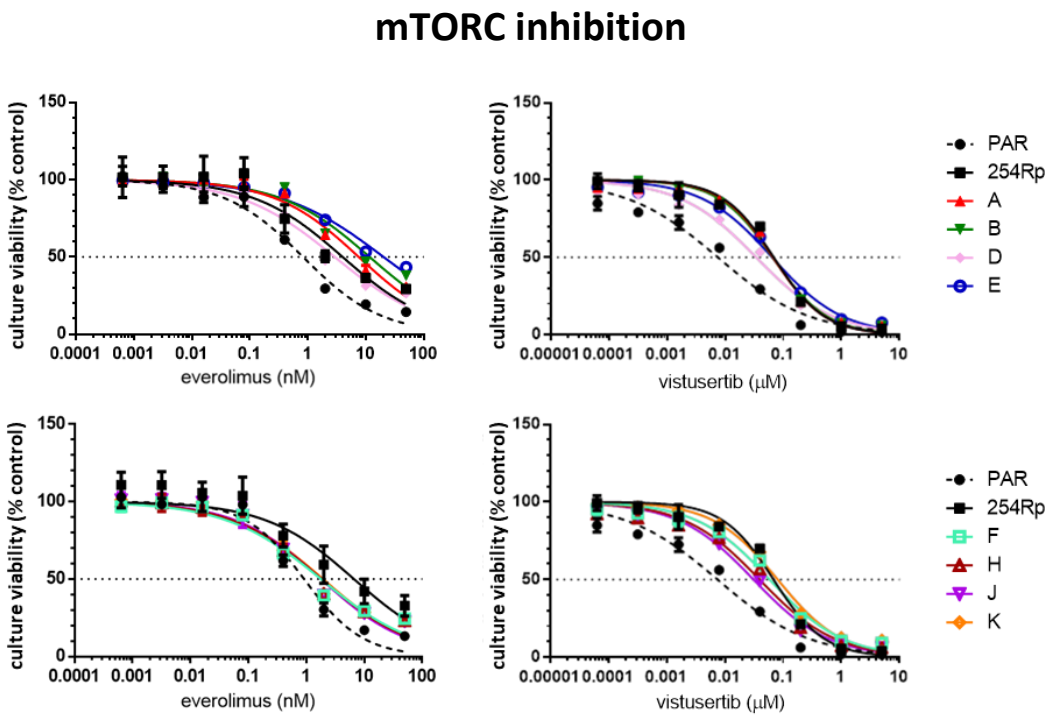

B

		PAR	A	B	D	E
everolimus (RAD001)	GI_{50} (nM)	0.87 ± 0.14	4.96 ± 2.39	8.51 ± 3.62	2.22 ± 0.62	10.90 ± 6.91
	RF	-	5.52$^{N.S}$	10.72$^{N.S}$	2.45$^{N.S}$	13.15$^{N.S}$
vistusertib (AZD2014)	GI_{50} (nM)	10.66 ± 3.72	59.56 ± 8.23	58.50 ± 9.01	35.62 ± 1.18	49.28 ± 10.86
	RF	-	6.08***	6.74**	3.58**	5.10***

		F	H	J	K	254Rp
everolimus (RAD001)	GI_{50} (nM)	2.29 ± 0.66	2.48 ± 0.80	2.17 ± 0.66	3.01 ± 2.52	4.33 ± 1.43
	RF	2.53$^{N.S}$	2.74$^{N.S}$	2.41$^{N.S}$	3.45$^{N.S}$	4.89*
vistusertib (AZD2014)	GI_{50} (nM)	52.50 ± 6.96	45.87 ± 10.74	29.46 ± 2.51	62.00 ± 16.44	63.91 ± 19.77
	RF	5.48***	4.41*	2.98**	6.57*	6.68*

Figure 4.3 – Determination of resistance of A2780 254Rp cells to mTORC inhibitors.
(A) Representative dose response curves for everolimus (left) and vistusertib (right), for 254R-A, B, D, E (top), F, H, J and K (bottom). SRB growth assay was performed and generation of dose response curves as described in Figure 4.2. Data representative of ≥three independent experiments. (B) Summary of GI_{50} concentrations and resistance factors (RF) to everolimus and vistusertib in A2780 PAR, 254Rp and 254Rp subclones, analysed and formatted as described in Figure 4.2.

Figure 4.4A shows a summary of RF values presented in Figures 4.2 and 4.3. Resistance to capivasertib was greater than CCT129254 in all resistant cell lines. Similarly to 254Rp, the RF values for most of the subclones for both AKT inhibitors were greater than either of the mTORC inhibitors, everolimus or vistusertib. Most of the 254Rp subclones exhibited a greater RF value to vistusertib than everolimus. The exceptions were 254R-B and E, by which resistance to everolimus was greater than vistusertib and greater than (254R-E) or equal (254R-B) to CCT129254. According to the Welch's t test, neither everolimus RF values for 254R-B or E were statistically significant. Taken together, the cross-resistance profiles can be divided into two groups: 1) high everolimus resistance (254R-B and E) and 2) and low everolimus resistance (254R-A, D, F, H, J and K).

Figure 4.4B shows for all 254R subclones, the baseline signalling of the PAM pathway downstream of mTORC1. Compared with PAR, the phosphorylation of threonine 389 (T389) on p70S6K was increased in every subclone, although none exhibited as great an increase as 254Rp. Phosphorylation at serines 235 and 236 (S235/6) on S6RP were equal to PAR in all subclones except 254R-A and F. Phosphorylation at threonine 37 and 46 (T37/46) on 4EBP1 was reduced compared to PAR in all resistant lines, with 254R-B, E and F exhibiting the least reduction. 254R-B, E and F also exhibited the greatest total 4EBP1 expression across the subclones.

4EBP1 phosphorylation and expression closest to the PAR level was present in both subclones with high RF value to everolimus (254R-B and E; group 1), and low 4EBP1 phosphorylation and expression was present in nearly all subclones with lower everolimus resistance (254R-A, D, F, H, J and K; group 2). 254R-F was the exception to this with high 4EBP1 but low everolimus resistance, in addition also exhibited fibroblastic morphology and was thus assigned to a third group.

Two subclones were selected for further investigation for candidate resistance mechanisms to capivasertib. 254R-B was selected from group 1 and 254R-D was selected from group 2 as these exhibited the greatest resistance to capivasertib for each group respectively.

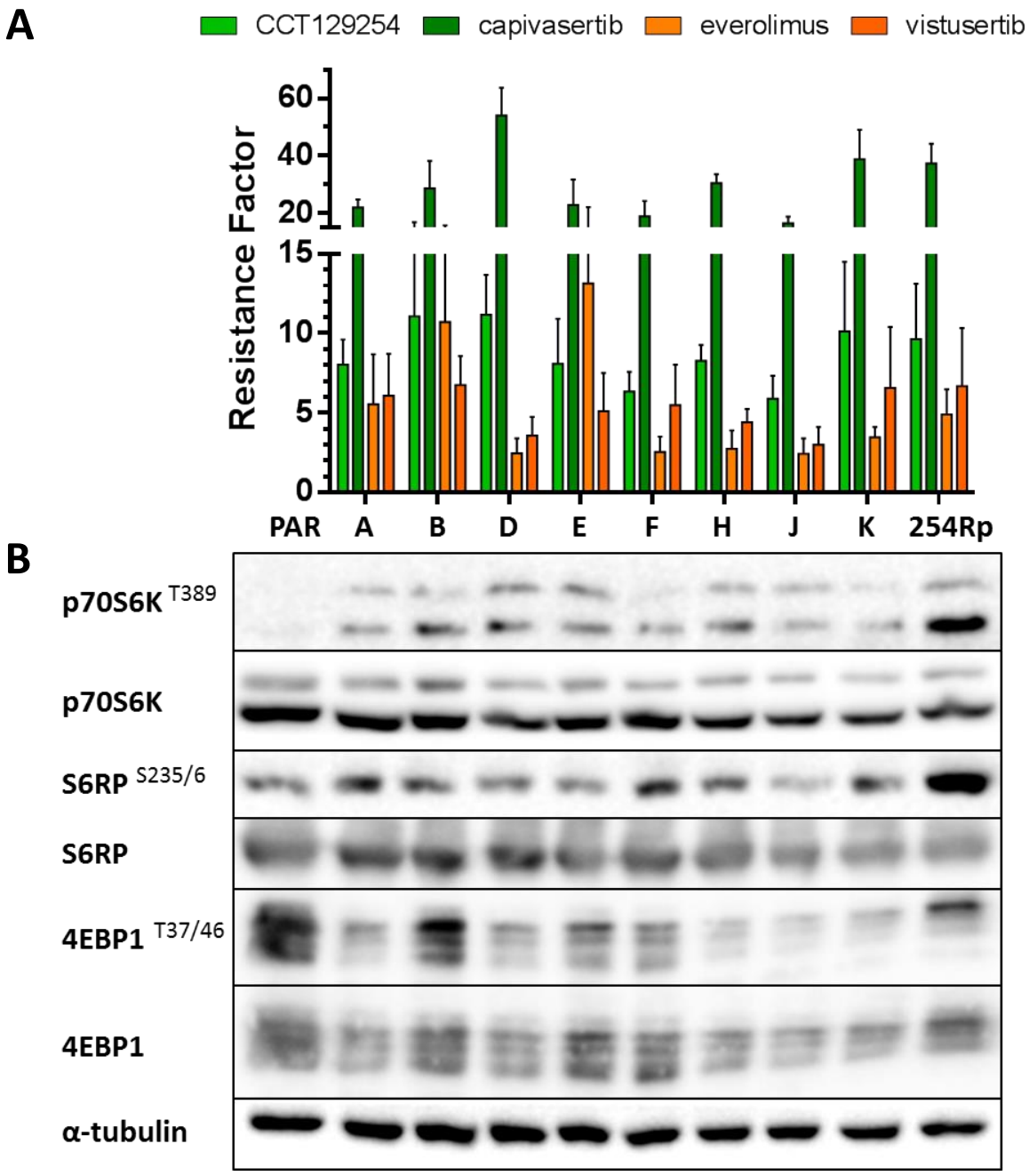

Figure 4.4 – Screening of A2780 254Rp clones for cross-resistance and baseline mTORC1 signalling
(A) Bar chart summary representing mean and error bars as SD for RF values of A2780 254Rp and 254Rp subclonal cell lines for AKT inhibitors (green) and mTORC inhibitors (orange), taken from Figures 4.2 and 4.3. Individual and mean RF values, SD and statistics calculated as Figure 4.2. (B) Western blot analysis of baseline mTORC1 signalling in A2780 PAR, 254Rp and 254Rp subclones. Cells were plated at $5x10^5$ in 10cm tissue culture dishes and incubated at normal growth conditions for 72 hours. All resistant cell lines were released from CCT129254 at least one week prior to plating cells for lysis. Lysate proteins were separated by SDS-PAGE, transferred to PVDF membranes and probed with antibodies against phosphorylated proteins and developed. Subsequently, blots were stripped and reprobed with antibodies against total proteins as indicated. Superscript (e.g. AKT ^{S473}) indicates phosphorylation at residues in superscript. Alpha-tubulin was used as a loading control. Representative of three independent experiments.

4.2.2. Cross-resistance profiling of A2780-254Rp subclones 254R-B and 254R-D to PAM inhibitiors.

The seeding concentration was optimised for the selected subclones, 254R-B and D in order to determine any changes in GI_{50} and RF values influenced by suboptimal seeding number.

Cross resistance profiling was repeated and expanded for 254R-B and D at the revised 1600 cells (Figure 2.3) per well seeding concentration. In Figure 4.5, 254R-B exhibited high cross-resistance to all ATP-competitive and allosteric AKT inhibitors tested (10-40 RF). Resistance to vistusertib was comparatively low (4 RF), however 254R-B exhibited greater than double the resistance factor to everolimus (96 RF) than capivasertib. 254R-B also showed no significant resistance to cap-dependent protein synthesis (CDPS) inhibitor 4EGI-1 (1.2 RF), compared to PAR.

Cross-resistance profiling for 254R-D was observed at the revised seeding concentration in Figure 4.6. 254R-D exhibited high cross-resistance to ATP-competitive inhibitors CCT129254 and capivasertib (11-40 RF). Interestingly, cross-resistance to the allosteric inhibitor MK-2206 was comparatively less (2.2 RF), but nonetheless statistically significant. 254R-D was also significantly resistant to the mTOR kinase inhibitor vistusertib (3.3 RF), and resistance to mTORC1-specific allosteric inhibitor everolimus was greater (12 RF). The large standard deviation exhibited with everolimus determined this phenomenon statistically non-significant by Welch's t test.

Resistance factors to CCT129254, capivasertib and vistusertib for both subclones showed less than two-fold difference between the original seeding concentration (3200 cells per well; Figures 4.2 and 4.3) and the final revised concentration (1600 cells per well; Figures 4.5 and 4.6). Interestingly, although the resistance factors for everolimus deviated largely between both seeding concentrations in both subclones, this was contributed by variations for both PAR and subclone GI_{50} values. This was a result of high standard deviation, which is a common phenomenon of this drug (Fallahi-Sichani *et al.*, 2013). Regardless, in both cell concentrations, the subclones demonstrated a trend towards resistance to everolimus.

A

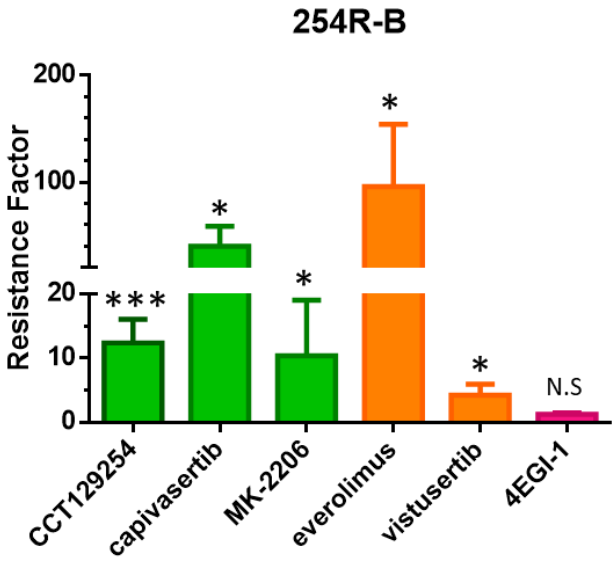

B

Drug	Target	GI50		Resistance Factor	N
		PAR	254R - B		
CCT129254 (µM)	AKT (ATP-competitive)	0.84 ± 0.25	9.73 ± 1.31	12.4***	4
capivasertib (µM) (AZD5363)	AKT (ATP-competitive)	0.10 ± 0.02	3.91 ± 2.17	40.1*	4
MK-2206 (µM)	AKT (allosteric)	0.25 ± 0.11	2.11 ± 1.42	10.4*	5
everolimus (nM) (RAD001)	mTORC1 only (substrate recruitment)	0.34 ± 0.17	26.9 ± 10.8	96.1*	4
vistusertib (nM) (AZD2014)	mTORC1/2 (ATP-competitive)	13.4 ± 5.51	51.8 ± 18.6	4.19*	4
4EGI-1 (µM)	eIF4F assembly	21.2 ± 7.80	25.9 ± 4.20	$1.22^{N.S}$	3

Figure 4.5 – Summary of cross-resistance profiling of A2780 254R-B to PAM pathway inhibitors at revised seeding concentrations.
(A) Bar chart representing mean and error bars as SD of RF values for AKT (green), mTORC (orange) and CDPS (pink) inhibitors in 254R-B cells plated at revised seeding concentration (1600 cells per well). Mean RF values and SD calculated as average of RF values and SD from ≥ three individual experiments. Individual RF values calculated as ratio of 254R-D GI_{50} to PAR GI_{50}. Statistics as calculated in Figure 4.2. (B) Summary of GI_{50} concentrations and RFs to PAM inhibitors indicated in A2780 PAR and 254R-D cells (plated at 1600 cells per well); analysed and formatted as described in Figure 4.2.

A

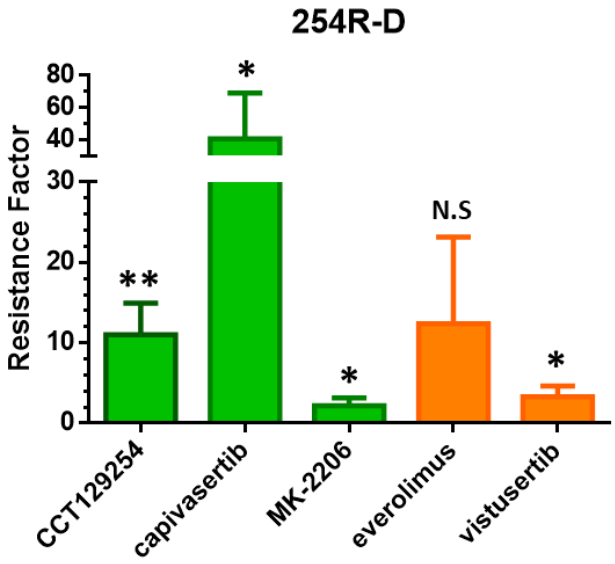

B

Drug	Target	GI50		Resistance Factor	N
		PAR	254R - D		
CCT129254 (µM)	AKT (ATP-competitive)	0.84 ± 0.25	8.73 ± 2.46	11.0**	4
capivasertib (µM) (AZD5363)	AKT (ATP-competitive)	0.10 ± 0.02	4.14 ± 3.51	40.6*	4
MK-2206 (µM)	AKT (allosteric)	0.25 ± 0.11	0.52 ± 0.19	2.19*	5
everolimus (nM) (RAD001)	mTORC1 only (substrate recruitment)	0.34 ± 0.17	3.76 ± 3.04	$12.4^{N.S}$	4
vistusertib (nM) (AZD2014)	mTORC1/2 (ATP-competitive)	13.4 ± 5.51	40.51 ± 13.1	3.31*	4

Figure 4.6 – Summary of cross-resistance profiling of A2780 254R-D at revised seeding concentration to PAM pathway inhibitors
(A) Bar chart representing mean and error bars as SD of RF values for AKT (green), mTORC (orange) and CDPS (pink) inhibitors in 254R-D cells plated at revised seeding concentration (1600 cells per well). Mean RF values and SD calculated as Figure 4.6. Statistics as calculated in Figure 4.2. (B) Summary of GI_{50} concentrations and RFs to PAM inhibitors indicated in A2780 PAR and 254R-D cells (plated at revised seeding concentration); analysed and formatted as described in Figure 4.2.

4.2.3. Baseline PAM pathway signalling in A2780 254R-B and 254R-D

Exploration of the baseline signalling of the PAM pathway was expanded in 254R-B and D to investigate signalling up- and downstream of mTORC1. There was little change in baseline signalling of PAM pathway components upstream of mTORC1 in 254R-B except for total GSK-3β expression. However, phosphorylation of serine 473 (S473) of AKT appeared reduced in 254R-D, indicative of decreased maximal activity of AKT (Pearce *et al.*, 2010). This correlated with a reduction in phosphorylation of threonine 246 (T246) of PRAS40. Phosphorylation at serine 9 (S9) on GSK-3β was

slightly reduced and total expression increased in 254R-D. Downstream of mTORC1, T389 of p70S6K was increased in both subclones, which was not due to a change in total p70S6K. Neither subclone exhibited an increase in S6RP phosphorylation but for both, 4EBP1 phosphorylation at T37/46 and total protein expression was reduced.

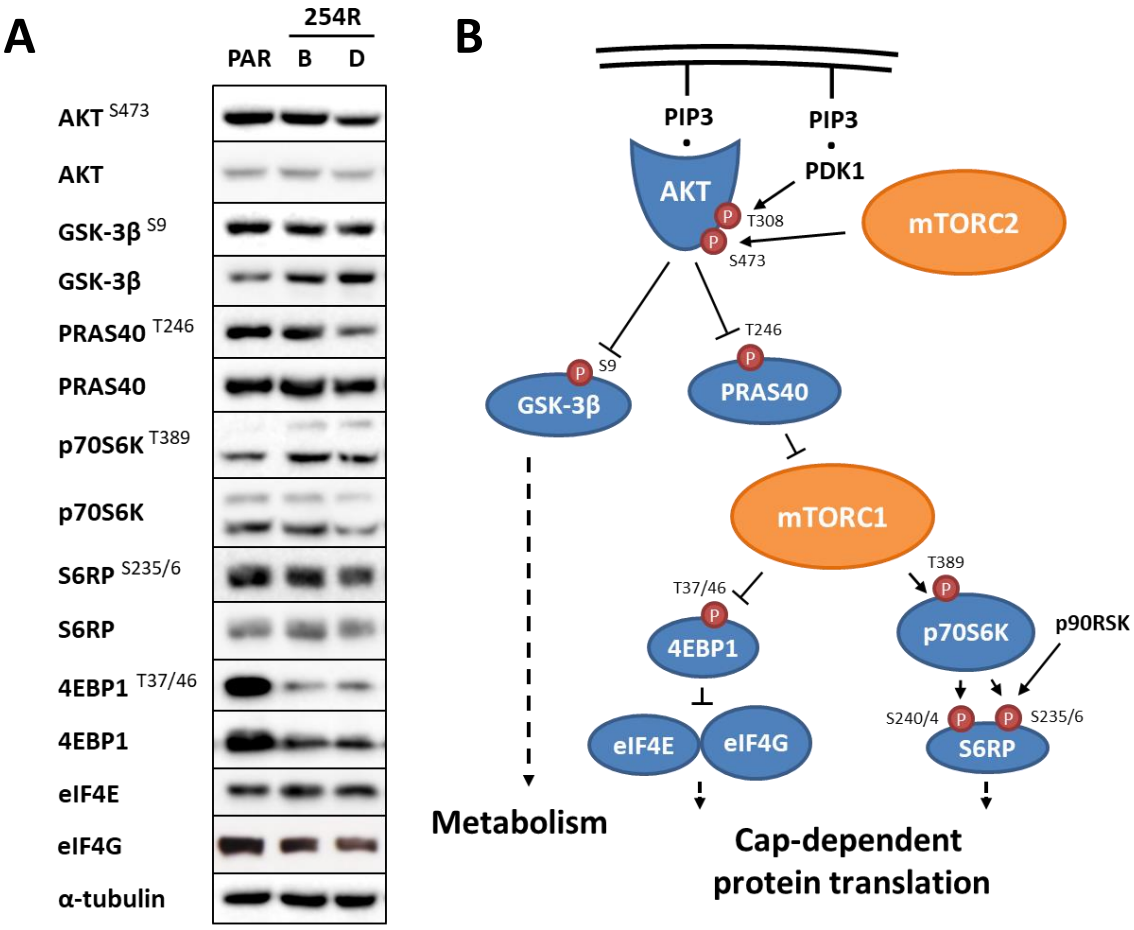

Figure 4.7 – Analysis of baseline PAM pathway signalling in A2780 PAR and 254Rp subclones 254R-B and 254R-D cell lines.
(A) A2780 PAR, 254R-B and D cells were released and plated and western blot performed on lysates as described in Figure 4.4. GAPDH was used as a loading control. Superscript (e.g. AKT ^{S473}) indicates signalling at phosphorylation site in superscript. Data are representative of two independent experiments. (B) A simplified schematic of the PAM pathway illustrating the relationship of the components (blue), investigated in (A). Phosphorylated residues are represented as dark red (P)s, with amino residue defined. Black arrows and block-headed arrows indicate phosphorylation of target induces activation or inhibition respectively. Black dotted arrows indicate phenotypic output.

In summary, changes in baseline PAM signalling in 254R-B were downstream of mTORC1, although GSK-3β expression was also increased. In contrast, 254R-D exhibited alterations in phosphorylation of all PAM pathway components investigated, except at S6RP. Taken with the cross-resistance profiling data from

Figures 4.5 and 4.6, these data suggest that 254R-B and D exhibit two distinctly different mechanisms of resistance. Additionally, the altered baseline signalling of p70S6K and 4EBP1 in both 254R-B and D may suggest that these mechanisms converge to confer resistant mTORC1 signalling. Therefore, the signalling of mTORC1 substrates in response to MK-2206 and everolimus was investigated in 254R-B and D compared with PAR.

4.2.4. Response of A2780 PAR and 254R-B to PAM inhibitors

MK-2206 was used to investigate the response to AKT inhibition instead of CCT129254 or capivasertib because MK-2206 is an allosteric inhibitor and thus more AKT-selective (Smyth and Collins, 2009; Hirai *et al.*, 2010). This is particularly important because both ATP-competitive inhibitors also target p70S6K, downstream of mTORC1 (Davies *et al.*, 2012; Addie *et al.*, 2013). PAR and 254R-B cells were exposed for 24 hours to a range of concentrations of drug and signalling was analysed by western blotting.

The response of 254R-B to MK-2206 is shown in Figure 4.8. The phosphorylation of S473 on AKT was undetectable by 0.1µM MK-2206 in both PAR and 254R-B. Total AKT in untreated cells was than drug-treated cells. This was likely because the antibody targeting total AKT was raised against the unphosphorylated carboxyl-terminal residues of AKT, which may overlap with S473 (*cellsignal.co.uk*) and thus have a greater affinity for non-phosphorylated AKT. T389 phosphorylation of p70S6K is undetectable in PAR whereas the baseline phosphorylation in 254R-B is considerably greater, and decreases in a dose-dependent manner. Despite the noteable increase in p70S6K phosphorylation, there was not a subsequent increase in phosphorylation of S6RP at S235/6 or S240/4 in 254R-B; in contrast, the baseline for both signals appeared reduced. T37/46 phosphorylation and total expression of 4EBP1 was reduced in 254R-B compared with PAR. Taken together, despite an increase in p70S6K phosphorylation, mTORC1 signalling in 254R-B was not resistant to MK-2206.

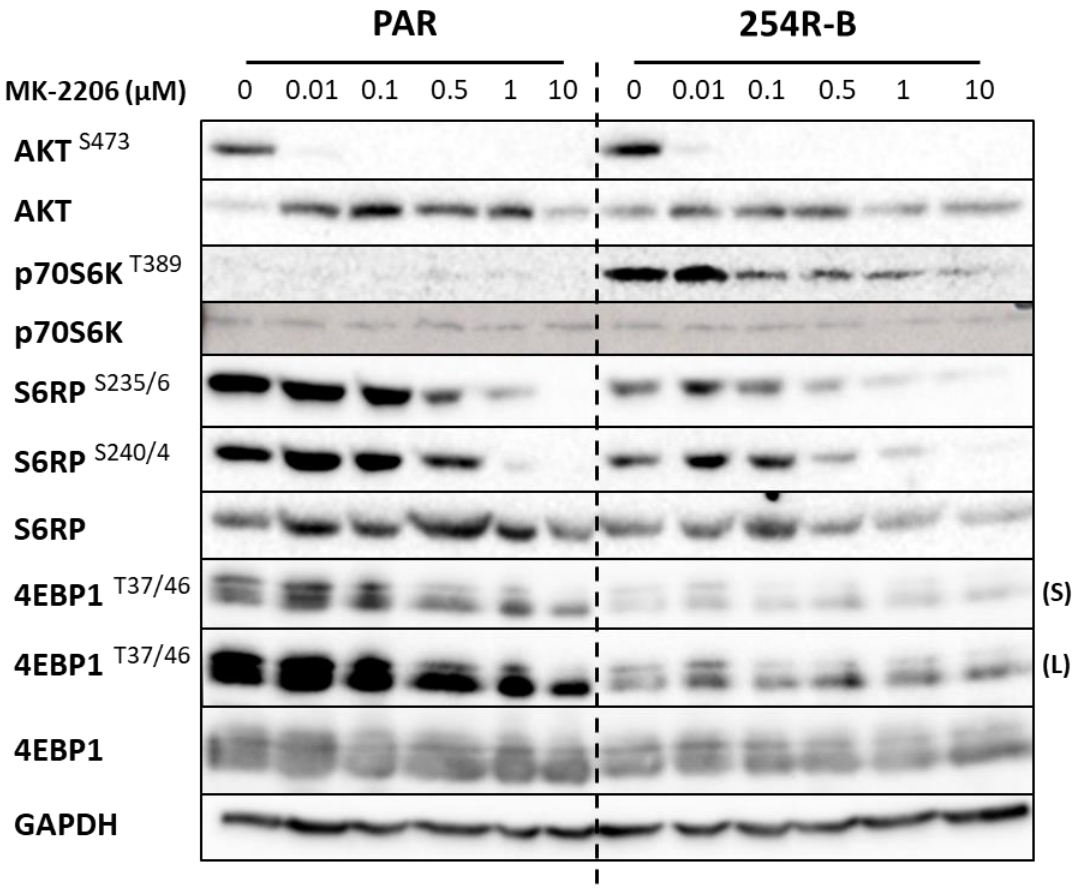

Figure 4.8 – PAM pathway signalling in A2780 PAR and 254R-B cells in response to MK-2206
A2780 PAR and 254R-B cells were plated at $5x10^5$ in 10cm tissue culture dishes and incubated in normal growth conditions for 72 hours. Plates were treated with a range of concentrations of MK-2206 for 24 hours prior to lysis. 254R-B cells were released from CCT129254 at least one week prior to plating. Western blot procedure used as described in Figure 4.4. Superscript (e.g. AKT ^{S473}) indicates signalling at phosphorylation site in superscript. GAPDH was used as a loading control. Data are representative of three independent experiments. S = short exposure; L = long exposure.

As 254R-B exhibited a high RF value to the allosteric mTORC1 inhibitor everolimus, the effect of this drug on AKT and mTORC1 substrate signalling was also investigated (Figure 4.9). AKT S473 phosphorylation was relatively unchanged in both cell lines. The phosphorylation of p70S6K (T389) and S6RP (S235/6 and S240/4) decreased with increasing concentrations of everolimus. For all these residues, the signal was undetectable by 1nM in both cell lines except S235/6 of S6RP of which a signal was still detectable at the highest 100nM dose in 254R-B. Interestingly, a reduction in signal at S6RP S235/6 was witnessed between 0.1 and 1nM in 254R-B.

The baseline phosphorylation of 4EBP1 (T37/46) was less in 254R-B compared with PAR (Figure 4.9). In both cell lines, high molecular weight (HMW)

hyperphosphorylated isoforms of 4EBP1 shifted to low molecular weight (LMW) hypophosphorylated isoforms with increasing concentrations of everolimus. However, in both cell lines, T37/46 phosphorylation of 4EBP1 was detectable in HMW isoforms at 1nM unlike T389 of p70S6K. It was previously published that rapalogues such as everolimus exhibit a greater affinity for inhibiting p70S6K signalling than 4EBP1 (Thoreen *et al.*, 2009). Therefore, 4EBP1 was not inhibited as effectively as p70S6K by everolimus. However, despite this phenomenon neither p70S6K nor 4EBP1 phosphorylation was more resistant to mTORC1 inhibition in 254R-B compared with PAR. Taken together, phosphorylation of S235/6 on S6RP was independent of mTORC1 inhibition by everolimus in 254R-B.

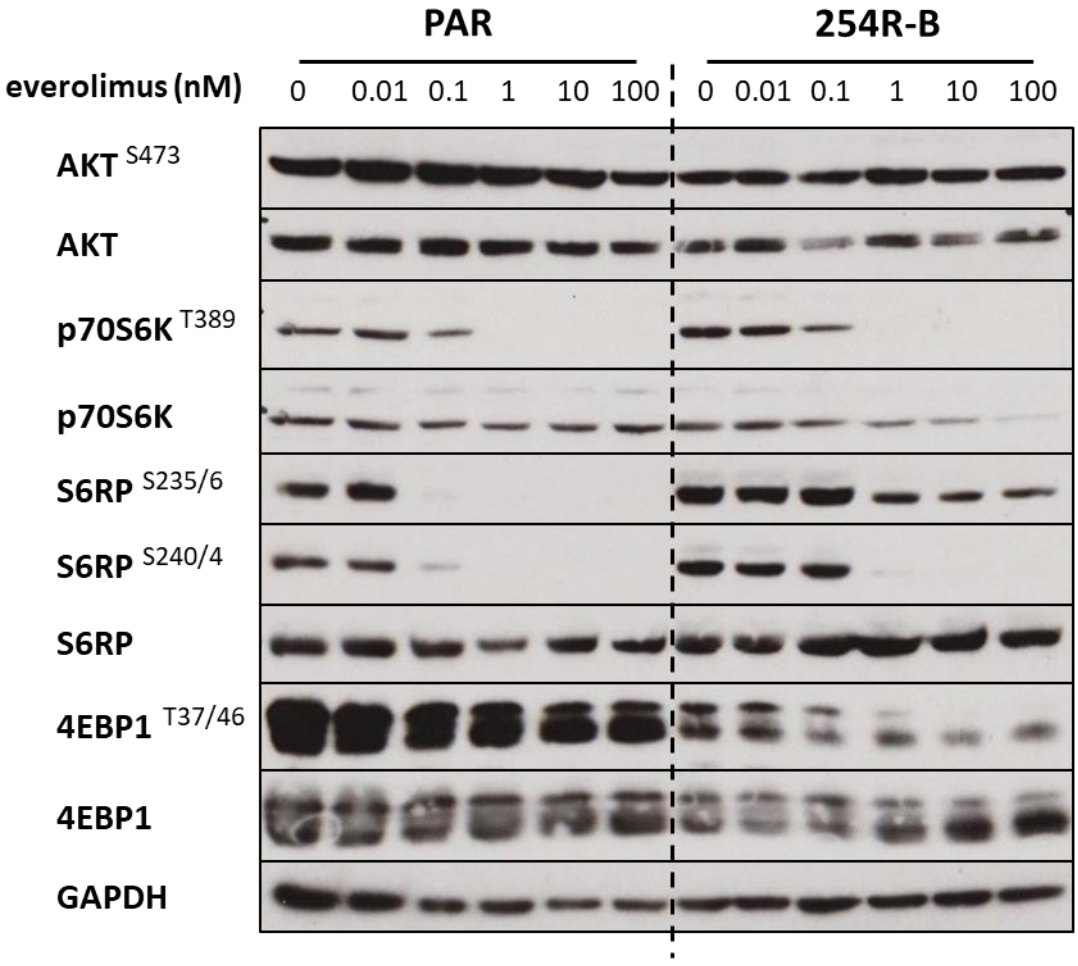

Figure 4.9 – PAM pathway signalling in A2780 PAR and 254R-B cells in response to everolimus
A2780 PAR and 254R-B cells were released and plated as described in Figure 4.8. Plates were treated with a range of concentrations of everolimus for 24 hours prior to lysis. Western blot procedure used as described in Figure 4.4. GAPDH was used as a loading control. Superscript (e.g. AKT ^{S473}) indicates signalling at phosphorylation site in superscript. Data are representative of two independent experiments. S = short exposure; L = long exposure

In Figures 4.4 and 4.8, baseline 4EBP1 expression in 254R-B appeared similar to the level of PAR, however in Figure 4.7 and 4.9, the expression appeared notably lower than PAR. 254R-B was selected in part because 4EBP1 expression was similar to PAR, unlike the low everolimus resistant subclones such as 254R-D. Therefore, the expression of 4EBP1 in 254R-B was investigated. Protein samples from three biological repeats were run in parallel and densitometric analysis performed to quantify the levels of T37/46 phosphorylated and total 4EBP1 in both cell lines. The relative density of the lysates, normalised to the GAPDH loading control showed a statistically significant 60% reduction in the T37/46 4EBP1 signal, however, despite a 30% reduction in 4EBP1 expression between PAR and 254R-B, this was not statistically significant. Between PAR and 254R-B, there was a 36.7% reduction in p4EBP1:4EBP1 ratio from 0.75 to 0.45, which suggests that the greater reduction in p4EBP1 than 4EBP1 in 254R-B is likely to alter the 4EBP1/eIF4E stoichiometry to favour increased 4EBP1 binding of eIF4E. In addition to this, densitometric analysis of the data in Figure 4.7 shows there is also a reduction in eIF4E:4EBP1 ratio from 0.73 to 0.42, indicating a 42.2% reduction. This may further impact the 4EBP1/eIF4E stoichiometry to favour increased 4EBP1 binding of eIF4E.

In summary, 254R-B exhibited some alterations in mTORC1 signalling in response to PAM inhibitor treatment. Although 254R-B exhibited no resistance to mTORC1 signalling to MK-2206, 4EBP1 phosphorylation and expression was reduced and less functionally active regardless of improved activity by drug action. Additionally, 254R-B also observed strong S235/6 S6RP resistance to everolimus, which was not observed with MK-2206 treatment.

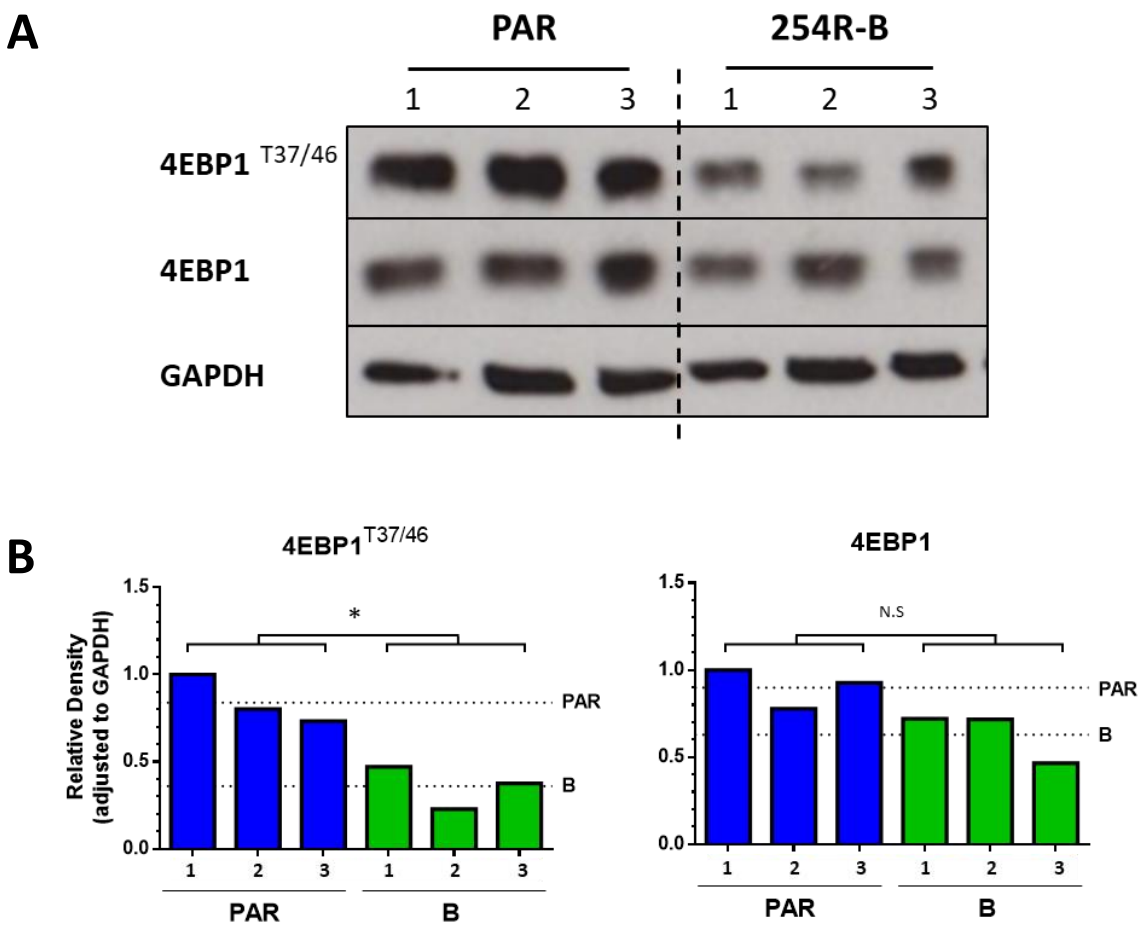

Figure 4.10 – Analysis of baseline 4EBP1 signalling across multiple A2780 PAR and 254R-B biological repeats.

(A) Untreated samples of A2780 PAR and 254R-B used in experiments for Figures 4.8 and 4.9 were analysed by western blot as described in Figure 4.4. Samples labelled as 1, 2 and 3 represent three separate biological repeats, plated identically on different days. GAPDH was used as a loading control. Superscript indicates signalling at respective phosphorylation site. (B) Bar charts of relative density of 4EBP1$^{T37/46}$ (left) and total 4EBP1 (right) bands from (A). Band intensities were determined using Image J, and relative densities calculated, adjusted to GAPDH loading, normalised to PAR n1 and analysed in GraphPad Prism 6. Dotted lines represent the mean of three biological repeats for A2780 PAR or 254R-B cells as indicated. Statistics: Welch's t test of PAR to 254R-B relative densities, *p<0.05, N.S = non-significant.

4.2.5. Response of A2780 PAR and 254R-D to PAM inhibitors

The response of 254R-D to MK-2206 was shown in Figure 4.11. MK-2206 reduced the phosphorylation of S473 on AKT with increasing concentrations of drug, indicative of reduced maximal activity of AKT (Pearce *et al.*, 2010). The phosphorylation was undetectable by 0.1µM in both PAR and 254R-D. Phosphorylation of T389 on p70S6K in PAR increased with greater concentrations of MK-2206, which was not exhibited in 254R-D, nor in previous MK-2206 treated blots for PAR (Figures 3.8 and 4.8). In both PAR and 254R-D, T389 p70S6K phosphorylation drops between 1 and 10µM. An equal dose-dependent reduction of S235/6 on S6RP was observed in both cell lines, and phosphorylation of S240/4 was slightly greater for each dose in PAR. The bandshift from high to low molecular weight forms of T37/46 phosphorylated 4EBP1 was observed at a lower concentration of MK-2206 in 254R-D (0.5µM) than PAR (1µM). Taken together, p70S6K and 4EBP1 phosphorylation were not resistant to AKT inhibition by MK-2206.

The effect of mTORC1-specific inhibition (everolimus) on these targets in 254R-D was also investigated (Figure 4.12). Consistent with Figure 4.7, baseline S473 phosphorylation of AKT was markedly less in 254R-D compared with PAR. S473 was also slightly reduced with increasing concentrations of everolimus in PAR, but slightly increased in 254R-D. The phosphorylation of T389 of p70S6K and S235/6 and S240/4 of S6RP decreased with increasing concentrations of everolimus. In all of these residues, the signal was undetectable by 1nM. Baseline T37/46 phosphorylation of 4EBP1 was markedly less in 254R-D compared with PAR (Figure 4.12). In both cell lines, HMW isoforms shifted to LMW isoforms with increasing concentrations of everolimus. The short exposure (S) for PAR and long (L) for 254R-D show that this band shift begins to occur between 0.1nm and 1nM in both cell lines. However, unlike with p70S6K and S6RP, T37/46 phosphorylation of 4EBP1 was still detectable in HMW isoforms even at 100nM for both cell lines. The bandshift at 1nM was also observed with total 4EBP1. Taken together, p70S6K and 4EBP1 phosphorylation were not resistant to mTORC1 inhibition.

In summary, mTORC1 signalling was not resistant to MK-2206 or everolimus in 254R-D cells.

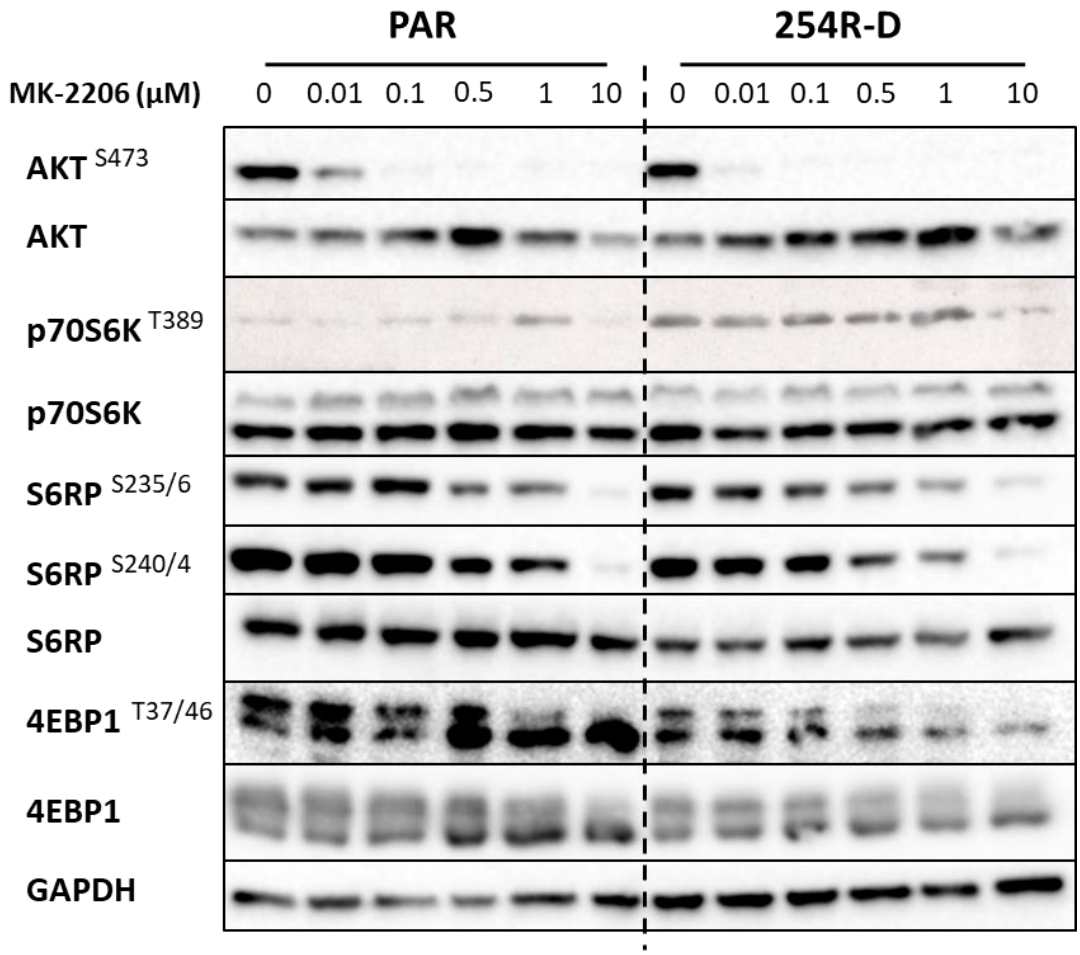

Figure 4.11 – PAM pathway signalling in A2780 PAR and 254R-D cells in response to MK-2206
A2780 PAR and 254R-D cells were released, plated and drug-treated as described in Figure 4.8. Western blot procedure used as described in Figure 4.4. Superscript (e.g. AKT ^{S473}) indicates signalling at phosphorylation site in superscript. GAPDH was used as a loading control. Data are representative of three independent experiments. S = short exposure; L = long exposure.

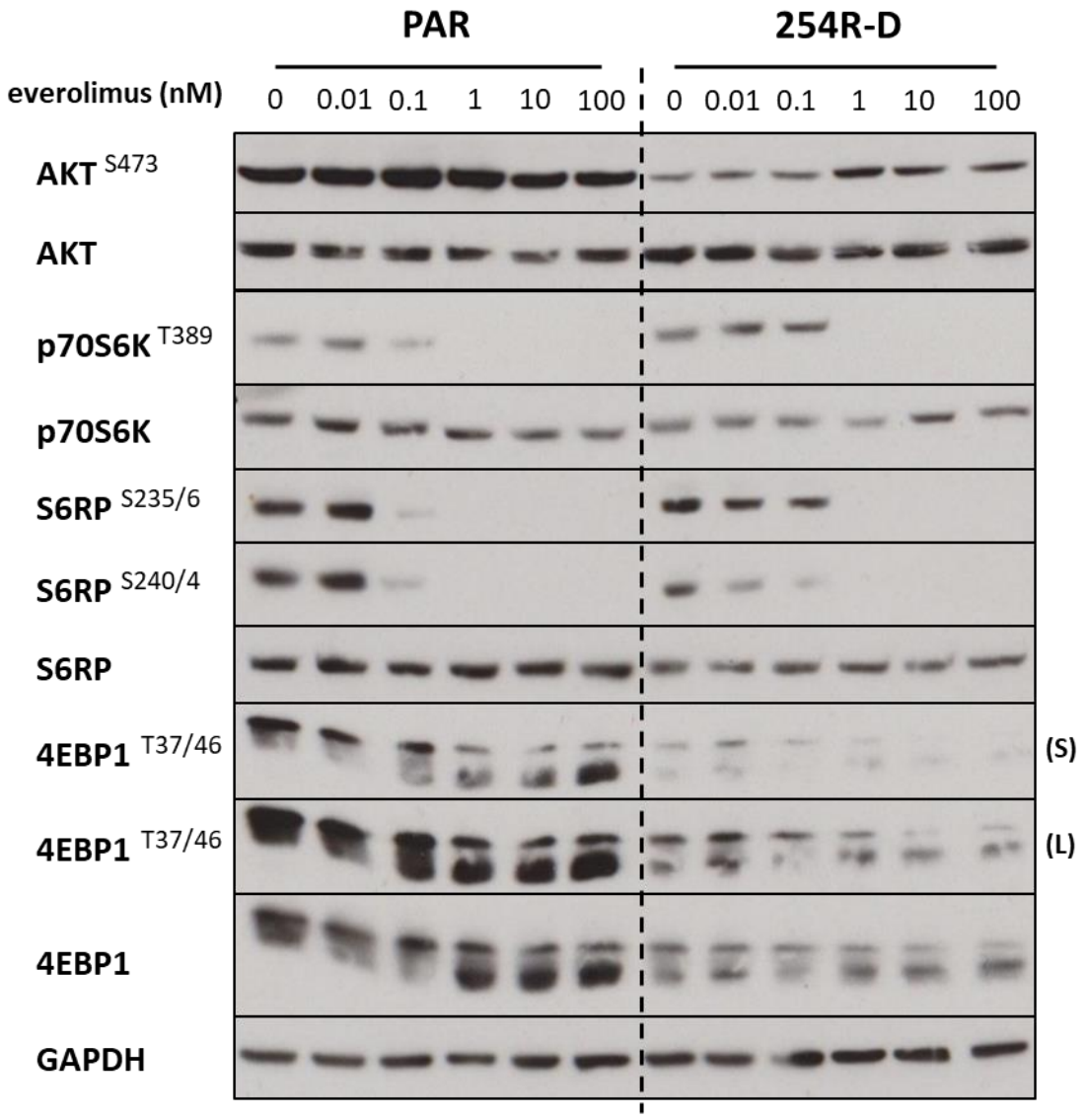

Figure 4.12 – PAM pathway signalling in A2780 PAR and 254R-D cells in response to everolimus
A2780 PAR and 254R-D cells were released, plated and drug-treated as described in Figure 4.9. Western blot procedure used as described in Figure 4.4. Superscript (e.g. AKT ^{S473}) indicates signalling at phosphorylation site in superscript. GAPDH was used as a loading control. Data are representative of two independent experiments.

4.3. Discussion

The primary aim of this chapter was to subclone the A2780 254Rp cell line and further examine subclonal populations to identify candidate mechanisms driving resistance to capivasertib.

4.3.1. Generation and screening of A2780 254Rp subclones

The subcloning of A2780 254Rp resulted in the generation of eight clonal 254R cell lines: 254R-A, B, D, E, F, H, J and K. All of the subclones were screened for morphological differences, cross-resistance to CCT129254, capivasertib, everolimus and vistusertib and changes in baseline signalling of mTORC1 substrates to identify subclones to take forward with distinctly different resistance mechanisms. The subclones revealed a diversity in cross-resistance profiling and mTORC1 signalling, however they could be broadly categorised into three groups (Figure 4.4).

The subclones in group 1 (254R-B and E) exhibited high RF values to everolimus and the phosphorylation and expression of 4EBP1 was similar to PAR. Group 2 subclones (254R-A, D, G, H, J and K) exhibited low everolimus resistance and phosphorylation and expression of 4EBP1 was reduced compared with PAR. Group 3 (254R-F only) exhibited low everolimus resistance, 4EBP1 phosphorylation and expression was similar to PAR and the morphology was more fibroblast-like than the epithelial-like shape of PAR and other resistant cell lines.

Two subclones were selected for further investigation for candidate resistance mechanisms to capivasertib. 254R-B was selected from group 1 and 254R-D was selected from group 2 as these exhibited the greatest resistance to capivasertib for each respective group. 254R-F would also be interesting to investigate further. An EMT phenotype has been previously associated with resistance to AKT inhibitors (MK-2206; Stottrup *et al.*, 2016) and can be further explored by assessing alterations in the levels of E-cadherin, N-cadherin and vimentin. Additionally, alterations in the signalling of mTORC1 substrates may suggest that alterations in E-cadherin may be dependent on mTORC1 signalling (Kim *et al.*, 2014).

Ultimately, the generation of only 8 254Rp subclones, provides a limited scope towards the potential diversity of capivasertib polyclonal resistance mechanisms which may be present in the heterogenetic 254Rp population. Additionally, the similarity of subclones to allow their categorisation into three distinct groups, may highlight a more restricted variety of mechanisms. The main cause of this may be the limited dilution technique used to generate capivasertib-resistant clonal populations. For this technique, the cells are required to be able to grow independently of one another, which may not necessarily be possible for every cell in a polyclonal resistant population. Therefore, not all resistance mechanisms can be isolated in this way. This is particularly true for resistance mechanisms that may have co-evolved together and form co-dependence (Burrell and Swanton, 2014). Furthermore, the use of resistant isogenic cell lines as models of drug resistance carry their own limitations altogether as they are less capable of properly representing a tumour environment in terms of the influences from intratumoural, microenvironment and immune interactions on resistance generation (McDermott *et al.*, 2014; Goodspeed *et al.*, 2016; Namekawa *et al.*, 2019).

4.3.2. Identification of candidate drivers of capivasertib resistance in 254R-B

After selection, cross-resistance profiling was repeated with a revised seeding concentration. 254R-B cells exhibited cross-resistance to all AKT inhibitors tested (10-40 RF; Figure 4.5) and even greater fold resistance to everolimus (96 RF).

Under AKT inhibition with MK-2206 (Figure 4.8), T389 phosphorylation of p70S6K was 254R-B was greater than PAR for each concentration and was likely due to the increase in baseline phosphorylation of this residue. Interestingly, this increase did not translate to increased or resistant phosphorylation of the p70S6K substrate, S6RP (S235/6 and S240/4). Nevertheless, this does not necessarily rule out p70S6K phosphorylation of other substrates such as eEF2K, eIF4B, PDCD4 and SKAR (Fenton and Gout, 2011). Therefore, the activity of these should be investigated. These data suggest that resistance of 254R-B to MK-2206 as observed in Figure 4.5 does not depend on altered signalling of mTORC1 substrates.

As 254R-B exhibited a large fold-resistance to the allosteric mTORC1 inhibitor everolimus, the effect of this drug on AKT and mTORC1 substrate signalling in 254R-B was also investigated (Figure 4.9). The most notable event was S6RP phosphorylation at S235/6. Although the signal was undetectable by 0.1nM in PAR, the signal in 254R-B dropped between 0.1nM and 1nM and did not decrease further with increasing concentrations of everolimus. The drop in signal between 0.1nM and 1nM in 254R-B correlated with a complete abolition of T389 p70S6K phosphorylation, and combined with no further drop in signal, suggested additional S235/6 phosphorylation by an mTORC1-independent kinase, such as p90RSK (Roux *et al.*, 2007). Interestingly, this resistant signalling was not observed with MK-2206 treatment, although previous studies have shown that resistance to PAM inhibitors associated with resistant S6RP S235/6 phosphorylation also harbour cross-resistance to MK-2206 (Serra *et al.*, 2013).

The baseline level of phosphorylation and total expression of 4EBP1 appeared inconsistent between Figures 4.4 and 4.7-9 and was further investigated in Figure 4.10. Densitometric analysis of 4EBP1 showed that phosphorylation at T37/46 was significantly reduced by 60% and total expression was reduced by 30%. This translated to a 36.7% reduction in p4EBP1:4EBP1 ratio between PAR and 254R-B, which suggests that the 4EBP1/eIF4E stoichiometry may be altered to favour increased 4EBP1 binding of eIF4E. Also, considering that in Figure 4.7, eIF4E showed minimal change between PAR and 254R-B, densitometric analysis of the data showed there was also a 42.2% reduction in eIF4E:4EBP1 ratio, which could further impact the 4EBP1/eIF4E stoichiometry to favour increased 4EBP1 binding of eIF4E, and therefore a reduction in eIF4F complex assembly and cap-dependent protein synthesis. Previous studies have shown that alterations of the balance of these two proteins can lead to resistance to mTORC inhibitors (Dilling et al., 2002; Alain et al., 2012; Cope et al., 2014). As discussed previously, 4EBP1 phosphorylation may be linked with its degradation. Similarly to Chapter 3, the effect of reduced 4EBP1 phosphorylation (60%; Figure 4.10) on 4EBP1 degradation in 254R-B (Yanagiya *et al.*, 2012), could be investigated using a cycloheximide half-life assay.

In summary, 254R-B exhibited changes in the activity of 4EBP1 and S6RP that may be involved in driving resistance to capivasertib. These may be independent of one another, with one or both driving resistance, or may be the result of a driver further upstream of both.

4.3.3. Identification of candidate drivers of capivasertib resistance in 254R-D

Cross-resistance profiling highlighted that 254R-D cells were resistant to both ATP-competitive AKT inhibitors, CCT129254 and capivasertib (11-40 RF; Figure 4.6). Interestingly, the RF value for the allosteric AKT inhibitor, MK-2206, although statistically significant was far lower (2.2 RF). This was lower than either of the mTORC inhibitors tested (3.3-12.4 RF). It was therefore unsurprising that mTORC1 signalling in 254R-D exhibited no resistance to MK-2206 (Figure 4.11). 254R-D also exhibited low RF to the mTOR kinase inhibitor vistusertib (3.3 RF), which indirectly affects AKT activity through mTORC2 phosphorylation of S473 (Pearce *et al.*, 2010). As 254R-D was resistant to the ATP-competitive inhibitors, CCT129254 and capivasertib, but less resistant to other direct or indirect forms of AKT inhibition, this suggests that the resistance mechanism may be specific to ATP-competitive AKT inhibitors. This can be confirmed through cross-resistance profiling with alternative ATP-dependent (e.g. ipatasertib) and independent AKT inhibitors (e.g. miltefosine, triciribine; Mundi *et al.*, 2016; Revathidevi and Munirajan, 2019). Sensitivity to MK-2206 implies that the drug can overcome and inhibit the resistance mechanism of capivasertib. As MK-2206 is a selective AKT inhibitor (Hirai *et al.*, 2010), it does not target additional nodes than those also targeted by capivasertib. Therefore the resistance mechanism may affect the shared drug target, AKT. Interestingly, baseline phosphorylation of S473 of AKT was reduced in 254R-D (Figure 4.7), indicative of a reduction in AKT activity (Pearce *et al.*, 2010), suggesting that 254R-D may be less dependent on AKT signalling. Despite this reduction, it would be useful to investigate whether this and AKT-substrate residues such as S9 GSK-3β and T246 PRAS40 are resistant to capivasertib, to indicate resistant activity of AKT. This may also be supplemented with an *in vitro* kinase assay. Previous studies have shown that mutations in AKT can lead to AKT inhibitor resistance (Carpten *et al.*, 2007),

therefore sequencing of all three isoforms in PAR and 254R-D may identify a mutation causing resistance to capivasertib.

Alternatively, resistance may be the result of a bypass mechanism from alterations of other AGC kinases targeted by capivasertib and CCT129254, such as p70S6K or PKA, which drive the same oncogenic output (Davies *et al.*, 2009; Addie *et al.*, 2013; Konieczkowski *et al.*, 2018). As S6RP phosphorylation was unchanged in 254R-D, at baseline or with MK-2206 or everolimus drug treatment, this suggests alterations of p70S6K function may be less likely, however it has yet to be investigated whether S6RP phosphorylation is resistant to capivasertib.

In summary, the data presented in this chapter suggest that A2780 254R-B and D exhibit two distinct phenotypes which were likely to correlate with two distinct resistant mechanisms. This would confirm that resistance to capivasertib in the original A2780 254Rp cell line was polyclonal, however this does not give insight into the respective proportions of different resistant populations within 254Rp. The following chapters will further investigate resistance mechanisms to capivasertib in 254R-B. The candidates identified in this chapter, alterations in 4EBP1 and S6RP both converge functionally to increase cap-dependent protein synthesis (CDPS). Chapter 5 aims to explore the role of CDPS in the resistance phenotype and Chapter 6 investigates the above candidates further.

Chapter 5

Investigating cap-dependent protein synthesis as a resistance phenotype in A2780 254R-B

5. Cap-dependent protein synthesis as a resistance phenotype in A2780 254R-B

5.1. Introduction

Protein synthesis is one of the most energy consuming processes of the cell, and when uncontrolled it can be highly advantageous for oncogenesis, promoting aberrant cell growth and proliferation. This highlights the importance of the high level of regulation overseeing protein synthesis (Nandagopal and Roux, 2015). There are two main methods: cap-dependent (CDPS) and cap-independent (IRES-mediated; CIPS) protein synthesis. The former is dominant under normal growth conditions, however in times of stress and low nutrients, CDPS is reduced to conserve cellular energy and IRES-mediated protein synthesis increases (Qin *et al.*, 2016).

CDPS requires the m^7G-cap at the 5' terminus of mRNA for ribosome docking involving a concerted effort of a number of eukaryotic initiation factors (eIFs) as illustrated in Figure 5.1. The mRNA cap is recognised by the cap-binding protein, eIF4E, through binding with the scaffold protein eIF4G (von der Haar *et al.*, 2000; Youtani *et al.*, 2000). eIF4E, eIF4G and the RNA-helicase, eIF4A, together form the heterotrimeric eIF4F complex. 4EBP1 inhibits eIF4F assembly by binding and sequestration of eIF4E (Figure 5.1; Gingras *et al.*, 2001; Nandagopal and Roux, 2015).

The eIF4F complex when assembled can initiate CDPS. eIF4G interacts with several translation factors, including eIF3 within the pre-initiation complex (PIC) in order to bridge the S6RP-bound 40S ribosomal subunit to the mRNA (Gingras *et al.*, 2001; Klann *et al.*, 2004). Subsequently, eIF4A can unwind secondary structures within the 5'-UTR of the mRNA and allow the ribosomal scanning for the AUG start codon (Figure 5.1). When the start codon is established, the initiation factors dissociate and allow recruitment of the 60S ribosomal subunit, forming a translation-competent 80S ribosome that can begin polypeptide chain synthesis, termed translation elongation (Gingras *et al.*, 2001; Nandagopal and Roux, 2015).

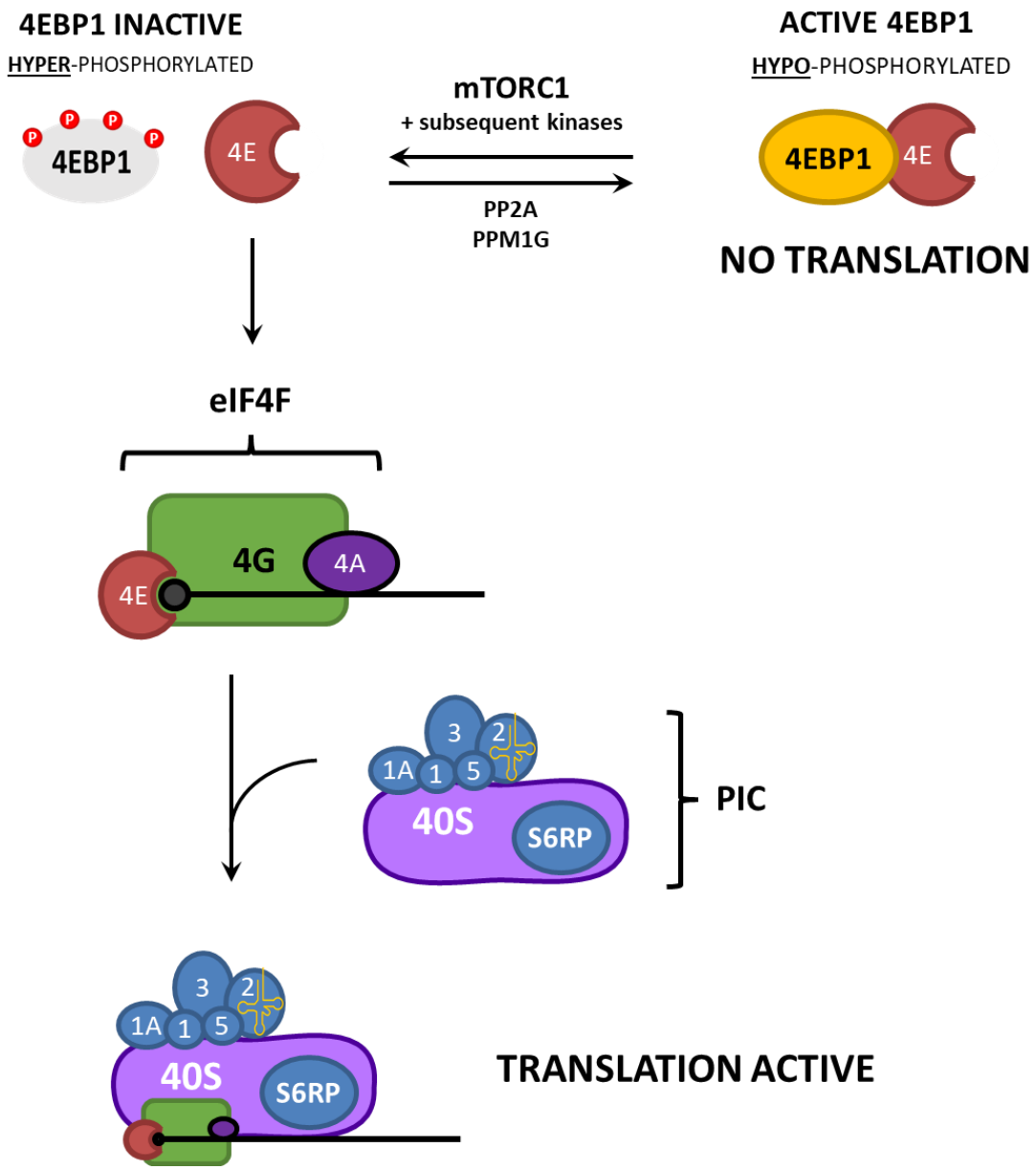

Figure 5.1 – Simplified schematic of the role of 4EBP1 and S6RP in cap-dependent protein synthesis.
When 4EBP1 is hypophosphorylated (yellow), it can bind to and sequester the mRNA cap-binding protein, eIF4E (4E). 4EBP1 becomes inactivated (grey) through phosphorylation of several residues and cannot bind with eIF4E. eIF4E brings the mRNA to the scaffold protein eIF4G (4G), and with eIF4A (4A) form the eIF4F initiation complex. This allows subsequent recruitment of the pre-initiation complex (PIC) for ribosomal docking. S6RP is bound to the 40S ribosomal subunit. 1 = eIF1; 1A = eIF1A; 2 = eIF2; 3 = eIF3; 5 = eIF5; 40S = 40S ribosomal subunit; P = phosphorylated residues; tRNA (yellow on eIF2). Black line with black and grey circle represents mRNA transcript with m^7G cap. Illustration based upon information from Ren-Jang, (2010).

The restricted availability of eIF4E makes this initiation factor a rate-limiting component of the eIF4F complex. The quantity of eIF4E that can bind with eIF4G is regulated by sequestration by eIF4E-binding proteins (4EBPs). When 4EBP1 is in a hypophosphorylated state, it strongly binds with eIF4E and sequesters its ability to

interact with eIF4G. When hyperphosphorylated, 4EBP1 becomes inactive and allows the formation of the eIF4F complex (Nandagopal 2016; Gingras 2001). mTOR is the main and best studied kinase of 4EBP1, which target the residues, T37 and T46 (Nandagopal 2016; Qin; Gingras). Phosphorylation of other less studied 4EBP1 residues may be phosphorylated by GSK-3β, p38MAPK, ERK, PIM1, ATM and CDK1 (Gingras *et al.*, 2001; Roux and Topisirovic, 2018).

CDPS is the convergence point of both PI3K/AKT/mTOR (PAM) and Mitogen-Activated Protein Kinase (MAPK) pathways, and thus it is unsurprising that components of CDPS are often altered and drive resistance to inhibitors of both pathways (Dilling *et al.*, 2002; Nina Ilic *et al.*, 2011; Alain *et al.*, 2012; Boussemart *et al.*, 2014; Cope *et al.*, 2014). Oncogenic alterations of such components often lead to increased CDPS, and therefore either increased global cell growth and proliferation, or increased translation of selective oncogenic mRNAs (Gingras *et al.*, 2001; Qin *et al.*, 2016).

Several mRNA transcripts contain long and structured 5'UTRs. These are highly dependent on eIF4A helicase activity in unwinding the structure in order to allow for effective ribosomal scanning. As eIF4A activity is dependent on eIF4E availability for assembling the eIF4F complex, these mRNAs are termed, eIF4E-sensitive. This regulation is commonly found on mRNA transcripts encoding for proto-oncogenes such as many growth factors, cytokines, protein kinases, transcription factors, polyamine biosynthesis proteins and cell cycle regulators (Figure 5.2; Polunovsky and Bitterman, 2002; Nandagopal and Roux, 2015; Qin *et al.*, 2016).

In Chapter 4, resistant subclones of A2780 254Rp were investigated for resistance mechanisms to capivasertib (AZD5363). 254R-B exhibited resistance to AKT and mTORC1 inhibitors, but not to the eIF4F complex assembly inhibitor, 4EGI-1. This in combination with reduced 4EBP1 expression and increased S6RP phosphorylation indicate that the resistance mechanism may converge at CDPS as a resistance phenotype in 254R-B. The aim of this chapter is to determine whether CDPS is altered in 254R-B and investigate the implications of phenotype.

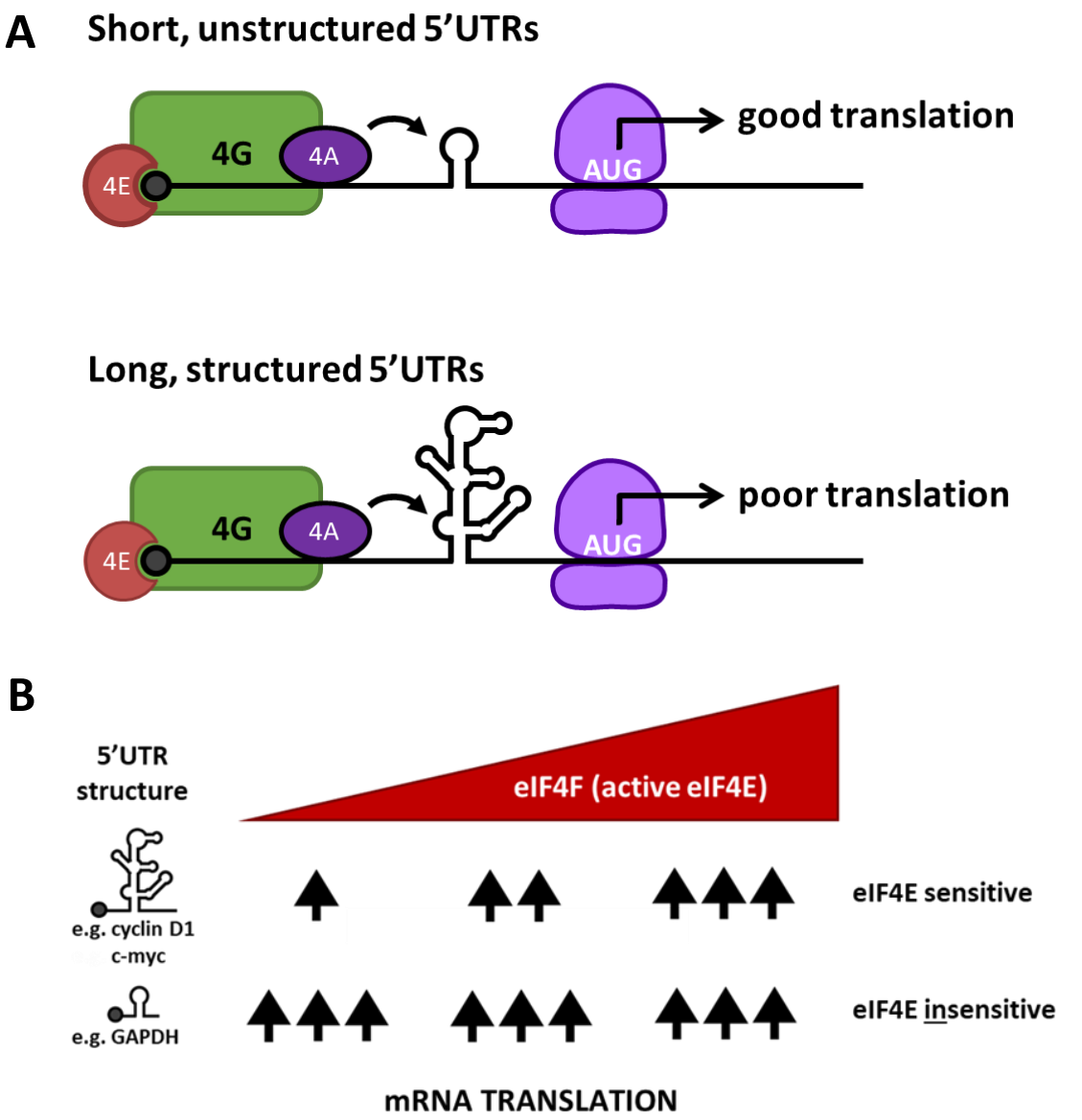

Figure 5.2 – Simplified schematic of protein synthesis of eIF4E-sensitive mRNA transcripts. Illustrations based and adapted from Roux and Topisirovic, (2012) and Leppek et al., (2018). (A) The complexity of the secondary structure of the 5'UTR of mRNA can influence cap-dependent protein synthesis. The greater the complexity, the greater the requirement for eIF4F complex helicase activity, which is dependent on availability of eIF4E – thus termed eIF4E-sensitive transcripts. 4A = eIF4A; 4E = eIF4E; 4G = eIF4G. Black line with black and grey circle represents mRNA transcript with m^7G cap. (B) The translational activity of eIF4E-insensitive mRNAs (top row) are marginally influenced by the changes in eIF4E availability, whereas eIF4E-sensitive mRNAs (bottom row) in contrast are strongly influenced by eIF4E availability.

5.2. Results

5.2.1. Dynamics of 4EBP1 and eIF4G binding to eIF4E in A2780 PAR and 254R-B cells

In Chapter 4, a reduction in 4EBP1 phosphorylation and expression alongside sensitivity to eIF4F complex assembly inhibitor, 4EGI-1 suggested that the resistance mechanism may directly or indirectly involve 4EBP1. As the best studied role of 4EBP1 is its binding and sequestration of mRNA cap-binding initiation factor, eIF4E (Gingras *et al.*, 2001; Nandagopal and Roux, 2015), this interaction was investigated by 7-methyl-GTP (m^7GTP) pull down assay to determine if the functional activity of 4EBP1 had changed in 254R-B.

PAR and 254R-B cell lines were treated for 24 hours with PAM inhibitors. All of the drugs tested inhibited the activity of mTORC1, directly or indirectly, and therefore decrease the phosphorylation of 4EBP1 at T37/46, and theoretically increase 4EBP1-eIF4E binding. Using agarose-bound m^7GTP, acting as a mimetic of the mRNA cap, eIF4E was isolated from non-denatured cell lysates, along with its associated proteins, as illustrated in Figure 5.3. These were analysed by western blot. The concentrations used for treatment corresponded with the half-maximal growth inhibition concentrations (GI_{50}) for PAR (low concentration) and 254R-B (high concentration) in each case respectively. In all of the pull downs in Figure 5.4, 4EBP1 was observed as a single band rather than multiple bands, as only the hypophosphorylated isoform of 4EBP1 can bind with eIF4E (Gingras *et al.*, 2001).

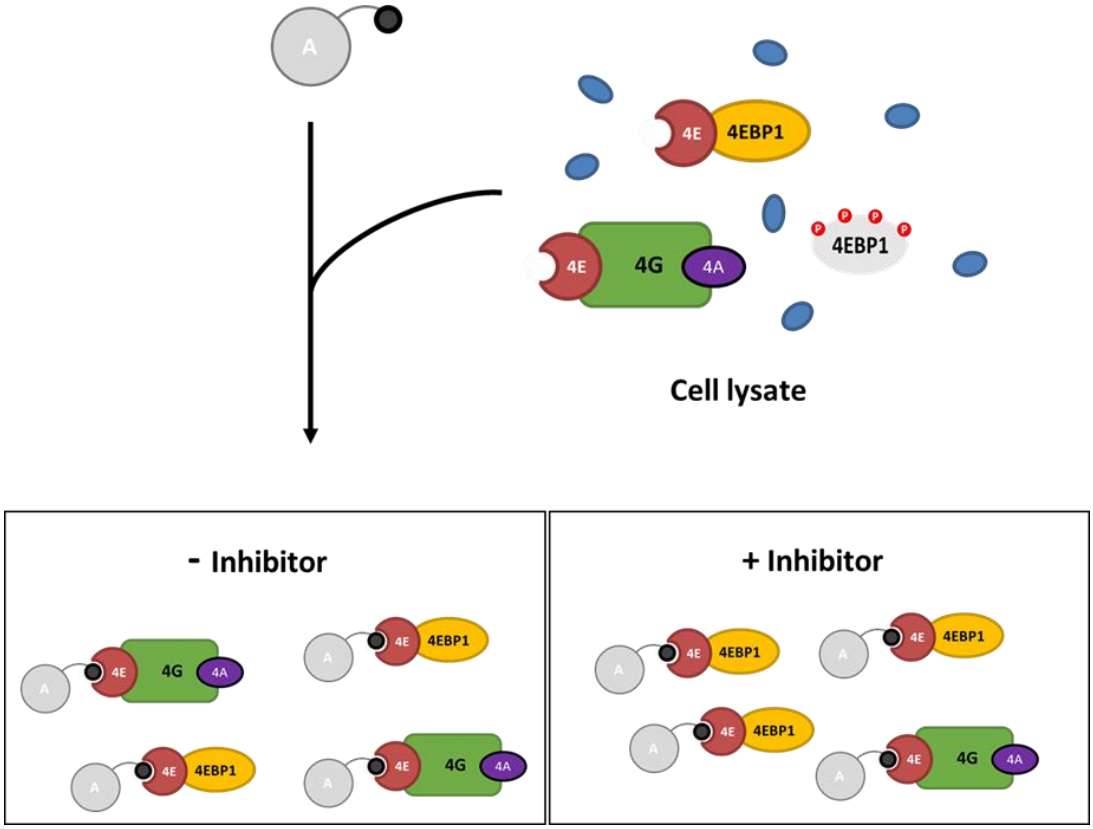

Figure 5.3 – Schematic of the m^{7}GTP pull down assay
Schematic based upon information from *www.thermofisher.com*. Agarose beads (light grey circle) bound with m^{7}GTP (black circle) were used to isolate eIF4E (4E) from cell lysate, and associated proteins were analysed by western blot. In the absence of an inhibitor (bottom left), some 4EBP1 will be phosphorylated and unable to bind with eIF4E, therefore facilitating eIF4E-eIF4G binding. In the presence of an inhibitor (MK-2206, capivasertib, everolimus or vistusertib), phosphorylation of 4EBP1 will be reduced and thus more 4EBP1 can actively bind with eIF4E, and thus greater levels of eIF4E found bound to 4EBP1 and less to eIF4G. 4A = eIF4A; 4G = eIF4G. Non-specific proteins in cell lysate are represented as blue ovals.

The proteins associated with eIF4E were first examined with treatment of MK-2206 (Figure 5.4A). This was used to investigate the response to AKT inhibition alone because MK-2206 is an allosteric inhibitor and thus more AKT-selective (Smyth and Collins, 2009; Hirai *et al.*, 2010). Figure 5.4A shows that the baseline binding of 4EBP1 to eIF4E appeared to be reduced in 254R-B compared with PAR. The level of 4EBP1 binding with eIF4E increases with MK-2206 in both cell lines, however on average the increase in 4EBP1 binding was much greater in PAR (16 fold) than 254R-B (4 fold; Figure 5.5A). eIF4G binding was dramatically reduced with 4μM MK-2206 in PAR (by 57%) compared to on average 17% reduction in 254R-B (Figure 5.5B).

With increasing concentrations of capivasertib (Figures 5.4B and 5.5), the level of 4EBP1 isolated with eIF4E also increased in PAR (6.5 fold) and a concomitant

reduction in eIF4G signal (39%) was observed. Similarly to MK-2206, despite the increase in 4EBP1 binding with increased capivasertib, in 254R-B, this increase was not to the same extent at 4μM (3.7 fold) as witnessed in PAR. Consequently, 254R-B exhibited only a 2.9% reduction in eIF4G binding between 0μM and 4μM capivasertib.

In Figure 5.4C, a similar result was also witnessed with treatment of the mTORC inhibitors, everolimus and vistusertib. With increasing concentrations of drug, there was an increase in 4EBP1 binding with eIF4E in PAR (everolimus 7.7 fold and vistusertib 6.2 fold). Concomitantly, both drugs also exhibited a reduction in eIF4G binding in PAR (66.3% and 39% respectively). Comparatively in 254R-B, 4EBP1 binding to eIF4E increased with drug concentration, however, these were not observed to the same extent as in PAR (both 4.5 fold). eIF4G-eIF4E binding was reduced by 30% for both drugs in 254R-B between the maximum concentration and DMSO control. Taken together, the binding of 4EBP1 to eIF4E was overall less responsive to 4EBP1 phosphorylation inhibition in 254R-B versus PAR.

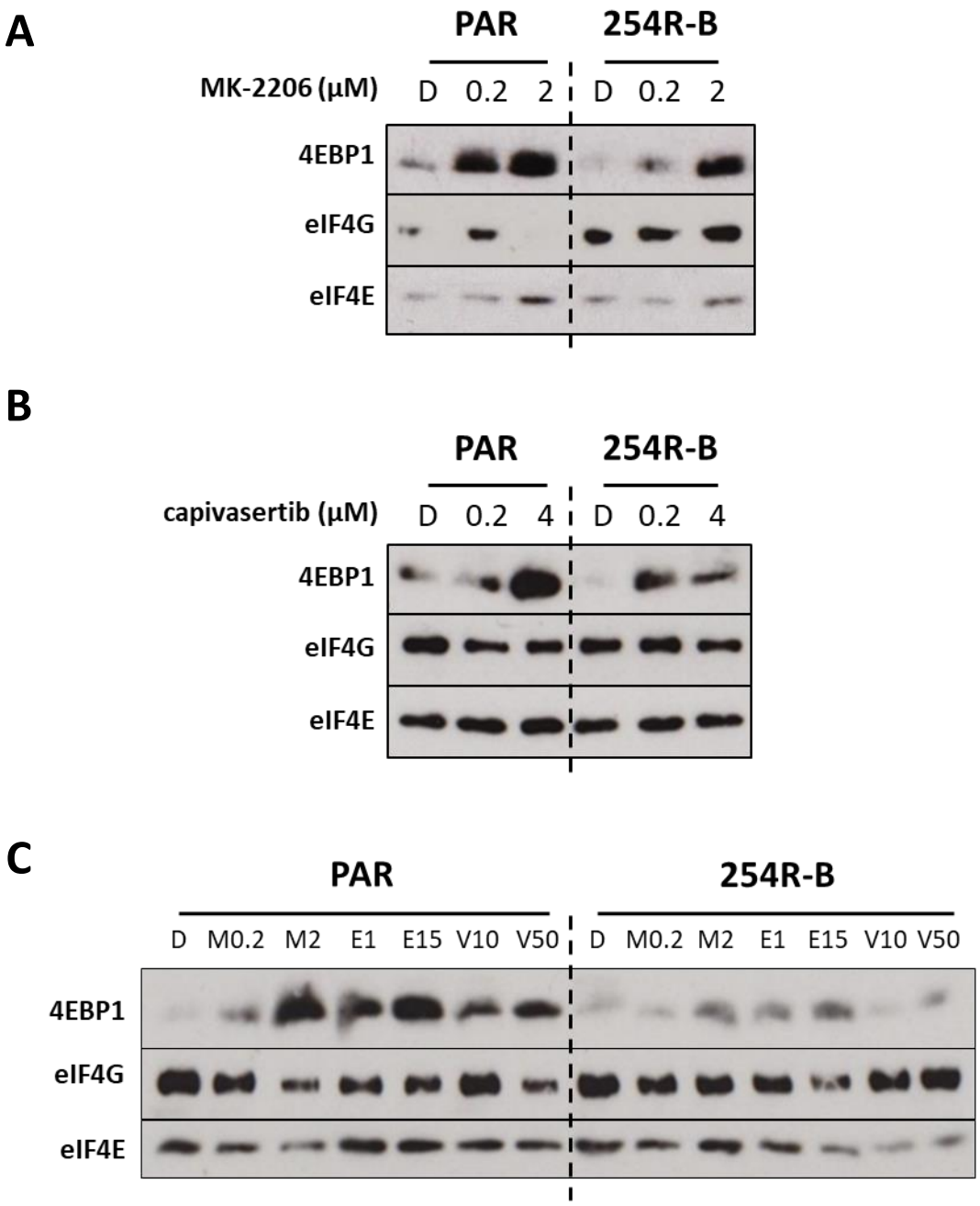

Figure 5.4 – Dynamics of 4EBP1 and eIF4G binding to eIF4E under PAM inhibitor treatment in A2780 PAR and 254R-B cells

Cells were plated at $5x10^5$ in 10cm tissue culture dishes and incubated at normal growth conditions for 72 hours. Cells were treated with (A) MK-2206, (B) capivasertib, (C) MK-2206 (M; µM), everolimus (E; nM) or vistusertib (V; nM) at PAR GI_{50}, 254R-B GI_{50} concentrations or DMSO-only (D; 0 µM), 24 hours prior to lysis in non-denaturing lysis buffer. 250µg protein was incubated with m^7GTP-bound agarose beads for 24 hours to isolate eIF4E and eIF4E-bound proteins. Beads were washed and proteins denatured in sample buffer at 60°C to minimise melting of beads. Bead-bound lysate proteins were separated by SDS-PAGE, transferred to PVDF membranes and probed with antibodies against total proteins and developed. Representative of ≥ two independent experiments.

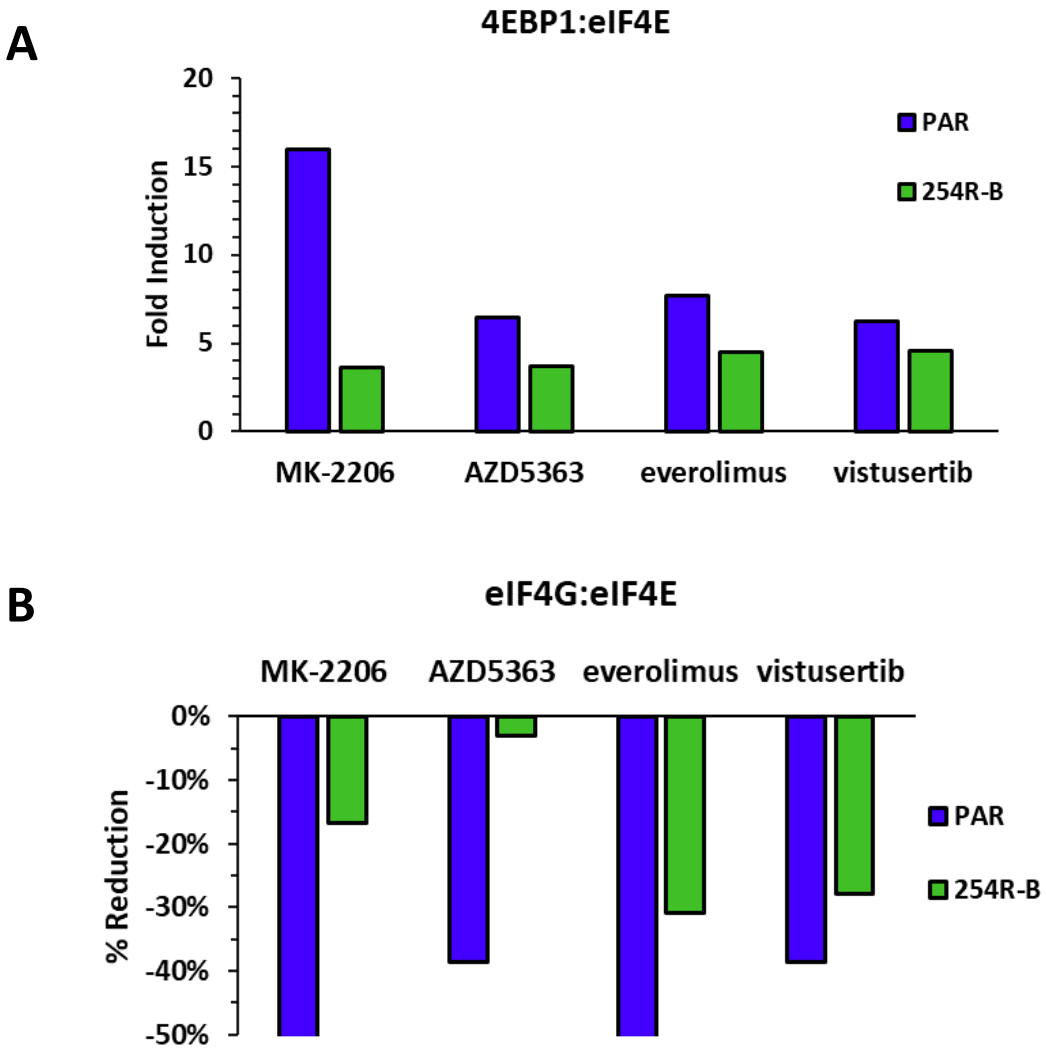

Figure 5.5 – Quantitative analysis of the dynamics of 4EBP1 and eIF4G binding to eIF4E under PAM inhibitor treatment in A2780 PAR and 254R-B cells
The relative induction of 4EBP1 or eIF4G binding to eIF4E with PAM inhibitor treatment. Pull down western blots as Figure 5.4 were quantified using densitometry. 4EBP1 or eIF4G band intensities were determined using Image J, adjusted to eIF4E loading and analysed in Microsoft Excel. (A) Induction was calculated as the fold difference between the adjusted area band intensity of 4EBP1 in DMSO control versus the maximum drug concentration per drug. (B) % Reduction was calculated as the % difference between the adjusted area band intensity of eIF4G in DMSO control versus the maximum drug concentration per drug. Average of ≥ two independent experiments.

5.2.2. Investigation of cap-dependent protein synthesis in A2780 PAR and 254R-B cells

Alterations in the ratio of 4EBP1 or eIF4G binding with eIF4E may suggest that cap-dependent protein synthesis was altered in 254R-B. The dual-luciferase reporter assay (DLRA) is a method by which the CDPS can be investigated between the two

cell lines. This method involves transfection of a bicistronic luciferase construct, and thus the method of transfection in these cell lines required optimisation.

Relative CDPS can be measured as a ratio of Cap-Dependent (CDPS) to Cap-Independent, IRES-mediated protein synthesis (CIPS). By transfecting the bicistronic pRL-IRES-FL plasmid (kindly gifted by Dr. Simon Cook; Babraham Institute, Cambridge), CDPS and CIPS were quantified within A2780 PAR and 254R-B cells. Figure 5.6A shows the pRL-IRES-FL plasmid contains two luciferase genes, *Renilla* and firefly luciferases, separated by the poliovirus internal ribosome entry site (IRES; Li *et al.*, 2002; Cope *et al.*, 2014). Expression of *Renilla* luciferase protein is indicative of CDPS, whereas firefly luciferase expression is regulated by CIPS. The level of luciferase expression is proportionate to the luciferase intensity which can be quantified using the DLRA. The *Renilla* luciferase intensity can be divided by the firefly luciferase signal to calculate the relative CDPS ratio (Figure 5.6B).

$$Relative\ CDPT = \frac{\text{Renilla}\ luciferase\ signal}{firefly\ luciferase\ signal}$$

In Figure 5.6C, *Renilla* expression was on average 200% greater in 254R-B than PAR and firefly luciferase was reduced by 83%. This suggests that CDPS was increased in 254R-B and CIPS was reduced, which overall resulted in a greater increase in relative CDPS. 254R-B exhibited a 9-fold increase in relative CDPS than PAR (Figure 5.6D).

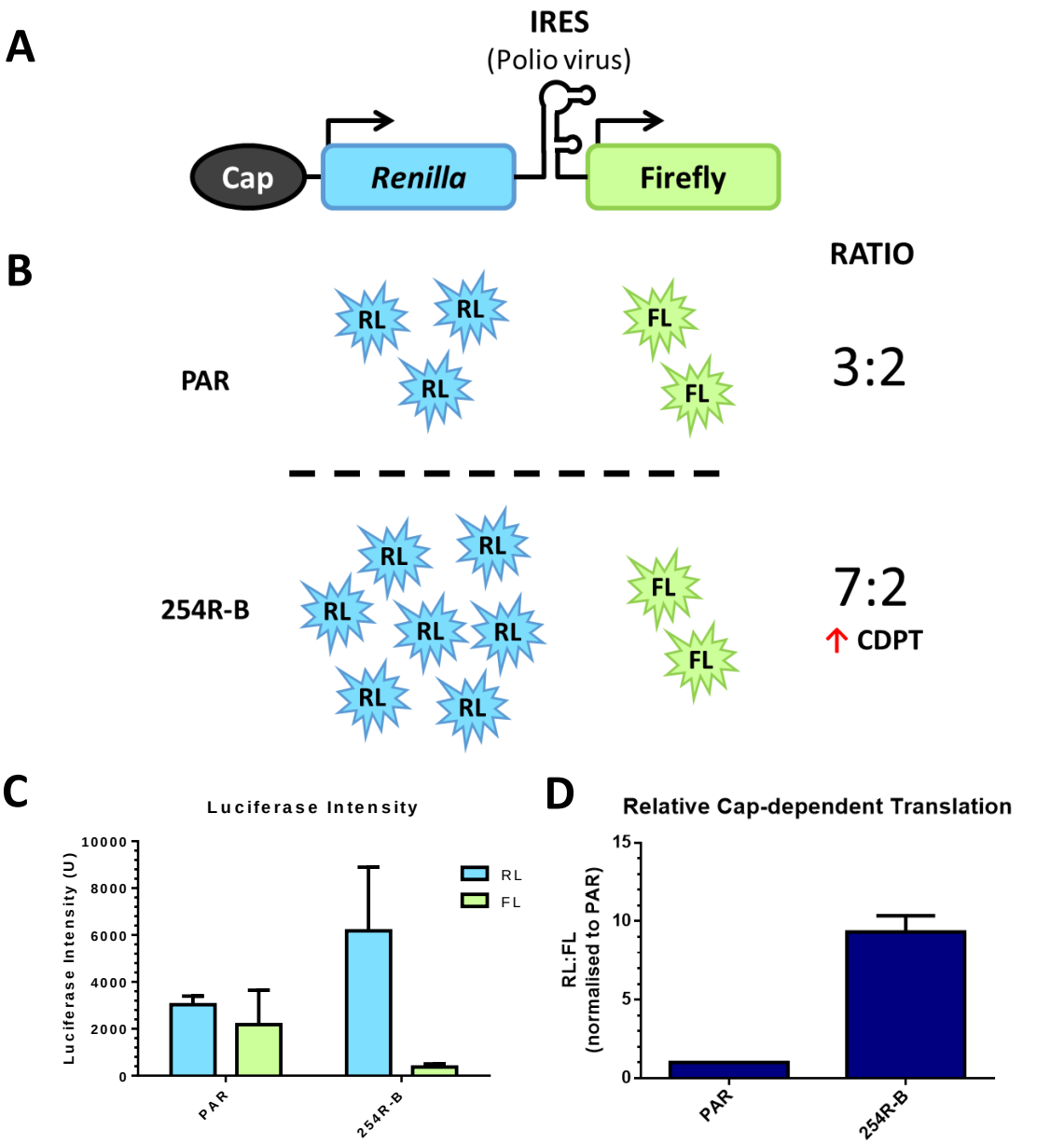

Figure 5.6 – Determination of relative levels of cap-dependent and IRES-dependent protein synthesis in A2780 PAR and 254R-B cell lines.

(A) Schematic of pRL-IRES-FL plasmid, based upon information from Li et al., (2002). Renilla luciferase expression is controlled by cap-dependent protein synthesis, whereas firefly luciferase expression is under the control of a polio-viral internal ribosome entry site (IRES). (B) Luciferase signal correlates with luciferase expression. Relative CDPS was calculated as the ratio of Renilla luciferase signal to firefly luciferase signal in PAR and 254R-B separately. RL = Renilla luciferase; FL = firefly luciferase. (C and D) Cells were plated at $3x10^5$ cells per well in a 6-well plate, 24 hours prior to transfection. 2.5µg of RNAse free water (mock), pRL-IRES-FL or pcDNA5-FRT-eGFP (eGFP) was complexed with Trans-IT LT1 transfection reagent at 3µl:1µg lipid:DNA ratio and added to cells as per manufacturer's instructions. 48 hours post-transfection, cells were lysed, protein concentration normalised and light emitted was measured for Renilla luciferase (RL) and firefly luciferase. Average of three independent experiments. Analysis performed using Graphpad Prism 6. (C) Bar graph depicting the luciferase signal intensities for Renilla and firefly luciferase. (D) Bar graph depicting the ratio of Renilla:firefly luciferase signals calculated by division of Renilla by firefly luciferase signals for each cell line, and normalised to PAR.

5.2.3. Investigation of global protein synthesis in A2780 PAR and 254R-B cells

The increase in CDPS observed in 254R-B, may increase global protein synthesis in the resistant cell line and so this was investigated using polysome profiling. Polysome profiling is a method to quantify altered protein synthesis via the assumption that mRNA with more ribosomes bound will have greater translational activity. Therefore, cells with more actively translated mRNA (polysomes) exhibit increased global protein synthesis. This can be measured as relative polysome and sub-polysome percentages (Warner *et al.*, 1963).

PAR and 254R-B cells were grown overnight and lysed using cycloheximide (CHX)-containing non-denaturing lysis buffer. CHX is an inhibitor of the elongation step of protein synthesis, thus immobilising ribosomes on mRNA and preserving their location at the time of drug exposure (Ingolia, 2010). Cleared lysates were ultracentrifuged through a 10-50% sucrose density to separate free RNA, free ribosomes and poorly translated mRNAs (sub-polysomes) into lighter fractions and actively translated mRNAs (polysomes) into heavier sucrose fractions (Figure 5.7A; Gingras *et al.*, 2001). The optical density of these fractions was measured at 254nm to produce traces as in Figure 5.7B, with an identifiable small peak for sub-polysomes (80S) and a larger stair-like curve for polysomes. The area under the curves were calculated as a percentage of the total area under both sub-polysome and polysome curves and are presented in Figure 5.7C.

254R-B exhibited a slight decrease in the percentage (13.4%) of the total ribosomes bound as sub-polysomes than PAR (16.1%). Consequently, polysome percentages were marginally increased (86.6% and 83.9% respectively). As these changes in in Figure 5.7C, were minimal and statistically insignificant, it was concluded that there was no increase in global protein synthesis.

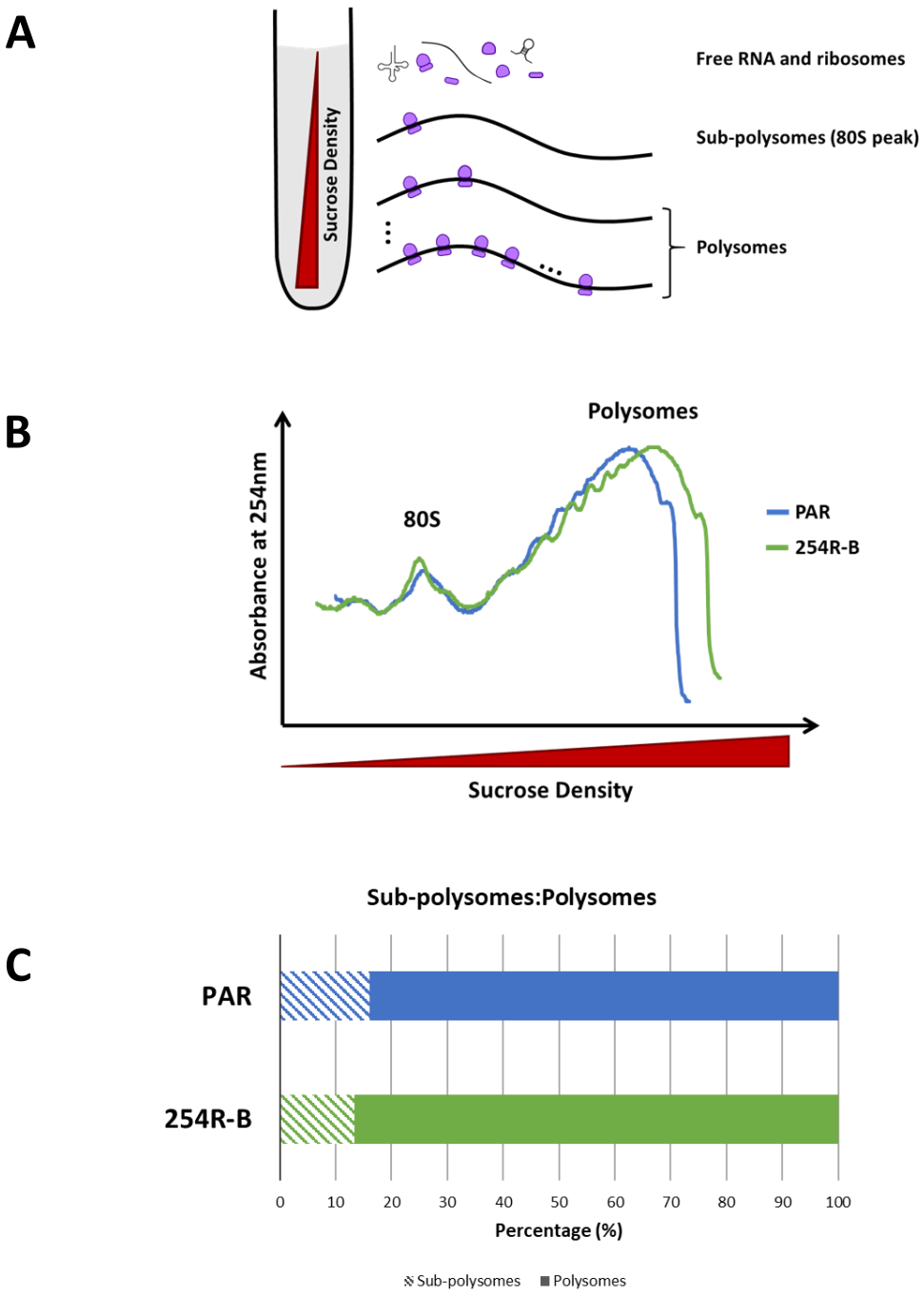

Figure 5.7 – Investigation of global protein synthesis in A2780 PAR and 254R-B cell lines
PAR and 254R-B cell lines were plated at 15x10^6 cells in T175 flasks and incubated in normal growth conditions for 24 hours. Cells were subsequently lysed in polysome profiling non-denaturing polysome profiling lysis buffer, and ultra-centrifuged through a 10-50% sucrose gradient in polyallomer tubes. The centrifugation separates free RNA and ribosomal subunits, sub-polysomes and polysomes by weight as illustrated by (A), adapted from Kapeli and Yeo, (2012) and Godfrey *et al.*, (2017). Absorbance of sucrose gradient fractions were analysed at 254nm to produce a trace such as example in (B), representative of three independent experiments. Increased absorbance correlates with increased levels of the relevant mRNA in the analysed fraction. (C) Bar graph of average polysome and sub-polysome percentages. The area under the polysome and sub-polysome curves were calculated in Microsoft Excel 2016 and analysed as a percentage of the total area under sub-polysome and polysome peaks. Average from three independent experiments.

5.2.4. Translation of eIF4E-sensitive mRNA transcripts in A2780 PAR and 254R-B cells

The increase in CDPS observed in **Error! Reference source not found.** may not necessarily correlate with increased global protein synthesis. It is well studied that increased eIF4F complex assembly increases the translation of eIF4E-sensitive mRNAs which contain long, highly structured 5' UTRs, such as cyclin D1 and c-myc (Polunovsky and Bitterman, 2002; Nandagopal and Roux, 2015; Qin *et al.*, 2016). These rely on the helicase activity of eIF4A in the eIF4F complex for ribosomal scanning and translation of the transcript, and thus the regulation of protein synthesis is dependent on the rate-limiting availability of eIF4E (Figure 5.8B; Roux and Topisirovic, 2012; Leppek *et al.*, 2018). As CDPS was increased in 254R-B (**Error! Reference source not found.**), it was hypothesized that the expression of eIF4E-sensitive transcripts would be increased. The expression of eIF4E-sensitive, cyclin D1 and c-myc was explored in Figure 5.8. Despite the reduction in 4EBP1 signalling and expression in 254R-B, the expression of both cyclin D1 and c-myc proteins was decreased in 254R-B compared with PAR. The reduction of cyclin D1 expression was pronounced, and the reduction c-myc was slight between PAR and 254R-B.

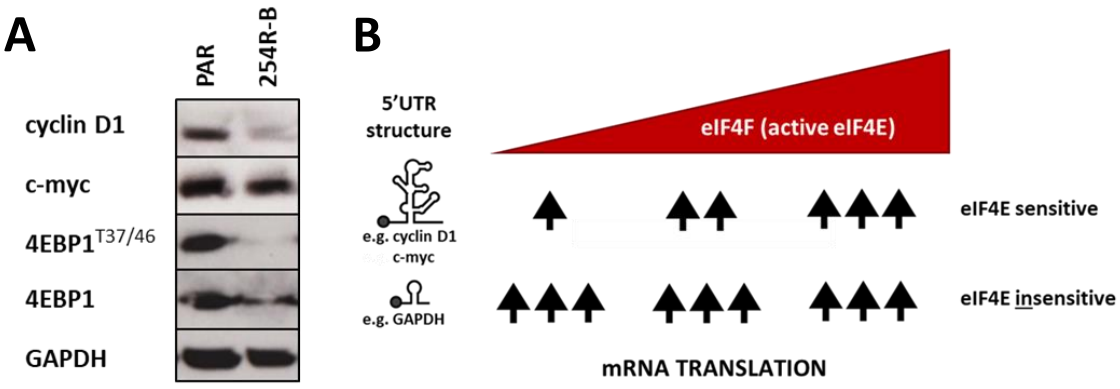

Figure 5.8 – Investigation of eIF4E sensitive protein expression in PAR and 254R-B cell lines
(A) Western blot analysis of baseline expression of cyclin D1, c-myc and 4EBP1 in A2780 PAR and 254R-B cell lines. Cells were plated at $5x10^5$ in 10cm tissue culture dishes and incubated at normal growth conditions for 72 hours. 254R-B was released from CCT129254 at least one week prior to plating cells for lysis. Lysis and western blotting performed as Figure 5.4. In the case of 4EBP1 and GAPDH, blots were stripped and reprobed with appropriate antibodies. GAPDH was used as a loading control. Representative of three independent biological repeats. (B) The translational activity of eIF4E-sensitive mRNAs (top row) are strongly influenced by the changes in eIF4E availability, whereas eIF4E-insensitive mRNAs (bottom row) in contrast are marginally influenced by eIF4E availability. Illustrations based and adapted from Roux and Topisirovic, (2012) and Leppek *et al.*, (2018).

5.3. Discussion

In previous chapters, alterations of 4EBP1 and S6RP were highlighted as candidate resistance mechanisms to capivasertib in A2780 254R-B cells. As both candidates converge on CDPS, the aim of this chapter was to determine whether the changes observed correlated with altered CDPS in 254R-B and investigate the implications of such a phenotype.

5.3.1. Dynamics of 4EBP1-eIF4E and eIF4G-eIF4E in A2780 PAR and 254R-B.

4EBP1 can play a part in both cap-dependent (via eIF4E interactions) and IRES-mediated protein synthesis (Qin *et al.*, 2016). As CDPS is the predominant method of protein synthesis (Qin *et al.*, 2016), the interactions between 4EBP1 and eIF4E were explored using an m^7GTP cap-mimetic pull down assay.

In Figure 5.4, at a baseline level, the binding of 4EBP1 to eIF4E is reduced between PAR and 254R-B cells, which may indicate that more eIF4E is available in 254R-B to bind with eIF4G. This is interesting as the ratio of p4EBP1:4EBP1 and 4EBP1:eIF4E at baseline level as determined by densitometry in Figure 4.7 and 4.10 suggested that 4EBP1 binding to eIF4E would be increased in 254R-B compared to PAR. The addition of PAM inhibitors, intended to reduce 4EBP1 phosphorylation, and thus increasing 4EBP1 activity prompted an increase in 4EBP1 binding to eIF4E in both cell lines. Interestingly, the degree of this binding was reduced in 254R-B for all drugs, which a 4-fold induction average across all drugs compared to 9-fold induction in 4EBP1 binding in PAR. This implies that the activity of 4EBP1 was less responsive to its hypophosphorylative state in 254R-B. As there was no alteration in expression of eIF4E or eIF4G in 254R-B (Figure 4.7), this result may suggest that there was less functionally available 4EBP1 to bind with eIF4E. One explanation for this is that there was less 4EBP1 to be able to bind with eIF4E (Figure 4.10), which may have contributed towards a reduced baseline 4EBP1-eIF4E binding in 254R-B (Figure 5.4). Using 5’ mRNA cap-mimetics as a pull down for eIF4E isolation has a main limitation in that the affinity for eIF4E is increased upon its binding to eIF4G.

Therefore, the degree of 4EBP1:eIF4E cannot be compared directly to eIF4G:eIF4E interactions.

Another explanation for reduced 4EBP1 activity may lie in alternative 4EBP isoforms to 4EBP1 predominating in activity (Tsukumo *et al.*, 2016), as the 4EBP1 antibody used in the pulldown does not cross-react with other 4EBP isoforms. This can be further investigated with pan-4EBP and 4EBP2 and 4EBP3 specific antibodies. However, as eIF4G did not reduce with drug to the same level as in PAR, this is unlikely.

The functional activity of 4EBP1 may also depend on alterations that directly affect its affinity for eIF4E. A mutation may exist in 4EBP1 that reduces the capacity for 4EBP1 to bind with eIF4E, for example within the canonical or non-canonical eIF4E-binding motifs (Igreja *et al.*, 2014; Peter *et al.*, 2015). This could be explored by sequencing 4EBP1 in both cell lines.

Alternatively, reduced functional 4EBP1 may be regulated independently of mTORC1. The mTORC1-dependent 4EBP1 phosphorylation sites investigated in this thesis, T37/46 do not directly affect eIF4E binding, although they are priming sites for S65 and T70 phosphorylation which impact on 4EBP1-eIF4E binding. Alterations of mTORC1-independent 4EBP1 kinase or phosphatase activity in 254R-B may also reduce 4EBP1 interaction with eIF4E.

Previous studies have shown that a reduction in 4EBP1 functionality (by reduced 4EBP1 relative to eIF4E), can lead to resistance to mTORC inhibitors (Dilling *et al.*, 2002; Alain *et al.*, 2012; Cope *et al.*, 2014). As reduced 4EBP1 increases the assembly of the eIF4F complex, these studies also highlight that CDPS is increased as a consequence.

5.3.2. Investigation of cap-dependent and global protein synthesis in A2780 PAR and 254R-B cells.

Relative CDPS was investigated in PAR and 254R-B cells using the dual luciferase reporter assay. Interestingly, there was a nine-fold increase in relative CDPS in

254R-B compared with the PAR (**Error! Reference source not found.**B). This was the result of a two-fold increase in *Renilla* luciferase (representing direct CDPS) and a 83% reduction in firefly luciferase (representing IRES-mediated PS; **Error! Reference source not found.**A). However, this increase in CDPS did not correlate with an increase in overall global protein synthesis (Figure 5.7). Interestingly, such a large reduction in CIPS in 254R-B may be in part due to a reduction in transfection efficiency compared to PAR (Figures 2.5-8), however it may also indicate a real reduction in CIPS in these cells, and requires further investigation.

The dual luciferase reporter assay is a useful means to quantify CDPS with reporter luciferases. However, in the construct used for this assay, the *Renilla* luciferase (representing CDPS) is under the control of one 5' UTR structure. As mRNAs exist with a variety of 5'UTR secondary structures, which vary in translation efficiency, the overall relative CDPS may be better represented using multiple constructs containing varied 5'UTR structures. The accuracy of the experiment is also highly dependent on the transfection efficiency of the construct, which was poor; therefore, the construct could be introduced into the cells by a more efficient means such as transduction.

Polysome profiling is a commonly used technique for investigating global protein synthesis activity as the fraction of ribosomes engaged in polysomes is directly proportional to the translation initiation rate (Warner *et al.*, 1963). However, this is not a method to directly measure polypeptide synthesis, which is highlighted by ribosomal stalling. Polysome profiling is unable to distinguish between ribosome dense mRNA (polysomes) resulted from increased translational activity or a backlog of ribosomes built up after a stalled ribosome (Chassé *et al.*, 2016). Polypeptide synthesis can be directly investigated using ^{35}S methionine labelling or via incorporation of puromycin or L-azidohomoalanine (Chen and Casadevall, 1999; Mallya *et al.*, 2014; Ge *et al.*, 2016)

5.3.3. Translation of eIF4E-sensitive mRNA transcripts in A2780 PAR and 254R-B cells.

Increased CDPS may not necessarily correlate with an increase in global protein synthesis, but instead reflect an increase in the translational activity of eIF4E-sensitive mRNAs (Polunovsky and Bitterman, 2002; Nandagopal and Roux, 2015; Qin *et al.*, 2016). As relative CDPS was increased in 254R-B, the expression of known eIF4E-sensitive mRNAs, cyclin D1 and c-myc were investigated in Figure 5.8. However, the baseline expression of both proteins was decreased in 254R-B compared with PAR, which may suggest that the expression of these proteins is unaffected by increased CDPS. This could be confirmed by quantifying the proportion of the mRNA for these proteins in polysomal and subpolysomal fractions from polysome profiling by quantitative PCR. Additionally, it is important to note that both *CCND1* (cyclin D1) and *MYC* genes also contain IRES, which can be enhanced by mTORC1 inhibition (rapamycin; Shi *et al.*, 2005). Capivasertib and CCT129254 also indirectly inhibit mTORC1 activity (Davies *et al.*, 2012; Addie *et al.*, 2013; Figure 6.12), however further investigation would be required to determine whether release of 254R-B from CCT129254 for one week prior to plating for the western blot (Section 2.2.3) was insufficient for the cellular drug concentration to influence CIPS. Alternatively, the PAR cell line could be equally treated and released from drug as 254R-B.

Regardless of reduced baseline expression, the synthesis of both proteins may be resistant to capivasertib. This can be further investigated by a capivasertib-treated western blot of both cell lines.

The sensitivity of protein synthesis to eIF4E availability may be context dependent for some highly complex 5'UTR transcripts (Roux and Topisirovic, 2018). Therefore, cyclin D1 and c-myc may not be eIF4E-sensitive in A2780 cells. Consequently, translation of other mRNAs known to be eIF4E-sensitive in A2780 cells such as BCL-2 and MCL-1 should be investigated (Lam *et al.*, 2014). However, it is worth noting that BCL-2 translation can also be mediated by IRES-dependent translation (Sherrill *et al.*, 2004).

In summary, the data presented in this chapter suggests that CDPS was significantly increased in A2780 254R-B versus PAR. This did not increase global protein synthesis, nor translation of 4E-sensitive mRNAs, although transcripts other than cyclin D1 and c-myc may be affected. Chapter 6 will further investigate the role of reduced 4EBP1 function and everolimus-resistant S6RP as candidate resistance mechanisms to capivasertib in 254R-B cells.

Chapter 6

Investigating 4EBP1 and S6RP alterations as candidate capivasertib resistance mechanisms

6. Investigating 4EBP1 and S6RP alterations as candidate capivasertib resistance mechanisms

6.1. Introduction

Cap-dependent protein synthesis (CDPS) is a convergence point of several signalling pathways including the mitogen-activated protein kinase (MAPK) and the PI3K/AKT/mTOR (PAM) pathways (Boussemart *et al.*, 2014). Alterations in the components of CDPS commonly appear as resistance mechanisms to inhibitors of both signalling pathways, especially PI3K, AKT, mTOR and B-Raf inhibitors (Dilling *et al.*, 2002; N. Ilic *et al.*, 2011; Mallya *et al.*, 2014; Nogami *et al.*, 2015). Many of these alterations commonly affect the efficiency of the eIF4F complex assembly by shifting the 4EBP1/eIF4E stoichiometry and enhancing CDPS (Alain *et al.*, 2012). This shift can occur through increased eIF4E expression (N. Ilic *et al.*, 2011; Hoang *et al.*, 2012; Cope *et al.*, 2014), reduced 4EBP1 expression (Dilling *et al.*, 2002; Mallya *et al.*, 2014; Martineau *et al.*, 2014), or increased hyperphosphorylated 4EBP1 (Mi *et al.*, 2015; Nogami *et al.*, 2015).

Previous studies have shown that resistance mechanisms at eIF4E or 4EBP1, may affect the proteins directly such as amplification of eIF4E (N. Ilic *et al.*, 2011), or complete loss of 4EBP1 (Mallya *et al.*, 2014). However, these proteins can also be indirectly targeted as well. For example, the activity of eIF4E can be increased through greater phosphorylation of serine 209 (S209) by ERK (extracellular signal-regulated kinase; Hoang *et al.*, 2012); *EIF4EBP1* transcription has been reported to be down-regulated by SNAIL (J. Wang *et al.*, 2017) and phosphorylation of 4EBP1 may be increased by mTORC1-dependent or independent mechanisms (Mi *et al.*, 2015; Nogami *et al.*, 2015).

Another component of CDPS, S6RP (S6 ribosomal protein) is a less common driver of drug resistance. Studies by Grasso *et al.*, (2014) and Theodosakis *et al.*, (2017) have shown that increased phosphorylation of serine 235 and 236 (S235/6) on S6RP is associated with resistance to MAPK pathway inhibitors. As S235/6 on S6RP can be phosphorylated by p90RSK (p90 ribosomal S6 kinase), resistance to selumetinib and

vemurafenib could be reversed using several p90RSK inhibitors, including BI-D1870 (Theodosakis *et al.*, 2017). Although neither of these studies investigated whether resistance to MAPK inhibition also correlated with cross resistance to PAM inhibitors, increased p90RSK3 and 4 expression (Serra *et al.*, 2013) as well as increased MAPK pathway activity have been previously associated with PI3K and mTORC inhibitor resistance (Carracedo *et al.*, 2008; Yu *et al.*, 2008; Hoang *et al.*, 2012; Muranen *et al.*, 2016).

The MAPK pathway has several nodes of crosstalk to the PAM pathway. Many of these crosstalk events positively regulate the activity of the PAM pathway (Figure 6.1). Due to their promiscuity, ERK and its substrate, p90RSK are the main nodes of crosstalk feeding from the MAPK pathway. ERK and p90RSK can directly phosphorylate TSC2 (tuberin; Mendoza *et al.*, 2011; Aksamitiene *et al.*, 2012) and also S8, S696 and S863 of RAPTOR (Carrière *et al.*, 2008; Carriere *et al.*, 2011). These all act to increase mTORC1 activity. ERK also phosphorylates MNK1 (MAPK-interacting kinases) which in turn targets S209 on eIF4E to increase its activity in CDPS (Siddiqui and Sonenberg, 2015; Brown and Gromeier, 2017). Additionally, the high kinase domain homology between p90RSK and p70S6K results in the sharing of several substrates including S235/6 of S6RP, eIF4B and eEF2K (Pearce *et al.*, 2010).

In previous chapters, alterations in 4EBP1 and S6RP were associated with resistance to capivasertib (AZD5363) and increased CDPS in 254R-B cells. The aim of this chapter was to validate the reduction of 4EBP1 expression observed in 254R-B as a candidate resistance mechanism to capivasertib and to further investigate the cause of S6RP S235/6 phosphorylation and its relevance in driving resistance.

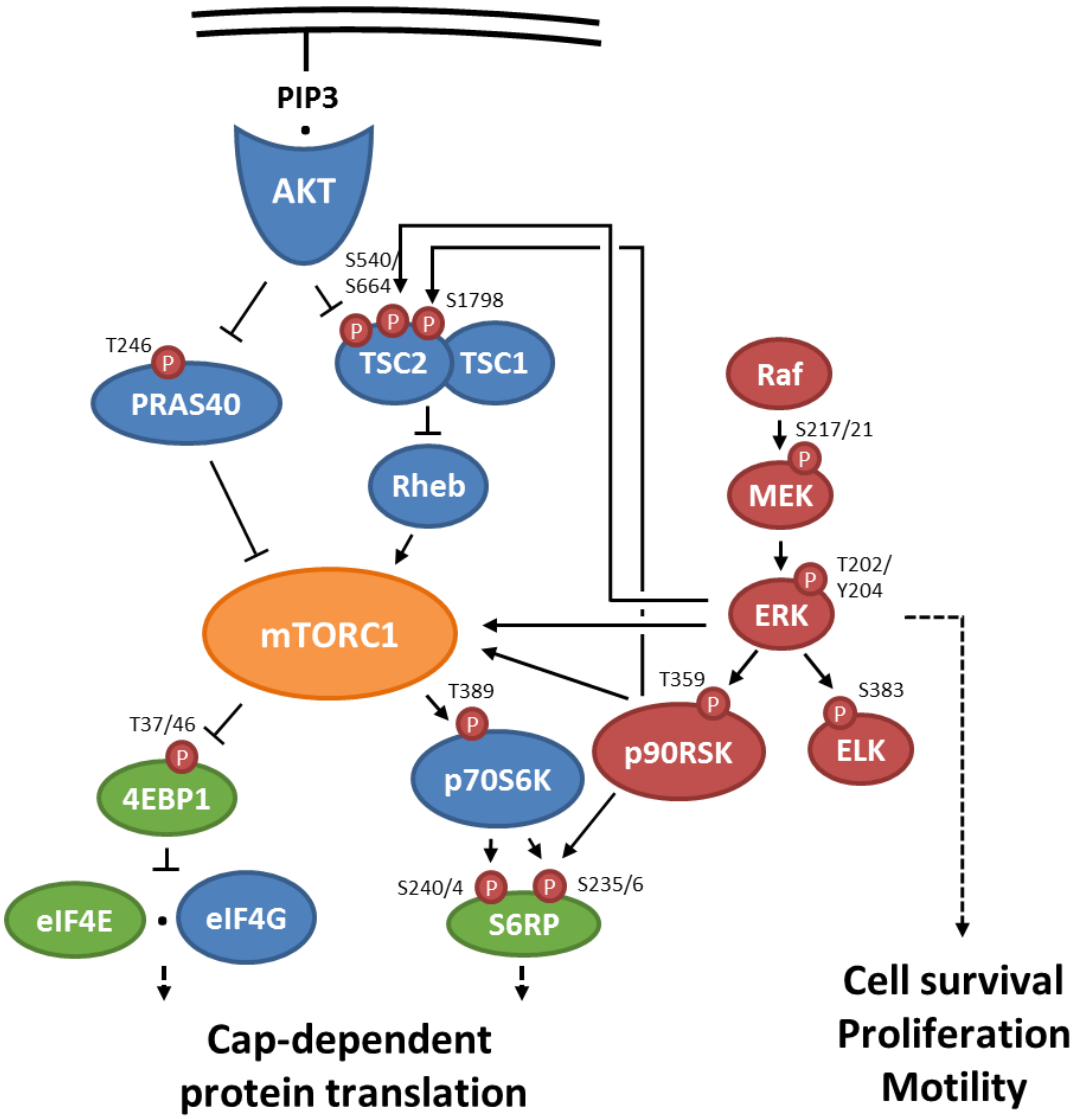

Figure 6.1 – Stimulatory crosstalk from MAPK pathway into the PAM pathway.
A simplified schematic of the PAM pathway illustrating the relationship of the components of MAPK pathway (dark red; ERK and p90RSK) with the PAM pathway (blue and orange). Proteins in green are CDPS components commonly altered in PAM inhibitor drug resistance. Phosphorylated residues are represented as dark red (P)s, with amino residue defined. Black arrows and block-headed arrows indicate phosphorylation of target induces activation or inhibition respectively. Black dotted arrows indicate phenotypic output. Periods (.) indicate protein interaction and binding. Illustration based upon information from Mendoza, et al., (2012) and Akasamitiene, et al., (2012).

6.2. Results

6.2.1. Validation of reduced 4EBP1 expression as a driver of resistance to capivasertib in 254R-B.

In previous chapters, 4EBP1 had been identified as a candidate for resistance to capivasertib due to a reduction in baseline phosphorylation and expression (Figure 4.7) and reduced interaction with eIF4E (Figure 5.4), which correlated with increased CDPS (Figure 5.6D). The dependence of the resistance mechanism on 4EBP1 was investigated by altering its functional activity in three ways: 1) reducing 4EBP1 activity in PAR via siRNA knockdown to induce resistance; or increasing 4EBP1 activity in 254R-B to reduce resistance by 2) small molecule inhibition of eIF4E-eIF4G interaction or 3) exogenous overexpression of 4EBP1.

6.2.1.1. Reduction of 4EBP1 activity in A2780 PAR by siRNA knockdown

Assays which can induce resistance in sensitive cell lines are typically more biologically insightful than increasing sensitivity of resistant cell lines, as the latter can be due to reduced cell fitness (Kaelin, 2017). If the alteration of the candidate alone can induce resistance in PAR cells, such is unlikely a result of off-target effects. In the case of capivasertib resistance, it was hypothesized that as 4EBP1 activity was reduced in 254R-B, reducing 4EBP1 activity in PAR cells via the knockdown of 4EBP1 expression by siRNA, may induce resistance to capivasertib.

To determine if loss of 4EBP1 expression could induce resistance to CCT129254 (analogue to capivasertib; Figure 1.10), 4EBP1 knockdown was performed on PAR cells. These were treated with CCT129254, 24 hours after plating, and incubated for an additional 72 hours, where the remaining cells were fixed and stained as the SRB growth assay. Cells were simultaneously plated into 6-well plates without drug treatment to observe knockdown at several time points throughout the assay (Figure 6.2A). 254Rp was used to represent CCT129254 resistance, as 4EBP1 expression was lower than 254R-B (Figure 4.4).

Figure 6.2 shows the effect of 4EBP1 knockdown on PAR cells exposed to CCT129254 for 72 hours. In Figure 6.2A, at 24 hours, when cells were drug treated, there was no knockdown of 4EBP1 with either Flexitube 2 or 5 oligonucleotides compared to the mock or NT controls. At 48 hours, 4EBP1 levels were lower with both oligonucleotides compared to the PAR NT or either mock-transfected PAR and 254Rp controls. 4EBP1 levels were lower in cells transfected with Flexitube 5 than 2 oligonucleotides. After 96 hours, 4EBP1 was still knocked down compared with the PAR mock and NT controls. Therefore, 4EBP1 expression was reduced for at least 48 of the 72-hour drug incubation period. Figure 6.2B shows that 4EBP1 knockdown with both oligonucleotides caused a significant reduction (up to 50%) in the viability of PAR cells under CCT129254 treatment. However, when the CCT129254 dose response curve for each transfection condition was normalised to its respective untreated control (Figure 6.2C), no change in the sensitivity to CCT129254 was observed with 4EBP1 knockdown when compared to the PAR mock and NT controls. Therefore, 4EBP1 knockdown reduced viability of PAR cells but did not increase resistance to CCT129254. Taken together, this would suggest that 4EBP1 knockdown was not sufficient to induce a CCT129254 resistance phenotype in the PAR cell line.

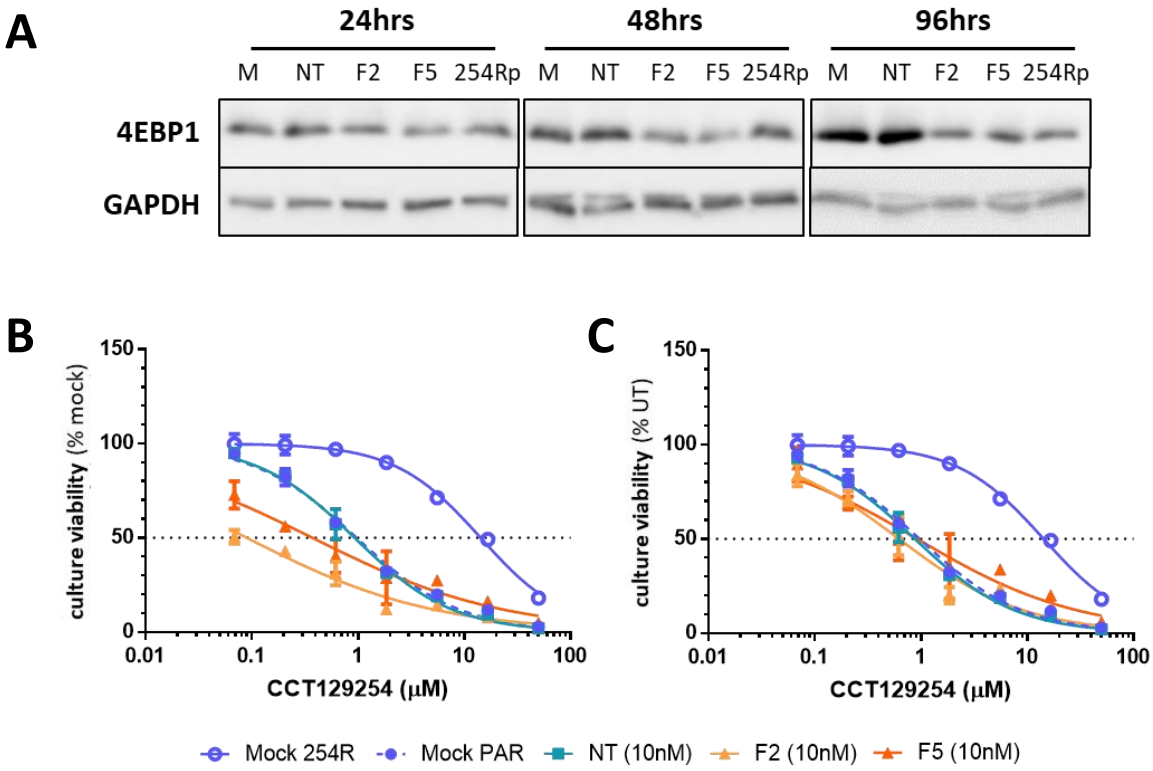

D

	M (PAR)	M (254Rp)	NT	F2	F5
GI_{50} (μM)	0.88 ± 0.1	11.7 ± 2.2	1.03 ± 1.2	0.97 ± 0.4	1.56 ± 1.8
RF	-	13.3**	$1.17^{N.S}$	$1.13^{N.S}$	$1.80^{N.S}$

Figure 6.2 – 4EBP1 knockdown in PAR cells by siRNA on the sensitivity to CCT129254.
A2780 PAR cells were reverse-transfected in 96 well plates with RNAse free water (mock; M), 10nM non-targeting Allstar negative control siRNA oligonucleotide (NT) or 4EBP1-targeting Flexitube 2 (F2) or 5 (F5) oligonucleotides, using 0.1% Lipofectamine. 24 hours after transfection, cells were treated with a serial dilution of CCT129254 for 48 hours and surviving cells were determined by SRB growth assay. (A) PAR cells were reverse-transfected and 254Rp cells were mock-transfected only as above in 6-well dishes simultaneously with 96-well plate transfection as knockdown efficiency controls. Plates were incubated for 24, 48 or 96 hours as indicated. Cells were subsequently lysed and analysed by western blotting. GAPDH was used as a loading control. (B and C) Dose response curves generated and half-maximal growth inhibition concentrations (GI_{50}) were calculated using GraphPad Prism 6. Growth curves for CCT129254 treatment were normalised to the untreated mock control (% mock; B) or to the untreated control (% mock) for each respective transfection condition (C). Data points present mean ± SD of three technical replicates. The broken line on the Y-axis indicates the points on the curves where growth was inhibited by 50% (GI_{50}). Data representative of ≥three independent experiments. (D) Summary of GI_{50} values for CCT129254 of transfected PAR cells and mock transfected 254Rp. Mean ± S.D. Welch's t test, *p<0.05, **p<0.01, N.S = non-significant, RF = resistance factor.

6.2.1.2. Increase of 4EBP1 activity in A2780 254R-B by chemical action to recapitulate sensitivity to capivasertib

The dependence of the resistance mechanism on 4EBP1 was also investigated by increasing its activity in 254R-B. One method to do this is by mimicking 4EBP1 inhibitory activity using the compound, 4EGI-1. This drug simultaneously disrupts the interaction of eIF4G-eIF4E (Moerke *et al.*, 2007) and enhances 4EBP1 binding to eIF4E (Sekiyama *et al.*, 2015). Cells were treated with the drug for 24 hours prior to lysis and the effect of 4EGI-1 on the sensitivity of 254R-B to capivasertib was measured using the apoptotic marker, cleaved PARP.

For this experiment, the concentrations of capivasertib and 4EGI-1 were optimised. The ideal concentration of capivasertib was that induced cleaved PARP in PAR cells but not 254R-B. As observed in Figure 6.3A, there was no detectable PARP cleavage in either PAR or 254R-B at baseline, however with increasing concentrations, PARP cleavage is increased in PAR. There was no clear PARP cleavage observed in any concentration of 254R-B. Based on this, any concentration at 1µM or above of capivasertib was ideal, however 1µM capivasertib was selected as this was the lowest concentration of capivasertib where PARP was notably cleaved in PAR. This concentration is also similar to the plasma concentration detected in patients during the Phase I clinical trial of capivasertib (Banerji *et al.*, 2018).

The ideal concentration of 4EGI-1 was one that can disrupt eIF4G-eIF4E binding in 254R-B cells. This was examined using the m^7GTP eIF4E pull down assay. Figure 6.3B shows that at 50µM and 100µM 4EGI-1, eIF4E binding with eIF4G was reduced and eIF4E binding to 4EBP1 was increased with increasing concentrations. Interestingly, the levels of eIF4E isolated with the m^7GTP beads was also reduced at 50µM and 100µM 4EGI-1 compared to the untreated control, although total eIF4E in the lysate remained unchanged. This phenomenon was expected as the affinity of eIF4E for the mRNA cap increases with binding to eIF4G (von der Haar *et al.*, 2000). These concentrations reduced the levels of phosphorylated 4EBP1 in the input lysate, observed by the band shift at 50µM, similar to the 2µM MK-2205 pull down positive control (P+). However, neither of these concentrations induced PARP cleavage in 254R-B to a detectable level as observed with 1µM capivasertib in PAR (C+). 50µM

4EGI-1 was selected as it was the lowest concentration tested that reduced eIF4G binding with eIF4E.

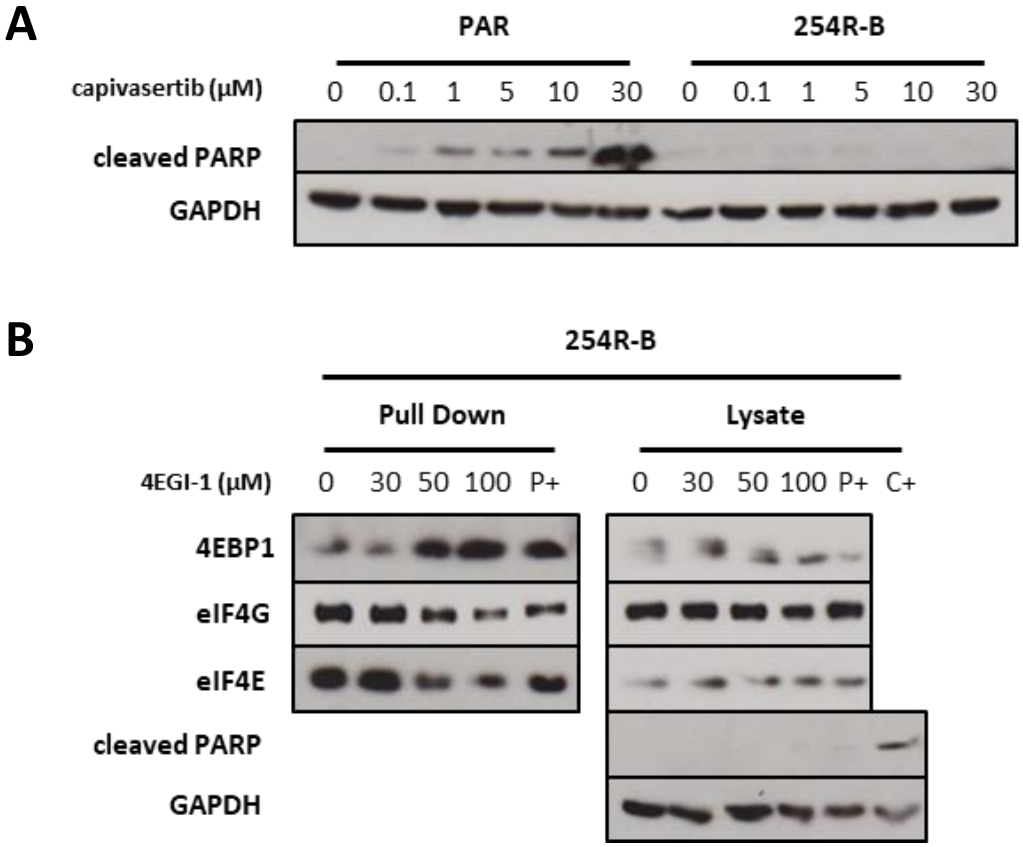

Figure 6.3 - Analysis of cleaved PARP with treatment of capivasertib (A) or 4EGI-1 (B)
Cells were plated at $5x10^5$ in 10cm tissue culture dishes and incubated at normal growth conditions for 72 hours. Cells were treated with capivasertib or 4EGI-1 at concentrations indicated, 24 hours prior to lysis. (A) Lysate proteins were analysed by western blotting. Membranes were probed with cleaved PARP or GAPDH as a loading control. (B) 250μg protein in non-denaturing lysis buffer was incubated with m^7GTP-bound agarose beads for 24 hours to isolate eIF4E and eIF4E-bound proteins. Beads were washed and proteins denatured in sample buffer at 60°C to minimise melting of beads. Bead-bound (left) and lysate only (right) proteins were analysed by western blotting. P+ = Pull down positive control (2μM MK-2206 treated 254R-B as Figure 5.4); C+ = cleaved PARP positive control (1μM capivasertib treated PAR from (A)). Representative of two independent experiments.

Figure 6.4 shows the effect of combined capivasertib and 4EGI-1 treatment in PAR and 254R-B cells. In Figure 6.4A, cleaved PARP increased in PAR cells with capivasertib or 4EGI-1 alone, but cleavage was much greater with the drug combination. In contrast, 254R-B cells have increased baseline PARP cleavage compared with PAR, but neither drug alone or combined increased PARP cleavage. As observed in the pull down in Figure 6.4B, 4EBP1 binding with eIF4E did not increase to the same level as PAR treated with the combination. In summary,

mimicking an increase of 4EBP1 activity using 4EGI-1 did not increase sensitivity of 254R-B to capivasertib when measured by apoptotic markers.

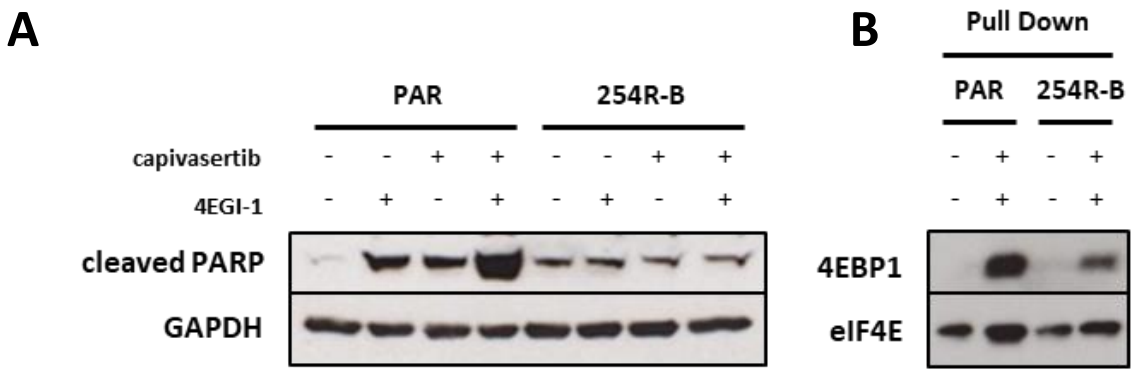

Figure 6.4 – Analysis of cleaved PARP with combined treatment of capivasertib and 4EGI-1. Cells were plated as Figure 4.7 and treated with capivasertib (1μM), 4EGI-1 (50μM) or both, 24 hours prior to lysis. (A) Lysate proteins were analysed by western blotting as Figure 4.7. Membranes were probed with cleaved PARP or GAPDH as a loading control. (B) eIF4E and eIF4E-bound proteins were isolated by pull down and analysed by western blotting as described in Figure 4.7. Representative of two independent experiments.

6.2.1.3. Increase of 4EBP1 activity in A2780 254R-B through exogenous protein expression to recapitulate sensitivity to capivasertib

Another method to increase 4EBP1 activity in 254R-B was to increase 4EBP1 expression. 254R-B cells were transfected with pcDNA3-4EBP1WT-HISMYC (human wildtype 4EBP1; WT) and pcDNA3-4EBP15A-HISMYC (human 5A-mutant 4EBP1; 5A), which were kind gifts from Dr Chris Proud (Australia; Tee and Proud, 2002; Wang *et al.*, 2003). The 5A mutant has five phosphorylated residues of 4EBP1 (T36, T47, T70, S83 and S65) mutated to alanine, and are thus unable to be phosphorylated, rendering exogenous 4EBP1 permanently active (Wang *et al.*, 2003).

Prior to initiating stable transfection, to confirm the nature of the plasmids, 254R-B were transiently transfected, lysed after 48 hours and levels of 4EBP1 expression was examined by western blotting (Figure 6.5). 4EBP1 was run as a single band rather than multiple bands for easier comparison. Both the phosphorylation and total expression of 4EBP1 was increased in 254R-B transfected with WT 4EBP1, however only total expression and not T37/46 of 4EBP1 was increased in 5A 4EBP1-transfected cells, as expected. 4EBP1 in these constructs was tagged with His and

Myc at the N-terminus (Wang *et al.*, 2003). The detection of the His-tag in only the WT and 5A lanes confirmed successful exogenous expression of the constructs.

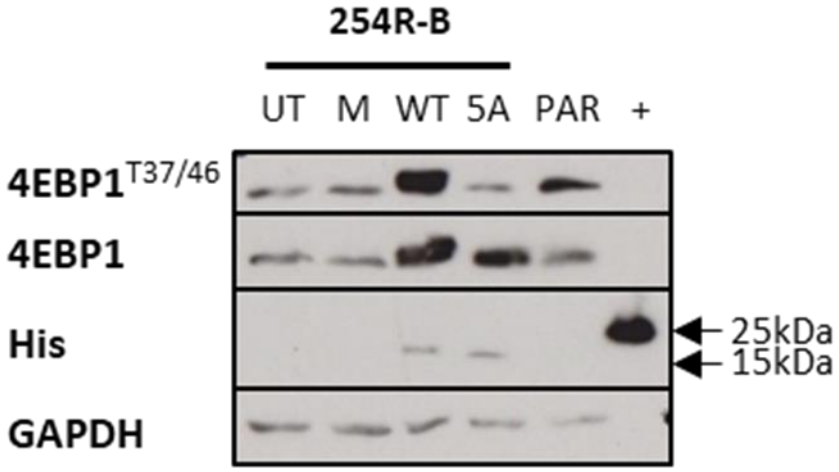

Figure 6.5 – Transient expression of wildtype and 5A-mutant 4EBP1 in 254R-B cells.
Cells were plated at $3x10^5$ cells per well in a 6-well plate, 24 hours prior to transfection. 2.5µg of RNAse free water (mock; M), pcDNA3-4EBP1WT-HISMYC (WT), or pcDNA3-4EBP15A-HISMYC (5A) were complexed with Trans-IT LT1 transfection reagent at 3µl:1µg lipid:DNA ratio and added to cells as per manufacturer's instructions. 48 hours post-transfection, cells were lysed and analysed by western blotting as Figure 6.4. UT = untransfected 254R-B cells; PAR = untransfected PAR cells; + = purified his-tagged protein used as positive control.

Both 4EBP1 expression plasmids contained resistance genes to geneticin (G418), which allowed for selection of transfected cells with plasmid incorporation. The optimal concentration of G418 was determined by SRB growth assay and kill curve (Figure 6.6). The optimal concentration kills all non-resistant cells by ten days. Preliminary optimisation was performed by titrating a range of concentrations of G418 into 254R-B cells plated in a 96-well format. Although stable transfection occurred in a T25 flask seeded at $5x10^5$, for the purposes of the SRB assay, the seeding concentration was scaled down to 8,000 cells per well as the equivalent seeding concentration for a 96-well plate. 254R-B cells were treated with G418 over a 96-hour period and the percentage of remaining surviving cells was determined using the SRB dye. Figure 6.6A shows that after 96 hours, there was 100% death at 0.25mg/ml of G418. This was therefore used as a starting concentration for the kill curve.

Cells were mock transfected and treated with G418 over a period of 10 days. Images were taken of the cells after G418-containing media was replenished (Figure

6.6B). After 10 days, there were very few cells attached to the bottom of the plate at 0.25 and 0.5mg/ml. No cells could be found attached to the plate after 10 days in 1.0mg/ml G418 and thus this concentration was taken forward as the dose to select for stable 4EBP1 expression clones.

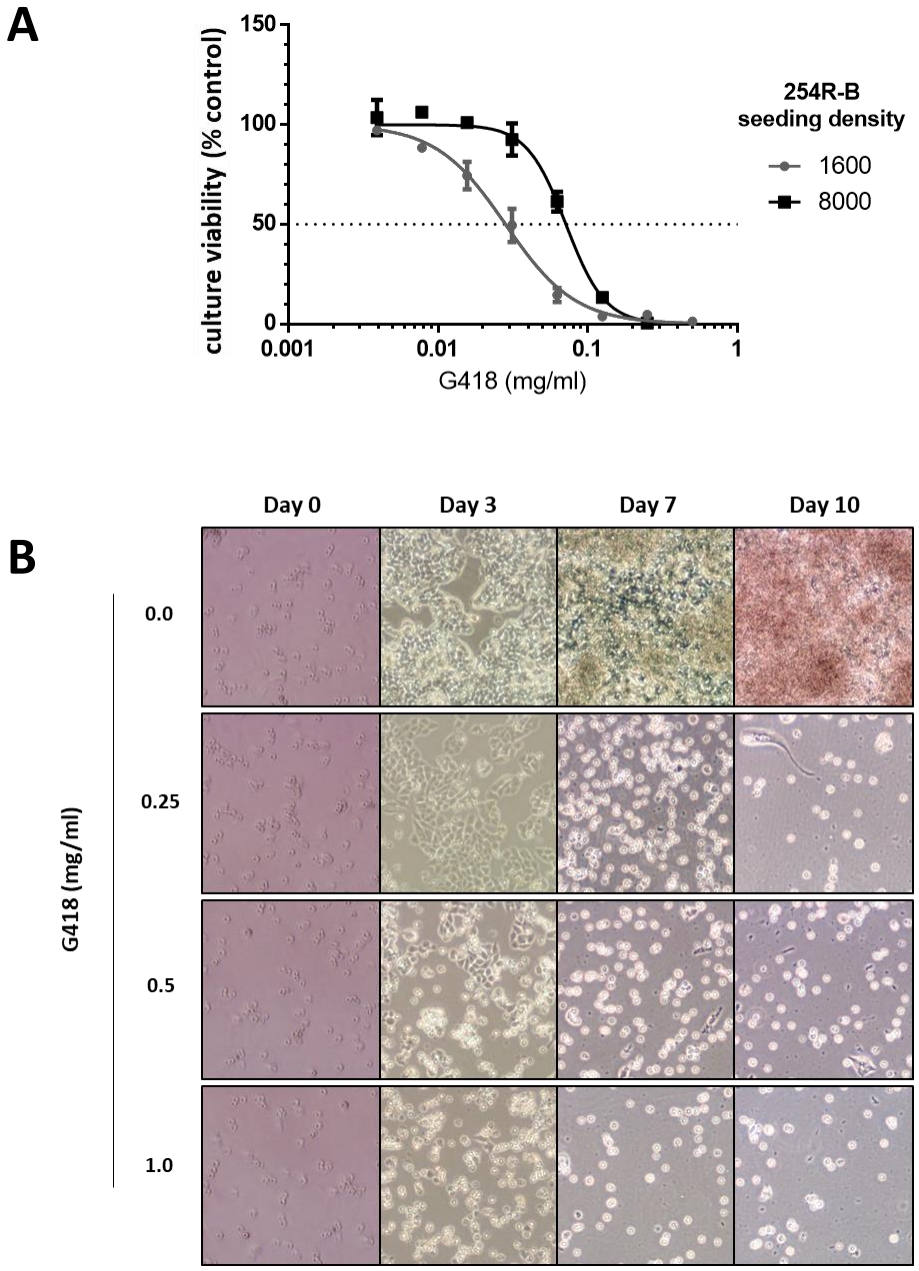

Figure 6.6 – Determination of optimal G418 concentration to select 4EBP1-transfected clones
(A) Representative dose response curve for G418 in A2780 254R-B cells only. Cells were plated at two seeding concentrations indicated and after 48 hours, treated with serially diluted concentrations of drug for 96 hours and surviving cells were determined by SRB growth assay. Dose response curve generated using GraphPad Prism 6. Data points present mean ± SD of three technical replicates. The broken line on the Y-axis indicates the points on the curves where growth was inhibited by 50% (GI_{50}). Data representative of three independent experiments. (B) Kill curve performed on 254R-B cells. Cells were treated with concentrations of G418 indicated from 48 hours post mock transfection. Drug-treated media was replenished every 2-3 days for 10 days. 400x magnification.

To generate 254R-B-4EBP1-WT or 5A populations, cells were plated, transfected with the appropriate plasmids and after 48 hours, treated with 1mg/ml G418 over a period of 10 days. Clonal and polyclonal populations were expanded. 15 WT (ten clonal; five polyclonal) and 11 5A colonies (eight clonal; three polyclonal) were successfully isolated. The phosphorylation and expression of 4EBP1 in the subpopulations is shown in Figure 6.7.

In 254R-B-4EBP1-WT subpopulations 3, 4, 6, 7, 9, 2P, 6P, and 8P, despite a slight increase in phosphorylated 4EBP1 compared with untransfected 254R-B, the total 4EBP1 expression was not increased, and were thus unsuccessful in expressing exogenous 4EBP1. 254R-B-4EBP1-WT subpopulations 7, 12P, 14, and 17-19 all exhibited an increase in 4EBP1 total expression, however WT18 and 19 did not exhibit an increase in phosphorylated 4EBP1. Therefore, WT subpopulations 7, 14, 17 and 12P were taken forward. The total expression of 1P was unclear and thus also taken forward.

For the 254R-B-4EBP1-5A subpopulations, there was an increase in 4EBP1 expression in 5A4, 11, 15P, 26, and 33. In each case phosphorylated 4EBP1 was not greater than untransfected 254R-B, as expected. Therefore, 5A subpopulations 4, 11, 15P, 26 and 33 were all taken forward.

The expression of selected populations was analysed again in Figure 6.8. As exogenous 4EBP1 was expressed as a heavier His-Myc fusion protein, endogenous and exogenous 4EBP1 could be separated by SDS-PAGE. Exogenous (Ex) and endogenous (En) 4EBP1 were separated, and revealed all selected WT and 5A subpopulations were successfully transfected except WT7 and WT1P. The two clonal WT subpopulations WT14 and WT17 were taken forward for further investigation. 5A4 exhibited less phosphorylated 4EBP1 than untransfected 254R-B and was also taken forward with 5A11.

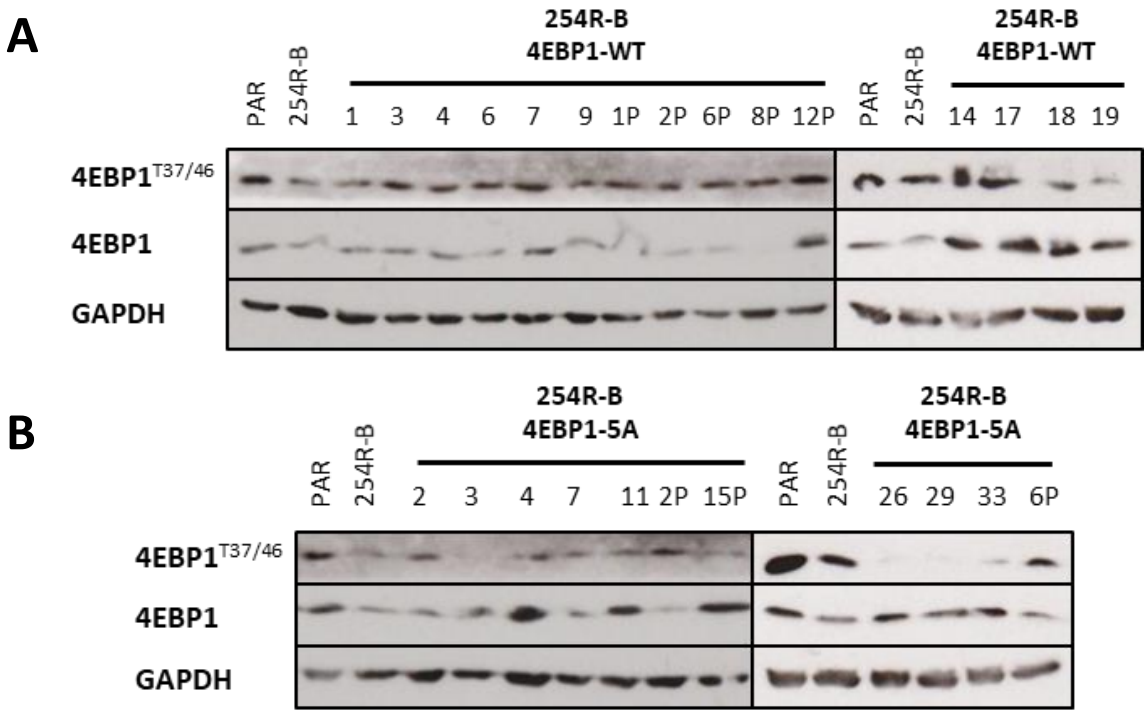

Figure 6.7 – Stable expression of wildtype (WT) or 5A-mutant (5A) 4EBP1 in 254R-B cells
Western blot analysis of 4EBP1 phosphorylation and expression in A2780 PAR, 254R-B and 254R-B pcDNA3-4EBP1WT-HISMYC (WT; A), or pcDNA3-4EBP15A-HISMYC (5A; B) transfected subpopulations. Cells were plated, lysed and analysed by western blotting as Figure 6.4. GAPDH was used as a loading control.

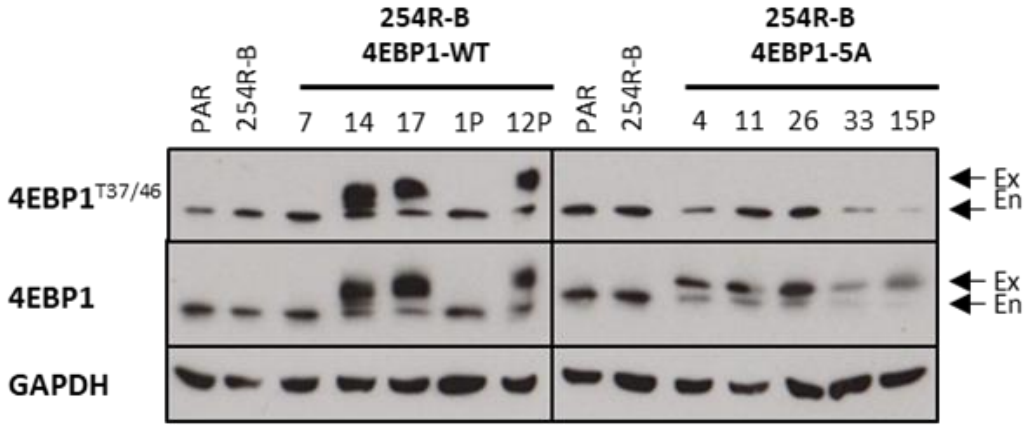

Figure 6.8 – Expression of selected wildtype (WT) or 5A-mutant (5A) 4EBP1 of selected stable transfection 254R-B cells
Western blot analysis of 4EBP1 phosphorylation and expression in 254R-B pcDNA3-4EBP1WT-HISMYC (WT), or pcDNA3-4EBP15A-HISMYC (5A) transfected subclones from Figure 6.7 with high 4EBP1. Cells were plated, lysed and analysed by western blotting as Figure 6.4. GAPDH was used as a loading control. Ex = exogenous band, En = endogenous band.

To investigate whether overexpression of 4EBP1 in the selected subpopulations increased 4EBP1 functional activity, the dynamics with eIF4E and eIF4G were examined using the m^7GTP eIF4E pull down assay. Figure 6.9 shows that in the presence of capivasertib, greater levels of 4EBP1 and lower levels of eIF4G were associated with eIF4E in PAR cells. The levels of 4EBP1 or eIF4G binding does not change with exposure to drug in 254R-B cells. With all four 254R-B-4EBP1 selected subpopulations, there was greater overall binding of 4EBP1 to eIF4E at baseline level than either PAR or 254R-B, and consequently eIF4G binding was lower than the baseline binding in PAR. For WT14 and 17, exogenous 4EBP1 binding to eIF4E increased with capivasertib exposure. This increase was not observed with 5A4 and 11, although a reduction in eIF4G binding was observed with drug treatment. The presence of exogenous 4EBP1 in all 254R-B-4EBP1 subpopulations reverted endogenous 4EBP1-eIF4E binding sensitive to capivasertib. In summary, 4EBP1 functional activity was increased in all 254R-B-4EBP1 subpopulations, compared to untransfected 254R-B cells.

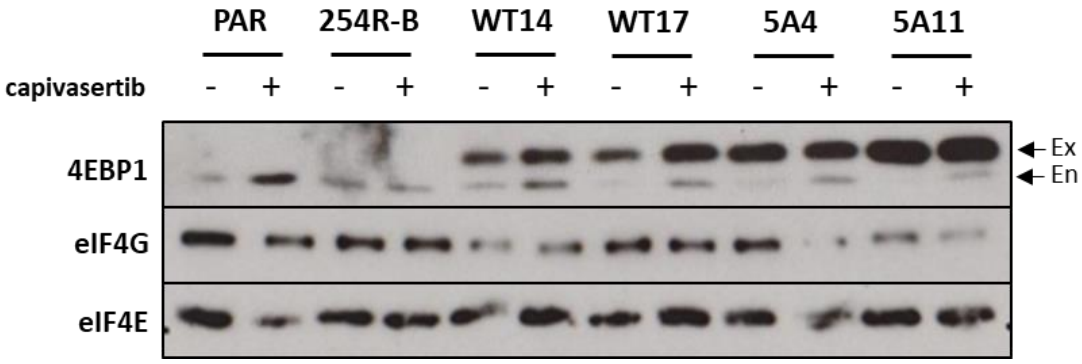

Figure 6.9 – Dynamics of 4EBP1 and eIF4G binding to eIF4E in A2780 PAR, 254R-B and 254R-B-4EBP1 cells
Cells were plated, treated with 254R-B GI_{50} concentration of capivasertib (4μM), eIF4E pull down assay and western blotting performed as Figure 6.4. Representative of two independent experiments.

The GI_{50} and RF values for capivasertib were determined in the 254R-B-4EBP1 subpopulations to observe whether increased 4EBP1 expression reduced 254R-B resistance to capivasertib. As shown in Figure 6.10, the RF values to capivasertib for all subpopulations were significantly reduced (8-14 RF) compared with untransfected 254R-B (84 RF), except 5A11 (99 RF). Apart from 5A11, increased 4EBP1 binding to eIF4E is associated with reduced capivasertib resistance (Figure

6.11). Taken together, the exogenous expression of WT or 5A-mutant 4EBP1 in 254R-B reduced resistance to capivasertib.

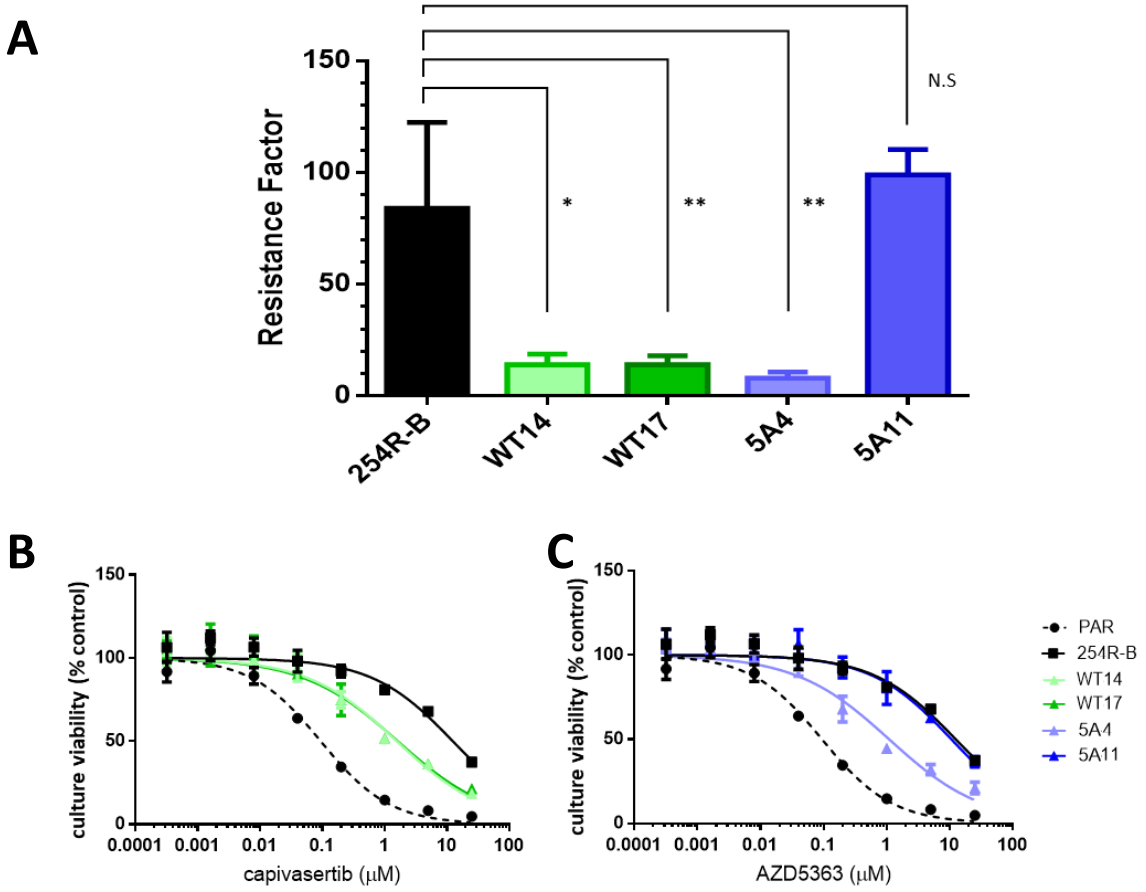

D

capivasertib	PAR	254R-B	WT14	WT17	5A4	5A11
GI_{50} (μM)	0.12 ± 0.03	9.8 ± 4.8	1.6 ± 0.6	1.6 ± 0.3	0.88 ± 0.2	11.5 ± 2.5
RF	-	84.0	14.2*	14.0**	7.6**	98.7

Figure 6.10 – 4EBP1 overexpression in 254R-B cells on the resistance to capivasertib
(A) Bar chart representing mean and error bars as SD of RF values for capivasertib in A2780 254R-B and 254R-B-4EBP1 subpopulations. Mean RF values and SD calculated as average of RF values and SD from ≥three individual experiments. Individual RF values calculated as ratio of 254R GI_{50} to PAR GI_{50}. (B and C) Representative dose response curves for capivasertib, for 254R-B-4EBP1-WT (B) and 5A (C) subpopulations. PAR, 254R-B and 254R-B-4EBP1 subpopulations were plated and after 48 hours treated with serially diluted concentrations of drug for 96 hours and surviving cells were determined by SRB growth assay. Data analysis as Figure 4.2. Data representative of ≥three independent experiments. (D) Summary of GI_{50} concentrations and resistance factors (RF) to capivasertib in A2780 PAR, 254R-B and 254R-B-4EBP1 subclones. Statistics as Figure 4.2.

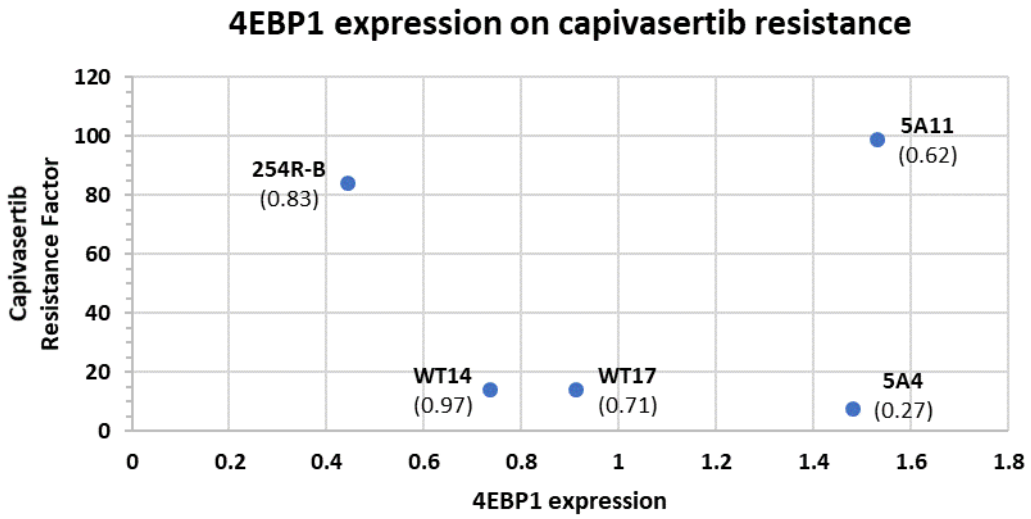

Figure 6.11 – 4EBP1 expression on capivasertib resistance
Capivasertib resistance factor (data from Figure 6.10) against the relative density of 4EBP1 expression with capivasertib treatment (+) from Figure 6.9. Band intensities were determined using Image J, adjusted relative to eIF4E and analysed in Microsoft Excel. The ratio of p4EBP1:4EBP1 for each cell line within brackets, calculated by densitometric analysis as described above (relative to GAPDH) for bands from Figure 6.8.

In summary, siRNA knockdown of 4EBP1 could not induce resistance to capivasertib in PAR and inhibition of eIF4E-eIF4G interactions using the compound 4EGI-1 in 254R-B cells did not increase drug sensitivity. Despite these, increasing exogenous expression of WT or 5A 4EBP1 in 254R-B, significantly reduced capivasertib resistance.

6.2.2. Investigation of MAPK pathway crosstalk in resistance to capivasertib

Alongside 4EBP1, S6RP was also considered as a candidate mechanism for resistance to capivasertib. In Chapter 4 (Figure 4.9), 254R-B exhibited strong resistant phosphorylation at serine 235 and 236 (S235/6) on S6RP to everolimus. To observe if this phenomenon was cross-resistant to capivasertib, PAM pathway signalling downstream of mTORC1 was examined in PAR and 254R-B cells treated with the drug. PAR and 254R-B cells were exposed for 24 hours to a range of concentrations of drug and signalling was analysed by western blotting.

The response of 254R-B to capivasertib is shown in Figure 6.12. The phosphorylation of serine 473 (S473) on AKT increased in both cell lines with increased concentrations of capivasertib. This was also observed in the

phosphorylation of threonine 389 (T389) of p70S6K. This was not observed in the phosphorylation of other proteins examined, and as both AKT and p70S6K are targets of capivasertib (Davies *et al.*, 2012; Addie *et al.*, 2013), this may be attributable to a conformational change induced by the ATP-competitive inhibitor which blocks phosphatase access to both proteins (Pearce *et al.*, 2010; Lin *et al.*, 2012). Total AKT was reduced in proportion to increased phosphorylated AKT, as observed in Figure 4.8. This was likely because it was raised against the unphosphorylated carboxyl-terminal residues of AKT, which may overlap with S473 (*cellsignal.co.uk*) and thus have a greater affinity for non-phosphorylated AKT.

Despite an increase in baseline phosphorylation of T389 on p70S6K in 254R-B versus PAR in the presence of capivasertib, there was no equivalent increase in the baseline phosphorylation of either S235/6 or serine 240 and 244 (S240/4) on S6RP. Both S6RP signals decreased in a dose-dependent manner in PAR and 254R-B. S235/6 was undetectable by 1μM in PAR and 30μM in 254R-B, suggesting these residues were more resistant to capivasertib than in PAR. Also, S240/4 exhibited slight resistance in which phosphorylation was undetectable by 5μM in PAR and 10μM in 254R-B.

Phosphorylation of 4EBP1 at threonine 37 and 46 (T37/46) clearly bandshifts from high molecular weight (HMW) hyperphosphorylated isoforms to low molecular weight (LMW) hypophosphorylated isoforms at 1μM in PAR, however 254R-B does not bandshift by 30μM. This resistant bandshifting was not observed with total 4EBP1. Taken together, phosphorylation at serine 235 and 236 (S235/6) on S6RP was cross-resistant to both everolimus and capivasertib in 254R-B cells.

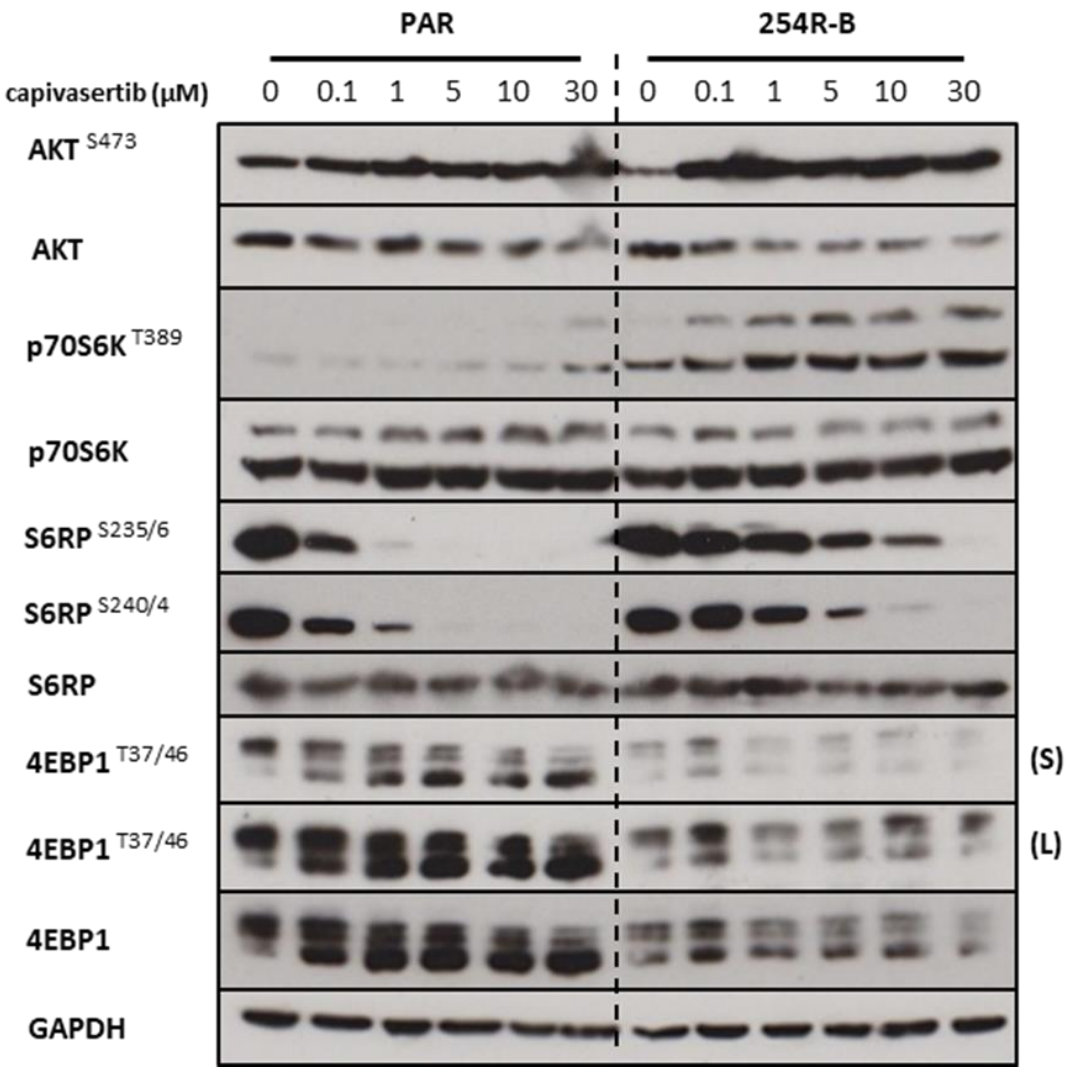

Figure 6.12 – PAM pathway signalling in A2780 PAR and 254R-B cells in response to capivasertib
A2780 PAR and 254R-B cells were plated, treated with a range of concentrations of capivasertib and lysed as Figure 6.4. 254R-B cells were released from CCT129254 at least one week prior to plating. Western blot procedure used as described in Figure 6.4. Superscript (e.g. AKT ^{S473}) indicates signalling at phosphorylation site in superscript. GAPDH was used as a loading control. S = short exposure; L = long exposure. Data are representative of two independent experiments.

S6RP phosphorylation of S235/6 can be directly regulated by a number of kinases including p70S6K, p90RSK, PKA and CK1 and the phosphatase PP1 (Meyuhas, 2015). S240/4 is only directly regulated by p70S6K and PP1, however the MAPK pathway may feed into S240/4 phosphorylation indirectly through crosstalk at TSC2 and mTORC1 (Figure 6.1; Mendoza *et al.*, 2011; Aksamitiene *et al.*, 2012). This combined with previous studies describing p90RSK signalling and S6RP phosphorylation driving drug resistance (Theodosakis *et al.*, 2017), the role of the MAPK pathway was investigated.

The baseline signalling of the MAPK pathway in PAR and 254R-B cells is shown in Figure 6.13A. Phosphorylation of serine 217 and 221 (S217/221) on MEK was decreased in 254R-B compared with PAR. Phosphorylation of threonine 202 and tyrosine 204 (T202/Y204) of ERK and its direct substrate, threonine 359 (T359) of p90RSK, and the total expression of p90RSK were all increased in 254R-B versus PAR. However, serine 383 (S383) of ELK (ETS domain-containing protein Elk-1), another direct substrate of ERK exhibited no change between PAR and 254R-B cells.

Cross-resistance profiling of PAR and 254R-B to MAPK pathway inhibitors (Figure 6.13C) was also investigated. Selumetinib (AZD6244) is an ATP-independent allosteric inhibitor of MEK, which upon binding induces a conformational change, allowing binding of ATP and substrate but inhibiting catalysis through inaccessibility to the activation loop of its substrate, ERK (Yeh *et al.*, 2007). Ravoxertinib is an ATP-competitive kinase inhibitor of ERK (Blake *et al.*, 2016; Roskoski, 2016, 2019). In Figure 6.13C, 254R-B on average exhibited cross-resistance to selumetinib (7.2 RF) compared with PAR, however due to a large standard deviation, this value was not statistically significant. Interestingly, the RF value was lower for ravoxertinib (1.8 RF) but statistically significant. According to McDermott *et al.*, (2014), clinically relevant resistance is defined as at least two-fold increase from the parental GI_{50}. Therefore, although statistically significant, the 1.8 RF value for ravoxertinib in 254R-B cells was not clinically relevant. Taken together, 254R-B cells exhibited alterations in baseline signalling in the MAPK pathway, particularly at ERK and p90RSK. 254R-B exhibited clinically relevant cross-resistance to MEK inhibition, although not statistically significant, and resistance to ERK inhibition was not clinically relevant.

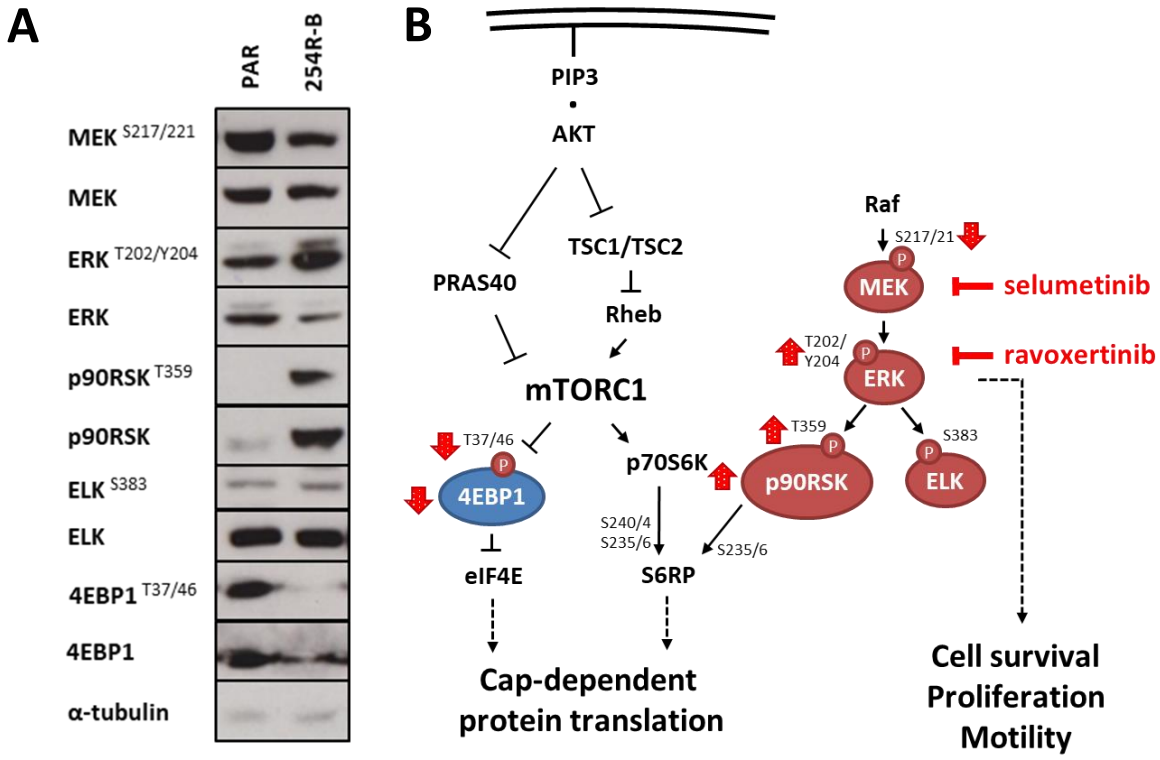

C

Drug	Target	GI_{50}		Resistance Factor	N
		PAR	254R-B		
selumetinib (μM) (AZD6244)	MEK (ATP-independent)	0.58 ± 0.1	3.6 ± 2.8	$7.2^{N.S}$	3
ravoxertinib (μM) (GDC-0994)	ERK1/2	0.59 ± 0.2	1.0 ± 0.1	1.8*	3

Figure 6.13 – Baseline signalling and resistance profiling of MAPK inhibitors in PAR and 254R-B.
A) A2780 PAR and 254R- B cells were released, plated and western blot performed on lysates as described in Figure 6.5. GAPDH was used as a loading control. Superscript (e.g. MEK $^{S217/221}$) indicates signalling at phosphorylation site(s) in superscript. Data are representative of three independent biological repeats. (B) A simplified schematic of the PAM pathway illustrating the relationship of the components investigated in (A) where blue are PAM and red are MAPK pathway components. Phosphorylated residues are represented as dark red (P)s, with amino residue defined. Black arrows and block-headed arrows indicate phosphorylation of target induces activation or inhibition respectively. Black dotted arrows indicate phenotypic output. Fat red arrows illustrate increase or decrease of phosphorylated residue or protein in 254R-B, as per western blot in (A). Absence of red arrow indicates no change. Red block-headed arrows indicate inhibition by drugs in (C). (C) Summary of GI_{50} concentrations and resistance factors (RF) values to selumetinib and ravoxertinib in A2780 PAR and 254R-B cells. GI_{50} values presented as mean ± SD of GI_{50} values from three independent experiments. RF values presented as mean RF of three independent experiments. Individual independent RF values calculated as the ratio of 254R-B GI_{50} to PAR GI_{50}. N = number of independent experiments. Statistics: Unpaired t test with Welch's correction of 254R-B to PAR GI_{50} values, *p<0.05, N.S = non-significant.

The increase in baseline phosphorylation of ERK and p90RSK, coupled with potential cross-resistance to MEK inhibitors but not ERK inhibitors may suggest that

capivasertib-resistant S235/6 S6RP phosphorylation may be dependent on ERK signalling. To investigate this hypothesis, the signalling of the MAPK pathway, and the components of which it feeds into the PAM pathway in PAR and 254R-B cell lines were investigated with treatment of the ERK inhibitor, ravoxertinib.

The results in Figure 6.14 show that with increasing concentrations of ravoxertinib, the phosphorylation of T202/Y204 of ERK increased in both cell lines. This may be the result of negative feedback, as nearly all components of the MAPK pathway upstream of ERK are regulated by negative feedback phosphorylation from ERK (Lake *et al.*, 2016). Alternatively, as ravoxertinib is an ATP-competitive kinase inhibitor (Blake *et al.*, 2016), this may be the result of a similar phenomenon observed with capivasertib and AKT/p70S6K (Figure 6.12), whereby a conformational change induced by the inhibitor blocks phosphatase access to the kinases (Pearce *et al.*, 2010; Lin *et al.*, 2012). Interestingly, the degree of increase of drug-induced ERK phosphorylation was greater in 254R-B than in PAR. The total expression of ERK conversely exhibited a drug-induced reduction in both cell lines. Similarly to AKT (as observed in Figure 6.12), this may be due to the epitope of the total antibody. As it was raised against the unphosphorylated carboxyl-terminal residues of ERK, this area may overlap with T202/Y204 (*cellsignal.co.uk*) and thus have a greater affinity for non-phosphorylated ERK, rather than both phosphorylated and non-phosphorylated protein.

In both cell lines, T359 of p90RSK was reduced in a dose-dependent manner, as observed in the long exposure of PAR and short exposure of 254R-B. The baseline phosphorylation of p90RSK was much greater in 254R-B than PAR, so that at 2µM of ravoxertinib, phosphorylation was undetectable in PAR, but detectable in 254R-B. As p90RSK expression was also increased in 254R-B, this may correspond with the increase in T359 phosphorylation.

In contrast to p90RSK phosphorylation, S383 phosphorylation on ELK was more sensitive to ravoxertinib in 254R-B compared with PAR. Conversely to p90RSK, this was likely due to a reduction in baseline S383 phosphorylation in 254R-B.

Interestingly, examination of signalling downstream of mTORC1 in the PAM pathway showed that p70S6K, S6RP and 4EBP1 did not observe a decrease in phosphorylation in a dose-dependent manner, but all observed a drop in signal between 5 and 10μM ravoxertinib in PAR cells. In 254R-B, the phosphorylation of p70S6K, S235/6 and S240/4 of S6RP but not T37/46 of 4EBP1 exhibited stronger bands at 5 and 10μM than PAR. Resistant S240/4 S6RP phosphorylation may be due to an increase in baseline phosphorylation at these residues. In total 4EBP1, there appeared less of a bandshift from HMW to LMW isoforms in 254R-B at 5 and 10μM, which may suggest other phosphorylation sites of 4EBP1 may be resistant to ravoxertinib, independently of phosphorylation of mTORC1-dependent priming residues T37/46.

In summary, S235/6 S6RP signalling was resistant to ERK inhibition by ravoxertinib. Although p90RSK phosphorylation was reduced in a dose-dependent manner to the drug in 254R-B, the increase in total expression resulted in resistant phosphorylation at concentrations of drug where the signal was undetectable in PAR cells (i.e. 2-10μM).

In Figure 6.13B, 254R-B cells exhibited a low RF value for ravoxertinib, however resistant S235/6 S6RP phosphorylation correlated with an increase in p90RSK expression and phosphorylation at T359. This site is phosphorylated by ERK as the first of a two-step process to activate the AGC kinase domain (Pearce *et al.*, 2010), and which decreased with ERK inhibition by ravoxertinib in a dose-dependent manner in both cell lines (Figure 6.14). To rule out the dependence of ERK signalling for p90RSK phosphorylation in 254R-B, it was investigated whether treatment with ravoxertinib increased sensitivity of 254R-B to capivasertib. Cells were treated with capivasertib and/or ravoxertinib for 24 hours prior to lysis and the sensitivity to drugs was measured using the apoptotic marker, cleaved PARP.

As the concentration of capivasertib was already optimised in Figure 6.3A, 1μM capivasertib was taken forward. The ideal concentration of ravoxertinib was such that significantly reduced p90RSK T389 phosphorylation in 254R-B, shown in Figure 6.14 to be 5 and 10μM. The degree of PARP cleavage at these concentrations in

both cell lines is shown in Figure 6.15A. PAR cells exhibited PARP cleaved in a dose-dependent manner. Interestingly, some PARP cleavage was exhibited at 5µM of ravoxertinib, but not at 10µM; therefore, 5µM ravoxertinib was taken forward.

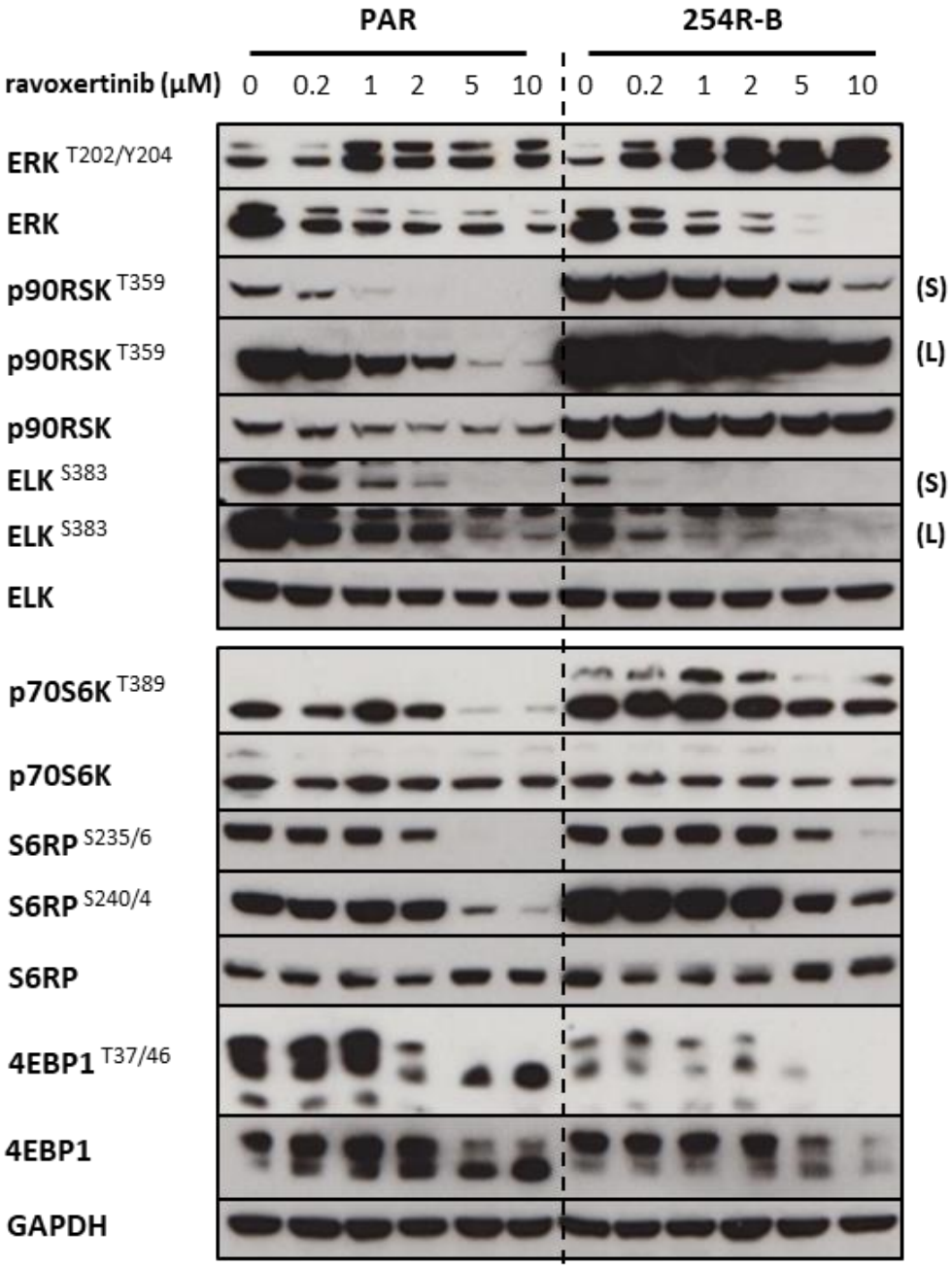

Figure 6.14 – PAM pathway signalling in A2780 PAR and 254R-B cells in response to ravoxertinib
A2780 PAR and 254R-B cells were released, plated and treated with a range of concentrations of ravoxertinib as described in Figure 6.7. Western blot procedure used as described in Figure 6.5. MAPK pathway components at top, PAM pathway components on bottom (separated by a gap). GAPDH was used as a loading control. Superscript (e.g. $ERK^{T202/Y204}$) indicates signalling at phosphorylation site in superscript. Data are representative of two independent experiments. S = short exposure; L = long exposure.

Figure 6.15B shows the effect of combined capivasertib and ravoxertinib treatment in PAR and 254R-B cells. Cleaved PARP increased in PAR cells with capivasertib or ravoxertinib alone and was greatest with combination of both drugs. In contrast, 254R-B cells observed a slight increase in cleaved PARP in ravoxertinib alone, but neither drugs alone nor combined increases cleavage to a level equal or greater than that observed in PAR. Taken together, treatment with ravoxertinib did not sensitise 254R-B cells to capivasertib.

In summary, S235/6 S6RP phosphorylation was resistant to capivasertib, which was fed by crosstalk from the MAPK pathway through p90RSK. The activity of p90RSK was not dependent on ERK signalling, despite 254R-B exhibiting a low RF value to the ERK inhibitor ravoxertinib.

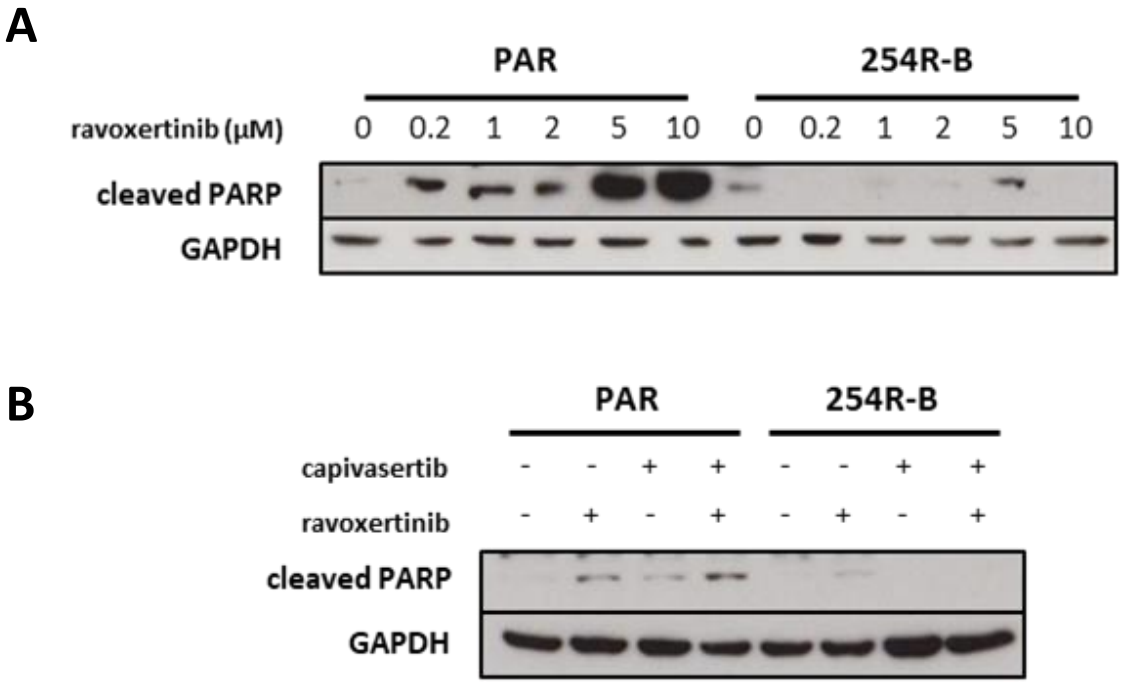

Figure 6.15 – Analysis of cleaved PARP with treatment of capivasertib and ravoxertinib
Cells were released, plated and drug treated with ravoxertinib concentrations indicated (A) or with capivasertib (1μM), ravoxertinib (5μM) or both (B) as Figure 6.7. Lysate proteins were analysed by western blotting as Figure 6.5. Membranes were probed with cleaved PARP or GAPDH as a loading control. Representative of ≥one independent experiment.

6.3. Discussion

The primary aim of this chapter was to validate the reduction of 4EBP1 function as a candidate resistance mechanism to capivasertib, and to further investigate the cause of S235/6 phosphorylation of S6RP as a candidate for driving resistance.

6.3.1. Validation of reduced 4EBP1 expression as a driver of resistance to capivasertib in 254R-B.

4EBP1 activity was found to be reduced in 254R-B compared with PAR in Chapters 4 and 5, which correlated with increased CDPS. To validate the importance of this in relation to the resistance mechanism, the functional activity of 4EBP1 was altered in three ways: 1) reducing 4EBP1 activity in PAR via siRNA knockdown to induce resistance; or increasing 4EBP1 activity in 254R-B to reduce resistance by 2) small molecule inhibition of the eIF4E-eIF4G interaction or 3) exogenous overexpression of 4EBP1.

Knockdown of 4EBP1 in PAR cells did not induce resistance to capivasertib (Figure 6.2). This may suggest that 4EBP1 knockdown alone was not sufficient enough to induce resistance to capivasertib and may require additional resistance drivers such as S6RP. Previous studies have shown that a double knockout of 4EBP1 in mouse embryonic fibroblasts can induce resistance to the mTORK inhibitor, torkinib (Alain *et al.*, 2012) and in pancreatic cell lines reduced 4EBP1 correlated with increased resistance to torkinib and everolimus (Martineau *et al.*, 2014). These highlight that reduced 4EBP1 expression alone is capable to induce resistance. These may be context-dependent, although alternatively, there were also several limitations of this experiment which may have influenced the result.

Use of siRNA inherently does not produce a long-term knockdown of a target protein and is largely dependent on the turnover of the protein. This may affect the duration and efficiency of the knockdown and thus a more stable knockdown with shRNA or complete knockout with CRISPR-cas9 may be more suitable for this experiment. As siRNA transfection requires a far greater seeding concentration to limit toxicity of the cell, the duration of the SRB growth assay was shortened to

prevent over confluent growth by the end of the assay. However, neither of these conditions dramatically affected the GI_{50} values for PAR and 254Rp. It is also worth noting that in Figure 6.6A, the knockdown was not as marked at 24 hours when capivasertib was added to the cells, compared to later timepoints (48 and 96 hours). A greater response may be observed if conditions were changed that drug was added to the cells at a timepoint in the assay when 4EBP1 was markedly reduced. Additionally, siRNA knockdown in cells was determined by western blot of transfected cells scaled up into a 6-well plate in order to yield sufficient detectable protein. This introduces an issue of cross-comparison, as knockdown may not necessarily the same in both plates. This could be overcome through the optimisation of a 4EBP1-specific cell-based ELISA to confirm knockdown in a 96-well plate format.

Whether an increase in 4EBP1 functional activity in 254R-B cells could reduce resistance to capivasertib was also investigated. 4EGI-1 was used to mimic the activity of 4EBP1 by disrupting eIF4G-eIF4E interactions. 4EGI-1 did not increase PARP cleavage in 254R-B in combination with capivasertib. This could be confirmed with a 4EGI-1 and capivasertib combination SRB growth assay, however Dr Denis Akan showed 4EGI-1 did not reduce capivasertib resistance to 254Rp (data unpublished). As observed in the eIF4E pull down, this was likely because the action of 4EGI-1 was not sufficient to increase 4EBP1 binding to eIF4E to the level observed in PAR (Figure 6.4).

In contrast, the 4EBP1-eIF4E binding in 254R-B with expression of exogenous WT or 5A-mutant 4EBP1 exceeded the levels observed in PAR (Figure 6.9). Introduction of the exogenous 4EBP1 was able to reduce resistance of 254R-B cells six-fold (254R-B-4EBP1-WT14 and 17) and 11-fold (254R-B-4EBP1-5A4; Figure 6.10). The fact that resistance to capivasertib was not abolished completely in these 254R-B-4EBP1 cell lines may suggest that there is only a partial target of the effect of the resistance mechanism, or that there is an additional mechanism that 254R-B are reliant upon for resistance, which may involve hyperactivation of the MAPK pathway, discussed in the next section.

The dynamics of endogenous and exogenous 4EBP1 binding in 254R-B-4EBP1 subpopulations with eIF4E (Figure 6.9), may give insight into the nature of the resistance mechanism as illustrated in Figure 6.16. As 254R-B exhibited no increase in 4EBP1 binding with eIF4E in the presence of capivasertib (Figure 6.16B), unlike PAR (Figure 6.16A), therefore hypophosphorylation of 4EBP1 did not increase its affinity for eIF4E. This highlights that there is an impairment in the activity of 4EBP1 as opposed to solely reliant on reduced 4EBP1 expression. This may be due to a mutation impairing 4EBP1 binding with eIF4E, alterations in other eIF4F complex or its binding proteins (e.g. LARP1; Stavraka and Blagden, 2015), a reduction in phosphatase activity or increased activity of a kinase that compensates for mTORC1 phosphorylation of 4EBP1 in 254R-B cells. However, an unexpected discovery in Figure 6.9 revealed that with the introduction of exogenous wildtype or 5A-mutant 4EBP1 into 254R-B, the phosphorylation of endogenous 4EBP1 reverted its sensitivity to capivasertib. This suggested that exogenous 4EBP1 is outcompeting endogenous 4EBP1 for an interaction that influences the affinity of 4EBP1 with eIF4E. This therefore suggests that reduced 4EBP1 phosphatase activity is unlikely. It may alternatively suggest the presence of a 4EBP1-targeting kinase (Kinase X; Figure 6.16C), which was unable to sufficiently phosphorylate all endogenous or exogenous wildtype 4EBP1, during capivasertib treatment as both exhibit increased binding with eIF4E. Furthermore, the 5A-mutants 5A4 and 5A11 did not increase exogenous 4EBP1 binding with eIF4E with capivasertib treatment, as these were unable to be phosphorylated and were permanently active. 5A4 exhibited greater binding of 4EBP1 than either WT14 or 17, indicating greater 4EBP1 activity, and may be the cause of a greater reduction in resistance to capivasertib (Figure 6.10).

Interestingly, 254R-B-4EBP1-5A11 appeared to observe the greatest exogenous 4EBP1 binding to eIF4E, and inducing endogenous binding with drug treatment (Figure 6.9/11), but surprisingly capivasertib resistance was greater than untransfected 254R-B (Figure 6.10). This may suggest that increased 4EBP1 binding was not the effect of exogenous 4EBP1 on the reduction of capivasertib resistance in the WT14, WT17 and 5A4 subpopulations. Alternatively, reduced resistance may correlate with both increased 4EBP1:eIF4E binding and reduced overall

p4EBP1:4EBP1 ratio, as 5A11 observed a greater ratio than 5A4 (Figure 6.11). This may indicate a feedback mechanism in 5A11 only, in which p4EBP1 is increased to counteract the rise in 4EBP1 expression and regulate 4EBP1:eIF4E stoichiometry. This feedback mechanism could in principle be triggered by 4EBP1:eIF4E binding, as 5A11 exhibited the greatest 4EBP1:eIF4E interaction of all 254R-B-4EBP1 selected subpopulations (Figure 6.9). Furthermore, as 5A11 still exhibits the greatest 4EBP1:eIF4E binding of all the cell lines, regardless of any feedback, the mechanism maintaining the capivasertib resistance is impacts an effector that is independent of 4EBP1:eIF4E stoichiometry.

However, it is also important to note that the introduction of exogenous 4EBP1 into 254R-B cells may cause a reduction in resistance due to off-target effects on overall cellular fitness rather than direct target of the resistance mechanism (Kaelin, 2017). The reduced resistance in WT14, WT17 and 5A, but not in 5A11 despite high 4EBP1 expression in 5A11 cells suggests the reduction in the former cell lines were likely to be a result of target of the resistance mechanism rather than off-target effects on overall cellular fitness (Kaelin, 2017). Further investigation of CDPS components in 254R-B and 254R-B-4EBP1 subpopulations is warranted to improve understanding of this mechanism.

In summary, validation of 4EBP1 as a candidate resistance mechanism outlined that 4EBP1 knockdown in PAR was insufficient to induce resistance to capivasertib, however introduction of exogenous 4EBP1 in 254R-B was sufficient to recapitulate sensitivity. Taken together, this may suggest that alterations in 4EBP1 alone were not sufficient to drive resistance to capivasertib, despite previous studies identifying that 4EBP1 alone is sufficient to drive resistance to other PAM inhibitors (Dilling *et al.*, 2002; Alain *et al.*, 2012; Mallya *et al.*, 2014; Martineau *et al.*, 2014).

6.3.2. Investigation of MAPK pathway crosstalk in resistance to capivasertib

Alongside 4EBP1, S6RP was also considered as a candidate mechanism for resistance to capivasertib. In Chapter 4 (Figure 4.9), 254R-B exhibited strong

resistant phosphorylation at serine 235 and 236 (S235/6) on S6RP to everolimus, which was also cross-resistant to capivasertib (Figure 6.12).

S6RP phosphorylation of S235/6 can be directly regulated by a number of kinases including p70S6K, p90RSK, PKA and CK1 and the phosphatase PP1 (Meyuhas, 2015). Of these, p90RSK phosphorylation of S6RP has been previously associated with drug resistance (Theodosakis *et al.*, 2017), and thus the MAPK pathway was investigated.

Observation of baseline signalling of the MAPK pathway revealed in 254R-B, an increase in p90RSK phosphorylation at T359, indicating its activation by ERK. Baseline phosphorylation at T202/Y204 of ERK was also increased, but phosphorylation of another substrate, ELK (S383) was not increased in 254R-B (Figure 6.13). The high T359 p90RSK phosphorylation correlated with increased total protein in 254R-B. The phosphorylation of p90RSK reduced in a dose-dependent manner with ERK inhibition but was still detectable with 10μM of the ERK inhibitor, ravoxertinib in 254R-B cells, unlike PAR (Figure 6.14). This dose-dependent reduction may continue with prolonged drug exposure and could explain why 254R-B exhibited a low RF value against ravoxertinib after drug incubation for 96 hours (Figure 6.14). The increase in p90RSK correlated with an increase in T389 p70S6K, S235/6 and S240/4 S6RP phosphorylation (Figure 6.14), of which both signals of S6RP phosphorylation were slightly resistant to capivasertib (Figure 6.12). As well as phosphorylation of S235/6 S6RP by p90RSK, the MAPK pathway may feed into S240/4 S6RP and T389 p70S6K phosphorylation indirectly through crosstalk at TSC2 and mTORC1 from ERK and p90RSK (Figure 6.1; Mendoza *et al.*, 2011; Romeo *et al.*, 2013). However, ELK phosphorylation was not resistant to ravoxertinib, nor did the drug sensitize 254R-B cells to capivasertib (Figure 6.15), therefore these were not dependent on ERK activity.

Taken together, this suggests that overexpression of p90RSK may drive resistant S235/6 S6RP phosphorylation. Treatment with a p90RSK inhibitor (such as LJH685, LJI308 or BI-D1870) alone in 254R-B cells would be expected to abolish resistant S235/6 S6RP phosphorylation, if this is the case. Inhibition of p90RSK may also increase 254R-B sensitivity to capivasertib, which can be explored by a drug

combination assay with apoptotic markers or SRB growth assay. Exploration of S6RP and other p90RSK outputs may highlight the function in drug resistance.

The mechanism of action of S6RP is currently not well understood. It is known to be involved in protein synthesis initiation through its binding with the 40S ribosomal subunit, and its phosphorylation increases CDPS (Williams *et al.*, 2003; Roux *et al.*, 2007). Additionally, S6RP may also have a role in cell size regulation, proliferation and in tissue-specific functions (Meyuhas, 2015). ERK has been previously identified as a kinase of 4EBP1, however there is currently little evidence that p90RSK directly or indirectly regulates the phosphorylation of 4EBP1 (Herbert *et al.*, 2002; Qin *et al.*, 2016). This may suggest that alterations in 4EBP1 and p90RSK may have arisen independently of one another, or further research is required to understand the link between them.

If increased p90RSK activity is validated as a driver of resistance to capivasertib, overexpression of the protein in 254R-B can be explored. Protein overexpression may be caused by multiple ways: the copy number of the gene may be amplified, transcription or translation may be overregulated, or degradation may be reduced (Fan *et al.*, 2009). Exploration of these levels may pinpoint the cause of p90RSK overexpression.

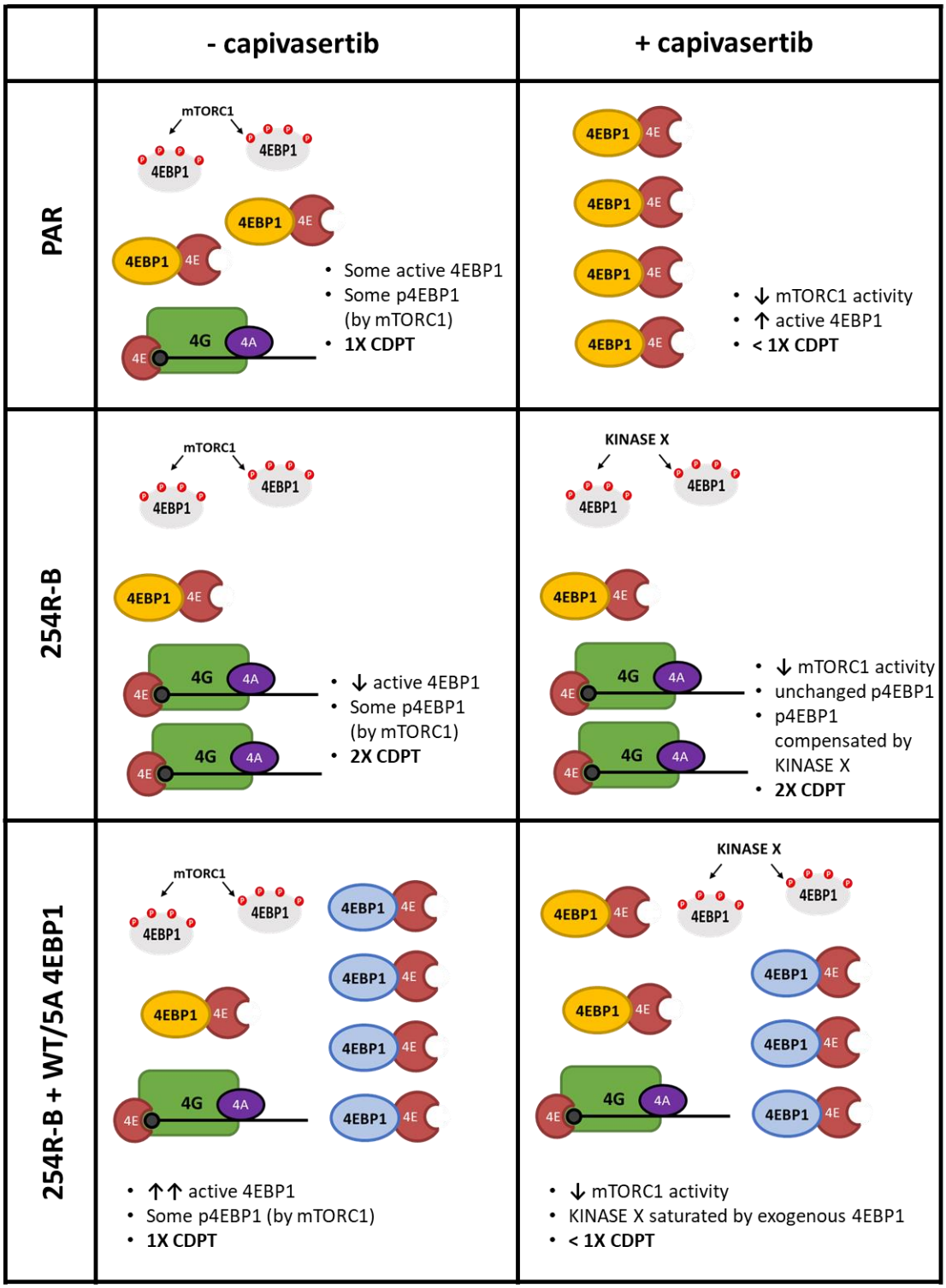

Figure 6.16 – Hypothesized model for role of unknown kinase X
Simplified model of the dynamics of 4EBP1 and eIF4G binding to eIF4E in A2780 PAR, 254R-B and 254R-B-4EBP1 cells in absence and presence of capivasertib (Figure 6.9). Kinase X may compensate for reduced mTORC1 activity in capivasertib-treated 254R-B cells. Endogenous 4EBP1 (yellow); exogenous 4EBP1 (blue); inactive 4EBP1 (grey); eIF4E (4E); eIF4G (4G); eIF4A (4A); P = phosphorylated residues; Black line with black and grey circle represents mRNA transcript with m7G cap.

In summary, the data presented in this chapter suggest that resistance to capivasertib in the A2780 254R-B cell line model is modulated by a mechanism proximal to 4EBP1. Knockdown of 4EBP1 in PAR did not induce the resistance phenotype, nor did disruption of eIF4G-eIF4E by 4EGI-1 action in 254R-B increase sensitivity to capivasertib. However, increased expression of wildtype or 5A-mutant 4EBP1 in 254R-B did recapitulate sensitivity. Additionally, 254R-B exhibited increased MAPK signalling through p90RSK, increasing the phosphorylation of S235/6 of S6RP. Whether this phenomenon is associated with reduced 4EBP1 activity in 254R-B needs to be investigated further. As both candidates converge at cap-dependent protein synthesis (CDPS), this highlights that components of CDPS may provide a potential point of therapeutic intervention if resistance to capivasertib emerges in the clinic.

Chapter 7

Final Discussion

7. Final Discussion

7.1. Introduction

The PI3K/AKT/mTOR (PAM) pathway is a signalling pathway important for regulating cell growth, proliferation, metabolism, survival and other cell phenotypes. As many of these phenotypes are important for oncogenesis, it is unsurprising that deregulation of the PAM pathway is commonly observed in many cancers and is therefore a target for therapeutic intervention (Fruman *et al.*, 2017).

AKT is an important node of the pathway, which phosphorylates over 100 different substrates required for many oncogenic processes (Fruman *et al.*, 2017; Cole *et al.*, 2019). For this reason, AKT inhibitors are undergoing development as a novel form of targeted cancer treatment. Acquired resistance is a major barrier to the clinical success of many cancer therapies, and the progression of these novel inhibitors will likely also be affected. Understanding potential resistance mechanisms can support the clinical utility of these drugs through screening patients for intrinsic or acquired resistance and determining effective therapeutic strategies to prevent or counteract resistance.

Capivasertib (AZD5363) and its derivative CCT129254 are both ATP-competitive pyrrolopyrimidine-derived AKT inhibitors (McHardy *et al.*, 2010; Davies *et al.*, 2012). Capivasertib has recently entered Phase III clinical trials as a combination with paclitaxel for the treatment of triple negative breast cancer, although the drug is in other Phase I/II trials for other cancers including breast, prostate and gynaecological cancers (*clinicaltrials.gov*). Although intrinsic resistance mechanisms have been previously reported to capivasertib and other AKT inhibitors (Davies, Greenwood et al. 2012; Sommer et al, 2013; Wehrenberg-Klee et al, 2015; Qi et al 2015), there are no publications identifying mechanisms of acquired resistance to this type of inhibitor.

Previous studies have successfully shown that cell line models can be used to identify clinically relevant drug resistance mechanisms (Nazarian *et al.*, 2010). The A2780 ovarian carcinoma cell line (PAR) was used to generate a subpopulation with

acquired resistance to the AKT inhibitor, CCT129254 (A2780 254Rp) by Dr Denis Akan (Akan, 2015). The aim of this project was to investigate the A2780 PAR and 254Rp cell lines to identify and validate candidate resistance mechanisms to capivasertib and associated oncogenic phenotypes. However, over the course of the project, it was identified that 254Rp populations were polyclonal and thus clonal subpopulations, 254R-B and 254R-D were also investigated.

7.2. Summary of main findings

7.2.1. A2780 254Rp exhibited polyclonal drug resistance

Characterisation of A2780 PAR and 254Rp cells was carried out in Chapter 3. Both cell lines exhibited an epithelial-like morphology and no stark changes were observed between PAR and 254Rp, indicating that a resistance mechanism is unlikely to involve an invasive, migratory phenotype for CCT129254-resistant oncogenesis.

Cross-resistance profiling revealed that 254Rp was 23-fold resistant to CCT129254, and 100-fold resistant to capivasertib, compared with PAR (Figure 3.2). 254Rp cells were also significantly resistant to the AKT kinase inhibitor ipatasertib (50 RF) and the allosteric AKT inhibitor MK-2206 (27 RF; Figure 3.3). Alongside cross-resistance to AKT inhibition, 254Rp cells also demonstrated statistically significant cross-resistance to PI3K (9.8 RF) and mTORC (2.8 and 4.6 RF; Figure 3.4) inhibition, although the level of resistance was not as great as observed with AKT inhibitors. The A2780 254Rp cell line may therefore be a useful model for investigation of general AKT, mTORC and PI3K inhibitor resistance. There was no cross-resistance to inhibitors of cap-dependent protein synthesis (CDPS), that target proteins downstream of mTORC1 (MNK, MRT00206081 and eIF4G-eIF4E binding, 4EGI-1; Figure 3.5). Taken together, these data suggest that the resistance mechanism may be proximal to mTORC1.

Observation of baseline PAM signalling revealed several alterations within the pathway between PAR versus 254Rp cells (Figure 3.7). Serine 473 (S473) AKT

phosphorylation was reduced in 254Rp, indicative of reduced AKT activity. The most marked changes observed were downstream of mTORC1 with a significant increase in phosphorylation of serine 235 and 236 (S235/6) on S6RP and a reduction in threonine 37 and 46 (T37/46) phosphorylation and total 4EBP1.

The response of these components to AKT inhibition was also investigated (Figure 3.8). Resistance of threonine 389 (T389) of p70S6K to MK-2206 in 254Rp highlighted that p70S6K is likely to contribute towards the increased baseline S6RP phosphorylation in Figure 3.7. Additionally, 4EBP1 phosphorylation was also resistant to MK-2206. When 254Rp cells were treated with the mTORC1 inhibitor everolimus, the resistant p70S6K and 4EBP1 phosphorylation was abolished (Figure 3.9). Since both T389 of p70S6K and T37/46 of 4EBP1 are phosphorylated by mTORC1 (Pearce *et al.*, 2010; Showkat *et al.*, 2014), increased mTORC1 activity was hypothesized as an output of the resistance mechanism in 254Rp.

SGK1 was hypothesized to increase mTORC1 activity in 254Rp, as previous studies have shown increased SGK1 can be associated with associated with PAM inhibitor resistance through increased mTORC1 signalling by SGK1 inhibition of TSC2 at AKT-targeted residues (Sommer *et al.*, 2013; Castel *et al.*, 2016). Microarray data (Table 3.1) showed a near eight-fold increase in SGK1 mRNA expression in 254Rp versus PAR cells. However, AKT-targeted residues on TSC2 were not resistant to MK-2206 in 254Rp cells, suggesting that SGK1 did not compensate for AKT inhibition (Figure 3.10). Therefore, overexpression of SGK1 was not taken forward as a candidate resistance mechanism.

In summary, 254Rp cells displayed conflicting results, as they were cross-resistant to both mTORC inhibitors, but AKT inhibitor-resistant mTORC1 signalling was sensitive to mTORC1 inhibition, which was not a product of SGK1 overexpression. This phenomenon may occur if 254Rp is a polyclonal drug resistant population. Therefore, in Chapter 4, 254Rp cells were subcloned by limited dilution to generate eight clonal 254R cell lines: 254R-A, B, D, E, F, H, J and K. The subclones were screened for morphological differences, cross-resistance to CCT129254, capivasertib, everolimus and vistusertib and differences in baseline mTORC1

signalling (Figure 4.4). The subclones revealed diversity in cross-resistance profiling and mTORC1 signalling but could be broadly categorised into three groups (Figure 4.4): 1) High everolimus resistance, 2) Reduced 4EBP1 phosphorylation and expression, and 3) Fibroblast-like morphology. Such variation in phenotype confirmed the polyclonal nature of 254Rp.

7.2.2. Resistance to capivasertib is associated with increased cap-dependent protein synthesis

Two 254Rp subclones, 254R-B (group 1) and 254R-D (group 2) were taken forward for further investigation in Chapter 4. 254R-B cells exhibited cross-resistance to all AKT inhibitors tested (10-40 RF; Figure 4.5) and even greater fold resistance to everolimus (96 RF). Western blotting of PAR and 254R-B lysates revealed a baseline reduction in 4EBP1 phosphorylation and expression (Figure 4.7 and 4.10) in 254R-B versus PAR. Additionally, S235/6 phosphorylation of S6RP was resistant to capivasertib and everolimus in 254R-B cells, compared with PAR (Figures 6.12 and 4.8). Both proteins have direct involvement in CDPS (Averous and Proud, 2006; Hutchinson *et al.*, 2011) and increase in this cellular process has been previously associated with resistance to PAM inhibitors (Dilling *et al.*, 2002; Alain *et al.*, 2012; Y Martineau *et al.*, 2014). Therefore, increased CDPS was hypothesized to drive resistance in 254R-B and was further investigated in Chapter 5.

The eIF4E pull down assay showed that reduced 4EBP1 phosphorylation by AKT and mTORC inhibitors prompted an increase in binding to eIF4E in both PAR and 254R-B cells, but the degree of binding was less in 254R-B for all drugs (Figure 5.4). This implied that the activity of 4EBP1 in 254R-B was less responsive to the maintenance of hypophosphorylated 4EBP1 action of the drugs and suggested that the functional activity of 4EBP1 was reduced. A minimal reduction in eIF4G-eIF4E binding despite drug treatment (Figure 5.4), combined with a nine-fold increase in relative CDPS determined by dual luciferase reporter assay (Figure 5.6), confirmed that increased CDPS was associated with reduced 4EBP1 functionality in 254R-B. Increased baseline CDPS did not increase baseline global protein synthesis (Figure 5.7), and

did not increase the expression of the two eIF4E-sensitive transcripts investigated, cyclin D1 and c-myc (Figure 5.8).

To validate loss of 4EBP1 function as a candidate resistance mechanism, the functional activity of this target was altered in three ways. Knockdown of 4EBP1 in PAR did not induce the resistance phenotype (Figure 6.2), nor did disruption of eIF4G-eIF4E binding by 4EGI-1 in 254R-B recapitulate sensitivity to capivasertib (Figure 6.4). However, increased expression of wildtype or 5A-mutant 4EBP1 did reduce capivasertib resistance in 254R-B by 10-fold (Figure 6.10).

The source of capivasertib-resistant S235/6 S6RP phosphorylation (Figure 6.12) was also investigated in 254R-B. This residue can be phosphorylated by p90RSK, which has been associated with resistance to PAM and MAPK pathway inhibitors (Serra *et al.*, 2013; Theodosakis *et al.*, 2017). Therefore, the role of the MAPK pathway was investigated.

Investigation of baseline MAPK pathway signalling revealed a clear increase in the pathway activity (Figure 6.13), observed by upregulated p90RSK T359 phosphorylation and expression. Phosphorylation at this residue was reduced in a dose-dependent manner with ERK inhibition by ravoxertinib, but the increase in baseline expression in 254R-B cells rendered the phosphorylation resistant (Figure 6.14). Ravoxertinib was unable to abolish S235/6 S6RP phosphorylation, nor induce PARP cleavage with capivasertib treatment in 254R-B cells (Figure 6.15); therefore, crosstalk from the MAPK pathway was not dependent on ERK activity. Taken together, loss of 4EBP1 function and enhanced p90RSK function were identified as candidate resistance mechanisms to capivasertib in A2780 254R-B cells.

7.2.3. Additional mechanisms of capivasertib resistance

Cross-resistance profiling highlighted that 254R-D cells were resistant to both ATP-competitive AKT inhibitors, CCT129254 and capivasertib (11-40 RF; Figure 4.6). Interestingly, the RF value for the allosteric AKT inhibitor, MK-2206, although statistically significant, was far lower (2.2 RF). This was also lower than either of the mTORC inhibitors tested (3.3-12.4 RF). Baseline phosphorylation of S473 on AKT

was reduced in 254R-D, compared with the PAR cell line. 4EBP1 phosphorylation and expression was also reduced (Figure 4.7). Consistent with low MK-2206 cross-resistance, 254R-D cells did not exhibit MK-2206-resistant mTORC1 signalling (Figure 4.11) or everolimus-resistant mTORC1 signalling (Figure 4.12). As 254R-D was resistant to ATP-competitive inhibitors but less resistant to other direct (MK-2206) or indirect forms of AKT inhibition (mTORC2; vistusertib), this suggested that the resistance mechanism may be specific to ATP-competitive AKT inhibitors. Sensitivity to MK-2206 implies that the drug can overcome and inhibit the resistance mechanism of capivasertib. As MK-2206 is a selective AKT inhibitor (Hirai *et al.*, 2010), it does not inhibit additional targets to those also targeted by capivasertib (i.e. AKT), which might overcome any resistance mechanism, therefore the resistance mechanism may affect the shared drug target, AKT.

Alternatively, resistance may be the result of a bypass mechanism from alterations of other AGC kinases targeted by capivasertib and CCT129254 and drive the same oncogenic output, such as p70S6K or PKA (Davies *et al.*, 2009; Addie *et al.*, 2013; Law *et al.*, 2017; Konieczkowski *et al.*, 2018).

7.3. Future work

7.3.1. Cap-dependent protein synthesis as a candidate capivasertib resistance output

The 254Rp cell line and nearly all of the 254Rp subclones exhibited a reduction in 4EBP1 phosphorylation and expression (Figure 4.4B). This may have arisen from the same mechanism occurring separately in multiple 254Rp clonal populations or may come about from an alteration that occurred early in resistance generation. Therefore, it may be useful to observe 4EBP1 expression over the course of CCT129254-resistance generation. A main shortcoming of this methodology is a lack of sequencing or microarray data to observe whether the changes in 4EBP1 phosphorylation and expression were due to alterations in the gene itself, or in mRNA turnover. Interestingly, exome sequencing and microarray analysis of PAR

and 254Rp by Dr Denis Akan did not reveal any clear alterations in 4EBP1 (Akan, 2015), although this does not necessarily mean that it may not be found in a 254Rp subclonal population which was of a too small proportion of 254Rp to be detected by these methods.

Introduction of 4EBP1 into 254R-B (254R-B-4EBP1-WT/5A cell lines) significantly reduced capivasertib resistance (Figure 6.10), however the rescue did not completely revert the sensitivity to the level of PAR cells. The fact that resistance to capivasertib was not abolished completely in these 254R-B-4EBP1 cell lines may suggest that there is only a partial target of the effect of the resistance mechanism, or that there exists additional signalling that 254R-B are reliant upon for resistance (Konieczkowski et al., 2018). This may involve hyperactivation of the MAPK pathway as elaborated later in this section, as is commonly observed in PAM inhibitor resistance (Carracedo et al., 2008; Yu et al., 2008; Hoang et al., 2012; Serra et al., 2013; Muranen et al., 2016). Additionally, the resistance mechanism may involve alternative bypass mechanisms (Konieczkowski et al., 2018), as many additional signalling cascades feed into the PAM pathway such as Wnt pathway, AMPK signalling, HIF1α signalling or input from amino acid availability as illustrated in Figure 1.4 (Kwiatkowski and Manning., 2005; Laplante and Sabatini., 2012; Kim and Guan., 2019). Alternatively, the resistance mechanism may be indifferent to the PAM pathway altogether (Konieczkowski et al., 2018).

Both reduced 4EBP1 expression and increased 4EBP1 phosphorylation have been separately associated with resistance to PAM inhibitors, but only one study had identified both occurring simultaneously in the same cell line (Dilling *et al.*, 2002; Alain *et al.*, 2012; Mallya *et al.*, 2014; Martineau *et al.*, 2014). This may be because resistant 4EBP1 phosphorylation can be masked by reduced 4EBP1 expression. There are several studies that suggest 4EBP1 phosphorylation is intimately linked with its degradation, however, studies contrast on whether phosphorylation positively or negatively regulates 4EBP1 degradation (Elia *et al.*, 2008; Yanagiya *et al.*, 2012). The regulation of 4EBP1 is an area that remains to be fully researched.

The reduced eIF4E-affinity of 4EBP1 in 254R-B may be due to a multiple of reasons, including a mutation in the binding domain of 4EBP1 and therefore sequencing 4EBP1 in 254R-B may indicate the presence of a mutation. The discovery that exogenous 4EBP1 (254R-B-4EBP1 populations) reverted endogenous 4EBP1-eIF4E binding sensitive to capivasertib such as observed in PAR (Figure 6.9) may highlight that the reduced eIF4E affinity of 4EBP1 in 254R-B may due to its being phosphorylated by an mTORC1-independent kinase (kinase X). Kinase X may be saturated by exogenous 4EBP1 in 254R-B 4EBP1 transfected populations (254R-B-4EBP1) and therefore unable to compensate for a lack of mTORC1 dependent signalling with capivasertib treatment.

Currently, the known 4EBP1 phosphorylated residues are: T37, T46, S65, T70, S83, S101 and S112 (Gingras *et al.*, 2001; Martineau *et al.*, 2013; Musa *et al.*, 2016; Qin *et al.*, 2016). Investigating the phosphorylation of all residues in response to capivasertib may identify which residues are the most resistant to the drug, and likely to be targets of kinase X. These can be confirmed through exogenous expression of alanine mutants of candidate resistant residues individually in 254R-B, or CRISPR-cas9 engineered phospho-mimetic mutants in PAR cells. Using these mutants, the dynamics of 4EBP1 with eIF4E, and resistance to capivasertib at a cellular level could be explored. Resistance of these residues to mTORC inhibitors, determined by immunoblotting with phospho-specific antibodies can be used to determine whether such sites are truly or partially mTORC1-independent. Co-immunoprecipitation of 4EBP1; examination of 4EBP1 phosphorylation with inhibitor treatments or phosphoproteomics algorithms (such as KSR-LIVE) can be used to determine the identify of kinase X (Domanova *et al.*, 2016). Exploration of the half-life of 4EBP1 in PAR, 254R-B and 254R-B-4EBP1 cell lines, through cycloheximide treatment time-lapse western blot can determine whether expression and phosphorylation of 4EBP1 are linked. As phosphorylation of T37/46 4EBP1 is reduced between PAR and 254R-B (Figure 4.10), this residue is likely to not be targeted by kinase X. Exploration of 4EBP1 expression with mutants of different residues may explain whether the degradation of the protein is dependent on the phosphorylation status of different residues.

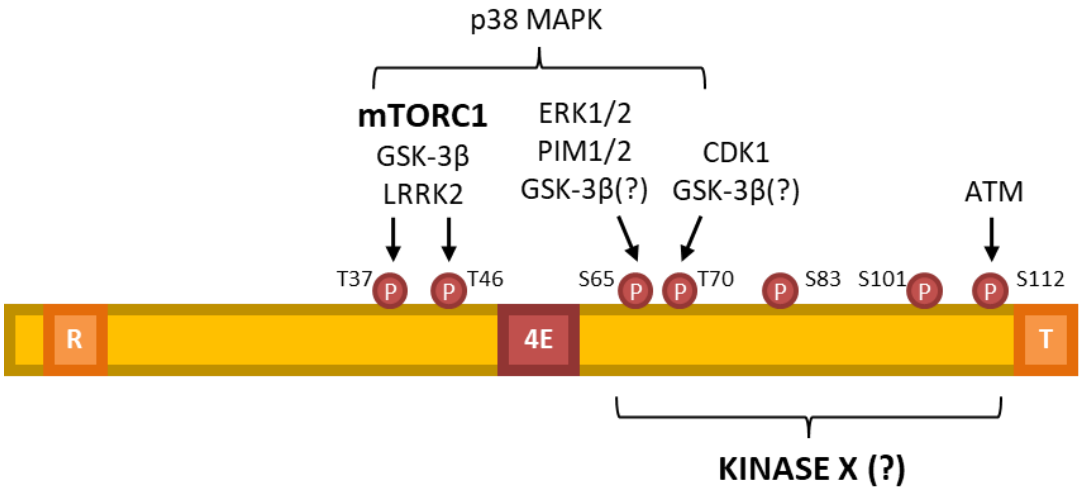

Figure 7.1 – 4EBP1 kinases and phosphorylated residues.
Protein structure and currently known phosphorylation sites of 4E-BP1. 4E-BP1 (yellow) contains three functional domains: an N-terminal RAIP mTORC1 binding motif (R), the eIF4E- binding domain (4E) and a C-terminal TOS mTORC1 binding motif (T). Phosphorylated residues are represented as dark red (P)s, with amino residue defined – threonine = T, serine = S. Black arrows indicate phosphorylation of residue by kinases indicated. Brackets indicate phosphorylation of multiple sites. (?) = Possible kinase. Model based upon information from Gingras et al., (2001), Martineau et al., (2013), Musa et al., (2016) and Qin et al., (2016).

Interestingly, increased p90RSK functionality was also identified as a candidate resistance mechanism, due to increased protein expression driving capivasertib-resistant S235/6 S6RP phosphorylation. This is yet to be validated as a driver of resistance and can be done by inducing p90RSK activity in PAR (overexpression), or inhibiting its activity (p90RSK inhibitor, siRNA, shRNA or CRISPR knockout) in 254R-B and monitoring the change in resistance to capivasertib. Although exogenous expression of 4EBP1 in 254R-B reduced the GI_{50} for capivasertib by 10-fold, it was not reduced to the level of PAR. 254R-B may be reliant on both reduced 4EBP1 functionality and increased p90RSK expression for complete abolition of capivasertib resistance, as illustrated in the model in Figure 7.2.

If p90RSK is validated to contribute towards capivasertib resistance, the phenotypic output may be explored. Phosphorylation by p90RSK on S235/6 S6RP is associated with formation of the cap-dependent pre-initiation complex (PIC) and increased CDPS. p90RSK can phosphorylate and regulate eIF4B (involved in potentiating eIF4A activity), TSC2 and RAPTOR, to increase CDPS. Other phenotypic roles of p90RSK include regulating transcription, the cell cycle and survival signalling (Anjum and Blenis, 2008).

The cause of the altered expression of p90RSK (and possibly 4EBP1) can be further explored through observation at a genetic level using quantitative PCR, for increase in copy number. Upregulated transcription can also be explored with reverse transcription of the mRNA transcripts. Alternatively, regulation at the protein level can be explored through cycloheximide or proteasome treated time-lapse western blotting. Identification of 4EBP1 kinase X, or how the expression of 4EBP1 and p90RSK is regulated may further identify whether these candidate resistance mechanisms are linked or independent.

Both 4EBP1 and p90RSK activity are known to converge at CDPS. Increased relative CDPS has been reported to drive resistance to mTORC and PI3K inhibitors, but none of these studies have reported whether cross-resistance to AKT inhibitors also occurred (Dilling *et al.*, 2002; Alain *et al.*, 2012; Y Martineau *et al.*, 2014). Relative CDPS was observed to be increased in 254R-B cells, but whether this is also refractory to capivasertib treatment can be investigated. Exploring relative CDPS levels in the 254R-B-4EBP1-WT/5A cell lines can further support the hypothesis that 4EBP1 alterations can drive resistance to capivasertib by increasing CDPS. In Chapter 5, the output of increased relative CDPS in 254R-B was not identified. Although global protein synthesis was not increased in 254R-B, whether global protein synthesis in 254R-B is resistant to capivasertib treatment is yet to be explored. Limitations of polysome profiling may be overcome by using ^{35}S methionine labelling or via incorporation of puromycin or L-azidohomoalanine to investigate direct polypeptide synthesis (Chen and Casadevall, 1999; Mallya *et al.*, 2014; Ge *et al.*, 2016). Alternatively, increased relative CDPS may result in increased translation of eIF4E-sensitive transcripts that were not investigated in Figure 5.8, such as BCL-2 and MCL-1, which are known eIF4E-sensitive transcripts in A2780 cells (Lam *et al.*, 2014).

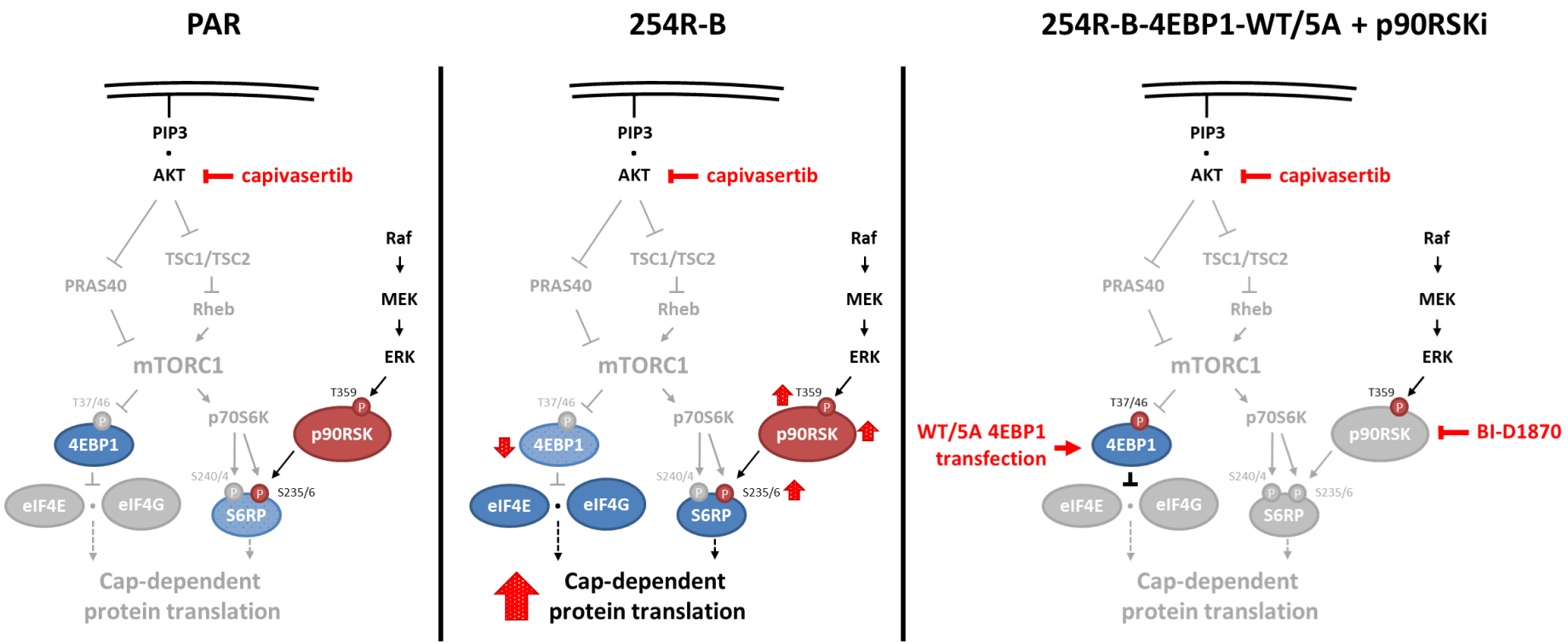

Figure 7.2 – Model of capivasertib resistance in 254R-B.
PAM pathway with treatment of capivasertib in PAR, 254R-B and 254R-B exogenous wildtype or 5A-mutant 4EBP1 transfected subpopulations (254R-B-4EBP1-WT/5A). Phosphorylated residues are represented as dark red (P)s, with amino residue defined. Black arrows and block-headed arrows indicate phosphorylation of target induces activation or inhibition respectively. Black dotted arrows indicate phenotypic output. p90RSKi = p90RSK inhibitor.

In conclusion, the work presented here provides strong evidence implicating that in A2780 254R-B cells, reduced 4EBP1 functional activity, increased p90RSK signalling and increased relative CDPS act as mediators of resistance to capivasertib. Future studies will therefore focus on determining the mechanism behind the reduced functional activity of 4EBP1 and further validating alterations of 4EBP1 and p90RSK together as drivers of resistance. These potential candidates are associated with increased CDPS, and the process by which this drives resistance is yet to be confirmed.

7.3.2. Additional mechanisms of capivasertib resistance

A2780 254R-D resistance may be associated with alterations at AKT or alternative AGC kinases. 254R-D was resistant to ATP-competitive inhibitors but less resistant to other forms of AKT inhibition, namely directly by MK-2206, or indirectly by vistusertib (mTORC2 inhibition). This suggested that the resistance mechanism may be specific to ATP-competitive AKT inhibitors (Figure 4.6). This can be confirmed through cross-resistance profiling with alternative ATP-dependent (e.g. ipatasertib) and independent AKT inhibitors (e.g. miltefosine, triciribine; Mundi *et al.*, 2016; Revathidevi and Munirajan, 2019).

254R-D cells exhibited reduced AKT activity, as observed by reduced phosphorylation of AKT substrates and S473 on the protein itself, which is phosphorylated by mTORC2 and is indicative of its maximal activity (Figure 4.7; Pearce et al., 2010). Despite sensitivity to MK-2206, it would be useful to investigate whether these residues are resistant to capivasertib in 254R-D. This may also be supplemented with an *in vitro* kinase assay in the presence of capivasertib. Previous studies have shown that mutations in AKT can lead to AKT inhibitor resistance (Carpten et al., 2007), therefore sequencing of all three isoforms in PAR and 254R-D may identify a mutation driving capivasertib resistance.

Involvement of alternative AGC kinases in the resistance mechanism can be further explored by determining cross-resistance to inhibitors specific to AGC kinase inhibitors, such as p70S6K (e.g. LY2584702) and PKA (e.g. H 89 2HCl), or sensitivity

to multi-AGC kinase inhibitor (i.e. AT13148). Limited alterations in baseline S6RP phosphorylation suggest alterations of p70S6K function may be less likely, however it has yet to be investigated whether S6RP phosphorylation is resistant to capivasertib.

As noted above, 4EBP1 expression was also reduced in 254R-D. This may be a passenger alteration in 254R-D but can be further investigated through expression of 4EBP1 WT or 5A constructs in the resistant cell line.

In conclusion, these studies show that capivasertib resistance in the A2780 254R-D cell line is associated with sensitivity to allosteric AKT inhibitors. Exploring the response of 254R-D to other methods of AKT inhibition and investigating alterations in CCT129254-targeted AGC kinases will be the focus of future work.

7.3.3. Clinical relevance of candidate resistance mechanisms

The data presented in this study have identified several potential resistance mechanisms to capivasertib, however the relevance of these findings to other cell lines and types requires investigation. Ultimately, the generation of only one polyclonal and 8 subclones populations of capivasertib resistant cells, provides a limited scope towards the potential diversity of polyclonal mechanisms of capivasertib resistance. Additionally, the similarity of subclones to allow their categorisation into three distinct groups, may highlight a more restricted variety of mechanisms. The main cause of this may be the limited dilution technique used to generate capivasertib-resistant clonal populations. For this technique, the cells are required to be able to grow independently of one another, which may not necessarily be possible for every cell in a polyclonal resistant population. Therefore, not all resistance mechanisms can be isolated in this way. This is particularly true for resistance mechanisms that may have co-evolved together and form co-dependence (Burrell and Swanton, 2014). Furthermore, the use of resistant isogenic cell lines as models of drug resistance carry their own limitations altogether as they are less capable of properly representing a tumour environment in terms of the influences from intratumoural, microenvironment and immune interactions on

resistance generation (McDermott *et al.*, 2014; Goodspeed *et al.*, 2016; Namekawa *et al.*, 2019).

Clinical trials have shown that capivasertib has been particularly effective in tumours with mutations eliciting PAM pathway addiction, in breast and gynaecological tumours (Banerji, *et al.*, 2018). Therefore, acquired capivasertib resistance could be generated in cell lines with similar mutations to validate alterations of 4EBP1, p90RSK and AGC kinases as capivasertib resistance drivers, as patients with these mutations in their tumours are more likely to be selected for treatment with capivasertib. A panel of such cell lines, besides A2780 cells could be also screened for intrinsic resistance mechanisms similar to those identified in this study. Alternatively, these mechanisms can be engineered into capivasertib-sensitive cell lines to observe if resistance is generated. These may therefore be used as biomarkers for intrinsic resistance to capivasertib to be screened in tumours to inform decisions for patient therapeutic strategies.

Ultimately, resistance mechanisms identified in these studies were determined in one artificially-induced capivasertib resistant cell line, and will only be truly validated as clinically relevant when acquired resistance to capivasertib and AKT inhibition emerges in the clinic.

7.4. Clinical implications of these findings

From the cross-resistance of 254Rp and subclones to capivasertib, it can be implied that generation of resistance in the clinic is probable. Although several intrinsic resistance mechanisms have been previously reported in AKT inhibitors (Davies, Greenwood et al. 2012; Sommer et al, 2013; Wehrenberg-Klee et al, 2015; Qi et al, 2015; Stottrup et al, 2016), as of August 2019, to my knowledge, there were no publications identifying acquired resistance mechanisms to AKT inhibitors. The candidate mechanisms identified in this study may have several clinical implications: 1) Determining biomarkers of resistance and 2) altering patient treatment strategies.

The candidate resistance mechanisms identified in this study (loss of 4EBP1 function and p90RSK overexpression) can be served as biomarkers for intrinsic resistance in capivasertib-naïve patients. Several papers have shown that reduced 4EBP1 expression is correlated with intrinsic resistance to PAM inhibitors (Dilling *et al.*, 2002; Mallya *et al.*, 2014; Martineau *et al.*, 2014). Levels of 4EBP1 expression can be identified in patient tumour samples using immunohistochemistry (Martineau *et al.*, 2014). In an ideal situation, tumour samples would be examined prior to treatment and after relapse to detect acquired resistance biomarkers, however obtaining biopsies are not clinically feasible, therefore relapse in ovarian patients is commonly determined by levels of CA125 in the blood.

In the occurrence of capivasertib-resistant tumour relapse, these findings may provide an insight into effective and ineffective secondary treatment strategies. For example, cross-resistance of these candidate resistance mechanisms to mTOR and PI3K inhibitors determine that the use of these will likely be ineffective. On the other hand, alterations of 4EBP1 may suggest that CDPS inhibitors may provide an effective strategy. Currently, there are no FDA-approved inhibitors of the eIF4F complex available for oncotherapy. However, the eIF4E-targeting antisense oligonucleotide, LY2275796, is currently in Phase I clinical trials (*clinicaltrials.*gov; Lu *et al.*, 2016).

In addition to replacement therapies, combination therapies may also provide another strategy for overcoming drug resistance (Al-Lazikani *et al.*, 2012; Holohan *et al.*, 2013)**.** The A2780 254Rp cell line can be used as a model to test effective novel drug combinations for overcoming capivasertib resistance, as observed with other drug-resistant isogenic cell lines (Katayama *et al.*, 2011). As this cell line has been identified to possess polyclonal drug resistance, the response to novel treatment strategies may reflect the polyclonal nature of tumours in the clinic. Testing these strategies *in vitro* may provide an insight into the most effective means to combat drug resistance to capivasertib and other AKT inhibitors.

7.5. Concluding remarks

The PAM pathway is one of the most commonly activated pathways in cancer and as such provides an attractive target for novel molecularly targeted cancer therapeutics. One such inhibitor is capivasertib, which has recently entered Phase III clinical trials. Unfortunately, despite the increase in development of molecularly targeted therapies, drug resistance is a major issue in the clinical success of such inhibitors, and the findings in this thesis outline that drug resistance is likely to also afflict capivasertib if progressed to drug approval.

Alterations in the function and expression of 4EBP1, p90RSK and potentially AGC kinases were identified as potential acquired resistance candidates to capivasertib, with associated increase in CDPS driving the phenotypic output of resistance. Further validation of resistance mechanisms is required to determine their clinical relevance and to devise suitable methods for overcoming capivasertib resistance.

In conclusion, if capivasertib progresses through clinical trials to drug approval, it is very likely that resistance will emerge in patients. This thesis provides an insight into candidate resistance mechanisms to capivasertib and other AKT inhibitors, as well as providing novel strategies for overcoming such drug resistance.

References

8. References

Addie, M., Ballard, P., Buttar, D., Crafter, C., Currie, G., Davies, B. R., Debreczeni, J., Dry, H., Dudley, P., Greenwood, R., Johnson, P. D., Kettle, J. G., Lane, C., Lamont, G., Leach, A., Luke, R. W. A., Ruston, L. (2013) 'Discovery of 4-Amino-N-[(1S)-1-(4-chlorophenyl)-3-hydroxypropyl]- 1-(7H-pyrrolo[2,3-d]pyrimidin-4-yl)piperidine-4-carboxamide (AZD5363), an Orally Bioavailable, Potent Inhibitor of Akt Kinases'. *Journal of Medicinal Chemistry*, 56(5):2059-73. doi: 10.1021/jm301762v.

Akan, D. T. (2015) 'Investigating mechanisms of acquired resistance to AKT inhibitors'.

Aksamitiene, E., Kiyatkin, A. and Kholodenko, B. N. (2012) 'Cross-talk between mitogenic Ras/MAPK and survival PI3K/Akt pathways: a fine balance', *Biochemical Society Transactions*, 40(1), pp. 139–146. doi: 10.1042/BST20110609.

Al-Lazikani, B., Banerji, U. and Workman, P. (2012) 'Combinatorial drug therapy for cancer in the post-genomic era', *Nature Biotechnology*, 30(7), pp. 679–692. doi: 10.1038/nbt.2284.

Alain, T., Morita, M., Fonseca, B. D., Yanagiya, A., Siddiqui, N., Bhat, M., Zammit, D., Marcus, V., Metrakos, P., Voyer, L.-A., Gandin, V., Liu, Y., Topisirovic, I. and Sonenberg, N. (2012) 'eIF4E/4E-BP ratio predicts the efficacy of mTOR targeted therapies.', *Cancer research*. American Association for Cancer Research, 72(24), pp. 6468–76. doi: 10.1158/0008-5472.CAN-12-2395.

Andjelković, M., Jakubowicz, T., Cron, P., Ming, X. F., Han, J. W. and Hemmings, B. A. (1996) 'Activation and phosphorylation of a pleckstrin homology domain containing protein kinase (RAC-PK/PKB) promoted by serum and protein phosphatase inhibitors.', *Proceedings of the National Academy of Sciences of the United States of America*. National Academy of Sciences, 93(12), pp. 5699–704. doi: 10.1073/pnas.93.12.5699.

Anjum, R. and Blenis, J. (2008) 'The RSK family of kinases: Emerging roles in cellular signalling', *Nature Reviews Molecular Cell Biology*. doi: 10.1038/nrm2509.

Arcaro, A. (2013) 'Targeting the insulin-like growth factor-1 receptor in human cancer.', *Frontiers in pharmacology*, 4, p. 30. doi: 10.3389/fphar.2013.00030.

Ardito, F., Giuliani, M., Perrone, D., Troiano, G. and Muzio, L. Lo (2017) 'The crucial role of protein phosphorylation in cell signaling and its use as targeted therapy (Review)', *International Journal of Molecular Medicine*. Spandidos Publications, pp. 271–280. doi: 10.3892/ijmm.2017.3036.

Averous, J. and Proud, C. G. (2006) 'When translation meets transformation: The mTOR story', *Oncogene*, 25(48), pp. 6423–6435. doi: 10.1038/sj.onc.1209887.

Aylett, Christopher H.S., Sauer, E., Imseng, S., Boehringer, D., Hall, M. N., Ban, N. and Maier, T. (2016) 'Architecture of human mTOR complex 1', *Science*, 351(6268). doi: 10.1126/science.aaa3870.

Aylett, Christopher H S, Sauer, E., Imseng, S., Boehringer, D., Hall, M. N., Ban, N. and Maier, T. (2016) 'STRUCTURAL BIOLOGY Architecture of human mTOR complex 1', *Science*, 351(6268), pp. 48–52. doi: 10.1126/science.aaa3870.

Baker, S. G. (2015) 'A cancer theory kerfuffle can lead to new lines of research.', *Journal of the National Cancer Institute*. Oxford University Press, 107(2). doi: 10.1093/jnci/dju405.

Banerji, U., Dean, Emma J, Pérez-Fidalgo, J. A., Batist, G., Bedard, P. L., You, B., Westin, S. N., Kabos, P., Garrett, M. D., Tall, M., Ambrose, H., Barrett, J. C., Carr, T. H., Cheung, S. Y. A., Corcoran, C., Cullberg, M., … Schellens, J. H. M. (2018) 'A Phase I Open-Label Study to Identify a Dosing Regimen of the Pan-AKT Inhibitor AZD5363 for Evaluation in Solid Tumors and in PIK3CA-Mutated Breast and Gynecologic Cancers.', *Clinical cancer research : an official journal of the American Association for Cancer Research*, 24(9), pp. 2050–2059. doi: 10.1158/1078-0432.CCR-17-2260.

Bast, R. C., Hennessy, B. and Mills, G. B. (2009) 'The biology of ovarian cancer: New opportunities for translation', *Nature Reviews Cancer*. doi: 10.1038/nrc2644.

Beaufort, C. M., Helmijr, J. C. A., Piskorz, A. M., Hoogstraat, M., Ruigrok-Ritstier, K., Besselink, N., Murtaza, M., van IJcken, W. F. J., Heine, A. A. J., Smid, M., Koudijs, M. J., Brenton, J. D., Berns, E. M. J. J. and Helleman, J. (2014) 'Ovarian cancer cell line panel (OCCP): clinical importance of in vitro morphological subtypes.', *PloS one*. Public Library of Science, 9(9), p. e103988. doi: 10.1371/journal.pone.0103988.

Bettegowda, C., Sausen, M., Leary, R. J., Kinde, I., Wang, Y., Agrawal, N., Bartlett, B. R., Wang, H., Luber, B., Alani, R. M., Antonarakis, E. S., Azad, N. S., Bardelli, A., Brem, H., Cameron, J. L., Lee, C. C., … Diaz, L. A. (2014) 'Detection of Circulating Tumor DNA in Early- and Late-Stage Human Malignancies', *Science Translational Medicine*, 6(224), pp. 224ra24-224ra24. doi: 10.1126/scitranslmed.3007094.

Bhat, M., Robichaud, N., Hulea, L., Sonenberg, N., Pelletier, J. and Topisirovic, I. (2015) 'Targeting the translation machinery in cancer', *Nature Reviews Drug Discovery*. Nature Publishing Group, 14(4), pp. 261–278. doi: 10.1038/nrd4505.

Blagden, S., Hamilton, A., Mileshkin, L., Hall, M., Meniawy, T., Wong, S., Anandra, S., Buck, M., McAleer, D., Reedy, B. A., Noble, R. B., Smith, D. A., Morris, S. R. and Gabra, H. (2014) '3 Afuresertib (GSK2110183), an oral AKT kinase inhibitor, in

combination with carboplatin and paclitaxel in recurrent ovarian cancer', *European Journal of Cancer*. Elsevier BV, 50, p. 7. doi: 10.1016/s0959-8049(14)70129-7.

Blagden, S. P., Hamilton, A. L., Mileshkin, L., Wong, S., Michael, A., Hall, M., Goh, J. C., Lisyanskaya, A. S., DeSilvio, M., Frangou, E., Stronach, E. A., Gopalakrishna, P., Meniawy, T. M. and Gabra, H. (2019) 'Phase IB dose escalation and expansion study of akt inhibitor afuresertib with carboplatin and paclitaxel in recurrent platinum-resistant ovarian cancer', *Clinical Cancer Research*. American Association for Cancer Research Inc., 25(5), pp. 1472–1478. doi: 10.1158/1078-0432.CCR-18-2277.

Blake, J. F., Burkard, M., Chan, J., Chen, H., Chou, K.-J., Diaz, D., Dudley, D. A., Gaudino, J. J., Gould, S. E., Grina, J., Hunsaker, T., Liu, L., Martinson, M., Moreno, D., Mueller, L., Orr, C., … Schwarz, J. B. (2016) 'Discovery of (*S*)-1-(1-(4-Chloro-3-fluorophenyl)-2-hydroxyethyl)-4-(2-((1-methyl-1 *H* -pyrazol-5-yl)amino)pyrimidin-4-yl)pyridin-2(1 *H*)-one (GDC-0994), an Extracellular Signal-Regulated Kinase 1/2 (ERK1/2) Inhibitor in Early Clinical', *Journal of Medicinal Chemistry*. American Chemical Society, 59(12), pp. 5650–5660. doi: 10.1021/acs.jmedchem.6b00389.

Blake, J. F., Xu, R., Bencsik, J. R., Xiao, D., Kallan, N. C., Schlachter, S., Mitchell, I. S., Spencer, K. L., Banka, A. L., Wallace, E. M., Gloor, S. L., Martinson, M., Woessner, R. D., Vigers, G. P. A., Brandhuber, B. J., Liang, J., … Skelton, N. J. (2012) 'Discovery and preclinical pharmacology of a selective ATP-competitive Akt inhibitor (GDC-0068) for the treatment of human tumors', *Journal of Medicinal Chemistry*, 55(18), pp. 8110–8127. doi: 10.1021/jm301024w.

Boussemart, L., Malka-Mahieu, H., Girault, I., Allard, D., Hemmingsson, O., Tomasic, G., Thomas, M., Basmadjian, C., Ribeiro, N., Thuaud, F., Mateus, C., Routier, E., Kamsu-Kom, N., Agoussi, S., Eggermont, A. M., Désaubry, L., … Vagner, S. (2014) 'eIF4F is a nexus of resistance to anti-BRAF and anti-MEK cancer therapies.', *Nature*, 513(7516), pp. 105–109. doi: 10.1038/nature13572.

Breuleux, M., Klopfenstein, M., Stephan, C., Doughty, C. A., Barys, L., Maira, S.-M., Kwiatkowski, D. and Lane, H. A. (2009) 'Increased AKT S473 phosphorylation after mTORC1 inhibition is rictor dependent and does not predict tumor cell response to PI3K/mTOR inhibition.', *Molecular cancer therapeutics*. NIH Public Access, 8(4), pp. 742–53. doi: 10.1158/1535-7163.MCT-08-0668.

Brognard, J., Sierecki, E., Gao, T. and Newton, A. C. (2007) 'PHLPP and a Second Isoform, PHLPP2, Differentially Attenuate the Amplitude of Akt Signaling by Regulating Distinct Akt Isoforms', *Molecular Cell*, 25(6), pp. 917–931. doi: 10.1016/j.molcel.2007.02.017.

Brown, M. C. and Gromeier, M. (2017) 'MNK Controls mTORC1:Substrate Association through Regulation of TELO2 Binding with mTORC1', *Cell Reports*. ElsevierCompany., 18(6), pp. 1444–1457. doi: 10.1016/j.celrep.2017.01.023.

Burrell, R. A. and Swanton, C. (2014) 'Tumour heterogeneity and the evolution of polyclonal drug resistance', *Molecular Oncology*, 8(6), pp. 1095–1111. doi: 10.1016/J.MOLONC.2014.06.005.

Cancer Research UK (2017) *Ovarian Cancer (C56), Proportion of Cases Diagnosed at Each Stage, All Ages, England 2014 and Northern Ireland 2010-2014*.

Cargnello, M., Tcherkezian, J. and Roux, P. P. (2015) 'The expanding role of mTOR in cancer cell growth and proliferation', *Mutagenesis*, 30(2), pp. 169–176. doi: 10.1093/mutage/geu045.

Carpten, J. D., Faber, A. L., Horn, C., Donoho, G. P., Briggs, S. L., Robbins, C. M., Hostetter, G., Boguslawski, S., Moses, T. Y., Savage, S., Uhlik, M., Lin, A., Du, J., Qian, Y. W., Zeckner, D. J., Tucker-Kellogg, G., … Thomas, J. E. (2007) 'A transforming mutation in the pleckstrin homology domain of AKT1 in cancer', *Nature*, 448(7152), pp. 439–444. doi: 10.1038/nature05933.

Carracedo, A., Ma, L., Teruya-Feldstein, J., Rojo, F., Salmena, L., Alimonti, A., Egia, A., Sasaki, A. T., Thomas, G., Kozma, S. C., Papa, A., Nardella, C., Cantley, L. C., Baselga, J. and Pandolfi, P. P. (2008) 'Inhibition of mTORC1 leads to MAPK pathway activation through a PI3K-dependent feedback loop in human cancer', *Journal of Clinical Investigation*, 118(9), pp. 3065–74. doi: 10.1172/JCI34739.

Carrière, A., Cargnello, M., Julien, L.-A., Gao, H., Bonneil, É., Thibault, P. and Roux, P. P. (2008) 'Oncogenic MAPK Signaling Stimulates mTORC1 Activity by Promoting RSK-Mediated Raptor Phosphorylation', *Current Biology*. Cell Press, 18(17), pp. 1269–1277. doi: 10.1016/J.CUB.2008.07.078.

Carriere, A., Romeo, Y., Acosta-Jaquez, H. A., Moreau, J., Bonneil, E., Thibault, P., Fingar, D. C. and Roux, P. P. (2011) 'ERK1/2 phosphorylate Raptor to promote Ras-dependent activation of mTOR complex 1 (mTORC1).', *The Journal of biological chemistry*. American Society for Biochemistry and Molecular Biology, 286(1), pp. 567–77. doi: 10.1074/jbc.M110.159046.

Castel, P., Ellis, H., Bago, R., Toska, E., Razavi, P., Carmona, F. J., Kannan, S., Verma, C. S., Dickler, M., Chandarlapaty, S., Brogi, E., Alessi, D. R., Baselga, J. and Scaltriti, M. (2016) 'PDK1-SGK1 Signaling Sustains AKT-Independent mTORC1 Activation and Confers Resistance to PI3Kα Inhibition', *Cancer Cell*, 30(2), pp. 229–242. doi: 10.1016/j.ccell.2016.06.004.

Castel, P. and Scaltriti, M. (2017) 'The emerging role of serum/glucocorticoid-regulated kinases in cancer', *Cell Cycle*. Taylor & Francis, 16(1), pp. 5–6. doi: 10.1080/15384101.2016.1232071.

Cencic, R., Hall, D. R., Robert, F., Du, Y., Min, J., Li, L., Qui, M., Lewis, I., Kurtkaya, S.,

Dingledine, R., Fu, H., Kozakov, D., Vajda, S. and Pelletier, J. (2011) 'Reversing chemoresistance by small molecule inhibition of the translation initiation complex eIF4F', *Proceedings of the National Academy of Sciences*. doi: 10.1073/pnas.1011477108.

Cencic, R., Robert, F., Galicia-Vázquez, G., Malina, A., Ravindar, K., Somaiah, R., Pierre, P., Tanaka, J., Deslongchamps, P. and Pelletier, J. (2013) 'Modifying chemotherapy response by targeted inhibition of eukaryotic initiation factor 4A', *Blood Cancer Journal*. doi: 10.1038/bcj.2013.25.

Chassé, H., Boulben, S., Costache, V., Cormier, P. and Morales, J. (2016) 'Analysis of translation using polysome profiling', *Nucleic Acids Research*. Narnia, 45(3), p. gkw907. doi: 10.1093/nar/gkw907.

Chen, L.-C. and Casadevall, A. (1999) 'Labeling of Proteins with [35S]Methionine and/or [35S]Cysteine in the Absence of Cells', *Analytical Biochemistry*, 269(1), pp. 179–188. doi: 10.1006/abio.1999.4023.

Chia, S., Gandhi, S., Joy, A., Edwards, S., Gorr, M., Hopkins, S., Kondejewski, J., Ayoub, J., Califaretti, N., Rayson, D. and Dent, S. (2015) 'Novel agents and associated toxicities of inhibitors of the pi3k/Akt/mtor pathway for the treatment of breast cancer', *Current Oncology*, 22(1). doi: 10.3747/co.22.2393.

Choi, Y. L., Soda, M., Yamashita, Y., Ueno, T., Takashima, J., Nakajima, T., Yatabe, Y., Takeuchi, K., Hamada, T., Haruta, H., Ishikawa, Y., Kimura, H., Mitsudomi, T., Tanio, Y., Mano, H. and ALK Lung Cancer Study Group (2010) 'EML4-ALK Mutations in Lung Cancer That Confer Resistance to ALK Inhibitors', *New England Journal of Medicine*, 363(18), pp. 1734–1739. doi: 10.1056/NEJMoa1007478.

Christofferson, T. (2014) *Tripping over the truth : how the metabolic theory of cancer is overturning one of medicine's most entrenched paradigms*.

clinicaltrials.gov (no date).

Cole, P. A., Chu, N., Salguero, A. L. and Bae, H. (2019) 'AKTivation mechanisms', *Current Opinion in Structural Biology*. Elsevier Current Trends, 59, pp. 47–53. doi: 10.1016/J.SBI.2019.02.004.

Cope, C. L., Gilley, R., Balmanno, K., Sale, M. J., Howarth, K. D., Hampson, M., Smith, P. D., Guichard, S. M. and Cook, S. J. (2014) 'Adaptation to mTOR kinase inhibitors by amplification of eIF4E to maintain cap-dependent translation', *J Cell Sci*. The Company of Biologists Ltd, 127(4), pp. 788–800. doi: 10.1242/JCS.137588.

Cross, D. A. E., Alessi, D. R., Cohen, P., Andjelkovich, M. and Hemmings, B. A. (1995)

'Inhibition of glycogen synthase kinase-3 by insulin mediated by protein kinase B', *Nature*. Nature Publishing Group, 378(6559), pp. 785–789. doi: 10.1038/378785a0.

van Dam, P. A., Vergote, I. B., Lowe, D. G., Watson, J. V, van Damme, P., van der Auwera, J. C. and Shepherd, J. H. (1994) 'Expression of c-erbB-2, c-myc, and c-ras oncoproteins, insulin-like growth factor receptor I, and epidermal growth factor receptor in ovarian carcinoma.', *Journal of clinical pathology*, 47(10), pp. 914–9. doi: 10.1136/jcp.47.10.914.

Davies, B. R., Dudley, P., Cosulich, S., Luke, R., Thompson, N., Collins, I., McHardy, T., Garrett, M. and Ogilvie, D. (2009) 'CCT129254 (AT11854) is a well tolerated, orally bioavailable inhibitor of AKT/PKB with pharmacodynamic and antitumor activity in a range of xenograft models', *Molecular Cancer Therapeutics*, 8(12), p. 129254.

Davies, B. R., Greenwood, H., Dudley, P., Crafter, C., Yu, D.-H., Zhang, J., Li, J., Gao, B., Ji, Q., Maynard, J., Ricketts, S.-A., Cross, D., Cosulich, S., Chresta, C. C., Page, K., Yates, J., … Pass, M. (2012) 'Preclinical Pharmacology of AZD5363, an Inhibitor of AKT: Pharmacodynamics, Antitumor Activity, and Correlation of Monotherapy Activity with Genetic Background', *Molecular Cancer Therapeutics*, 11(4), pp. 873–887. doi: 10.1158/1535-7163.MCT-11-0824-T.

Dever, T. E. and Green, R. (2012) 'The Elongation, Termination, and Recycling Phases of Translation in Eukaryotes', *Cold Spring Harbor Perspectives in Biology*, 4, p. a013706. doi: 10.1101/cshperspect.a013706.

Deyoung, M. P., Horak, P., Sofer, A., Sgroi, D. and Ellisen, L. W. (2008) 'Hypoxia regulates TSC1/2-mTOR signaling and tumor suppression through REDD1-mediated 14-3-3 shuttling', *Genes and Development*. doi: 10.1101/gad.1617608.

Dibble, C. C., Elis, W., Menon, S., Qin, W., Klekota, J., Asara, J. M., Finan, P. M., Kwiatkowski, D. J., Murphy, L. O. and Manning, B. D. (2012) 'TBC1D7 Is a Third Subunit of the TSC1-TSC2 Complex Upstream of mTORC1', *Molecular Cell*. Elsevier, 47(4), pp. 535–546. doi: 10.1016/j.molcel.2012.06.009.

Dilling, M. B., Germain, G. S., Dudkin, L., Jayaraman, A. L., Zhang, X., Harwood, F. C. and Houghton, P. J. (2002) '4E-binding proteins, the suppressors of eukaryotic initiation factor 4E, are down-regulated in cells with acquired or intrinsic resistance to rapamycin.', *The Journal of biological chemistry*. American Society for Biochemistry and Molecular Biology, 277(16), pp. 13907–17. doi: 10.1074/jbc.M110782200.

Do, K., Speranza, G., Bishop, R., Khin, S., Rubinstein, L., Kinders, R. J., Datiles, M., Eugeni, M., Lam, M. H., Doyle, L. A., Doroshow, J. H. and Kummar, S. (2015) 'Biomarker-driven phase 2 study of MK-2206 and selumetinib (AZD6244, ARRY-142886) in patients with colorectal cancer', *Investigational New Drugs*. Springer

New York LLC, 33(3), pp. 720–728. doi: 10.1007/s10637-015-0212-z.

Domanova, W., Krycer, J., Chaudhuri, R., Yang, P., Vafaee, F., Fazakerley, D., Humphrey, S., James, D. and Kuncic, Z. (2016) 'Unraveling Kinase Activation Dynamics Using Kinase-Substrate Relationships from Temporal Large-Scale Phosphoproteomics Studies', *PLOS ONE*. Public Library of Science, 11(6), p. e0157763. doi: 10.1371/journal.pone.0157763.

Donald, A., McHardy, T., Rowlands, M. G., Hunter, L.-J. K., Davies, T. G., Berdini, V., Boyle, R. G., Aherne, G. W., Garrett, M. D. and Collins, I. (2007) 'Rapid Evolution of 6-Phenylpurine Inhibitors of Protein Kinase B through Structure-Based Design', *Journal of Medicinal Chemistry*, 50(10), pp. 2289–2292. doi: 10.1021/jm0700924.

Donzelli, S., Mori, F., Biagioni, F., Bellissimo, T., Pulito, C., Muti, P., Strano, S. and Blandino, G. (2014) 'MicroRNAs: short non-coding players in cancer chemoresistance', *Molecular and Cellular Therapies*. River Publishers, 2(1), p. 16. doi: 10.1186/2052-8426-2-16.

Dorrello, N. V., Peschiaroli, A., Guardavaccaro, D., Colburn, N. H., Sherman, N. E. and Pagano, M. (2006) 'S6k1- and βTRCP-mediated degradation of PDCD4 promotes protein translation and cell growth', *Science*, 314(5798), pp. 467–471. doi: 10.1126/science.1130276.

Douglas, D. A., Zhong, H., Ro, J. Y., Oddoux, C., Berger, A. D., Pincus, M. R., Satagopan, J. M., Gerald, W. L., Scher, H. I., Lee, P. and Osman, I. (2006) 'Novel mutations of epidermal growth factor receptor in localized prostate cancer.', *Frontiers in bioscience*, 11, pp. 2518–25.

Druker, B. J., Tamura, S., Buchdunger, E., Ohno, S., Segal, G. M., Fanning, S., Zimmermann, J. and Lydon, N. B. (1996) 'Effects of a selective inhibitor of the Abl tyrosine kinase on the growth of Bcr–Abl positive cells', *Nature Medicine*. Nature Publishing Group, 2(5), pp. 561–566. doi: 10.1038/nm0596-561.

Earwaker, P., Anderson, C., Willenbrock, F., Harris, A. L., Protheroe, A. S. and Macaulay, V. M. (2018) 'RAPTOR up-regulation contributes to resistance of renal cancer cells to PI3K-mTOR inhibition', *PLoS ONE*, 13(2). doi: 10.1371/journal.pone.0191890.

Elia, A., Constantinou, C. and Clemens, M. J. (2008) 'Effects of protein phosphorylation on ubiquitination and stability of the translational inhibitor protein 4E-BP1', *Oncogene*, 27(6), pp. 811–822. doi: 10.1038/sj.onc.1210678.

Elkabets, M., Vora, S., Juric, D., Morse, N., Mino-Kenudson, M., Muranen, T., Tao, J., Campos, A. B., Rodon, J., Ibrahim, Y. H., Serra, V., Rodrik-Outmezguine, V., Hazra, S., Singh, S., Kim, P., Quadt, C., … Baselga, J. (2013) 'mTORC1 inhibition is required for

sensitivity to PI3K p110α inhibitors in PIK3CA-mutant breast cancer.', *Science translational medicine*, 5(196), p. 196ra99. doi: 10.1126/scitranslmed.3005747.

Fadden, P., Haystead, T. A. J. and Lawrence, J. C. (1997) 'Identification of phosphorylation sites in the translational regulator, PHAS-I, that are controlled by insulin and rapamycin in rat adipocytes', *Journal of Biological Chemistry*, 272(15), pp. 10240–10247. doi: 10.1074/jbc.272.15.10240.

Falzone, L., Salomone, S. and Libra, M. (2018) 'Evolution of Cancer Pharmacological Treatments at the Turn of the Third Millennium', *Frontiers in Pharmacology*. Frontiers, 9, p. 1300. doi: 10.3389/fphar.2018.01300.

Fan, D., Kim, S., Langley, R. L. and Fidler, I. J. (2009) *Drug Resistance in Cancer Cells*. doi: 10.1007/978-0-387-89445-4.

Fenton, T. R. and Gout, I. T. (2011) 'Functions and regulation of the 70 kDa ribosomal S6 kinases', *The International Journal of Biochemistry & Cell Biology*. Pergamon, 43(1), pp. 47–59. doi: 10.1016/J.BIOCEL.2010.09.018.

Folkes, A. J., Ahmadi, K., Alderton, W. K., Alix, S., Baker, S. J., Box, G., Chuckowree, I. S., Clarke, P. A., Depledge, P., Eccles, S. A., Friedman, L. S., Hayes, A., Hancox, T. C., Kugendradas, A., Lensun, L., Moore, P., … Shuttleworth, S. J. (2008) 'The Identification of 2-(1 *H* -Indazol-4-yl)-6-(4-methanesulfonyl-piperazin-1-ylmethyl)-4-morpholin-4-yl-thieno[3,2- *d*]pyrimidine (GDC-0941) as a Potent, Selective, Orally Bioavailable Inhibitor of Class I PI3 Kinase for the Treatment of Can', *Journal of Medicinal Chemistry*, 51(18), pp. 5522–5532. doi: 10.1021/jm800295d.

Fruman, D. A., Chiu, H., Hopkins, B. D., Bagrodia, S., Cantley, L. C. and Abraham, R. T. (2017) 'The PI3K Pathway in Human Disease', *Cell*. Elsevier Inc., 170(4), pp. 605–635. doi: 10.1016/j.cell.2017.07.029.

Garraway, L. A. and Jänne, P. A. (2012) 'Circumventing Cancer Drug Resistance in the Era of Personalized Medicine', *Cancer Discovery*, 2(3), pp. 214–226. doi: 10.1158/2159-8290.CD-12-0012.

Gasparri, M. L., Bardhi, E., Ruscito, I., Papadia, A., Farooqi, A. A., Marchetti, C., Bogani, G., Ceccacci, I., Mueller, M. D. and Benedetti Panici, P. (2017) 'PI3K/AKT/mTOR Pathway in Ovarian Cancer Treatment: Are We on the Right Track?', *Geburtshilfe und Frauenheilkunde*, pp. 1095–1103. doi: 10.1055/s-0043-118907.

Ge, J., Zhang, C.-W., Ng, X. W., Peng, B., Pan, S., Du, S., Wang, D., Li, L., Lim, K.-L., Wohland, T. and Yao, S. Q. (2016) 'Puromycin Analogues Capable of Multiplexed Imaging and Profiling of Protein Synthesis and Dynamics in Live Cells and Neurons', *Angewandte Chemie International Edition*, 55(16), pp. 4933–4937. doi:

10.1002/anie.201511030.

Gingras, A. C., Raught, B., Gygi, S. P., Niedzwiecka, A., Miron, M., Burley, S. K., Polakiewicz, R. D., Wyslouch-Cieszynska, A., Aebersold, R. and Sonenberg, N. (2001) 'Hierarchical phosphorylation of the translation inhibitor 4E-BP1.', *Genes & development*. Cold Spring Harbor Laboratory Press, 15(21), pp. 2852–64. doi: 10.1101/gad.912401.

Gingras, A., Raught, B. and Sonenberg, N. (2001) 'Regulation of translation initiation by FRAP / mTOR', *Genes & development*, 15, pp. 807–826. doi: 10.1101/gad.887201.

Godfrey, C. L., Mead, E. J., Daramola, O., Dunn, S., Hatton, D., Field, R., Pettman, G. and Smales, C. M. (2017) 'Polysome profiling of mAb producing CHO cell lines links translational control of cell proliferation and recombinant mRNA loading onto ribosomes with global and recombinant protein synthesis.', *Biotechnology journal*, 12(8). doi: 10.1002/biot.201700177.

Goodspeed, A., Heiser, L. M., Gray, J. W. and Costello, J. C. (2016) 'Tumor-Derived Cell Lines as Molecular Models of Cancer Pharmacogenomics', *Molecular cancer research : MCR*, 14(1), pp. 3–13. doi: 10.1158/1541-7786.MCR-15-0189.

Gottesman, M. M., Fojo, T. and Bates, S. E. (2002) 'Multidrug resistance in cancer: role of ATP–dependent transporters', *Nature Reviews Cancer*. Nature Publishing Group, 2(1), pp. 48–58. doi: 10.1038/nrc706.

Grasso, S., Tristante, E., Saceda, M., Carbonell, P., Mayor-López, L., Carballo-Santana, M., Carrasco-García, E., Rocamora-Reverte, L., García-Morales, P., Carballo, F., Ferragut, J. A. and Martínez-Lacaci, I. (2014) 'Resistance to Selumetinib (AZD6244) in colorectal cancer cell lines is mediated by p70S6K and RPS6 activation.', *Neoplasia (New York, N.Y.)*, 16(10), pp. 845–60. doi: 10.1016/j.neo.2014.08.011.

Groenewoud, M. J., Goorden, S. M. I., Kassies, J., Pellis-van Berkel, W., Lamb, R. F., Elgersma, Y. and Zwartkruis, F. J. T. (2013) 'Mammalian Target of Rapamycin Complex I (mTORC1) activity in Ras homologue enriched in brain (Rheb)-deficient mouse embryonic fibroblasts', *PLoS ONE*, 8(11), pp. 1–15. doi: 10.1371/journal.pone.0081649.

Guertin, D. A., Stevens, D. M., Thoreen, C. C., Burds, A. A., Kalaany, N. Y., Moffat, J., Brown, M., Fitzgerald, K. J. and Sabatini, D. M. (2006) 'Ablation in Mice of the mTORC Components raptor, rictor, or mLST8 Reveals that mTORC2 Is Required for Signaling to Akt-FOXO and PKCα, but Not S6K1', *Developmental Cell*, 11(6), pp. 859–871. doi: 10.1016/j.devcel.2006.10.007.

Gupta, S. V., Sass, E. J., Davis, M. E., Edwards, R. B., Lozanski, G., Heerema, N. A., Lehman, A., Zhang, X., Jarjoura, D., Byrd, J. C., Pan, L., Chan, K. K., Kinghorn, A. D., Phelps, M. A., Grever, M. R. and Lucas, D. M. (2011) 'Resistance to the Translation Initiation Inhibitor Silvestrol is Mediated by ABCB1/P-Glycoprotein Overexpression in Acute Lymphoblastic Leukemia Cells', *The AAPS Journal*. doi: 10.1208/s12248-011-9276-7.

Von Der Haar, T., Ball, P. D. and Mccarthy, J. E. G. (2000) *Stabilisation of eukaryotic initiation factor 4E-binding to the mRNA 5`-cap by domains of eIF4G*. JBC Papers in Press. Available at: http://www.jbc.org/ (Accessed: 9 April 2019).

Haddadi, N., Lin, Y., Travis, G., Simpson, A. M., McGowan, E. M. and Nassif, N. T. (2018) 'PTEN/PTENP1: "Regulating the regulator of RTK-dependent PI3K/Akt signalling", new targets for cancer therapy', *Molecular Cancer*. doi: 10.1186/s12943-018-0803-3.

Hanahan, D. and Weinberg, R. A. (2011) 'Hallmarks of Cancer: The Next Generation', *Cell*, 144(5), pp. 646–674. doi: 10.1016/j.cell.2011.02.013.

Harrington, L. S., Findlay, G. M., Gray, A., Tolkacheva, T., Wigfield, S., Rebholz, H., Barnett, J., Leslie, N. R., Cheng, S., Shepherd, P. R., Gout, I., Downes, C. P. and Lamb, R. F. (2004) 'The TSC1-2 tumor suppressor controls insulin-PI3K signaling via regulation of IRS proteins.', *The Journal of cell biology*. The Rockefeller University Press, 166(2), pp. 213–23. doi: 10.1083/jcb.200403069.

Harrington, L. S., Findlay, G. M. and Lamb, R. F. (2005) 'Restraining PI3K: mTOR signalling goes back to the membrane', *Trends in Biochemical Sciences*, 30(1), pp. 35–42. doi: 10.1016/j.tibs.2004.11.003.

Haslehurst, A. M., Koti, M., Dharsee, M., Nuin, P., Evans, K., Geraci, J., Childs, T., Chen, J., Li, J., Weberpals, J., Davey, S., Squire, J., Park, P. C. and Feilotter, H. (2012) 'EMT transcription factors snail and slug directly contribute to cisplatin resistance in ovarian cancer', *BMC Cancer*, 12(1), p. 91. doi: 10.1186/1471-2407-12-91.

Hassan, B., Akcakanat, A., Sangai, T., Evans, K. W., Adkins, F., Eterovic, A. K., Zhao, H., Chen, K., Chen, H., Do, K.-A., Xie, S. M., Holder, A. M., Naing, A., Mills, G. B. and Meric-Bernstam, F. (2014) 'Catalytic mTOR inhibitors can overcome intrinsic and acquired resistance to allosteric mTOR inhibitors.', *Oncotarget*, 5(18), pp. 8544–57. doi: 10.18632/oncotarget.2337.

Herbert, T. P., Tee, A. R. and Proud, C. G. (2002) 'The extracellular signal-regulated kinase pathway regulates the phosphorylation of 4E-BP1 at multiple sites', *Journal of Biological Chemistry*, 277(13), pp. 11591–11596. doi: 10.1074/jbc.M110367200.

Higashitsuji, Hisako, Higashitsuji, Hiroaki, Masuda, T., Liu, Y. and Fujita, J. (2007)

'Enhanced Deacetylation Of P53 By The Anti-Apoptotic Protein Hsco In Association With Histone Deacetylase 1'. *Journal of Biological Chemistry* (18):13716-25. doi: 10.1074/jbc.M609751200.

Hindupur, S. K., Gonza´lez, A. and Hall, M. N. (2015) 'The Opposing Actions of Target of Rapamycin and AMP-Activated Protein Kinase in Cell Growth Control', *Cold Spring Harbor Perspectives in Biology*, 7(a019141). doi: 10.1101/cshperspect.a019141.

Hirai, H., Sootome, H., Nakatsuru, Y., Miyama, K., Taguchi, S., Tsujioka, K., Ueno, Y., Hatch, H., Majumder, P. K., Pan, B.-S. and Kotani, H. (2010) 'MK-2206, an Allosteric Akt Inhibitor, Enhances Antitumor Efficacy by Standard Chemotherapeutic Agents or Molecular Targeted Drugs In vitro and In vivo', *Molecular cancer therapeutics*. American Association for Cancer Research, 9(7), pp. 1956–67. doi: 10.1158/1535-7163.mct-09-1012.

Hirano, H., Komatsu, S., Kajiwara, H., Takagi, Y. and Tsunasawa, S. (1993) 'Microsequence analysis of the N-terminally blocked proteins immobilized on polyvinylidene difluoride membrane by western blotting.', *Electrophoresis*, 14(9), pp. 839–46.

Hoang, B., Benavides, A., Shi, Y., Yang, Y., Frost, P., Gera, J. and Lichtenstein, A. (2012) 'The PP242 mammalian target of rapamycin (mTOR) inhibitor activates extracellular signal-regulated kinase (ERK) in multiple myeloma cells via a target of rapamycin complex 1 (TORC1)/eukaryotic translation initiation factor 4E (eIF-4E)/RAF pathway and activ', *The Journal of biological chemistry*, 287(26), pp. 21796–805. doi: 10.1074/jbc.M111.304626.

Hollestelle, A., Elstrodt, F., Nagel, J. H. A., Kallemeijn, W. W. and Schutte, M. (2007) 'Phosphatidylinositol-3-OH kinase or RAS pathway mutations in human breast cancer cell lines.', *Molecular cancer research : MCR*, 5(2), pp. 195–201. doi: 10.1158/1541-7786.MCR-06-0263.

Holohan, C., Van Schaeybroeck, S., Longley, D. B. and Johnston, P. G. (2013) 'Cancer drug resistance: An evolving paradigm', *Nature Reviews Cancer*. Nature Publishing Group, 13(10), pp. 714–726. doi: 10.1038/nrc3599.

Holz, M. K. and Blenis, J. (2005) 'Identification of S6 Kinase 1 as a Novel Mammalian Target of Rapamycin (mTOR)-phosphorylating Kinase', *Journal of Biological Chemistry*, 280(28), pp. 26089–26093. doi: 10.1074/jbc.M504045200.

Hsieh, A. C., Nguyen, H. G., Wen, L., Edlind, M. P., Carroll, P. R., Kim, W. and Ruggero, D. (2015) 'Cell type – specific abundance of 4EBP1 primes prostate cancer sensitivity or resistance to PI3K pathway inhibitors', *Science Signaling*, 8(403), pp. 1–11. doi: 10.1126/scisignal.aad5111.

Huang, J. and Manning, B. D. (2008) 'The TSC1–TSC2 complex: a molecular switchboard controlling cell growth', *Biochemical Journal*, 412(2), pp. 179–190. doi: 10.1042/BJ20080281.The.

Huang, K. and Fingar, D. (2012) 'Growing knowledge of the mTOR signaling network', *Seminars in Cell and Developmental Biology,* 1(3), pp. 233–245. doi: 10.1016/j.dcn.2011.01.002.The.

Hutchinson, J. A., Shanware, N. P., Chang, H. and Tibbetts, R. S. (2011) 'Regulation of ribosomal protein S6 phosphorylation by casein kinase 1 and protein phosphatase 1', *Journal of Biological Chemistry*, 286(10), pp. 8688–8696. doi: 10.1074/jbc.M110.141754.

I. Brian Greenwell., (2017) 'PI3K Inhibitors: Understanding Toxicity Mechanisms and Management', *Oncology* 15;31(11):821-8.

Igreja, C., Peter, D., Weiler, C. and Izaurralde, E. (2014) '4E-BPs require non-canonical 4E-binding motifs and a lateral surface of eIF4E to repress translation', *Nature Communications*, 5(May), pp. 1–14. doi: 10.1038/ncomms5790.

Ilic, N., Utermark, T., Widlund, H. R. and Roberts, T. M. (2011) 'PI3K-targeted therapy can be evaded by gene amplification along the MYC-eukaryotic translation initiation factor 4E (eIF4E) axis', *Proceedings of the National Academy of Sciences*, 108(37), pp. E699–E708. doi: 10.1073/pnas.1108237108.

Ingolia, N. T. (2010) 'Genome-Wide Translational Profiling by Ribosome Footprinting', *Methods in Enzymology*. Academic Press, 470, pp. 119–142. doi: 10.1016/S0076-6879(10)70006-9.

Inoki, K., Ouyang, H., Zhu, T., Lindvall, C., Wang, Y., Zhang, X., Yang, Q., Bennett, C., Harada, Y., Stankunas, K., Wang, C. yu, He, X., MacDougald, O. A., You, M., Williams, B. O. and Guan, K. L. (2006) 'TSC2 Integrates Wnt and Energy Signals via a Coordinated Phosphorylation by AMPK and GSK3 to Regulate Cell Growth', *Cell*. doi: 10.1016/j.cell.2006.06.055.

Jacinto, E., Facchinetti, V., Liu, D., Soto, N., Wei, S., Jung, S. Y., Huang, Q., Qin, J. and Su, B. (2006) 'SIN1/MIP1 Maintains rictor-mTOR Complex Integrity and Regulates Akt Phosphorylation and Substrate Specificity', *Cell*, 127(1), pp. 125–137. doi: 10.1016/j.cell.2006.08.033.

Jackson, R. J. (2013) 'The current status of vertebrate cellular mRNA IRESs.', *Cold Spring Harbor perspectives in biology*. Cold Spring Harbor Laboratory Press, 5(2). doi: 10.1101/cshperspect.a011569.

Jackson, R. J., Hellen, C. U. T. and Pestova, T. V. (2010) 'The mechanism of eukaryotic translation initiation and principles of its regulation', *Nature Reviews Molecular Cell Biology*, pp. 113–127. doi: 10.1038/nrm2838.

Jhanwar-Uniyal, M., Amin, A. G., Cooper, J. B., Das, K., Schmidt, M. H. and Murali, R. (2017) 'Discrete signaling mechanisms of mTORC1 and mTORC2: Connected yet apart in cellular and molecular aspects', *Advances in Biological Regulation*. Elsevier Ltd, 64, pp. 39–48. doi: 10.1016/j.jbior.2016.12.001.

Johnson, A. G., Grosely, R., Petrov, A. N. and Puglisi, J. D. (2017) 'Dynamics of IRES-mediated translation.', *Philosophical transactions of the Royal Society of London. Series B, Biological sciences*. The Royal Society, 372(1716). doi: 10.1098/rstb.2016.0177.

Juric, D., Castel, P., Griffith, M., Griffith, O. L., Won, H. H., Ellis, H., Ebbesen, S. H., Ainscough, B. J., Ramu, A., Iyer, G., Shah, R. H., Huynh, T., Mino-Kenudson, M., Sgroi, D., Isakoff, S., Thabet, A., … Scaltriti, M. (2015) 'Convergent loss of PTEN leads to clinical resistance to a PI(3)Kα inhibitor', *Nature*, 518(7538). doi: 10.1038/nature13948.

Kaelin, W. G. (2017) 'Common pitfalls in preclinical cancer target validation', *Nature Reviews Cancer*. Nature Publishing Group, 17(7), pp. 441–450. doi: 10.1038/nrc.2017.32.

Kapeli, K. and Yeo, G. W. (2012) 'Genome-Wide Approaches to Dissect the Roles of RNA Binding Proteins in Translational Control: Implications for Neurological Diseases', *Frontiers in Neuroscience*. Frontiers, 6, p. 144. doi: 10.3389/fnins.2012.00144.

Katayama, R., Khan, T. M., Benes, C., Lifshits, E., Ebi, H., Rivera, V. M., Shakespeare, W. C., Iafrate, A. J., Engelman, J. A. and Shaw, A. T. (2011) 'Therapeutic strategies to overcome crizotinib resistance in non-small cell lung cancers harboring the fusion oncogene EML4-ALK', *Proceedings of the National Academy of Sciences*, 108(18), pp. 7535–7540. doi: 10.1073/pnas.1019559108.

Keisell, D. P., Black, D. M., Bishop, D. T. and Spurr, N. K. (1993) 'Genetic analysis of the BRCA1 region in a large breast/ovarian family: refinement of the minimal region containing BRCA1', *Human Molecular Genetics*, 2(11), pp. 1823–1828. doi: 10.1093/hmg/2.11.1823.

Kim, E., Kim, A., Kim, S., Kim, H., Chang, J., Ahn, C. and Chang, Y. (2014) 'Inhibition of mTORC1 induces loss of E-cadherin through AKT/GSK-3β signaling-mediated upregulation of E-cadherin repressor complexes in non-small cell lung cancer cells', *Respiratory Research*. BioMed Central, 15(1), p. 26. doi: 10.1186/1465-9921-15-26.

Kim, J. and Guan, K.-L. (2019) 'mTOR as a central hub of nutrient signalling and cell growth', *Nature Cell Biology*. Nature Publishing Group, 21(1), pp. 63–71. doi: 10.1038/s41556-018-0205-1.

Kim, J., Kundu, M., Viollet, B. and Guan, K.-L. (2011) 'AMPK and mTOR regulate autophagy through direct phosphorylation of Ulk1', 13(2), pp. 132–141. doi: 10.1038/ncb2152.AMPK.

Klann, E., Antion, M. D., Banko, J. L. and Hou, L. (2004) 'Synaptic Plasticity and Translation Initiation', *Learning & Memory*. Cold Spring Harbor Laboratory Press, 11(4), pp. 365–372. doi: 10.1101/LM.79004.

Konieczkowski, D. J., Johannessen, C. M. and Garraway, L. A. (2018) 'A Convergence-Based Framework for Cancer Drug Resistance', *Cancer Cell*. Elsevier Inc., 33(5), pp. 801–815. doi: 10.1016/j.ccell.2018.03.025.

Konopleva, M. Y., Walter, R. B., Faderl, S. H., Jabbour, E. J., Zeng, Z., Borthakur, G., Huang, X., Kadia, T. M., Ruvolo, P. P., Feliu, J. B., Lu, H., Debose, L. K., Burger, J. A., Andreeff, M., Liu, W., Baggerly, K. A., … Kantarjian, H. M. (2014) 'Preclinical and early clinical evaluation of the oral AKT inhibitor, MK-2206, for the treatment of acute myelogenous leukemia', *Clinical Cancer Research*. American Association for Cancer Research Inc., 20(8), pp. 2226–2235. doi: 10.1158/1078-0432.CCR-13-1978.

Kumar, C. C. and Madison, V. (2005) 'AKT crystal structure and AKT-specific inhibitors', *Oncogene*. Nature Publishing Group, 24(50), pp. 7493–7501. doi: 10.1038/sj.onc.1209087.

Kwiatkowski, D. J. and Manning, B. D. (2005) 'Tuberous sclerosis: A GAP at the crossroads of multiple signaling pathways', *Human Molecular Genetics*, 14(SUPPL. 2). doi: 10.1093/hmg/ddi260.

LAEMMLI, U. K. (1970) 'Cleavage of Structural Proteins during the Assembly of the Head of Bacteriophage T4', *Nature*, 227(5259), pp. 680–685. doi: 10.1038/227680a0.

Lahr, R. M., Fonseca, B. D., Ciotti, G. E., Al-Ashtal, H. A., Jia, J.-J., Niklaus, M. R., Blagden, S. P., Alain, T. and Berman, A. J. (2017) 'La-related protein 1 (LARP1) binds the mRNA cap, blocking eIF4F assembly on TOP mRNAs', *eLife*, 6. doi: 10.7554/eLife.24146.

Lake, D., Corrêa, S. A. L. and Müller, J. (2016) 'Negative feedback regulation of the ERK1/2 MAPK pathway', *Cellular and Molecular Life Sciences*. doi: 10.1007/s00018-016-2297-8.

Lam, F., Abbas, A. Y., Shao, H., Teo, T., Adams, J., Li, P., Bradshaw, T. D., Fischer, P. M., Walsby, E., Pepper, C., Chen, Y., Ding, J. and Wang, S. (2014) 'Targeting RNA transcription and translation in ovarian cancer cells with pharmacological inhibitor CDKI-73.', *Oncotarget*. Impact Journals, LLC, 5(17), pp. 7691–704. doi: 10.18632/oncotarget.2296.

Lamoureux, F., Thomas, C., Crafter, C., Kumano, M., Zhang, F., Davies, B. R., Gleave, M. E. and Zoubeidi, A. (2013) 'Blocked Autophagy Using Lysosomotropic Agents Sensitizes Resistant Prostate Tumor Cells to the Novel Akt Inhibitor AZD5363', *Clinical Cancer Research*, 19(4), pp. 833–844. doi: 10.1158/1078-0432.CCR-12-3114.

Laplante, M. and Sabatini, D. M. (2009) 'mTOR signaling at a glance', *Journal of Cell Science*, 122(20), pp. 3589–3594. doi: 10.1242/jcs.051011.

Laplante, M. and Sabatini, D. M. (2012) 'mTOR signaling in growth control and disease', *Cell,* 30(7), p. 631. doi: 10.1016/j.cell.2012.03.017.mTOR.

Law, N. C., Donaubauer, E. M., Zeleznik, A. J. and Hunzicker-Dunn, M. (2017) 'How Protein Kinase A Activates Canonical Tyrosine Kinase Signaling Pathways To Promote Granulosa Cell Differentiation.', *Endocrinology*, 158(7), pp. 2043–2051. doi: 10.1210/en.2017-00163.

Lawrence, M. S., Stojanov, P., Mermel, C. H., Robinson, J. T., Garraway, L. A., Golub, T. R., Meyerson, M., Gabriel, S. B., Lander, E. S. and Getz, G. (2014) 'Discovery and saturation analysis of cancer genes across 21 tumour types.', *Nature*. NIH Public Access, 505(7484), pp. 495–501. doi: 10.1038/nature12912.

Le, X., Antony, R., Razavi, P., Treacy, D. J., Luo, F., Ghandi, M., Castel, P., Scaltriti, M., Baselga, J. and Garraway, L. A. (2016) 'Systematic functional characterization of resistance to PI3K inhibition in breast cancer', *Cancer Discovery*. doi: 10.1158/2159-8290.CD-16-0305.

Leppek, K., Das, R. and Barna, M. (2018) 'Functional 5' UTR mRNA structures in eukaryotic translation regulation and how to find them.', *Nature reviews. Molecular cell biology*, 19(3), pp. 158–174. doi: 10.1038/nrm.2017.103.

Leprivier, G., Remke, M., Rotblat, B., Dubuc, A., Mateo, A.-R. F., Kool, M., Agnihotri, S., El-Naggar, A., Yu, B., Somasekharan, S. P., Faubert, B., Bridon, G., Tognon, C. E., Mathers, J., Thomas, R., Li, A., … Sorensen, P. H. (2013) 'The eEF2 Kinase Confers Resistance to Nutrient Deprivation by Blocking Translation Elongation', *Cell*, 153(5), pp. 1064–1079. doi: 10.1016/j.cell.2013.04.055.

Li, B., Yuan, M., Kim, I.-A., Chang, C.-M., Bernhard, E. J. and Shu, H.-K. G. (2004) 'Mutant epidermal growth factor receptor displays increased signaling through the phosphatidylinositol-3 kinase/AKT pathway and promotes radioresistance in cells of astrocytic origin.', *Oncogene*, 23(26), pp. 4594–602. doi: 10.1038/sj.onc.1207602.

Li, S., Jia, Y., Jacobson, B., McCauley, J., Kratzke, R., Bitterman, P. B. and Wagner, C. R. (2013) 'Treatment of breast and lung cancer cells with a N-7 benzyl guanosine monophosphate tryptamine phosphoramidate pronucleotide (4Ei-1) results in chemosensitization to gemcitabine and induced eIF4E proteasomal degradation', *Molecular Pharmaceutics*. 10(2):523-31, doi: 10.1021/mp300699d.

Li, S., Sonenberg, N., Gingras, A.-C., Peterson, M., Avdulov, S., Polunovsky, V. a and Bitterman, P. B. (2002) 'Translational control of cell fate: availability of phosphorylation sites on translational repressor 4E-BP1 governs its proapoptotic potency.', *Molecular and cellular biology*, 22(8), pp. 2853–61. doi: 10.1128/MCB.22.8.2853.

Li, X., Dai, D., Chen, B., Tang, H., Xie, X. and Wei, W. (2018) 'Efficacy of PI3K/AKT/mTOR pathway inhibitors for the treatment of advanced solid cancers: A literature-based meta-analysis of 46 randomised control trials', *PLoS ONE*. doi: 10.1371/journal.pone.0192464.

Lin, J., Sampath, D., Nannini, M. A., Lee, B. B., Degtyarev, M., Oeh, J., Savage, H., Guan, Z., Hong, R., Kassees, R., Lee, L. B., Risom, T., Gross, S., Liederer, B. M., Koeppen, H., Skelton, N. J., … Lin, K. (2013) 'Targeting activated Akt with GDC-0068, a novel selective Akt inhibitor that is efficacious in multiple tumor models', *Clinical Cancer Research*, 19(7), pp. 1760–1772. doi: 10.1158/1078-0432.CCR-12-3072.

Lin, K., Lin, J., Wu, W.-I., Ballard, J., Lee, B. B., Gloor, S. L., Vigers, G. P. A., Morales, T. H., Friedman, L. S., Skelton, N. and Brandhuber, B. J. (2012) 'An ATP-Site On-Off Switch That Restricts Phosphatase Accessibility of Akt', *Science Signaling*, 5(223), pp. ra37–ra37. doi: 10.1126/scisignal.2002618.

Lindsley, C. (2010) 'The Akt/PKB Family of Protein Kinases: A Review of Small Molecule Inhibitors and Progress Towards Target Validation: A 2009 Update', *Current Topics in Medicinal Chemistry*, 10(4), pp. 458–477. doi: 10.2174/156802610790980602.

Liu, R. and Proud, C. G. (2016) 'Eukaryotic elongation factor 2 kinase as a drug target in cancer, and in cardiovascular and neurodegenerative diseases', *Acta Pharmacologica Sinica*. Nature Publishing Group, pp. 285–294. doi: 10.1038/aps.2015.123.

Liu, S. L., Wang, Z. G., Hu, Y., Xin, Y., Singaram, I., Gorai, S., Zhou, X., Shim, Y., Min, J. H., Gong, L. W., Hay, N., Zhang, J. and Cho, W. (2018) 'Quantitative Lipid Imaging Reveals a New Signaling Function of Phosphatidylinositol-3,4-Bisphophate: Isoform- and Site-Specific Activation of Akt', *Molecular Cell*, 71(6). doi: 10.1016/j.molcel.2018.07.035.

Livasy, C. A., Reading, F. C., Moore, D. T., Boggess, J. F. and Lininger, R. A. (2006) 'EGFR expression and HER2/neu overexpression/amplification in endometrial carcinosarcoma.', *Gynecologic oncology*, 100(1), pp. 101–6. doi: 10.1016/j.ygyno.2005.07.124.

Longley, D. and Johnston, P. (2005) 'Molecular mechanisms of drug resistance', *The Journal of Pathology*, 205(2), pp. 275–292. doi: 10.1002/path.1706.

Lord, C. J. and Ashworth, A. (2012) 'The DNA damage response and cancer therapy', *Nature*, 481(7381), pp. 287–294. doi: 10.1038/nature10760.

Lovejoy, C. A. and Cortez, D. (2009) 'Common mechanisms of PIKK regulation.', *DNA repair*. NIH Public Access, 8(9), pp. 1004–8. doi: 10.1016/j.dnarep.2009.04.006.

Lu, C., Makala, L., Wu, D. and Cai, Y. (2016) 'Targeting translation: EIF4E as an emerging anticancer drug target', *Expert Reviews in Molecular Medicine*, 18. doi: 10.1017/erm.2015.20.

Ma, L., Chen, Z., Erdjument-Bromage, H., Tempst, P. and Pandolfi, P. P. (2005) 'Phosphorylation and Functional Inactivation of TSC2 by Erk: Implications for Tuberous Sclerosisand Cancer Pathogenesis', *Cell*. Cell Press, 121(2), pp. 179–193. doi: 10.1016/J.CELL.2005.02.031.

Malka-Mahieu, H., Newman, M., Désaubry, L., Robert, C. and Vagner, S. (2017) 'Molecular pathways: The eIF4F translation initiation complex-newopportunities for cancer treatment', *Clinical Cancer Research*, 23(1), pp. 21–25. doi: 10.1158/1078-0432.CCR-14-2362.

Mallya, S., Fitch, B. A., Lee, J. S., So, L., Janes, M. R. and Fruman, D. A. (2014) 'Resistance to mTOR kinase inhibitors in lymphoma cells lacking 4EBP1.', *PloS one*. Edited by R. W. Sobol, 9(2), p. e88865. doi: 10.1371/journal.pone.0088865.

Mansoori, B., Mohammadi, A., Davudian, S., Shirjang, S. and Baradaran, B. (2017) 'The Different Mechanisms of Cancer Drug Resistance: A Brief Review.', *Advanced pharmaceutical bulletin*. Tabriz University of Medical Sciences, 7(3), pp. 339–348. doi: 10.15171/apb.2017.041.

Martelli, A. M., Buontempo, F. and McCubrey, J. A. (2018) 'Drug discovery targeting the mTOR pathway', *Clinical Science*, 132(5), pp. 543–568. doi: 10.1042/CS20171158.

Martineau, Y., Azar, R., Bousquet, C. and Pyronnet, S. (2013) 'Anti-oncogenic potential of the eIF4E-binding proteins', *Oncogene*, 32(6), pp. 671–677. doi: 10.1038/onc.2012.116.

Martineau, Y, Azar, R., Müller, D., Lasfargues, C., El Khawand, S., Anesia, R., Pelletier, J., Bousquet, C. and Pyronnet, S. (2014) 'Pancreatic tumours escape from translational control through 4E-BP1 loss', *Oncogene*, 33(11), pp. 1367–1374. doi: 10.1038/onc.2013.100.

Martineau, Yvan, Müller, D. and Pyronnet, S. (2014) 'Targeting protein synthesis in cancer cells', *Oncoscience*, 1(7), p. 484. doi: 10.18632/oncoscience.63.

Martini, M., Ciraolo, E., Gulluni, F. and Hirsch, E. (2013) 'Targeting PI3K in Cancer: Any Good News?', *Frontiers in Oncology*. Frontiers, 3, p. 108. doi: 10.3389/fonc.2013.00108.

McDermott, M., Eustace, A. J., Busschots, S., Breen, L., Crown, J., Clynes, M., Donovan, N., Stordal, B., O'Donovan, N. and Stordal, B. (2014) 'In vitro Development of Chemotherapy and Targeted Therapy Drug-Resistant Cancer Cell Lines: A Practical Guide with Case Studies', *Frontiers in Oncology*. Frontiers Media SA, 4(March), p. 40. doi: 10.3389/fonc.2014.00040.

McHardy, T., Caldwell, J. J., Cheung, K.-M., Hunter, L. J., Taylor, K., Rowlands, M., Ruddle, R., Henley, A., de Haven Brandon, A., Valenti, M., Davies, T. G., Fazal, L., Seavers, L., Raynaud, F. I., Eccles, S. A., Aherne, G. W., … Collins, I. (2010) 'Discovery of 4-Amino-1-(7 *H* -pyrrolo[2,3- *d*]pyrimidin-4-yl)piperidine-4-carboxamides As Selective, Orally Active Inhibitors of Protein Kinase B (Akt)', *Journal of Medicinal Chemistry*, 53(5), pp. 2239–2249. doi: 10.1021/jm901788j.

Meinhold-Heerlein, I. and Hauptmann, S. (2014) 'The heterogeneity of ovarian cancer.', *Archives of gynecology and obstetrics*, 289(2), pp. 237–9. doi: 10.1007/s00404-013-3114-3.

Mendoza, M. C., Er, E. E. and Blenis, J. (2011) 'The Ras-ERK and PI3K-mTOR pathways: cross-talk and compensation.', *Trends in biochemical sciences*. NIH Public Access, 36(6), pp. 320–8. doi: 10.1016/j.tibs.2011.03.006.

Menon, S., Dibble, C. C., Talbott, G., Hoxhaj, G., Valvezan, A. J., Takahashi, H., Cantley, L. C. and Manning, B. D. (2014) 'Spatial Control of the TSC Complex Integrates Insulin and Nutrient Regulation of mTORC1 at the Lysosome', *Cell*, 156(4), pp. 771–785. doi: 10.1016/j.cell.2013.11.049.

Menon, S. and Manning, B. D. (2008) 'Common corruption of the mTOR signaling network in human tumors.', *Oncogene*, 27 Suppl 2, pp. S43-51. doi: 10.1038/onc.2009.352.

Metzger, B., Chambeau, L., Begon, D. Y., Faber, C., Kayser, J., Berchem, G., Pauly, M., Boniver, J., Delvenne, P., Dicato, M. and Wenner, T. (2011) 'The human epidermal growth factor receptor (EGFR) gene in European patients with advanced colorectal cancer harbors infrequent mutations in its tyrosine kinase domain', *BMC Medical Genetics*. doi: 10.1186/1471-2350-12-144.

Meyuhas, O. (2015) 'Ribosomal Protein S6 Phosphorylation: Four Decades of Research', *International Review of Cell and Molecular Biology*, 320. doi: 10.1016/bs.ircmb.2015.07.006.

Mi, W., Ye, Q., Liu, S. and She, Q.-B. (2015) 'AKT inhibition overcomes rapamycin resistance by enhancing the repressive function of PRAS40 on mTORC1/4E-BP1 axis', *Oncotarget*, 6(16), pp. 13962–77. doi: 10.18632/oncotarget.3920.

Moerke, N. J., Aktas, H., Chen, H., Cantel, S., Reibarkh, M. Y., Fahmy, A., Gross, J. D. D., Degterev, A., Yuan, J., Chorev, M., Halperin, J. A. and Wagner, G. (2007) 'Small-Molecule Inhibition of the Interaction between the Translation Initiation Factors eIF4E and eIF4G', *Cell*, 128(2), pp. 257–267. doi: 10.1016/j.cell.2006.11.046.

Morrow, J. K., Du-Cuny, L., Chen, L., Meuillet, E. J., Mash, E. A., Powis, G. and Zhang, S. (2011) 'Recent Development of Anticancer Therapeutics Targeting Akt', *Recent patents on anti-cancer drug discovery*. NIH Public Access, 6(1), p. 146.

Mundi, P. S., Sachdev, J., McCourt, C. and Kalinsky, K. (2016) 'AKT in cancer: new molecular insights and advances in drug development', *British Journal of Clinical Pharmacology*, 110, pp. 943–956. doi: 10.1111/bcp.13021.

Mura, M., Hopkins, T. G., Michael, T., Abd-Latip, N., Weir, J., Aboagye, E., Mauri, F., Jameson, C., Sturge, J., Gabra, H., Bushell, M., Willis, A. E., Curry, E. and Blagden, S. P. (2014) 'LARP1 post-transcriptionally regulates mTOR and contributes to cancer progression', *Oncogene*, 34, pp. 5025–5036. doi: 10.1038/onc.2014.428.

Muranen, T., Selfors, L. M., Hwang, J., Gallegos, L. L., Coloff, J. L., Thoreen, C. C., Kang, S. A., Sabatini, D. M., Mills, G. B. and Brugge, J. S. (2016) 'ERK and p38 MAPK Activities Determine Sensitivity to PI3K/mTOR Inhibition via Regulation of MYC and YAP', *Cancer Research*, 76(24), pp. 7168–7180. doi: 10.1158/0008-5472.CAN-16-0155.

Murugan, A. K., Liu, R. and Xing, M. (2019) 'Identification and characterization of two novel oncogenic mTOR mutations', *Oncogene*. Nature Publishing Group, p. 1. doi: 10.1038/s41388-019-0787-5.

Musa, J., Orth, M. F., Dallmayer, M., Baldauf, M., Pardo, C., Rotblat, B., Kirchner, T., Leprivier, G. and Grünewald, T. G. P. (2016) 'Eukaryotic initiation factor 4E-binding protein 1 (4E-BP1): A master regulator of mRNA translation involved in tumorigenesis', *Oncogene*. Nature Publishing Group, 35(36), pp. 4675–4688. doi: 10.1038/onc.2015.515.

Namekawa, T., Ikeda, K., Horie-Inoue, K. and Inoue, S. (2019) 'Application of Prostate Cancer Models for Preclinical Study: Advantages and Limitations of Cell Lines, Patient-Derived Xenografts, and Three-Dimensional Culture of Patient-Derived Cells', *Cells*. MDPI AG, 8(1), p. 74. doi: 10.3390/cells8010074.

Nandagopal, N. and Roux, P. P. (2015) 'Regulation of global and specific mRNA translation by the mTOR signaling pathway.', *Translation (Austin, Tex.)*. Taylor & Francis, 3(1), p. e983402. doi: 10.4161/21690731.2014.983402.

Nazarian, R., Shi, H., Wang, Q., Kong, X., Koya, R. C., Lee, H., Chen, Z., Lee, M. K., Attar, N., Sazegar, H., Chodon, T., Nelson, S. F., McArthur, G., Sosman, J. A., Ribas, A. and Lo, R. S. (2010) 'Melanomas acquire resistance to B-RAF(V600E) inhibition by RTK or N-RAS upregulation', *Nature*, 468(7326), pp. 973–977. doi: 10.1038/nature09626.

Ng, T. H., Sham, K. W. Y., Xie, C. M., Ng, S. S. M., To, K. F., Tong, J. H. M., Liu, W. Y. Z., Zhang, L., Chan, M. T. V, Wu, W. K. K. and Cheng, C. H. K. (2019) 'Eukaryotic elongation factor-2 kinase expression is an independent prognostic factor in colorectal cancer', *BMC Cancer*, 19(649). doi: 10.1186/s12885-019-5873-0.

Nitulescu, G. M., Margina, D., Juzenas, P., Peng, Q., Olaru, O. T., Saloustros, E., Fenga, C., Spandidos, D. A., Libra, M. and Tsatsakis, A. M. (2016) 'Akt inhibitors in cancer treatment: The long journey from drug discovery to clinical use (Review)', *International Journal of Oncology*. doi: 10.3892/ijo.2015.3306.

Nogami, A., Oshikawa, G., Okada, K., Fukutake, S., Umezawa, Y., Nagao, T., Kurosu, T. and Miura, O. (2015) 'FLT3-ITD confers resistance to the PI3K/Akt pathway inhibitors by protecting the mTOR/4EBP1/Mcl-1 pathway through STAT5 activation in acute myeloid leukemia', *Oncotarget*, 6(11). doi: 10.18632/oncotarget.3279.

O'Reilly, K. E., Rojo, F., She, Q.-B., Solit, D., Mills, G. B., Smith, D., Lane, H., Hofmann, F., Hicklin, D. J., Ludwig, D. L., Baselga, J. and Rosen, N. (2006) 'mTOR inhibition induces upstream receptor tyrosine kinase signaling and activates Akt.', *Cancer research*. NIH Public Access, 66(3), pp. 1500–8. doi: 10.1158/0008-5472.CAN-05-2925.

Oda, K., Okada, J., Timmerman, L., Rodriguez-Viciana, P., Stokoe, D., Shoji, K., Taketani, Y., Kuramoto, H., Knight, Z. A., Shokat, K. M. and McCormick, F. (2008) 'PIK3CA Cooperates with Other Phosphatidylinositol 3-Kinase Pathway Mutations to

Effect Oncogenic Transformation', *Cancer research*. American Association for Cancer Research, 68(19), pp. 8127–36. doi: 10.1158/0008-5472.can-08-0755.

Papadopoulos, E., Jenni, S., Kabha, E., Takrouri, K. J., Yi, T., Salvi, N., Luna, R. E., Gavathiotis, E., Mahalingam, P., Arthanari, H., Rodriguez-Mias, R., Yefidoff-Freedman, R., Aktas, B. H., Chorev, M., Halperin, J. A. and Wagner, G. (2014) 'Structure of the eukaryotic translation initiation factor eIF4E in complex with 4EGI-1 reveals an allosteric mechanism for dissociating eIF4G', *Proceedings of the National Academy of Sciences*, 111(31), pp. E3187–E3195. doi: 10.1073/pnas.1410250111.

Parmar, N. and Tamanoi, F. (2010) 'Rheb G-Proteins and the Activation of mTORC1', *The Enzymes*. NIH Public Access, 27, p. 39. doi: 10.1016/S1874-6047(10)27003-8.

Parmer, T. G., Ward, M. D., Yurkow, E. J., Vyas, V. H., Kearney, T. J. and Hait, W. N. (1999) 'Activity and regulation by growth factors of calmodulin-dependent protein kinase III (elongation factor 2-kinase) in human breast cancer', *British Journal of Cancer*, 79(1), pp. 59–64. doi: 10.1038/sj.bjc.6690012.

Pearce, Laura R., Alton, G. R., Richter, D. T., Kath, J. C., Lingardo, L., Chapman, J., Hwang, C. and Alessi, D. R. (2010) 'Characterization of PF-4708671, a novel and highly specific inhibitor of p70 ribosomal S6 kinase (S6K1)', *Biochemical Journal*, 431(2), pp. 245–255. doi: 10.1042/BJ20101024.

Pearce, Laura R., Komander, D. and Alessi, D. R. (2010) 'The nuts and bolts of AGC protein kinases', *Nature Reviews Molecular Cell Biology*. Nature Publishing Group, 11(1), pp. 9–22. doi: 10.1038/nrm2822.

Pecorino, L. (2016) *Molecular biology of cancer : mechanisms, targets, and therapeutics*.

Pelletier, J., Graff, J., Ruggero, D. and Sonenberg, N. (2015) 'Targeting the eIF4F translation initiation complex: A critical nexus for cancer development', *Cancer Research*, 75(2). doi: 10.1158/0008-5472.CAN-14-2789.

Peter, D., Igreja, C., Weber, R., Wohlbold, L., Weiler, C., Ebertsch, L., Weichenrieder, O. and Izaurralde, E. (2015) 'Molecular Architecture of 4E-BP Translational Inhibitors Bound to eIF4E', *Molecular Cell*, 57(6), pp. 1074–1087. doi: 10.1016/j.molcel.2015.01.017.

Pike, K. G., Malagu, K., Hummersone, M. G., Menear, K. A., Duggan, H. M. E., Gomez, S., Martin, N. M. B., Ruston, L., Pass, S. L. and Pass, M. (2013) 'Optimization of potent and selective dual mTORC1 and mTORC2 inhibitors: The discovery of AZD8055 and AZD2014', *Bioorganic and Medicinal Chemistry Letters*, 23(5), pp. 1212–1216. doi: 10.1016/j.bmcl.2013.01.019.

Qi, L., Toyoda, H., Xu, D. qing, Zhou, Y., Sakurai, N., Amano, K., Kihira, K., Hori, H., Azuma, E. and Komada, Y. (2015) 'PDK1-mTOR signaling pathway inhibitors reduce cell proliferation in MK2206 resistant neuroblastoma cells', *Cancer Cell International*. BioMed Central, 15(1), pp. 1–14. doi: 10.1186/s12935-015-0239-4.

Qin, X., Jiang, B. and Zhang, Y. (2016) '4E-BP1, a multifactor regulated multifunctional protein', *Cell Cycle*. Taylor & Francis, 15(6), pp. 781–786. doi: 10.1080/15384101.2016.1151581.

Ravegnini, G., Sammarini, G., Moran, S., Calice, G., Indio, V., Urbini, M., Astolfi, A., Zanotti, F., Pantaleo, M. A., Hrelia, P. and Angelini, S. (2019) 'Mechanisms of resistance to a PI3K inhibitor in gastrointestinal stromal tumors: an omic approach to identify novel druggable targets.', *Cancer management and research*, 11, pp. 6229–6244. doi: 10.2147/CMAR.S189661.

Rees, D. C., Congreve, M., Murray, C. W. and Carr, R. (2004) 'Fragment-based lead discovery', *Nature Reviews Drug Discovery*, 3(8), pp. 660–672. doi: 10.1038/nrd1467.

Regad, T. (2015) 'Targeting RTK Signaling Pathways in Cancer.', *Cancers*, 7(3), pp. 1758–84. doi: 10.3390/cancers7030860.

Ren-Jang, L. (2010) 'Maternal mRNA and the PolyA Tail in Oocytes', *Nature Education*, 3(9), p. 47.

Revathidevi, S. and Munirajan, A. K. (2019) 'Akt in cancer: Mediator and more', *Seminars in Cancer Biology*. doi: 10.1016/j.semcancer.2019.06.002.

Richardson, P. G., Eng, C., Kolesar, J., Hideshima, T. and Anderson, K. C. (2012) 'Perifosine, an oral, anti-cancer agent and inhibitor of the Akt pathway: mechanistic actions, pharmacodynamics, pharmacokinetics, and clinical activity', *Expert Opinion on Drug Metabolism & Toxicology*, 8(5), pp. 623–33. doi: 10.1517/17425255.2012.681376.

Rinnerthaler, G., Gampenrieder, S. P. and Greil, R. (2018) 'ASCO 2018 highlights: metastatic breast cancer', *Memo - Magazine of European Medical Oncology*. doi: 10.1007/s12254-018-0450-9.

Rodon, J., Dienstmann, R., Serra, V. and Tabernero, J. (2013) 'Development of PI3K inhibitors: Lessons learned from early clinical trials', *Nature Reviews Clinical Oncology*. Nature Publishing Group, 10(3), pp. 143–153. doi: 10.1038/nrclinonc.2013.10.

Romeo, Y., Moreau, J., Zindy, P.-J., Saba-El-Leil, M., Lavoie, G., Dandachi, F., Baptissart, M., Borden, K. L. B., Meloche, S. and Roux, P. P. (2013) 'RSK regulates activated BRAF signalling to mTORC1 and promotes melanoma growth', *Oncogene*. NIH Public Access, 32(24), p. 2917. doi: 10.1038/ONC.2012.312.

Roskoski, R. (2016) 'Classification of small molecule protein kinase inhibitors based upon the structures of their drug-enzyme complexes', *Pharmacological Research*, 103, pp. 26–48. doi: 10.1016/j.phrs.2015.10.021.

Roskoski, R. (2019) 'Targeting ERK1/2 protein-serine/threonine kinases in human cancers', *Pharmacological Research*. Academic Press, 142, pp. 151–168. doi: 10.1016/J.PHRS.2019.01.039.

Roux, P. P., Ballif, B. A., Anjum, R., Gygi, S. P. and Blenis, J. (2004) 'Tumor-promoting phorbol esters and activated Ras inactivate the tuberous sclerosis tumor suppressor complex via p90 ribosomal S6 kinase', *Proceedings of the National Academy of Sciences*. doi: 10.1073/pnas.0405659101.

Roux, P. P., Shahbazian, D., Vu, H., Holz, M. K., Cohen, M. S., Taunton, J., Sonenberg, N. and Blenis, J. (2007) 'RAS/ERK signaling promotes site-specific ribosomal protein S6 phosphorylation via RSK and stimulates cap-dependent translation.', *The Journal of biological chemistry*. American Society for Biochemistry and Molecular Biology, 282(19), pp. 14056–64. doi: 10.1074/jbc.M700906200.

Roux, P. P. and Topisirovic, I. (2012) 'Regulation of mRNA Translation by Signaling Pathways', *Cold Spring Harbor Perspectives in Biology*, 4(11), pp. a012252–a012252. doi: 10.1101/cshperspect.a012252.

Roux, P. P. and Topisirovic, I. (2018) 'Signaling Pathways Involved in the Regulation of mRNA Translation', *Molecular and Cellular Biology*, 38(12). doi: 10.1128/MCB.00070-18.

Rutkovsky, A. C., Yeh, E. S., Guest, S. T., Findlay, V. J., Muise-Helmericks, R. C., Armeson, K. and Ethier, S. P. (2019) 'Eukaryotic initiation factor 4E-binding protein as an oncogene in breast cancer', *BMC Cancer*. BioMed Central, 19(1), p. 491. doi: 10.1186/s12885-019-5667-4.

Saito, M., Okamoto, A., Kohno, T., Takakura, S., Shinozaki, H., Isonishi, S., Yasuhara, T., Yoshimura, T., Ohtake, Y., Ochiai, K., Yokota, J. and Tanaka, T. (2000) 'Allelic imbalance and mutations of the PTEN gene in ovarian cancer', *International Journal of Cancer*. John Wiley & Sons, Ltd, 85(2), pp. 160–165. doi: 10.1002/(SICI)1097-0215(20000115)85:2<160::AID-IJC2>3.0.CO;2-5.

Sampath, D., Malik, A., Plunkett, W., Nowak, B., Williams, B., Burton, M., Verstovsek, S., Faderl, S., Garcia-Manero, G., List, A. F., Sebti, S., Kantarjian, H. M.,

Ravandi, F. and Lancet, J. E. (2013) 'Phase I clinical, pharmacokinetic, and pharmacodynamic study of the Akt-inhibitor triciribine phosphate monohydrate in patients with advanced hematologic malignancies', *Leukemia Research*. doi: 10.1016/j.leukres.2013.07.034.

Saura, Cristina, Roda, Desamparados, Roselló, Susana, Oliveira, Mafalda, Macarulla, Teresa, Alejandro Pérez-Fidalgo, J., Morales-Barrera, Rafael, Manuel Sanchis-García, J., Musib, Luna, Budha, Nageshwar, Zhu, Jin, Nannini, Michelle, Chan, W. Y., Sanabria Bohórquez, S. M., Meng, R. D., Lin, Kui, … Tabernero Study supervision, J (2017) 'A First-in-Human Phase I Study of the ATP-Competitive AKT Inhibitor Ipatasertib Demonstrates Robust and Safe Targeting of AKT in Patients with Solid Tumors', *Cancer Discovery*, 7(1), pp. 102–113. doi: 10.1158/2159-8290.CD-16-0512.

Saxton, R. A. and Sabatini, D. M. (2017) 'mTOR Signaling in Growth, Metabolism, and Disease', *Cell*, 168(6), pp. 960–976. doi: 10.1016/j.cell.2017.02.004.

Schmid, P., Abraham, J., Chan, S., Wheatley, D., Brunt, M., Nemsadze, G., Baird, R., Park, Y. H., Hall, P., Perren, T., Stein, R. C., László, M., Ferrero, J.-M., Phillips, M., Conibear, J., Sarker, S.-J., … Turner, N. C. (2018) 'AZD5363 plus paclitaxel versus placebo plus paclitaxel as first-line therapy for metastatic triple-negative breast cancer (PAKT): A randomised, double-blind, placebo-controlled, phase II trial.', *Journal of Clinical Oncology*. American Society of Clinical Oncology, 36(15_suppl), pp. 1007–1007.

Schuler, W., Sedrani, R., Cottens, S., Häberlin, B., Schulz, M., Schuurman, H. J., Zenke, G., Zerwes, H. G. and Schreier, M. H. (1997) 'SDZ RAD, a new rapamycin derivative: pharmacological properties in vitro and in vivo.', *Transplantation*, 64(1), pp. 36–42.

Sedrani, R., Cottens, S., Kallen, J. and Schuler, W. (1998) 'Chemical modification of rapamycin: the discovery of SDZ RAD.', *Transplantation proceedings*, 30(5), pp. 2192–4. Available at: http://www.ncbi.nlm.nih.gov/pubmed/9723437.

Sekiyama, N., Arthanari, H., Papadopoulos, E., Rodriguez-Mias, R. A., Wagner, G. and Léger-Abraham, M. (2015) 'Molecular mechanism of the dual activity of 4EGI-1: Dissociating eIF4G from eIF4E but stabilizing the binding of unphosphorylated 4E-BP1', *Proceedings of the National Academy of Sciences*, 112(30), pp. E4036–E4045. doi: 10.1073/pnas.1512118112.

Serra, V., Eichhorn, P. J. A., García-García, C., Ibrahim, Y. H., Prudkin, L., Sánchez, G., Rodríguez, O., Antón, P., Parra, J.-L., Marlow, S., Scaltriti, M., Pérez-Garcia, J., Prat, A., Arribas, J., Hahn, W. C., Kim, S. Y. and Baselga, J. (2013) 'RSK3/4 mediate resistance to PI3K pathway inhibitors in breast cancer', *The Journal of Clinical Investigation*. American Society for Clinical Investigation, 123(6), pp. 2551–2563. doi: 10.1172/JCI66343.

Seyfried, T. N. (2015) 'Cancer as a mitochondrial metabolic disease.', *Frontiers in cell and developmental biology*. Frontiers Media SA, 3, p. 43. doi: 10.3389/fcell.2015.00043.

Sherrill, K. W., Byrd, M. P., Van Eden, M. E. and Lloyd, R. E. (2004) 'BCL-2 translation is mediated via internal ribosome entry during cell stress', *Journal of Biological Chemistry*, 279(28), pp. 29066–29074. doi: 10.1074/jbc.M402727200.

Shi, Y. J., Sharma, A., Wu, H., Lichtenstein, A. and Gera, J. (2005) 'Cyclin D1 and c-myc internal ribosome entry site (IRES)-dependent translation is regulated by AKT activity and enhanced by rapamycin through a p38 MAPK- and ERK-dependent pathway', *Journal of Biological Chemistry*. American Society for Biochemistry and Molecular Biology, 280(12), pp. 10964–10973. doi: 10.1074/jbc.M407874200.

Showkat, M., Beigh, M. A. and Andrabi, K. I. (2014) 'mTOR Signaling in Protein Translation Regulation: Implications in Cancer Genesis and Therapeutic Interventions', *Molecular Biology International*, 2014, pp. 1–14. doi: 10.1155/2014/686984.

Siddiqui, N. and Sonenberg, N. (2015) 'Signalling to eIF4E in cancer', *Biochemical Society Transactions*, 43(5), pp. 763–772. doi: 10.1042/BST20150126.

Skehan, P., Storeng, R., Scudiero, D., Monks, A., McMahon, J., Vistica, D., Warren, J. T., Bokesch, H., Kenney, S. and Boyd, M. R. (1990) 'New colorimetric cytotoxicity assay for anticancer-drug screening.', *Journal of the National Cancer Institute*, 82(13), pp. 1107–12.

Smith, P. K., Krohn, R. I., Hermanson, G. T., Mallia, A. K., Gartner, F. H., Provenzano, M. D., Fujimoto, E. K., Goeke, N. M., Olson, B. J. and Klenk, D. C. (1985) 'Measurement of protein using bicinchoninic acid.', *Analytical biochemistry*, 150(1), pp. 76–85.

Smyth, L. A. and Collins, I. (2009) 'Measuring and interpreting the selectivity of protein kinase inhibitors.', *Journal of chemical biology*. Springer, 2(3), pp. 131–51. doi: 10.1007/s12154-009-0023-9.

Sommer, E. M., Dry, H., Cross, D., Guichard, S., Davies, B. R. and Alessi, D. R. (2013) 'Elevated SGK1 predicts resistance of breast cancer cells to Akt inhibitors', *Biochemical Journal*, 452(3), pp. 499–508. doi: 10.1042/BJ20130342.

Spencer, A., Yoon, S.-S., Harrison, S. J., Morris, S. R., Smith, D. A., Brigandi, R. A., Gauvin, J., Kumar, R., Opalinska, J. B. and Chen, C. (2014) 'The novel AKT inhibitor afuresertib shows favorable safety, pharmacokinetics, and clinical activity in multiple myeloma.', *Blood*, 124(14), pp. 2190–5. doi: 10.1182/blood-2014-03-559963.

Stavraka, C. and Blagden, S. (2015) 'The La-related proteins, a family with connections to cancer', *Biomolecules*. MDPI AG, pp. 2701–2722. doi: 10.3390/biom5042701.

Stella, A., Lonoce, A., Resta, N., Gentile, M., Susca, F., Mareni, C., Brescia, G., Origoni, P., Montero, M. P. and Guanti, G. (1992) 'Familial adenomatous polyposis: identification of a new frameshift mutation of the APC gene in an Italian family.', *Biochemical and biophysical research communications*, 184(3), pp. 1357–63. doi: 10.1016/s0006-291x(05)80032-4.

Stottrup, C., Tsang, T. and Chin, Y. R. (2016) 'Upregulation of AKT3 Confers Resistance to the AKT Inhibitor MK2206 in Breast Cancer', *Molecular Cancer Therapeutics*. American Association for Cancer Research, 15(8), pp. 1964–1974. doi: 10.1158/1535-7163.MCT-15-0748.

Tabernero, J., Cervantes, A., Saura, C. and Roda, D. (2011) 'Targeting the PI3K-Akt-mTOR pathway with GDC-0068 , a novel selective ATP competitive Akt inhibitor', *Cell*.

Tamura, K., Hashimoto, J., Tanabe, Y., Kodaira, M., Yonemori, K., Seto, T., Hirai, F., Arita, S., Toyokawa, G., Chen, L., Yamamoto, H., Kawata, T., Lindemann, J. and Esaki, T. (2016) 'Safety and tolerability of AZD5363 in Japanese patients with advanced solid tumors', *Cancer Chemotherapy and Pharmacology*. doi: 10.1007/s00280-016-2987-9.

Tang, H., Hornstein, E., Stolovich, M., Levy, G., Livingstone, M., Templeton, D., Avruch, J. and Meyuhas, O. (2001) 'Amino Acid-Induced Translation of TOP mRNAs Is Fully Dependent on Phosphatidylinositol 3-Kinase-Mediated Signaling, Is Partially Inhibited by Rapamycin, and Is Independent of S6K1 and rpS6 Phosphorylation', *Molecular and Cellular Biology*, 21(24), pp. 8671–8683. doi: 10.1128/MCB.21.24.8671-8683.2001.

Tavares, M. R., Pavan, I. C. B., Amaral, C. L., Meneguello, L., Luchessi, A. D. and Simabuco, F. M. (2015) 'The S6K protein family in health and disease', *Life Sciences*. doi: 10.1016/j.lfs.2015.03.001.

Tee, A. R. and Proud, C. G. (2002) 'Caspase cleavage of initiation factor 4E-binding protein 1 yields a dominant inhibitor of cap-dependent translation and reveals a novel regulatory motif.', *Molecular and cellular biology*, 22(6), pp. 1674–83. doi: 10.1128/mcb.22.6.1674-1683.2002.

Teng, Q.-X., Ashar, Y. V., Gupta, P., Gadee, E., Fan, Y.-F., Reznik, S. E., Wurpel, J. N. D. and Chen, Z.-S. (2019) 'Revisiting mTOR inhibitors as anticancer agents', *Drug Discovery Today*. Elsevier Current Trends. doi: 10.1016/J.DRUDIS.2019.05.030.

The Human Protein Atlas (2020). Available at: https://www.proteinatlas.org/ (Accessed: 21 January 2020).

Theodosakis, N., Micevic, G., Langdon, C. G., Ventura, A., Means, R., Stern, D. F. and Bosenberg, M. W. (2017) 'p90RSK Blockade Inhibits Dual BRAF and MEK Inhibitor-Resistant Melanoma by Targeting Protein Synthesis', *The Journal of investigative dermatology*. NIH Public Access, 137(10), p. 2187. doi: 10.1016/J.JID.2016.12.033.

Thoreen, C. C. (2017) 'The molecular basis of mTORC1-regulated translation', *Biochemical Society Transactions*, 45(1), pp. 213–221. doi: 10.1042/BST20160072.

Thoreen, C. C., Kang, S. A., Chang, J. W., Liu, Q., Zhang, J., Gao, Y., Reichling, L. J., Sim, T., Sabatini, D. M. and Gray, N. S. (2009) 'An ATP-competitive mammalian target of rapamycin inhibitor reveals rapamycin-resistant functions of mTORC1', *Journal of Biological Chemistry*, 284(12), pp. 8023–8032. doi: 10.1074/jbc.M900301200.

Thorpe, L. M., Yuzugullu, H. and Zhao, J. J. (2015) 'PI3K in cancer: Divergent roles of isoforms, modes of activation and therapeutic targeting', *Nature Reviews Cancer*. doi: 10.1038/nrc3860.

Tomasetti, C. and Vogelstein, B. (2015) 'Variation in cancer risk among tissues can be explained by the number of stem cell divisions', *Science*, 347(6217), pp. 78–81. doi: 10.1126/science.1260825.

Torti, D. and Trusolino, L. (2011) 'Oncogene addiction as a foundational rationale for targeted anti-cancer therapy: Promises and perils', *EMBO Molecular Medicine*, 3(11), pp. 623–636. doi: 10.1002/emmm.201100176.

Tsukumo, Y., Alain, T., Fonseca, B. D., Nadon, R. and Sonenberg, N. (2016) 'Translation control during prolonged mTORC1 inhibition mediated by 4E-BP3', *Nature Communications*. Nature Publishing Group, 7, pp. 1–13. doi: 10.1038/ncomms11776.

Türk, D. and Szakács, G. (2009) 'Relevance of multidrug resistance in the age of targeted therapy.', *Current opinion in drug discovery & development*, 12(2), pp. 246–52.

Tzatsos, A. and Kandror, K. V. (2006) 'Nutrients Suppress Phosphatidylinositol 3-Kinase/Akt Signaling via Raptor-Dependent mTOR-Mediated Insulin Receptor Substrate 1 Phosphorylation', *Molecular and Cellular Biology*, 26(1), pp. 63–76. doi: 10.1128/MCB.26.1.63-76.2006.

Vanhaesebroeck, B., Guillermet-Guibert, J., Graupera, M. and Bilanges, B. (2010) 'The emerging mechanisms of isoform-specific PI3K signalling', *Nature Reviews Molecular Cell Biology*, 11(5), pp. 329–341. doi: 10.1038/nrm2882.

Vanhaesebroeck, B., Stephens, L. and Hawkins, P. (2012) 'PI3K signalling: The path to discovery and understanding', *Nature Reviews Molecular Cell Biology*. Nature Publishing Group, 13(3), pp. 195–203. doi: 10.1038/nrm3290.

Wang, H., Huang, F., Wang, J., Wang, P., Lv, W., Hong, L., Li, S. and Zhou, J. (2015) 'The synergistic inhibition of breast cancer proliferation by combined treatment with 4EGI-1 and MK2206', *Cell Cycle*, 14(2), pp. 232–242. doi: 10.4161/15384101.2014.977096.

Wang, J., Ye, Q., Cao, Y., Guo, Y., Huang, X., Mi, W., Liu, S., Wang, C., Yang, H.-S., Zhou, B. P., Evers, B. M. and She, Q.-B. (2017) 'Snail determines the therapeutic response to mTOR kinase inhibitors by transcriptional repression of 4E-BP1', *Nature Communications*. Nature Publishing Group, 8(1), p. 2207. doi: 10.1038/s41467-017-02243-3.

Wang, L., Harris, T. E., Roth, R. A. and Lawrence, J. C. (2007) 'PRAS40 regulates mTORC1 kinase activity by functioning as a direct inhibitor of substrate binding', *Journal of Biological Chemistry*, 282(27), pp. 20036–20044. doi: 10.1074/jbc.M702376200.

Wang, X., Li, W., Parra, J.-L., Beugnet, A. and Proud, C. G. (2003) 'The C Terminus of Initiation Factor 4E-Binding Protein 1 Contains Multiple Regulatory Features That Influence Its Function and Phosphorylation', *Molecular and Cellular Biology*, 23(5), pp. 1546–1557. doi: 10.1128/MCB.23.5.1546-1557.2003.

Wang, X., Li, W., Williams, M., Terada, N., Alessi, D. R. and Proud, C. G. (2001) 'Regulation of elongation factor 2 kinase by p90RSK1 and p70 S6 kinase', *EMBO Journal*, 20(16), pp. 4370–4379. doi: 10.1093/emboj/20.16.4370.

Wang, X. and Proud, C. G. (2011) 'mTORC1 signaling: what we still don't know', *Journal of Molecular Cell Biology*. Oxford University Press, 3(4), pp. 206–220. doi: 10.1093/jmcb/mjq038.

Wang, X., Xie, J. and Proud, C. G. (2017) 'Eukaryotic elongation factor 2 kinase (eEF2K) in cancer', *Cancers*. MDPI AG. doi: 10.3390/cancers9120162.

WARNER, J. R., KNOPF, P. M. and RICH, A. (1963) 'A multiple ribosomal structure in protein synthesis.', *Proceedings of the National Academy of Sciences of the United States of America*. National Academy of Sciences, 49(1), pp. 122–9.

Webster, K. R., Goel, V. K., Hung, I. N., Parker, G. S., Staunton, J., Neal, M., Molter, J., Chiang, G. G., Jessen, K. A., Wegerski, C. J., Sperry, S., Huang, V., Chen, J., Thompson, P. A., Appleman, J. R., Webber, S. E., … Reich, S. H. (2015) 'eFT508, a Potent and Selective Mitogen-Activated Protein Kinase Interacting Kinase (MNK) 1 and 2 Inhibitor, Is Efficacious in Preclinical Models of Diffuse Large B-Cell Lymphoma (DLBCL)', *Blood*, 126(23), pp. 1554–1554.

Wehrenberg-Klee, E., Turker, N. S., Heidari, P., Larimer, B., Juric, D., Baselga, J., Scaltriti, M. and Mahmood, U. (2016) 'Differential Receptor Tyrosine Kinase PET Imaging for Therapeutic Guidance', *Journal of Nuclear Medicine*, 57(9), pp. 1413–1419. doi: 10.2967/jnumed.115.169417.

Weinstein, I. B. and Joe, A. K. (2006) 'Mechanisms of Disease: oncogene addiction—a rationale for molecular targeting in cancer therapy', *Nature Clinical Practice Oncology*, 3(8), pp. 448–457. doi: 10.1038/ncponc0558.

Williams, A. J., Werner-Fraczek, J., Chang, I.-F. and Bailey-Serres, J. (2003) 'Regulated Phosphorylation of 40S Ribosomal Protein S6 in Root Tips of Maize', *PLANT PHYSIOLOGY*, 132(4), pp. 2086–2097. doi: 10.1104/pp.103.022749.

Wiza, C., Nascimento, E. B. M. and Ouwens, D. M. (2012) 'Role of PRAS40 in Akt and mTOR signaling in health and disease', *AJP: Endocrinology and Metabolism*, 302(12), pp. E1453–E1460. doi: 10.1152/ajpendo.00660.2011.

Yanagiya, A., Suyama, E., Adachi, H., Svitkin, Y. V, Aza-Blanc, P., Imataka, H., Mikami, S., Martineau, Y., Ronai, Z. A. and Sonenberg, N. (2012) 'Translational homeostasis via the mRNA cap-binding protein, eIF4E.', *Molecular cell*. NIH Public Access, 46(6), pp. 847–58. doi: 10.1016/j.molcel.2012.04.004.

Yap, T. A., Garrett, M. D., Walton, M. I., Raynaud, F., de Bono, J. S. and Workman, P. (2008) 'Targeting the PI3K–AKT–mTOR pathway: progress, pitfalls, and promises', *Current Opinion in Pharmacology*, 8(4), pp. 393–412. doi: 10.1016/j.coph.2008.08.004.

Yeh, T. C., Marsh, V., Bernat, B. A., Ballard, J., Colwell, H., Evans, R. J., Parry, J., Smith, D., Brandhuber, B. J., Gross, S., Marlow, A., Hurley, B., Lyssikatos, J., Lee, P. A., Winkler, J. D., Koch, K. and Wallace, E. (2007) 'Biological Characterization of ARRY-142886 (AZD6244), a Potent, Highly Selective Mitogen-Activated Protein Kinase Kinase 1/2 Inhibitor', *Clinical Cancer Research*, 13(5), pp. 1576–1583. doi: 10.1158/1078-0432.CCR-06-1150.

Yip, C. K., Murata, K., Walz, T., Sabatini, D. M. and Kang, S. A. (2010) 'Structure of the Human mTOR Complex I and Its Implications for Rapamycin Inhibition', *Molecular Cell*. Elsevier Ltd, 38(5), pp. 768–774. doi: 10.1016/j.molcel.2010.05.017.

Youtani, T., Tomoo, K., Ishida, T., Miyoshi, H. and Miura, K.-I. (2000) 'Regulation of Human eIF4E by 4E-BP1: Binding Analysis Using Surface Plasmon Resonance', *IUBMB Life*. John Wiley & Sons, Ltd, 49(1), pp. 27–31. doi: 10.1080/713803582.

Yu, K., Toral-Barza, L., Shi, C., Zhang, W.-G. and Zask, A. (2008) 'Response and determinants of cancer cell susceptibility to PI3K inhibitors: Combined targeting of PI3K and Mek1 as an effective anticancer strategy', *Cancer Biology & Therapy*, 7(2), pp. 310–318. doi: 10.4161/cbt.7.2.5334.

Zhang, M., Fu, W., Prabhu, S., Moore, J. C., Ko, J., Kim, J. W., Druker, B. J., Trapp, V., Fruehauf, J., Gram, H., Fan, H. Y. and Ong, S. T. (2008) 'Inhibition of Polysome Assembly Enhances Imatinib Activity against Chronic Myelogenous Leukemia and Overcomes Imatinib Resistance', *Molecular and Cellular Biology*. doi: 10.1128/mcb.00477-08.

Zorea, J., Prasad, M., Cohen, L., Li, N., Schefzik, R., Ghosh, S., Rotblat, B., Brors, B. and Elkabets, M. (2018) 'IGF1R upregulation confers resistance to isoform-specific inhibitors of PI3K in PIK3CA-driven ovarian cancer.', *Cell death & disease*, 9(10), p. 944. doi: 10.1038/s41419-018-1025-8.

Zuccotti, P. and Modelska, A. (2016) 'Studying the translatome with polysome profiling', in *Methods in Molecular Biology*. 1358:59-69. doi: 10.1007/978-1-4939-3067-8_4.